2016

Study of cable bolt shear strength characteristics for ground reinforcement in mines

Xuwei Li
University of Wollongong

UNIVERSITY OF WOLLONGONG

Faculty of Engineering & Information Sciences

School of Civil, Mining and Environmental Engineering

STUDY OF CABLE BOLT SHEAR STRENGTH CHARACTERISTICS FOR GROUND REINFORCEMENT IN MINES

XUWEI LI

"This thesis is presented as part of the requirements for the award of the Degree of Doctor of Philosophy at the University of Wollongong"

2016

DECLARATION

I, Xuwei Li, hereby declare that all material in this thesis, submitted in fulfilment of the requirements for the award of the degree of Doctor of Philosophy, in the School of Civil, Mining and Environmental Engineering, University of Wollongong, is wholly my own work unless otherwise referenced or acknowledged. This document has not been submitted for qualification at any other academic institution.

Xuwei Li
2016

PUBLICATIONS

The following publications are the result of this thesis:

[1] **Li, X.**, Nemcik, J., Mirzaghorbanali, A., Aziz, N. and Rasekh, H. (2015). Analytical model of shear behaviour of a fully grouted cable bolt subjected to shearing. *International Journal of Rock Mechanics and Mining Sciences*, 80, 31-39.

[2] **Li, X.**, Aziz, N., Mirzaghorbanali, A. and Nemcik, J. (2016). Behaviour of fiber glass bolts, rock bolts and cable bolts in shear. *Rock Mechanics and Rock Engineering*, 49(7), 2723-2735.

[3] **Li, X.**, Aziz, N., Mirzaghorbanali, A. and Nemcik, J. (2017). Comparison of the shear test results of a cable bolt on three laboratory test apparatuses. *Tunnelling and Underground Space Technology*, 61, 82-89.

[4] **Li, X.**, Nemcik, J., Aziz, N., Mirzaghorbanali, A. and Rasekh, H. (2015). Modelling of rebar and cable bolt behaviour in tension/shear. *In: Proceddings of the 15th Coal Operators' Conference*, Wollongong, NSW, Australia.

[5] Aziz, N., Nemcik, J., Mirzaghorbanali, A., Foldi, S., Joyce, D., Moslemi, A., Ghojavand, H., Ma, S., **Li, X.** and Rasekh, H. (2014). Suggested methods for the preparation and testing of various properties of resins and grouts. *In: Proceddings of the 14th Coal Operators' Conference*, Wollongong, NSW, Australia.

[6] David, J., Mirzaghorbanali, A., **Li, X.**, Rasekh H., Aziz, N. and Nemcik, J. (2015). Strength properties of fibre glass dowels used for strata reinforcement in coal mines. *In: Proceddings of the 14th Coal Operators' Conference*, Wollongong, NSW, Australia.

[7] Rasekh, H., Aziz, N., Nemcik, J., Mirzaghorbanali, A. and **Li, X.** (2015). An experimental study on the contact surface area of cabled bolted strata. *In: Proceddings of the 15th Coal Operators' Conference*, Wollongong, NSW, Australia.

[8] Aziz, N., Craig P., Mirzaghorbanali A., Rasekh, H., Nemcik, J. and **Li, X.** (2015). Behaviour of cable bolts in shear; experimental study and mathematical modelling. *In: Proceddings of the 15th Coal Operators' Conference*, Wollongong, NSW, Australia.

[9] Aziz, N., Hawker, R., Mirzaghorbanali, A., Nemcik J., **Li, X.** and Rasekh, H. (2015). Strength characteristics of secura hollow groutable cable bolts. *In: Proceddings of the 15th Coal Operator' Conference*, Wollongong, NSW, Australia.

[10] Rasekh, H., Mirzaghorbanali, A., Aziz, N., Nemcik, J. and **Li, X.** (2016). Modelling simulation of the performance of cable bolts in shear. *In: Proceddings of the 16th Coal Operators' Conference*, Wollongong, NSW, Australia.

[11] Aziz, N., Mirzaghorbanali, A., Nemcik, J., Rasekh, H. and **Li, X.** (2016). A follow up to study the behaviour of cable bolts in shear: experimental study and mathematical modelling. *In: Proceddings of the 16th Coal Operators' Conference*, Wollongong, NSW, Australia.

[12] Aziz, N., Mirzaghorbanali, A., Nemcik, J., **Li, X.**, Rasekh, H. and Wang G. (2016). Load transfer characteristics of plain and spiral cable bolts tested in new non rotating pull testing apparatus. *In: Proceddings of the 16th Coal Operators' Conference*, Wollongong, NSW, Australia.

ACKNOWLEDGEMENTS

I would like to show my sincere gratitude and appreciation to my thesis supervisors Dr Jan Nemcik and Prof. Naj Aziz, the Faculty of Engineering and Information Sciences, the University of Wollongong, for their ongoing guidance, assistance and support over the course of my doctorate thesis. They have always been available to communicate with, showing their enthusiasm in helping students to succeed and to realise their goals. Their patience and kindness showed in the whole research process and leisure-time activities really helped to ease my anxiety and uneasiness about my study and life, providing me a relaxing environment to focus my energy on research. I am very lucky to have had two great supervisors mentoring me to become a mature researcher in the field of rock reinforcement by bolting. This wonderful research experience with my supervisors will surely be a great memory in my future life.

I wish to extend my thanks to the technical staff in the laboratory of the School of Civil, Mining and Environmental Engineering, especially Mr Colin Delvinish, Mr Duncan Best, Mr Rick McLean, Mr Cameron Neilson and Mr Alan Grant for their assistance in the completion of the experimental procedures and testing of specimens. Without their arrangement and help, the research program would not have been finished smoothly.

Also, I want to give my thanks to members in the bolting research team in the University of Wollongong for their helpful and mind-stimulating advices and full support in test performing, including Dr Ali Mirzaghorbanali, Haleh Rasekh, David Gilbert, Guanyu Yang and others.

The University of Wollongong and the China Scholarship Council (CSC) jointly funded my research and life here in Australia. Their financial support made it possible for me to explore in a new research area as well as a different culture.

My thanks also go to many friends for their encouragement and bringing joyfulness that has helped to uplift my research work, such as Jian Zhang, Weiguo Zeng, Matthew William Goldston, Gongda Wang, Qiuqiu Qiao and Jia Lin.

A special thank is also given to Bob Kininmonth for his careful check of grammatical and spelling errors.

Finally, I want to thank my family members for their ongoing support and love without which I would not have been able to finish my doctorate study. Especially, I am grateful to my younger brother for his care of my parents and also wish all the best to my niece.

ABSTRACT

Bolting is currently the most commonly accepted rock reinforcing method of dealing with rock strata instability in both surface and underground mines as well as civil engineering. Bolts are installed in fractured rock mass to build composite beams in weak strata or to attach weak excavation surfaces to deeper and competent rock layers to achieve stability.

After opening, rock mass around the excavation space experiences stress redistribution and rock fracturing occurs in this process. Bolts installed in the fractured rock mass around excavations normally bear combined tensile and shear loads due to the opening and sliding of rock fractures. Direct shear restraint and high normal stress are applied by the bolt to the fracture surfaces to minimise their displacements. This mechanism allows the excavation surfaces to stabilise and makes them self-supporting. In the interactive process of rock mass and bolt, two load transfer mechanisms are involved: the axial tensioning (axial shearing at the bolt-grout interface, in essence) and the lateral shearing. Axial tensioning was the common focus in past studies, whereas lateral shearing is attracting more attention at present. The strength of the bolt when subjected to both shear and tensile loads is smaller than bolt strength when subjected to tensile load only. Thus, ignoring the shear load in bolting design probably leads to a higher safety factor. Hence, a deep understanding of bolt behaviour subjected to combined loads is essential in bolting system design and assessment.

In the past, a number of experimental and theoretical investigations were conducted on the shear behaviour of the rock discontinuity reinforced by rock bolts and a few preliminary conclusions were drawn. Yet, few studies were performed on the shear behaviour of cable bolted rock discontinuities. Thus, this research investigated the shear performance of cable bolted rock discontinuities both experimentally and theoretically to provide more knowledge in this area.

A series of experimental studies were undertaken to investigate the shear behaviour of cable bolted concrete joints (representing rock discontinuity) and relevant influencing factors. Double shear tests with joint friction were carried out and test results were analysed in respect of joint shear strength, joint shear displacement,

joint shear stiffness, cable pre-tension effect, cable wire surface profile effect, cable failure mode and the shear force-axial force relationship. Double shear tests without joint friction were also carried out using a modified double shear test apparatus. By comparing the double shear tests with and without joint friction, the joint friction and the cable dowel effects on the shear behaviour of cabled concrete joints were studied. British standard single shear tests were also carried out on four cable bolts and were compared with double shear tests. The comparison showed that the joint shear strength from the British standard single shear tests was much smaller than the double shear test results and the reason was analysed.

Bolts used in underground rock engineering include Fibre Glass (FG) bolts, steel rebar bolts and cable bolts. Since these three types of bolts have different mechanical properties, such as tensile strength, shear strength and axial tensile modulus, their reinforcing effect on rock discontinuities are expected to be different. Thus in this study, cable bolts were compared with FG bolts and steel rebar bolts in terms of reinforcing concrete joints with consideration of their basic mechanical properties. Comparison showed that the influence of their basic mechanical properties on their reinforcing effect on concrete joints was evident. Since the mechanical properties of FG bolts was completely different from the other two types, the FG bolt reinforcing effect on the concrete joint was entirely different. The reinforcing effect of cable bolts and steel rebar bolts was more similar due to their similar mechanical properties.

Apart from the experimental investigations, an analytical study was also carried out based on the statically indeterminate beam theory and some conclusions drawn from existing test results, with consideration of most pertinent influencing factors. An analytical model was proposed and compared with the double shear test results, which showed close agreement. In the light of the proposed theoretical method, parametric investigations were performed on four influencing factors, including cable pre-tension, joint friction coefficient, concrete strength and cable installation angle. From the parametric investigations, it was known that the joint friction coefficient and the concrete strength influenced the cable bolted joint shear strength in a consistent manner. However, the cable pre-tension and the cable installation angle affected the cabled joint shear strength in an inconsistent manner. In addition,

the cable pre-tension showed opposite influences on cabled joint shear strength when changing the cable failure modulus, which was consistent with the double shear tests on the plain wire cable and the indented wire cable.

CONTENTS

LIST OF FIGURES

LIST OF TABLES

LIST OF SYMBOLS AND ABBREVIATIONS

SYMBOLS

a, b, a', b'	Regression coefficients
A_b	Bolt cross section area
b_c	Width of the concrete substrate
b_f	Width of the FRP strip
B	Static moment on the bar
c	Cohesion
c_1	Coefficient
C_0	Ratio of cable length to applied load
d_b	Diameter of bolt
E	Elastic modulus of the cable strand
E_c	Modulus of elasticity of concrete
E_f	Elastic modulus of FRP strip
E_m	Modulus of elasticity of support material
EM	Stiffness of mortar and rock
f_{ij}	Displacement along the direction of R_i caused by the unit of R_j
F_{bs}	Shear force acting in the bar at joint
F_{max}	Tensile failure load (strength) of cable bolt
F_n	Confining force on joint
F_s	Shear force of the whole double shear system;

F_p	Axial force of bolt at the distance of L_x
i	Angle of the saw-tooth face
i_d	Angle of joint dilatancy
I	Inertia moment of a cable strand
JCS	Joint wall compressive strength
JRC	Joint roughness coefficient and
k	Concentration coefficient of the shear stress distribution at the cable cross section
k'_{bc}	Bar curvature
K	Stiffness of the elastic foundation
K_m	Lateral stiffness of support material
l_{pl}	Yielding length of subgrade
l_y	Distance from the start position of cable yielding to the joint plane
L	Plastic hinge distance from the joint plane to hinges
L_0	Distance of strain gauge from applied load or point of dilation
L_c	Edge dimension of concrete cross section
L_{ti}	Length of the inner tensioning section
L_{to}	Length of the outer tensioning section
L_x	Distance of a specific point from the loaded end
m_F	Influence of rock strength
m_R	Influence of joint friction angle

M	Bending moment at a cross section of a cable strand
M_{pl}	Plastic bending moment of a bolt
M_{yield}	Yield bending moment
n	Coefficient of local compression of concrete
N	Normal force on joint shearing surface
N_b	Tensile force in the bolt due to shear displacement
$N_{deflection}$	Normal force induced by bolt deflection on the joint plane
N_e	Normal force on the joint plane caused by initial external confining stress
N_f	Ultimate tensile strength of a bolt
N_{joint}	Total normal force on the joint plane
N_o	Tensile force at the failure location of a bolt
N_{oe}	Axial force at point O at bolt yielding stress
N_{of}	Axial force at point O at bolt failure
$N_{pretension}$	Normal force induced by pre-tension on the joint plane
N_y	Tensile force inducing yield in pure tension
N_{yield}	Tensile yield strength of a bolt
p	Support reaction
p_u	Yield strength of the support host materials
P_0	Applied load required to initiate deformation of strain gauge
P_t	Maximum tension load of the bolt,

Q	Shear force of bolt at intersection
Q_{Ay}	Cable shear force at yielding location when the cable yielding starts
Q_f	Ultimate shear strength of a bolt
Q_o	Shear force at the failure location of a bolt
Q_{oy}	Shear force at bolt-joint intersection when a cable starts to yield
Q_{oe}	Shear force acting at point O at bolt yielding stress
Q_{of}	Shear force at point O at bolt failure
Q_{yield}	Yield strength of a cable strand in shear
R_b	Bolt contribution to the shear resistance of a bolted joint
$s(x)$	Displacement of FRP strip relative to the concrete substrate
t_c	Thickness of the concrete substrate
t_f	Thickness of the FRP strip
T	Shear force applied on the shear system
T_{bp}	Tension in the bar at plastic moment
T_c	Direct cable contribution to joint shear strength, also called 'dowel effect' by some researchers
T_{dowel}	Joint shear resistance due to dowel effect
T_f	Shear force of the shear system at bar failure
T_{nbc}	Normalized bolt contribution to joint shear strength
T_r	Axial tensile force of bolt at intersection
T_s	Bolt shear load at the joint intersection

T_t	Axial bolt load at the joint intersection
T_u	Ultimate axial load of bolt
T_y	Yield strength of bar
u	Lateral deformation of support material
u_l	Lateral deformation of support material at which the cable yielding occurs
u_s	Lateral bolt deformation at the joint intersection.
u_t	Axial bolt deformation at the joint intersection;
V_d	Dowel force at the shear displacement of Δ at a crack
V_j	Joint shear displacement
V_u	Ultimate dowel force
y_{bd}	Bolt deflection.
y_n	Distance from the neutral axis of the cable strand;
α	Bolt installation angle to joint
α_{bj}	Angle between the bolt axial and the shearing plane
α_f	Failure angle of concrete specimen
γ	Constant
Δ_s	Slip along the loading direction
Δ	Angle of bar
$\Delta\sigma_{nb}$	Additional confining stress provided by the bolt
Δ_i, $i = 1,2,3,$ at point O	Axial extension, the lateral deflection and the deflection angle of bolt

Δ_{iq}	Displacement along the R_i direction caused by the grout reaction force
Δc_b	Additional cohesion provided by the bolt
ΔN_e	Additional external confining stress
ΔT_{A+G}	Influence of bolt inclination (installation) angle and joint dilatancy
ε_u	Ultimate strain of bolt
θ	Bolt deflection angle
θ_δ	Angle between the bar and the normal direction of the joint
ϵ	Constant
μ	Coefficient of jointfriction
ρ	Stiffness ratio of the FRP strip to the concrete block calculated
ρ_d	Concrete density
σ_{bf}	Bolt failure strength
σ_{by}	Bolt yield stress
σ_c	Compressive strength of the concrete
σ_h	Average rock strength under bolt compression
σ_n	Normal stress
σ_{n0}	Initial confining stress on the joint
τ	Joint shear strength
τ_{bf}	Bolt failure strengths in pure shear
τ_P	Peak shear strength

τ_r	Residual shear strength
φ	Joint frictionAngle
φ_b	Basic friction angle
φ_i	Internal friction angle of concrete
φ_r	Residual angle of friction

ABBREVIATIONS

BS	British Standard
BSSST	British Standard Single Shear Test
CFC	Continuously Frictionally Coupled
CMC	Continuously Mechanically Coupled
DEPT	Double Embedment Pull Test
DMFC	Discretely Mechanically or Frictionally Coupled
DST	Double Shear Test
FG	Fibre Glass
JM	Jennmar
RT	Rio Tinto
LSEPT	Laboratory Short Encapsulation Pull Test
MASDEA	Minova Axially Split Double Embedment Apparatus
SBSPUL	Shear Bond Stiffness Per Unit Length
SHGC	Secura Hollow Groutable Cable
SR	Spirally Ribbed
UCS	Uniaxial Compression Strength

CHAPTER ONE
INTRODUCTION

1.1 General

In rock engineering, the stability of rock strata at surface slopes and around underground openings is of a major concern. Support and reinforcement measures must be taken to control the rock deformation to ensure safety in these areas. Rock support technique is to install supporting elements externally to the rock surface to provide a passive resistance to the deformed and fractured rock masses. Rock control devices belonging to supporting elements include wooden packs, wooden and steel props, steel sets, steel arches, mesh and sprayed materials. All of these supporting elements generate and apply external resistance forces to rock surfaces. In most cases the supported rock mass will experience large fracturing and deformation before the supports provide sufficient resistance. The passive support is less competent in stabilising rock masses mainly because it cannot resist early rock deformation.

Rock reinforcement refers to improving the mechanical properties of the rock mass by internally installing reinforcing elements which includes rock bolts, cable bolts and ground anchors (Windsor, 1997). They are the three main reinforcing techniques widely used in the world. These three reinforcing techniques evolved naturally through a trial and error process to address different classes of problem, which led to the "reinforcement length – capacity relationship". In practice, reinforcing elements have evolved to deal with three different scales of rock mass instability and the relationship is listed below (Windsor, 1999):

- Surface instability: 0-3 m long elements or rock bolts;
- Near surface instability: 3-15 m long elements or cable bolts;
- Deep seated instability: 10-30 m long elements or ground anchors.

In underground coal mines, only rock bolts and cable bolts are adopted to solve the excavation surface and near surface instability problems, whereas no ground anchors longer than 10-30 m are used. Rock bolting and cable bolting are undoubtedly regarded as fundamentally effective reinforcement techniques to stabilise underground openings. The application of rock bolting in coal mines commenced in the early 1900's and became a systematic practice in the late 1950's. Yet, it was not until the mid-1960's that cable bolting was initially used in coal mines (Goris, 1990; Windsor, 1999). After that, these two reinforcing methods have been developing and improving continuously, including reinforcing and structural components, reinforcing scheme design, bolt installation as well as monitoring and assessment of bolt performance.

After excavating, the rock mass around the excavation experiences stress redistribution and rock fracturing. To stabilise the excavation, rock needs to be reinforced at early stages of mining to prevent large displacements and form a self-supporting structure. Compared to external support measures, bolting can provide immediate resistance to stabilise the surrounding rock mass. The wide use of bolts has proven its effectiveness in reinforcing rock strata.

The bolt reinforcement of rock mass is achieved through the load transfer between the bolt and the surrounding strata. Effective and sufficient load transfer helps to improve the stress distribution and the integrity of surrounding rock mass. As bolts are mostly installed in already fractured strata, the main feature of bolting is to provide direct shear restraint and high normal stress to the fracture surfaces to minimise their displacements. The applied confining stress to rock fractures is mainly from the bolt axial loading, while the direct shear restraint of bolt to rock fractures is from the bolt shear loading. These are the two main research areas in the bolt load transfer.

A typical bolting reinforcement system comprises four components: the rock, the bolting element, the internal fixture and the external fixture (Thompson *et al.*, 2012). All adjacent components interact and form four interactions: the rock and the internal fixture, the bolting element and the internal fixture, the bolting element and the external fixture as well as the external fixture and the rock. In the axial load transfer,

the interaction between the bolting element, the internal fixture and the rock is the most important part. Regarding the internal fixture, there are: mechanical point anchor, mechanical friction and grouting. Among them, grouting is the most effective way of transferring loads between the bolting element and the rock because of its high stiffness and great reliability. Currently, the majority of bolts used in underground coal mines are anchored by grouting. In the study of load transfer between bolt element and the rock via grout, the main concerns are the bolt axial stress distribution, the shear stress distribution at the bolt-grout-rock interface, their relationship with the bolt displacement and the applied load at the loading point. To obtain these stress distributions and their relationships in analytical investigation, the bond-slip model at the interface is the core issue. The used bond-slip models in the past research include the linear model (Martin *et al.*, 2004), the tri-linear model (Ren *et al.*, 2010) and nonlinear model (Ma *et al.*, 2013; Ma *et al.*, 2014; Zhou *et al.*, 2010).

Field observations indicated that many bolts failed due to a combination of tension and shear loading, which demonstrated the influence of the lateral shear force on bolt failure. Lateral shearing of bolts contributes to the shear resistance of fractures both directly and indirectly. The lateral shear loading involves not only the bolt shear behaviour at the shearing plane but also the axial tensioning behaviour along the bolt axis, which is a more complex problem. Moreover, due to the small shear strength of bolt, the bolt failure strength is more easily exceeded when subjected to combined shear and tension loads. In this case bolts tend to fail at reduced loads. The traditional design method of a bolting scheme considering only the bolt tensile strength but not the influence of both tensile and shear forces is thought to be less reliable with elevated risk.

In terms of reinforcing rock discontinuities with bolts, more attention was given to rock bolting rather than cable bolting, especially in the last few decades. This was mainly due to the difficulties of studying the cable bolting in nature. To be exact, after the initial adoption of rock bolting in the early 1900's, with increasing understanding of the axial load transfer mechanism of rock bolting, researchers in the 70's, 80's, and 90's started to turn their attention to lateral interaction between

rock bolts and rock discontinuities. During this period, a great number of papers were published on the mechanical behaviour of rock discontinuities reinforced by rock bolts subjected to shearing, such as Dulacka (1972), Bjurstrom (1974), Fuller and Cox (1978); Haas (1981), Hibino and Motojima (1981), Dight (1982, 1983), Ludvig (1983), Egger and Fernandes (1983), Stillborg (1984), Ge and Liu (1988), Aydan (1989); Spang and Egger (1990), Pellet (1994), Pellet *et al.* (1995), Ferrero (1995), Pellet and Egger (1996), Kharchafi *et al.* (1999), McHugh and Signer (1999). However, fewer studies were undertaken on cable bolting subjected to shearing during the same period. To the author's knowledge, the earliest published investigations on cable bolted rock discontinuities exposed to shear loading were conducted by Goris *et al.* (1996) as well as Dolinar *et al.* (1996), followed by Craig and Aziz (2010) and Aziz *et al.* (2014).

Recently, increasing attentions have been turned to cable bolts loaded in shear due to not only limited research on cable bolting in the past, but also the increasing significance of cable bolting in reinforcing strata in areas of thinly-laminated rock and/or high horizontal stress.

The interaction between bolt and rock discontinuities is heavily influenced by a great number of factors, such as strength of rock and grout (Aziz *et al.*, 2003; Ferrero, 1995; Jalalifar *et al.*, 2006b; Spang and Egger, 1990), grout annulus thickness (Aziz *et al.*, 2015a), bolt pretension (Aziz *et al.*, 2003; Ferrero, 1995; Haas, 1981; Hibino and Motojima, 1981; Jalalifar *et al.*, 2006b), grouted or un-grouted conditions (Goris *et al.*, 1996), bolt installation angle (Azuar, 1977; Bjurstrom, 1974; Egger and Fernandes, 1983; Ge and Liu, 1988; Grasselli, 2005; Haas, 1981; Hibino and Motojima, 1981; Spang and Egger, 1990), joint friction coefficient (Goris *et al.*, 1996; Spang and Egger, 1990), loading rate, loading time (creep effect), bolt geometry (Spang and Egger, 1990) and bolt strength. In general, rock strength and bolt pretension have been studied systematically in terms of rock bolting, whereas other influencing factors were rarely investigated. Moreover, some conclusions in the reported publications even contradict each other (Azuar, 1977; Ge and Liu, 1988; Grasselli, 2005; Hibino and Motojima, 1981; Spang and Egger, 1990). A great deal of work about the impact of these influencing factors on the shear performance of

bolted discontinuities needs to be undertaken. Tests and analysis have been systematically performed on rock bolting in general, and cable bolting and rock bolting are analogous to some extent with regards to reinforcing rock discontinuities. Thus existing investigations of rock bolting can be used in the study on cable bolted rock joint shear behaviour.

A correct understanding of the bolt reinforcing effect on rock discontinuities is essential in designing and assessing a reliable bolting scheme. The limited knowledge of cable bolts in reinforcing rock discontinuities has hindered its application. Thus, this aspect of the topic is currently being investigated both experimentally and theoretically, which is the subject of this thesis.

1.2 Key objectives

- Studying and comparing the failure mechanism (pattern) of various cable bolts in the laboratory conditions.
- Investigating the effects of cable pre-tension, cable wire profile and concrete strength on the reinforced joint shear strength and joint shear displacement at cable failure.
- Examining the joint friction effect and the dowel effect of cable bolts by conducting double shear tests with and without joint friction.
- Comparing the shear performance of cable bolts, steel rebar bolts and FG bolts in reinforcing concrete joints.
- Building a theoretical model to predict the shear strength and shear displacement of a cable bolted concrete joint with consideration of most pertinent parameters.
- Performing parametric studies on a number of influencing factors of the cable bolted joint shear performance, including cable pre-tension, joint friction coefficient, concrete strength and cable installation angle.

1.3 Methodology

Primarily, the shear performance of cable bolted concrete joints was the focus of this study. To investigate the load transfer mechanism of cable bolted concrete joints, both experimental and theoretical analyses were performed. Experimental tests on materials used in the shear test of cable bolted joint were undertaken to obtain their basic mechanical properties. These tested materials included cementitious and resin grouts, concrete blocks and cable bolts. Both double shear tests and single shear tests were carried out to study the cable bolted concrete joint shear behaviour. In double shear tests, a number of influencing factors were investigated including cable pretension, cable wire profile and concrete strength. Based on the double shear test results, the joint shear strength, joint shear displacement, joint shear stiffness, cable failure mode and the shear force-axial force relationship were analysed. Apart from double shear tests with joint friction, double shear tests without joint friction were also carried out using a modified double shear test apparatus. By comparing double shear tests with and without joint friction, the joint friction effect and the cable dowel effect on the shear behaviour of cabled concrete joints were studied. Comparisons were also made between double and single shear test results and problems of single shear tests in testing cable shear performance were discovered from the comparison. Cable bolts were compared with FG bolts and steel rebar bolts in reinforcing concrete joints, which showed the influence of the basic mechanical properties on their different shear behaviours.

In addition to the experimental investigations, an analytical investigation was also carried out based on the statically indeterminate beam theory and some existing test results with consideration of most pertinent parameters. In the light of the proposed theoretical method, parametric investigations were performed on four influencing factors including cable pre-tension, joint friction coefficient, concrete block strength and cable installation angle.

1.4 The Scope of the thesis

This thesis is comprised of eight chapters, covering all the research objectives.

Chapter 1 presents the research background, the key objectives and the research methodology of this thesis.

Chapter 2 reviews the bolt classifications, the development of cable bolts, the bolting mechanism, the rock reinforcement theories and the instrumentation of bolt systems.

Chapter 3 reviews the shear behaviour of cable bolted rock discontinuities subjected to combined tensile and shear loads. A great number of shear test methods are compared and the principles to consider when designing a new shear apparatus are summarised and analysed. Bolt failure modes in field conditions, bolt failure mechanism and the influencing factors of bolt shear behaviour are also reviewed. Since the shear performance of bolted rock discontinuities involves both the bolt lateral shear behaviour and the axial behaviour, theoretical analysis of both aspects is reviewed.

Chapter 4 studies the mechanical properties of the experimental materials used in the shear tests including cementitious and resin grouts, concrete blocks and cable bolts.

Chapter 5 presents the experimental procedure and test results including double shear tests with and without joint friction and single shear tests. Results from different shear tests are compared and analysed in terms of joint shear strength, joint shear displacement, joint shear stiffness, cable pre-tension effect, cable wire surface profile effect, cable failure mode and the shear force-axial force relationship.

Chapter 6 compares the shear behaviour of cable bolts, steel rebar bolts and FG bolts in reinforcing concrete joints. The comparison is made with consideration of their basic mechanical properties.

Chapter 7 proposes a theoretical method to predict the shear behaviour of a cable bolted rock discontinuity exposed to shearing. Based on the theoretical method, parametric investigation is made on four influencing factors, cable pre-tension, joint friction angle, concrete strength and cable installation angle.

Chapter 8 summarises the main conclusions drawn in this thesis and several recommendations for future research.

CHAPTER TWO
REVIEW OF BOLTING TECHNIQUES IN ROCK REINFORCEMENT

2.1 Introduction

Rock bolting is a reinforcement technique widely used to reinforce slopes, tunnels, underground excavations and other engineering projects to control rock deformation by enhancing the strength and stiffness of fractured rock masses. When tunnels and underground openings are excavated, rock mass around the excavation experiences stress redistribution. Due to stress changes the surrounding rock mass fails, deforms and expands into the excavation space. This deformation in the surrounding rock mass is unavoidable. In practical applications, what is possible and meaningful is to control the rock deformation according to the requirements of a particular project instead of attempting to avoid it.

The purpose of the rock bolting design is to improve the mechanical properties of fractured rock mass to stabilize rock strata. The role of rock reinforcement is to minimise excessive displacements along fractures within the failed rock. This in turn will minimise bulking of the softened rock mass and maximise confining stresses (σ_3) within the fractured strata. This will reduce the extent of the roof softening zone and maximise the confining stresses further away from the excavation thus preventing rock from falling. Basically, the reinforced rock mass retains a small portion of its original rock strength. All reinforcing mechanisms using rock bolts are established in this way.

With the wide use of rock bolts, a great variety of bolts have been developed and currently in use. Windsor (1999) categorised the existing bolts on the basis of the bonding mechanism. However, as this name system is too general and academic and each category includes a variety of bolts with different names, it is never used beyond academic writing. So when talking about bolting technology, one should be very careful and make it clear exactly what type of bolt is discussed.

A typical bolting reinforcement system comprises four components as shown in Figure 2.1. All adjacent components interact and form four interactions which determine the performance of a bolting reinforcement system. Based on the basic performance of a bolting system, a set of bolting reinforcement systems is combined in a certain pattern to form a bolting reinforcement scheme. The bolting reinforcement scheme helps rock mass surrounding an excavation to form a structure to self-stabilise.

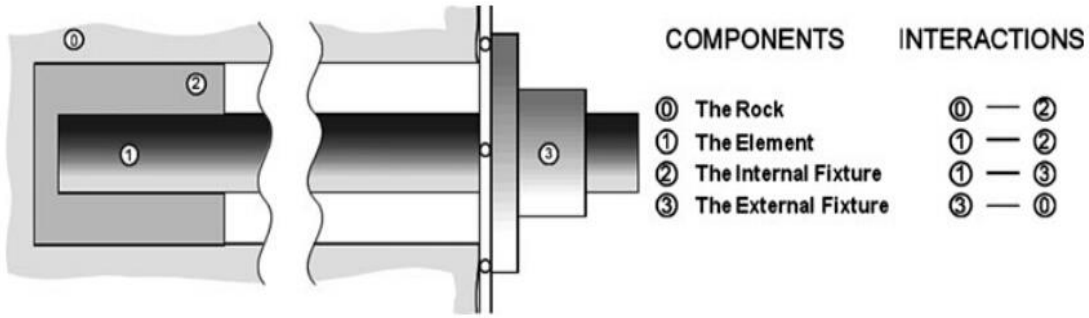

Figure 2.1 A typical bolting reinforcement system
(Thompson *et al.*, 2012)

2.2 Bolt type classification and terminology used in this thesis

With the development and popularity of rock reinforcement techniques, a great variety of reinforcement devices have been developed. It is stated by Thompson *et al.* (2012) that all existing rock reinforcement devices can be classified as rock bolts, cable bolts and ground anchors on the basis of the reinforcement length and the reinforcement capacity as shown in Figure 2.2. This classification is also widely used in industry and research sectors. It is worth noting that the tensile capacity of those reinforcement devices is related to the reinforcement device length and this is termed the "length-capacity relation" of reinforcement. It is suggested that this is a natural selection in response to rock instability problems over three scales (Windsor, 1997).

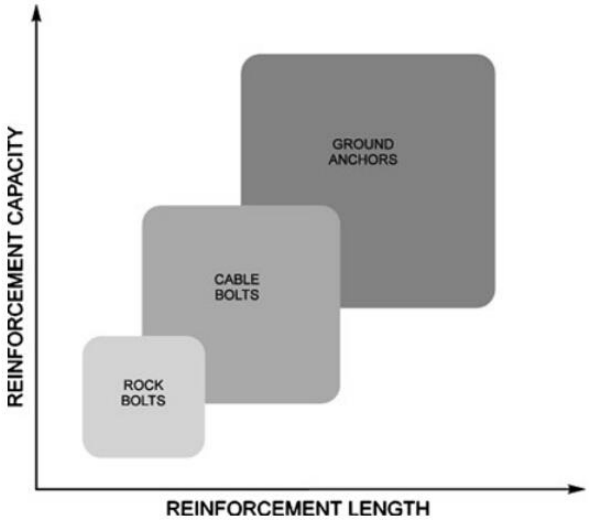

Figure 2.2 Classification of reinforcement systems based on length and capacity (Thompson *et al.*, 2012)

Regarding terms used in rock reinforcement techniques, there is always confusion about the range of rock bolt and rock bolting. Literally understanding, rock bolt refers to all types of bolts used to reinforce rock mass including different bars, cable bolts and ground anchors. Yet, when cable bolt was developed, people tended to highlight the difference of cable bolts and thus put them in the same level as rock bolt instead of a subset of the rock bolt. Actually, cable bolt is just one type of rock bolt. The same thing also happened to ground anchor which has a larger length and capacity. At present, rock bolt is normally used to refer to all types of bolts except cable bolts and ground anchors.

Rock bolting is also used to represent two different things by site operators and researchers. Often, rock bolting is used to refer to rock reinforcement by solid or hollow bars only, while sometimes it is used to represent rock reinforcement by all types of bolts. Especially, it is always used to express both meanings interchangeably in the same document, which makes it difficult for readers to accurately understand what it exactly refers to in a particular position. It is necessary to clarify the exact meaning of these terms in a particular work and maintain the consistency afterwards.

The development and evolution of bolting technology has led to a variety of terms used to describe different reinforcing elements (Windsor, 1999; Windsor and

Thompson, 1996). Due to the diversity of bolt types and techniques in use, they are named differently. To avoid misinterpretation, definition is given here for a range of bolts and bolting terminology used in this thesis, which is primarily based on Windsor's definition:

- Bolt: straight reinforcement element used to internally strengthen rock or concrete, including rock bolt, cable bolt and ground anchor.
- Rock bolt/bar: single straight reinforcement element, mainly including fibre glass (FG) bar, steel bar and wooden bar.
- FG bolt: a main subset of rock bolt, single straight reinforcement element made of fibre glass.
- Steel rebar bolt: a main subset of rock bolt, single straight reinforcement element made of steel rebar.
- Cable wire: a steel wire used to form a cable bolt or cable strand.
- Cable strand or Cable bolt: a set of helically spun cable wires.
- Tendon: pre-tensioned bolts.
- Dowel: un-tensioned bolts.
- Bolting: rock reinforcement by rock bolts, cable bolts and ground anchors.
- Rock bolting: rock reinforcement by rock bolts.
- Cable bolting: rock reinforcement by cable bolts.
- Ground anchoring: rock reinforcement by ground anchors.

2.3 Development of cable bolts

Cable bolts are flexible reinforcement elements consisting of multiple steel wires arranged together. Although closely related to rock bolting, cable bolting has developed into an independent reinforcement method in strengthening rock mass

primarily due to its structural difference. Table 2.1 summarises configurations of cable bolts developed so far.

Table 2.1 Cable bolt types (Windsor, 1992)

Type	Longitudinal section	Cross section	Comment
Multi-wire tendon			Earliest cable bolt
Bird-caged multi-wire tendon	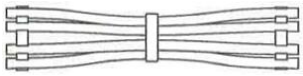	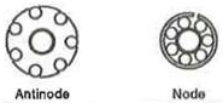	Spacer and tie arrangement used to improve load transfer capacity
Single strand		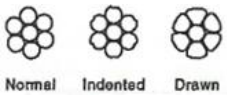	Evolvement from plain multiple wires to strand structure
Coated single strand		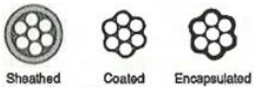	Corrosion resistant
Barrel and wedge anchor on strand	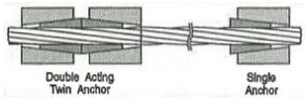	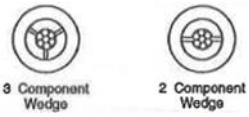	Actively reinforced
Swaged anchor on strand			Strengthened load transfer
Bird-caged strand		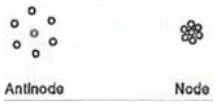	Strengthened load transfer
Bulbed strand			Strengthened load transfer
Ferruled strand			Strengthened load transfer
Hollow strand			Fully encapsulated
Multi-layer strand			Increased cable strength
Multi strands			Increased cable strength

Since the earliest use of the cable bolt at the Willroy mine in Canada and at the Geduld Mines in South Africa (Windsor, 1999), cable bolts have evolved into many different structures that have different performances. The earliest cable bolts were direct combination of smooth steel wires without any internal structures. Since the load transfer characteristics of plain wires is quite poor due to their smooth, straight profile the spacer and tie arrangements were used to improve the load transfer (Jirovec, 1978). Compared to currently used cable bolts, the primary difference of the early cable bolts is the untwisted steel wire.

Helical structure cable bolts were developed and used in the early 1970's. The conversion from straight wire to helical structure was revolutionary and made vast improvements in productivity, adaptability and mechanical performance (Windsor, 1999). The 7-wire, 15.2 mm nominal diameter strand is the most classical type and is still commonly used throughout the world. The load transfer capacity of cable bolts could be strengthened by changing the steel wire surface profile to increase the surface roughness, and adopted surface profiles include indentation, spiral rib, and other drawn patterns. Also, cable bolts are available in stainless steel variety or may be galvanized, sheathed, coated or encapsulated for corrosion protection. All subsequent cable bolts were designed based on the helical strand structure with modification of local structure.

In addition to profiling the wire surface, two different ways are used to increase the load transfer capacity of cable bolts: adding anchors on strands and deforming cable strands to make anchors. The added anchors on strands could be the barrel and wedge system bonded with cable strands by friction (Matthews *et al.*, 1983) or steel blocks swaged on strand (Schmuck, 1979). The deformed strand cable bolts include bird-caged strand (Hutchins *et al.*, 1990), bulbed strand (Garford, 1990) and ferruled strand (Windsor, 1990). All deformed strands are enlarged in diameter at intervals to increase resistance at the bonding interface. They differ mainly in the manufacturing procedure. Bird-caged strand consists of an unraveled and rewound strand that results in an open-weave cross section with greatly enhanced load transfer characteristics (Hutchins *et al.*, 1990). Bulbed strand is formed by gripping the strand and compressing it axially to separate and deform the wires over a small

interval (Garford, 1990). Ferruled strand may be formed by spinning the peripheral wires during manufacture over a ferrule placed on the king wire (Windsor, 1990).

To fully encapsulate the strand during installation for corrosion protection, hollow cable strands were developed with the replacement of the king wire by a hollow steel tube (Faulkner, 2012). The hollow tube provides a path for grout to go in or escape out of the borehole.

Cable strands having more than two layers were also developed and they do not have hollow tubes normally. The advantage of multi-layer strands is that higher tensile strength is provided by strands with small diameter, which allows installation of cable strands in small boreholes.

2.4 Load transfer in bolting

2.4.1 Loading sources of bolting

Generally, there could be three types of load source in a bolting system, i.e., bolt pretension and post-tension, the deformation of surrounding rock mass and the displacement of rock discontinuities. If pretension or post-tension is applied to bolts, axial loads will be generated in the general bolt body. The deformation of surrounding rock mass causes relative axial displacement between the surrounding rock mass and the bolt, which leads to force transfer due to the friction or mechanical interlocking at the bolt-grout-rock interface. Opening of rock discontinuities loads the bolt in the form of applying a concentrated pulling force at the discontinuity and both sides of the bolt are pulled towards the opening point. If rock mass slides along a discontinuity reinforced by a bolt, bending moment and shear force will be generated in the bending section of the bolt.

2.4.2 Load transfer classification of bolting

The load transfer in a reinforcement system involves four types of interaction between reinforcement components as shown in Figure 2.1. Among these interactions, the load transfer between the surrounding rock masses and the reinforcement element is the most important one and it involves the internal fixture,

the surrounding rock and the reinforcement element as shown in Figure 2.3 (Thompson *et al.*, 2012). On the basis of all existing reinforcement systems, Windsor (1997) classified them into three categories as follows:

- Continuously Mechanically Coupled (CMC);
- Continuously Frictionally Coupled (CFC);
- Discretely Mechanically or Frictionally Coupled (DMFC);

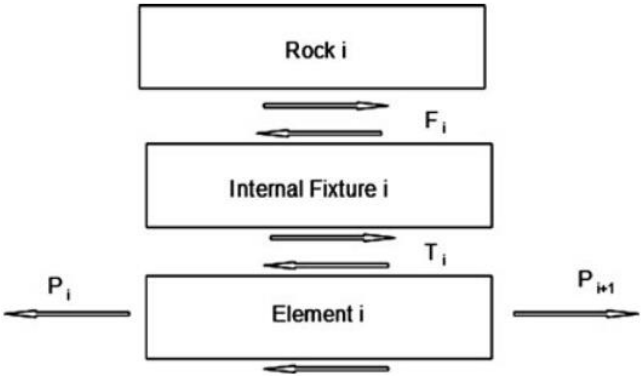

Figure 2.3 Load transfer mechanisms within a reinforcement system (Thompson *et al.*, 2012)

2.5 Rock reinforcement theory in bolting

Based on the bolting mechanism introduced above, researchers established and developed a variety of rock reinforcement theories to control rock masses under different field conditions. Considering the interaction between a bolting system and the surrounding rock mass based on field conditions, a group of bolts with different dimensions, profiles and structures are installed in a designed pattern to strengthen the fractured rock mass and to help rock mass form a stable rock structure. All established theories are based on field conditions. When field conditions change, the effectiveness of a theory will change accordingly. The field conditions in consideration are the rock layer characteristics, the existing structures in rock mass, the existence of stable rock layers, the stress state in rock mass and the rock strength. Although the bolting reinforcement interpretation differs from one theory to another, in practice, bolting may function as a combination of different theories. In particular

conditions, one theory may play a dominant role and the others assist. A few typical rock reinforcement theories are introduced as follows.

Suspension theory:

After excavating roadways in underground mines, the immediate roof rock mass of low grade rock has poor self-stability and may fall away from the deeper roof rock layers. Normally, this kind of rock masses is fractured and/or thinly stratified, which hardly forms a stable structure after losing its support due to excavation. If the rock mass beyond this immediate roof layer is strong and stable, then the weak immediate roof rock can be suspended from the strong roof layer using bolts. Thus the weak immediate roof layer can be reinforced and stabilised. The suspension theory is schematically shown in Figure 2.4. The suspension theory requires bolts to be long enough to reach the stable roof layers at a certain depth which should provide a bonding strength to hang the weak strata below. Pretension is normally required to compress the weak rock discontinuities to improve the rock mass integrity. Otherwise, if the displacements along the weak rock discontinuities become excessive, the rock mass becomes unstable and can easily fall down. Steel mesh and straps are mostly used together with bolts to improve the integrity of rock mass.

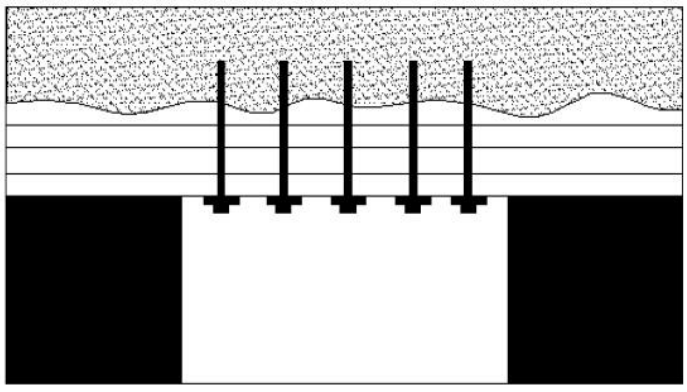

Figure 2.4 Suspension of weak surface rock to the deeper stable rock (Karabin and Debevec, 1976)

Beam building theory:

If the strong and stable rock layers do not exist or are beyond the reach of the bolt anchors, then the beam building theory applies where bolts installed in laminated and/or weak rock layers form a composite beam. The ability of a composite beam to

resist the shear and tensile deformation of rock mass is much higher than the individual rock layers would provide. Likewise, bolt pretension is essential to maintain rock layers integrated, which helps to form a competent composite beam. Figure 2.5 shows the mechanism of beam building theory.

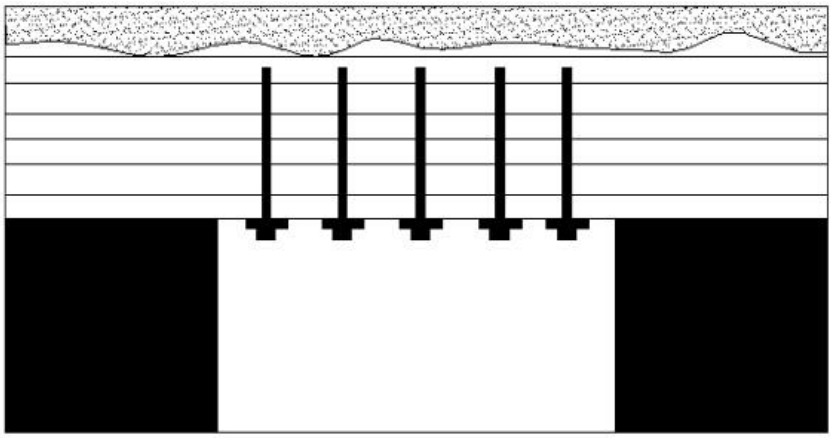

Figure 2.5 Composite rock beam formed by bolt reinforcement (Karabin and Debevec, 1976)

Keying theory:

When a large number of weak discontinuities are present within the rock mass, the rock mass can be visualised as individual rock pieces keyed together. If not reinforced/supported this strata could fall. In this case the use of the suspension theory or the beam building theory to stabilize this rock masses is inappropriate. The decision has to be made where and how many bolts need to be installed to effectively reinforce the keyed strata together to minimise deformation and stop unravelling of the keyed rock pieces. Bolts in tension compress/clamp fractured rock together which increases the frictional resistance along the discontinuities and enables a small lateral compressive stress to remain within the strata. Thus the stability of fractured rock masses is improved. Therefore, the keying theory features improving the stability of individual fractured rock masses by applying additional compressive stress to increase the mutual frictional resistance of rock masses. The size and shape of rock masses and the installation angle of bolt are some important factors controlling the bolt reinforcement effect. The keying effect of bolting is shown in Figure 2.6.

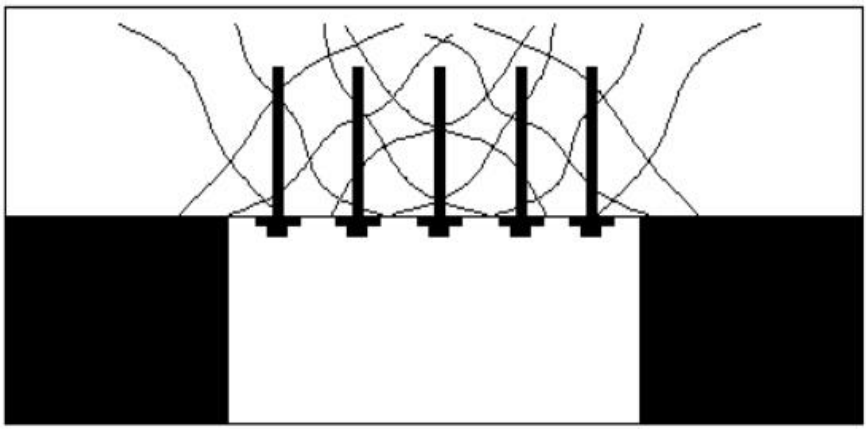

Figure 2.6 Keying effect of bolting (Karabin and Debevec, 1976)

Arching theory:

When it was initially proposed, the concept of arching was mainly related to bedded strata (Li, 2006). Yet, it was also effectively employed in other types of rock masses. Naturally, when underground roadways are excavated, the rock weight of overlaying rock mass is redistributed sideways and applies pressure on the abutments, forming the pressure arch. The excavation-influenced rock zone between the pressure arch and the excavation is in a different stress state. The stresses within the pressure arch are elevated, while the stresses below diminished (Li, 2006). In an un-reinforced stratified roof, the naturally formed pressure arch is thought to be located deep within the roof, depending on geological conditions and the thickness of rock strata.

The rock strata in the near field of excavations (mainly immediate roof) are the concern of collapse hazard, which is in the destressed zone of the natural pressure arch. When bolts are installed in the destressed rock surface, rock strata are bound together to form a thicker rock layer, which can carry more than the bending load carried by unbolted rock strata. A stable thick pressure arch is formed in the surface unstable rock strata when it is subjected to an external transverse load as shown in Figure 2.7. In addition, it is stated that the arching theory is a typical case of the beam building theory when transverse fractures exist in the stratified roof strata (Li, 2006).

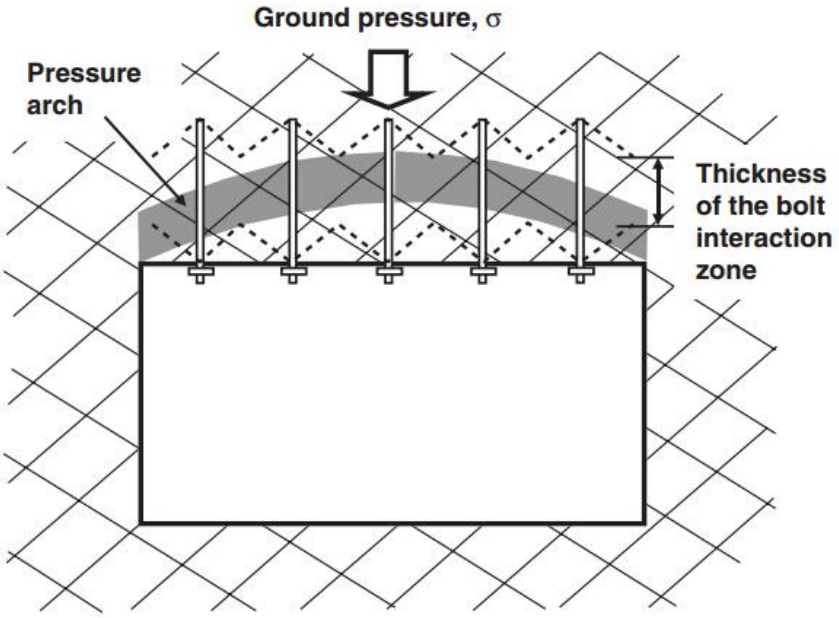

Figure 2.7 Pressure arch formed in the bolted surface fractured roof (Li, 2006)

2.6 Instrumentation systems in bolting

Instrumentation of rock bolting and cable bolting mainly involves the measurement of strain induced during the loading process, which can be converted into load according to the Hooke formula or an experimentally tested stress-strain relationship of the bolt material. Electrical resistance strain gauges and optical fibre are currently the main tools used to measure and monitor the strain in bolts.

When using strain gauges to measure the axial strain of rebar bolts, in general, a groove is machined on opposing sides of a rebar bolt (Li *et al.*, 2014; McHugh and Signer, 1999; Signer *et al.*, 1997) as shown in Figure 2.8, which provides space for the attachment and protection of strain gauges. As the machined groove reduces the axial tensile strength of bolts to some degree which is related to the groove dimension, this needs to be corrected when evaluating the measured data. For example, in the study of McHugh and Signer (1999) the tensile strength declined by approximately 10% due to two 6.4 mm by 3.2 mm grooves on a bolt 22 mm in diameter. This method was effectively used *in situ* to monitor the loading state of rebar bolts, which helped to assess the effectiveness and safety conditions of existing support design and to design a new support scheme where necessary (Signer *et al.*,

1997). This method was also useful and widely accepted in experimental investigations (Jalalifar *et al.*, 2006a; Li *et al.*, 2014; McHugh and Signer, 1999). However the effect of grooves on the bolt performance was not studied or assessed in detail. The groove influence might not be noticeable and could be taken into account with the consideration of the loss of axial tensile strength in the elastic stage of bolts loaded in tension. But the groove influence could be remarkable when bolts are in a plastic state or loaded in shear.

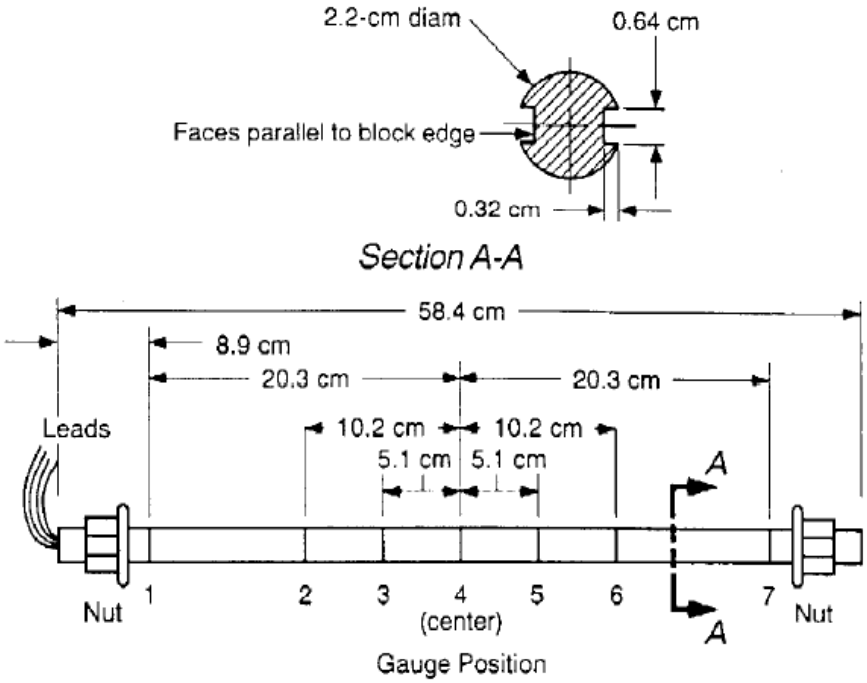

Figure 2.8 Instrumented rebar bolt (McHugh and Signer, 1999)

The strains occurring in loaded cable bolts are very difficult to measure. In general, the instrumentation can be divided into two types, the internal instrumentation and the external instrumentation. The internal instrumentation refers to instruments mounted inside the king strand wire, such as the Smart cable (Hyett *et al.*, 1997) and the SRL cable (Martin *et al.*, 2004), while the external instrumentation refers to instruments mounted externally on the outer layer of cable strands, such as the Tensmeg cable (Lewis *et al.*, 2002).

Compared to internal instruments, the external instruments are easier to assemble. Instruments can be mounted on each cable wire to measure strains of all cable wires. The weakness of external instruments is that they potentially interfere with the

interface between the cable bolt and grout, and thus affect the bond strength in the measured area (Hyett *et al.*, 1997). However, the internal instrument does not affect the bond strength of cable bolts. The weakness of the internal instrumentation is that strains of different strand wires cannot be measured because strain gauges are all mounted in the king strand wire as shown in Figure 2.9. This is not desirable when the loading states are different in different strand wires, for example, when cable bolts are bent in shear. Moreover, the manufacturing of internal instrumented king strand wire and the assembly of the king wire with the outer wires are much more complex.

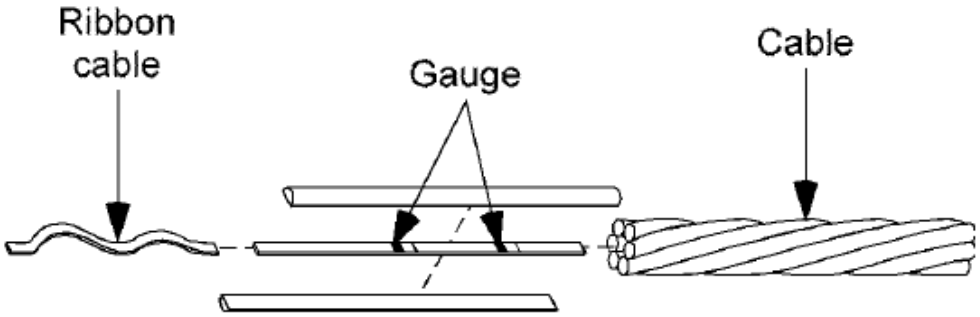

Figure 2.9 Instrumented king wire with gauges and connecting cable (Lewis *et al.*, 2002)

When optic fibre is used to measure the strain in bolts, the installation of optic fibre and other preparation requirement for bolt testing are similar to using strain gauges. The advantage of optic fibre is that one optic fibre is capable of measuring the strain of the whole bolt, which requires much less space for optic fibres when multiple points need to be measured and has little influence on bolt anchorage (Gao *et al.*, 2005). In the experimental study by Gao *et al.* (2005), the difference between the optic fibre and the strain gauge measurements was within 4% when a bolt was loaded in tension, which demonstrated the effectiveness and reliability of the optic fibre method.

From measured strains both the tensile and bending stresses could be obtained for rebar bolts, whereas it is difficult to acquire the bending stress for cable bolts. This is due to the spiral structure of cable bolts.

When bolts bend, bending stresses are generated in each of the bolt wires. The bending stress distribution in a rebar bolt can be easily measured and calculated while the induced bending stress distribution in a cable bolt is nearly impossible to calculate and therefore must be measured due to the relative wire movement. This is schematically illustrated in Figure 2.10. In a cable bolt, the overall bending stress distribution is a combination of the typical bending stress and the transferred stress induced by the relative movement of cable wires. Up to date, no research has been undertaken to establish the bending stress distribution on the cable bolt. Hence the true bending stress distribution in a cable bolt is not yet known.

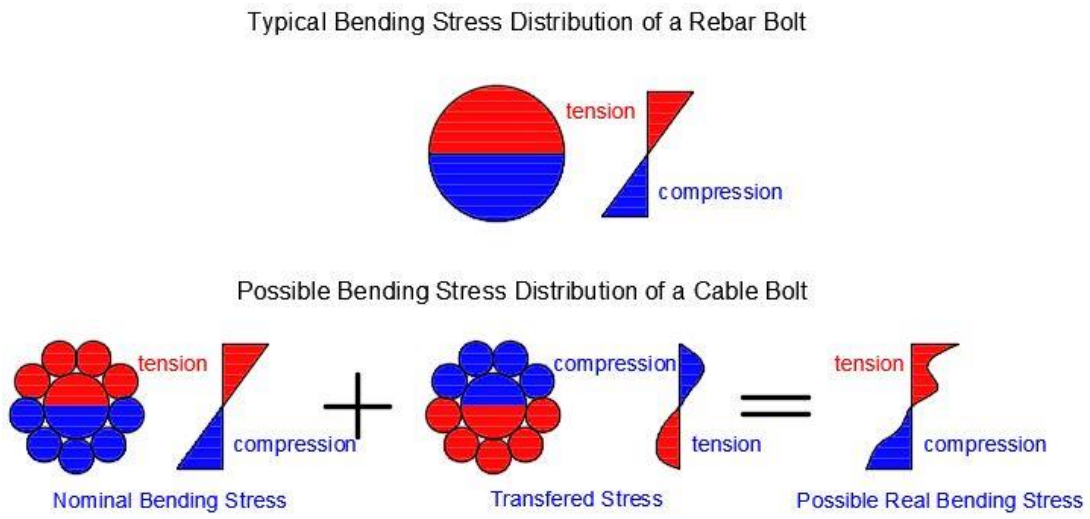

Figure 2.10 Schematic distribution of bending stress in rebar and cable bolts

2.7 Summary

Bolting is practically an effective reinforcement technique in reinforcing stratified and fractured rock mass to maintain the stability and control the deformation of underground excavations and surface slopes. The understanding of the bolting mechanism and the requirement of field conditions have driven the development of new bolt types with improved structures, surface profiles and other features. Based on the length and capacity of existing bolts, they can be divided into rock bolts, cable bolts and ground anchors.

Cable structure has evolved substantially from the earliest multi-wire tendons to currently used steel strands with different diameters, surface profiles and anchorage-

strengthening components. The structure difference affects the performance of cable bolts, thus tests need to be conducted to individually assess the behaviour of each cable design.

A bolt anchored in a rock borehole interacts with the surrounding rock masses and loads are generated and transferred between them when relative movement occurs. The interactions between bolt and rock mass are in the form of friction and mechanical locking. Loads induced in bolts are basically from three sources, bolt pretension, opening of rock discontinuity and rock deformation. A bolt helps to restrain rock deformation by providing clamping action in the rock mass and thus minimise the movement within the fractured ground.

Based on the reinforcing behaviour of a single bolt, a set of bolts are installed in a designed pattern to form a reinforcement scheme. According to the strength, integrity and stress state in rock mass, a variety of rock reinforcement theories were proposed with various reinforcement design configurations, including suspension, beam building, keying and arching.

No matter whether it is in the field applications or in laboratory studies, the stress state and the deformation of bolts need to be monitored for analysis and assessment of its performance and safety. The bolt instrumentation involves attaching stain gauges or optic glass fibres in the groove machined on a bolt surface or on the central hollow grouting tube or inside the king wire of cable bolts.

CHAPTER THREE
REVIEW OF BOLTS SUBJECTED TO COMBINED TENSILE AND SHEAR LOADS

3.1 Introduction

Bolts are widely used to build composite beams in weak strata or to attach weak excavation surfaces to deeper and competent rock layers. Bolts are efficient to reinforce and support excavations in both surface and underground mines and civil engineering projects (Windsor, 1999). As bolts are mostly installed in already fractured strata, the main feature of bolting is to provide direct shear restraint and high normal stress (confinement $= \sigma_n \tan(\varphi + i)$) to the fracture surfaces to minimise their displacements. This mechanism allows the excavation surfaces to stabilise and makes them self-supporting. This mechanism significantly improves the fractured rock integrity and allows for beam building, effective arching and suspension of weak layers while the fractured rock remains keyed together without unravelling. Bolting increases the strength of fractured rock mass and helps to retain some of the compressive stress within the failed strata.

A bolt anchored in rock mass will be loaded when it experiences rock deformation. The loading state of a bolt is controlled by the relative displacement between bolt and rock. Generally, a bolt is loaded by a combination of tension and shear forces. The shear force could be an important factor or even the main force component contributing to bolt failure, especially in areas of severe rock slide due to high lateral stress. If the shear force is ignored, the reinforcement design may not be correct. Measurements and observations indicate that many bolts fail due to a combination of tension and shear loading in field applications, which demonstrates the influence of shear force on bolt failure.

Regarding the shear characteristics of bolting in reinforcing rock strata, a variety of experimental and analytical studies as well as field observations have been performed. The reported studies are reviewed in the following sections.

3.2 Test methods of evaluating the load transfer behaviour of bolts

Regarding the load transfer between bolts and reinforced rock strata, there are two cases to study, the axial load transfer and lateral shear load transfer. When loaded axially, only the tensile behaviour of bolt is relevant, whilst when loaded laterally, both the tensile and shear behaviours are involved.

Table 3.1 and Table 3.2 chronologically list currently used methods and apparatuses used in the laboratory to investigate the behaviour of bolts loaded axially and laterally and their features.

Regarding the bond-slip behaviour of bolts, there are basically two types of test methods, the push test and the pull test. Only a few researchers used the push test method, and most researchers adopted the pull test method to study the bolt bond-slip behaviour. Pull test methods include single encapsulation test and double encapsulation test. All test apparatuses can be used for rebar bolts, while only some specialised apparatuses are available for cable strands due to their spiral wire structure. Special considerations are required to prevent rotation and unwinding of the test device and cable strands. Based on the assessment and comparison of existing test apparatuses, a good test apparatus that could replicate the field conditions to study the axial loading behaviour of bolt should meet the following requirements:

- Initial confining pressure is available and adjustable to simulate different stress states in the field;
- Rock or concrete samples are required to simulate the grout-rock interface, thereby making the failure at grout-rock interface possible;
- Rock samples should be large enough to avoid size effects;
- Bearing plate size should be suitable to allow all possible failure modes to occur (applying to test method in which a hydraulic tensioner is used);
- The whole test apparatus should be gripped together to prevent the rotation and unwinding of a cable strand sample.

In general, as for the lateral shear behaviour of bolts, the shear apparatuses can be divided into single shear and double shear test methods. The earliest traceable investigation of bolt shear performance in a laboratory was conducted by Dulacka in 1972. The test rig used by Dulacka was a single shear test apparatus in which the bolt installation angle was adjustable, and thus allowed the investigation of varied bolt installation angles (Dulacka, 1972). In 1974, Bjurstrom used another single shear test rig, in which, aside from the abilities of Dulacka's design, normal stresses were applied and precisely controlled during the shearing process (Bjurstrom, 1974). From then on, similar single shear test designs were developed during the 80s and 90s and into the 21st century as shown in Table 3.2. Several double shear test apparatuses are also included in Table 3.2. The earliest reported double shear tests were performed by Haile *et al.* (1995), followed by Aziz *et al.* (2003), then Li *et al.* (2014). These shear test methods mainly differ in the following aspects.

- The consideration of joint friction or without joint friction;
- The size of rock or concrete samples;
- The constraint condition of rock or concrete samples;
- The availability of different installation angles of bolts;
- The availability of applying pretension load to bolts;
- The constraint condition of bolt ends.

By analysing and comparing these shear test apparatuses, it is known that when developing a new laboratory shear test rig attention needs to be placed on the following factors:

1. **The joint friction:** The joint friction is one of the main sources of shear resistance of bolted rock masses. During the shearing process, the bent bolt interacts with rock mass and thus changes the normal force on the shear joint planes. The joint friction coefficient varies during the shearing process due to the damage to joint plane asperities and the crush of rock mass around bolts. The difficulty in measuring and recording the variance of joint friction

coefficient and normal force on joint planes makes it practically impossible to accurately investigate the joint friction effect in shear tests.

2. **The bolt de-bonding:** When shear-loaded, the bolt bends and axial force is generated and propagates along the bolt axis to its end. Thus, with the increase of bolt axial force, bolt de-bonding might occur and develop along the bolt axis as well. The extent of bolt de-bonding will affect the shear stiffness and shear strength of the entire shear system, thereby influencing the overall performance of a bolt in reinforcing jointed rock masses. Factors controlling bolt de-bonding primarily include the cross section area of the laboratory rock samples (diameter for circular samples) (Hagan *et al.*, 2015), the bolt encapsulation length (McKenzie and King, 2015), the external confining stress of rock samples and the bolt end constraint condition.

3. **The boundary conditions:** The performance of bolts could be expected to be variable under different field conditions. If possible, the assessment of bolt performance should be related to a particular field condition to make it comparable to other tests. The field condition primarily refers to the normal confining condition and the radial confining condition of the whole shear system. Currently in existing studies, the radial confining condition is always zero load and the normal confining condition is either constant load or no load.

4. **The bolt installation angle:** To allow the adjustment of bolt installation angle, normally large rock samples are required to allow bolts to be sheared to failure in a wide range of initial bolt installation angle. Moreover, the apparatus tends to have more complex structure. In most of the existing shear test apparatuses, it is impossible to adjust the bolt installation angle.

5. **The contact condition between the bolt and steel mould:** During the shearing process, the bolt is expected to interact with and crush into the surrounding rock mass. Theoretically, the bolt will only be in contact with the encapsulation material and rock mass before the final failure. No contact occurs between the bolt and the steel mould frame at the sheared joint area.

Any contact between the bolt and streel frame may lead to severe stress concentration and premature failure of bolts.

6. **The loading manner:** In field conditions, the loading process of a bolt crossing rock joints is very complex. The bolt could be loaded at both the axial and the shear directions at the same time. In each direction the bolt could be loaded by force, by displacement or a combination of both. Besides, the loading rate in the two directions might be proportional to each other due to the relative rock movement. When the loading manner changes, the shear performance of a bolted joint can be expected to change accordingly. Thus, when designing a new shear test machine or apparatus, it should be envisaged first what kind of loading condition is expected to study. Then the testing machine and/or apparatus should be capable of applying and accurately recording loads in the desired manner in both directions.

Table 3.1 Summary of apparatuses used to study the axial tensile behaviour of bolts

Method	Test arrangement	Advantage	Disadvantage
Short single-encapsulation push test (Aziz *et al.*, 2006; Fabjanczyk and Tarrant, 1992)		Constant encapsulation length during loading.	No grout-rock interface; No initial confining pressure; High induced confining pressure due to the small diameter of steel tubes.
Short single-encapsulation pull test (Aziz *et al.*, 2006)	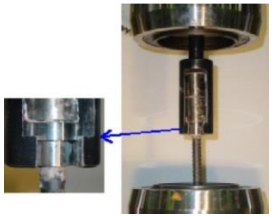	Similar to above	Similar to above
Unconstrained pull test (Hutchinson and Diederichs, 1996)	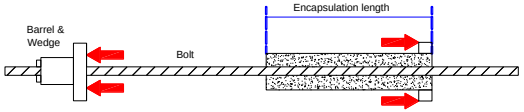	Similar to above	Similar to above
Constrained pull test (Hutchinson and Diederichs, 1996)	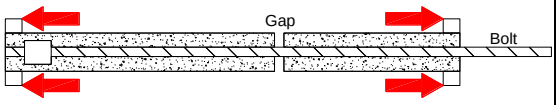	Constant encapsulation length during loading; Mitigation of the influence of the loading section of bolt	No grout-rock interface; No initial confining pressure; High induced confining pressure.
Long double-encapsulation pull test (Goris, 1990; Lewis *et al.*, 2002)	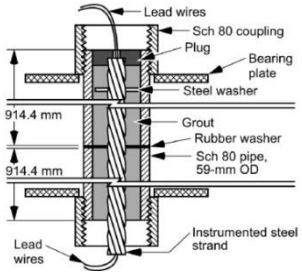	Similar to above	Similar to above

Double embedment pull test (DEPT) (Thomas, 2012)	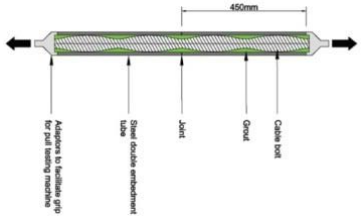	Repeatable test mould; Mitigation of the influence of the loading section of bolt.	No grout-rock interface; Rotation and unwinding of cable bolt; High induced confining pressure.
Laboratory short encapsulation pull test (LSEPT) (Thomas, 2012)	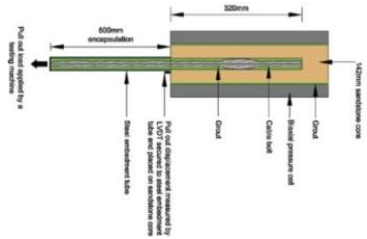	Replication of bolt-ground and gout-rock interfaces and hole rifling; Fixed confining pressure can be applied by a biaxial pressure cell.	Rotation and unwinding of cable bolt; Medium induced confining pressure.
Modified LSEPT (Thomas, 2012)	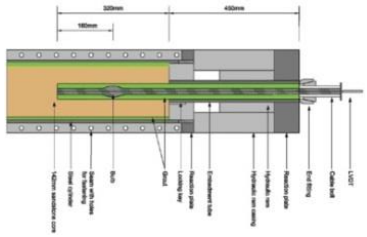	Replication of bolt-ground and gout-rock interfaces and hole rifling; Anti-rotation device to avoid the cable unwinding; a thick walled steel cylinder is used to replace the fixed confining pressure by a constant stiffness boundary condition.	Medium induced confining pressure.
Single-encapsulation pull test (Ito *et al.*, 2001)	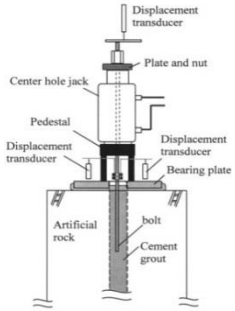	Anti-rotation device to avoid the cable unwinding; Replication of bolt-ground and gout-rock interfaces and hole rifling; Small induced confining pressure.	

Short single-encapsulation pull test (Aziz, 2004)	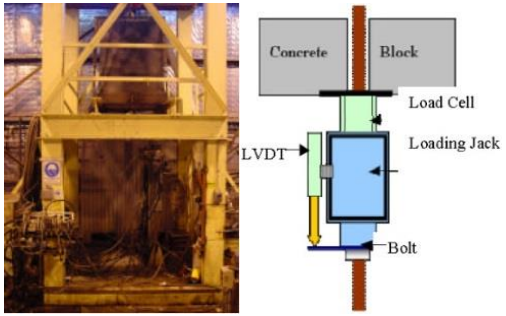	Replication of bolt-ground and gout-rock interfaces and hole rifling; Small induced confining pressure; Repeatable concrete sample.	Rotation and unwinding of cable bolt; large heavy concrete sample.
Modified LSEPT (Hagan *et al.*, 2014)	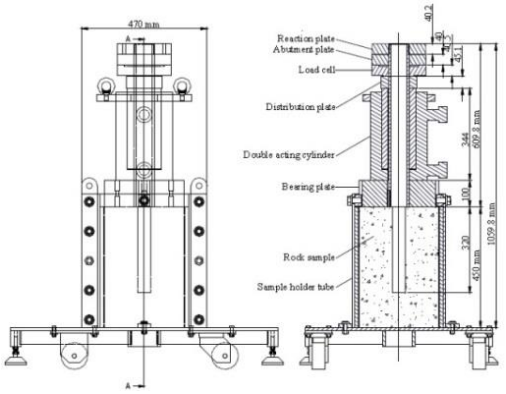	Lock system to prevent cable rotation and unwinding; Available initial confining pressure; All five failure modes can be studied with bearing plates of a suitable diameter; Small induced confining pressure; Repeatable test mould.	/
Minova Axially Split Double Embedment Apparatus (MASDEA) (Aziz 2016)		Repeatable test mould; Prevention of cable rotation and unwinding;	Difficult to cast a straight sample; No initial confining pressure; No grout-rock interface; High induced confining pressure.

Table 3.2 Summary of shear test apparatus

Method	Schematic test arrangement	Advantages	Disadvantages
Single shear (Dulacka, 1972)	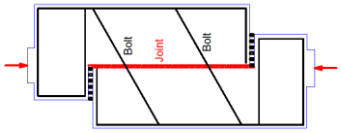	Different installation angles are possible.	Only thin bolts can be tested due to small allowable shear displacement.
Single shear (Bjurstrom, 1974)	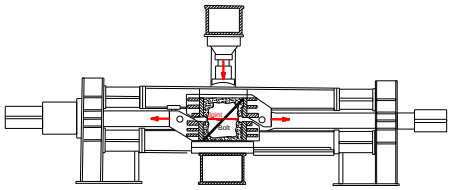	The normal stress can be smoothly adjusted; Different installation angles are possible.	Specially designed complex apparatus is required.
Single shear (Dight, 1983)	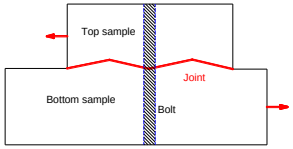	Dilation angle is possible.	Specially designed complex apparatus is required.
Single shear (Ge and Liu, 1988)	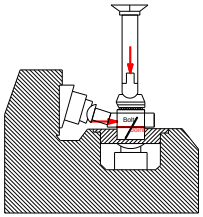	The normal stress can be smoothly adjusted; Different installation angles are possible;	Specially designed complex apparatus is required.
Single shear (Spang and Egger, 1990)	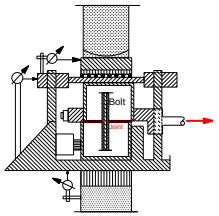	Normal force is possible;	No bolt pretension; Specially designed machine is required.

Single shear (Pellet, 1994)	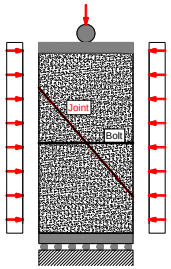	Different bolt installation angles can be studied; Tri-axial stress state is provided.	Specially designed complex apparatus is required.
Single shear (Bawden *et al.*, 1994; Hutchinson and Diederichs, 1996)	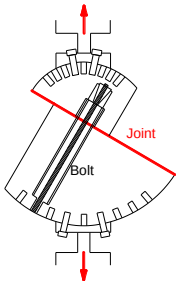	Different installation angles are possible.	The apparatus does not produce the maximum capacity of standard cable bolts in most cases.
Single shear (Haile *et al.*, 1995)	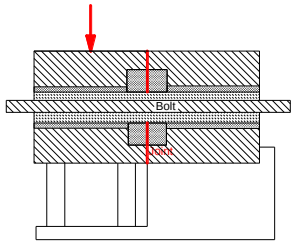	No contact between shear box and bolts during shearing.	No bolt installation angle; Samples tend to collapse when testing; Specially designed machine is required.
Single shear (Ferrero, 1995)	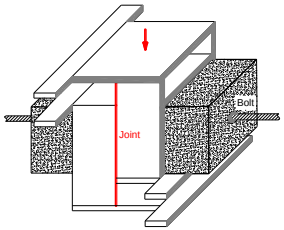	No contact between shear box and bolts during shearing; Able to be tested in general compression machines.	Samples tend to collapse when testing

Single shear (Goris *et al.*, 1996)	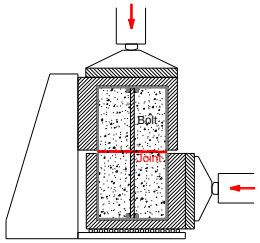	Normal force is possible;	No bolt pretension; Specially designed complex apparatus is required.
Symmetric single shear (Grasselli, 2005)	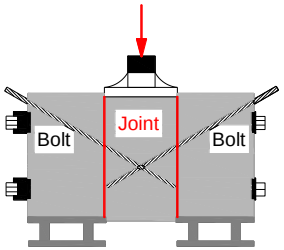	Different installation angles can be studied. Symmetric setup intrinsically avoids rotation of concrete during shearing.	Only thin weak bolts can be loaded to failure due to the collapse of concrete; Samples are very large.
Single shear (British Standard Institution, 2009)	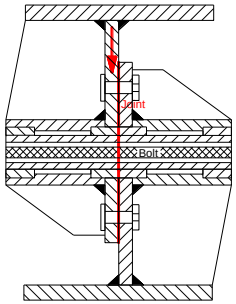	The setup is simple and can be loaded in general compression machines.	Peak shear load is small; Contact between steel shear tubes and bolts get bolts snapped prematurely; No bolt pretension and bolt installation angle cannot be adjusted.
Symmetric single shear (Tanaka and Murakoshi, 2011)	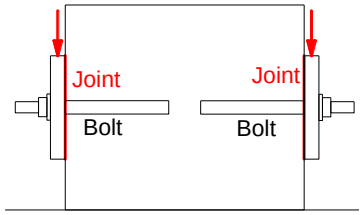	The test assembly is very simple.	The shearing behaviour between steel plates and bolts cannot represent the real rock joint shear.

Single shear (Ayres and Gardner, 2014)	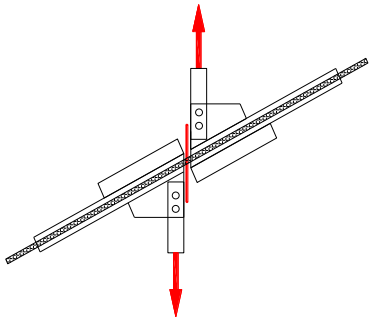	Different bolt installation angle; Simple rig structure;	Rig failure may occur; Not capable of testing strong bolts (cable);
Single shear (McKenzie and King, 2015)		No contact between steel shear tubes and bolts; No de-bonding occurs during testing; A compression machine is integrated to the system.	Samples are large, and difficult to prepare and test; Bolt installation angle cannot be adjusted.
Single shear (Srivastava and Singh, 2015)		Normal force is available; Shear box of large size allows a set of jointed blocks assembled together to study a complex situation.	No bolt pretension; Specially designed complex apparatus is required.
Double shear (Haile *et al.*, 1995)	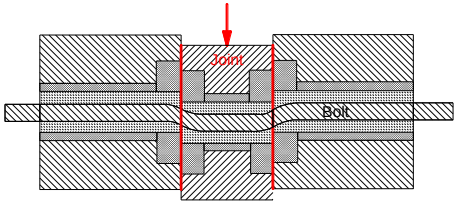	Pretension effect of bolts can be studied; Both shear force and axial confining force can be recorded; Able to be tested in a general compression machine	Thick bolts cannot be loaded to failure due to the collapse of concrete.

Double shear (Aziz *et al.*, 2003; Aziz *et al.*, 2014)	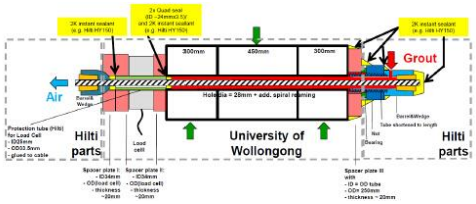	Pretension effect of bolts can be studied; Both shear force and axial confining force can be recorded; Steel frame avoids the collapse of the concrete; Able to be tested in general compression machines.	Simultaneous failure of bolt at both joints is not ensured.
Double shear (Li *et al.*, 2014)	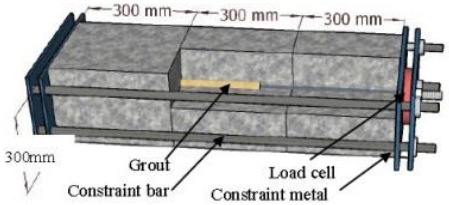	Pretension effect of bolts can be studied; Both shear force and axial confining force can be recorded; Able to be tested in a general compression machine;	Thick bolts cannot be loaded to failure due to the collapse of concrete.

3.3 Field observation of bolt shear failure

The stress state and deformation of rock mass in which bolts are installed determines the bolt performance exposed to rock loading. Figure 3.1 shows typical rock deformation and stress redistribution around an underground excavation reinforced by rock bolts and cable bolts.

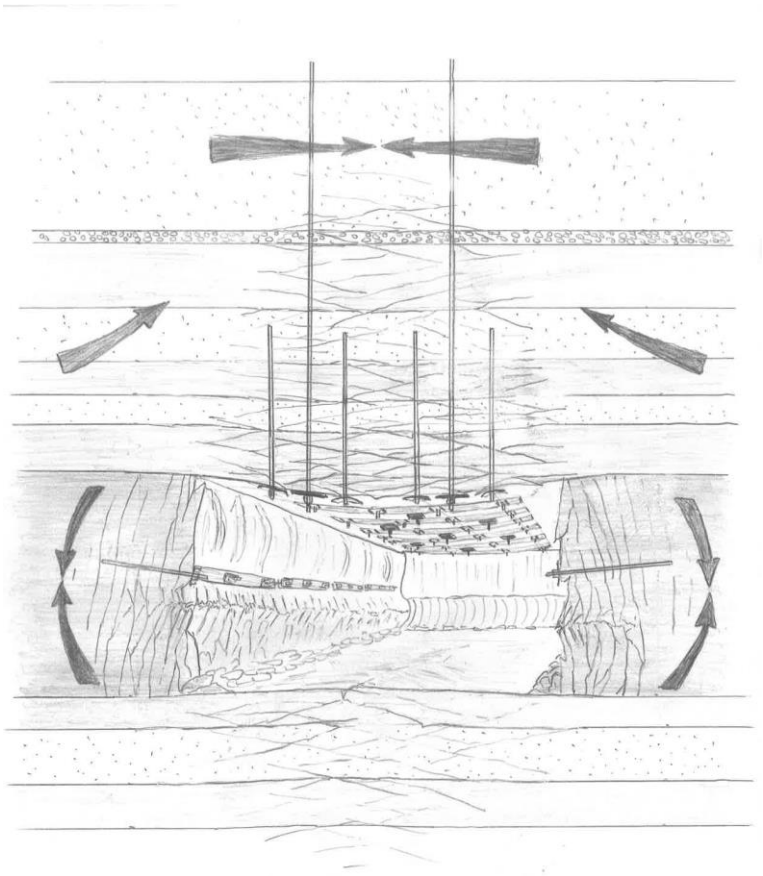

Figure 3.1 Sketch of deformation and stress redistribution in rock masses around an excavation reinforced by rock bolts and cable bolts (Nemcik *et al.*, 2009)

After excavation, rock layers bulk and fractures occur in rock masses when stresses in them exceed the rock strength. Fractures develop further away from the excavation with the stress redistribution around the excavation. In the roof, the rock stress state is mainly determined by the horizontal tectonic stress and the stiffness of rock layers. If the loading condition is identical, the higher the rock stiffness, the more stress is retained in the rock layer. In the surface roof rock mass of the excavation, the vertical stress is zero, which allows the stress in the rock mass to easily exceed its strength. The surface rock mass fails and stresses originally carried by the surface rock mass

are forced further away from the excavated opening. With the transfer of stresses deeper into the rock mass, the rock failure may also develop to deeper rock mass if the rock stress exceeds its strength. In general, the closer to the excavation the rock mass is, the severer the rock failure is. The bulking rock masses move towards the excavation and cause visible deformation around the excavation.

Both rock bolts and cable bolts are commonly used to control the excavation deformation. In shallow mining, bolting was initially used to secure surface loose rock blocks to deeper competent rock masses in underground openings. The requirement for bolts, in this case, is to provide enough tension force to hang the unstable loose rock blocks (Li, 2010). Therefore, the tensile strength of the bolt plays the most significant role in deciding the performance limit in shallow mining. In deep mining, bolts do not always function as hanging elements to secure surface loose rock blocks because high *in situ* stress may prevent rock blocks from loosening after excavation, while rock failure can still occur due to the high *in situ* stress (Li, 2010). In many cases, bolts do not provide enough reinforcement because of their premature failure in high stress conditions. Field observations showed that most bolts failed under the combined loading conditions of tensioning and shearing (Li, 2007, 2010). In deep rock mass where high stresses exist, the shear strength of bolts is equally important as the tensile strength.

In the field observations performed by Li (2010), it was observed that rock bolts were loaded in the portion close to the collar of the borehole in high stress rock masses, and usually at a distance of about 0.5 m from the face plate in a dilating rock mass as shown in Figure 3.2. In addition, since the deformation capacity of a fully bonded bolt was mobilized only in a small bolt segment near fractures, a small amount of fracture opening could result in premature bolt failure. Moreover, rock mass dilation is not preventable in high stress rock masses, thus rock bolts should be able to accommodate large rock deformations.

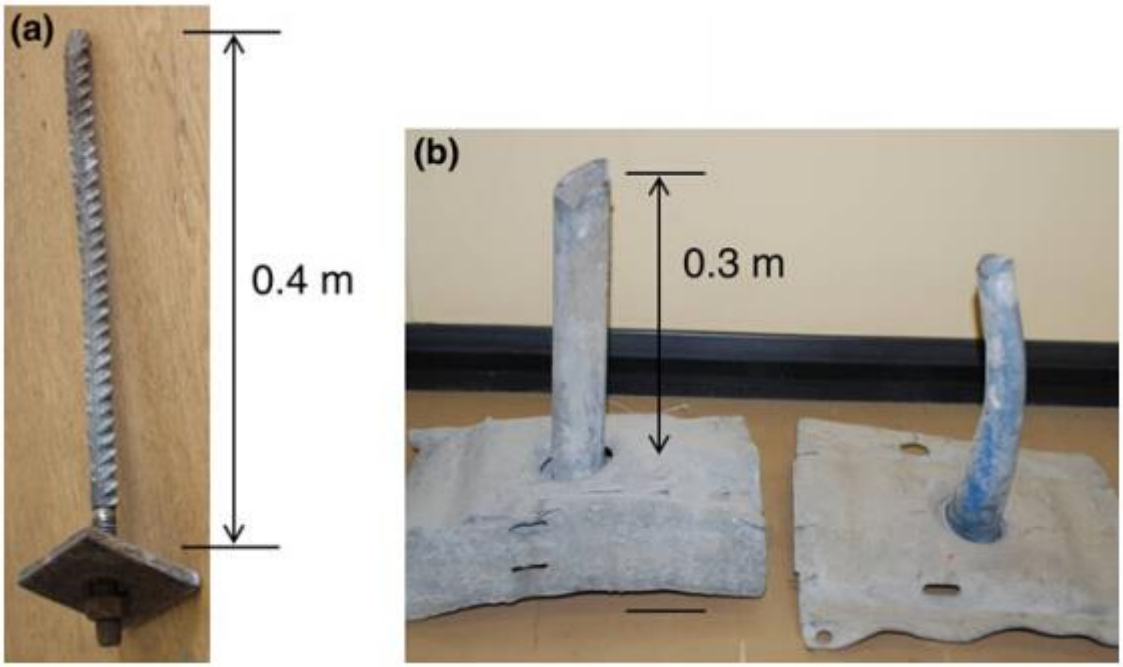

Figure 3.2 Failed rock bolts: (a) A failed rebar bolt in a creeping rock mass; (b) Failed split sets in a weak rock mass (Li, 2010)

3.4 Failure mechanism of bolts loaded in shear

As for the failure mechanism of rock bolts and cable bolts, researchers agree that the combination of tension and shear forces mobilised in bolts is the primary mechanism of bolt failure (Bjurstrom, 1974; Craig and Aziz, 2010; Ferrero, 1995; Grasselli, 2005). While some believe that tension in the vicinity of reinforced joints plays the critical role in some cases, others argue that the shear force is the decisive influencing factor of bolt failure. In addition, at various stages of laboratory or field tests, bolts may fail due to different mechanisms (tension failure, shear failure, or the combination of tension and shear failures) in different parts of their cross-section. Hence, what is required is to clarify why bolts fail in tension rather than shear in a certain case, and vice versa.

Bolt installation angle affects the generation and ratio of tensile and shear forces when subjected to shear loading. The larger the bolt installation angle to the joint, the larger the shear force will be at a particular shear displacement. In tests performed by Bjurstrom (1974), bolt failures which occurred for bolt installation angles of less than 35° appeared to be of tension type as shown in Figure 3.3. Bolts installed at an angle

of more than 40-45° tended to fail in a combination of shear and tension as shown in Figure 3.4.

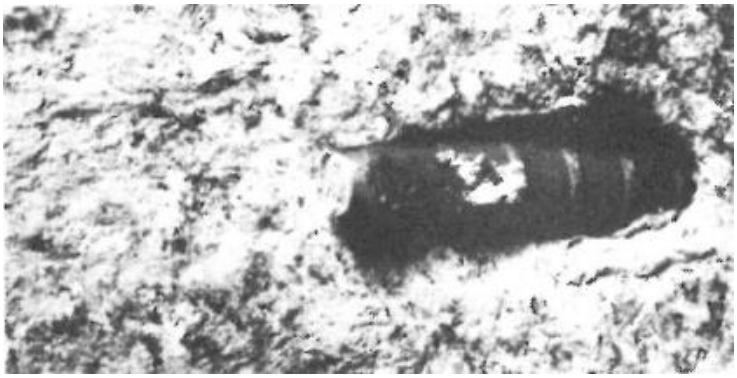

Figure 3.3 Bolt failure mainly in tension as a result of direct shear of a bolted granite joint at the installation angle of 28° (Bjurstrom, 1974)

Figure 3.4 Shear-tension failure as a result of direct shear of a bolted granite joint at the installation angle of 50° (Bjurstrom, 1974)

As expected, the rock strength could be a factor influencing the failure mode of bolts subjected to shear loading. This was confirmed by experimental studies conducted by Ferrero (1995). When strong rock was used in tests, bolts failed due to a combination of shear and tensile forces. Yet, when weak rock was used, bolts failed in tension due to either the tensile strength or the tensile strain limit being reached.

Grasselli (2005) carried out experimental and numerical studies on fully grouted steel bar and Swellex bolts used to reinforce rock joints to examine their mechanical behaviour. It was found that plastic hinges were mobilised on a fully grout-bonded bolt while Swellex stabiliser didn't experience plastic hinges during the shearing process. The failure of fully grouted bolt was principally due to the traction

concentrated between two plastic hinges mobilised in the vicinity of the joint plane, whereas the failure of Swellex was due to the shear stress developed on the shearing plane.

Craig and Aziz (2010) and Aziz *et al.* (2014) performed double shear tests on 28 mm hollow 'TG' cable bolts and solid Hilti superstrand cable bolts to investigate the failure pattern and mechanism. All steel wires of hollow TG cable bolts failed in tension with obvious necking phenomena in the vicinity of joints, whilst steel wires of the solid superstrand cable bolts failed in different manners. Steel wires of the outer layer were snapped in both tension and shear, whereas wires of the inner layer were broken in tension. The entire cable bolt did not break at the same time but in sequence which were proven by multiple load drops.

3.5 Influencing factors of bolt shear characteristics

The interaction of bolts and joints is heavily influenced by a great number of factors, such as strength of rock and grout, grout annulus thickness (Aziz *et al.*, 2015a), bolt pretension, grouted or un-grouted conditions, bolt installation angle, joint friction coefficient, loading rate, loading time (creep effect), bolt geometry, bolt strength and bolt de-bonding. Comparatively, influencing factors such as the strength of the rock and bolt pretension have been studied deeply, whereas others were rarely analysed.

The strength of rock or grout has a vital influence on the deformation and stress distribution of bolts placed across joints. The range of the plastic zone in the vicinity of bolt-rock intersection determined by rock strength influences the distribution and development of shear and tensile stresses along a bolt, which affects the eventual deformation and mode of failure. This was proved by the laboratory and numerical studies conducted by Jalalifar *et al.* (2006b). In addition, in tests on rock bolts conducted by Ferrero (1995), mechanisms of reinforcement failure were related to the characteristics of rock material. In the strong and stiff rock material, bolt failure was determined by shear and tensile stresses at the joint intersection; In the weak rock, bolt failure was due to either the tensile strength or the ultimate elongation of the reinforcing element being reached. Spang and Egger (1990) conducted tests on three different rocks, results of which demonstrated that, generally, the shear

capacity of a bolted joint was higher in soft rock than in hard rock. This feature could be observed in tests with a very low friction angle. The stress-strain relationship is stiffer in hard rock than in soft rock. Craig and Aziz (2010) carried out double shear tests on cable bolts to study the shearing characteristics and the failure mode. The test results showed that cable bolt failure occurred due to the tensile stress of cable bolts in the vicinity of a shearing plane reaching the tensile strength of the steel wires. Another sets of double shear test on rock bolts carried out by Aziz *et al.* (2003) indicated that the shear strength and shear load at the turning point of the load-displacement curve are higher in 40 MPa concrete than in 20 MPa concrete.

Spang and Egger (1990) indicated in their tests that the shear strength of bolted rough joints is 50% more than that of very smooth joint surfaces, and the larger friction angle of bolted joints increases the joint shear stiffness. Goris *et al.* (1996) conducted a series of tests to assess the resistance capability of cable bolts placed across concrete blocks joints ranging from rough to smooth. The test results indicated that the shear resistance more than doubled for reinforced concrete blocks with both rough and smooth joints as opposed to non-reinforced concrete blocks. In addition, all tested cable bolts did not fail at the maximum displacement of 38 mm which was the allowable shear displacement of the testing machine. For shear displacement at failure, tests carried out by both Stillborg (1984) and Craig and Aziz (2010) indicated that the cable bolt failure occurred when the joint shear displacement reached about 50 mm and 59 mm, respectively. In field tests and subsequent observations, it was estimated that cable bolts failed at between 50 -100 mm of lateral movement (Dolinar *et al.*, 1996). Tests conducted by Grasselli (2005) on fully bonded bolts demonstrated that the shear displacement at failure of concrete blocks reinforced by two bolts was slightly larger than by one bolt, whereas the shear displacement at failure was larger for bolts with large diameter than that with small diameter.

Shear tests conducted by Bjurstrom (1974) on fully grouted rock bolts demonstrated that the installation angle of bolt across the joint influenced the mode of bolt failure as well as the joint shear strength and stiffness. In addition, Haas (1981) reported that inclined bolts in bolted blocks were stiffer in terms of the shear resistance than the perpendicular bolts. Also, Azuar (1977) reported that the maximum bolt contribution

to the joint shear resistance was controlled by the installation angle of bolt. When installed perpendicular to the joint surface, the maximum bolt contribution was 60% of the bolt tensile strength and it increased up to 90% at the inclined angle of installation. Egger and Fernandes's (1983) shear tests showed that the joint shear displacement at failure was minimum for bolt installation angle between 40° and 50°, whereas the joint shear displacement indicated a minimum for bolt installation angle between 30° and 45° in Spang and Egger's (1990) tests. In addition, Spang and Egger (1990) found that, for joints of a high friction angle the shear resistance capacity of bolted joints increased with the increase of bolt installation angle. However for joints of a very low friction angle there was no relationship between bolt installation angle and the shear capacity of bolted joints. Also, inclined bolts reacted in a stiffer way than the bolts installed in a perpendicular direction. In Ge and Liu's (1988) direct shear tests on thin steel rebar bolts with the joint friction coefficient of 0.77, the maximum joint shear strength was achieved at the bolt installation angle of 60°, and a similar result was obtained in their analytical analysis. Moreover, in their analysis with the increase of joint friction angle, the maximum joint shear strength was achieved at an increased bolt installation angle. The optimum joint strength was achieved at an angle of 30° for joint friction angle of 0° while the optimum strength was achieved at an installation angle of 90° for the joint friction angle of 60°. Grasselli's (2005) tests on comparison between the full steel bar and Swellex bolts indicated that the variation of bolt installation angle influenced both the maximum shear strength developed by the reinforcement and the stiffness of the bolted joint. Also, the post-failure deformation angle between plastic hinges showed a linearly decreasing trend with the increase of initial bolt installation angle. However, Hibino and Motojima (1981) argued that the initial inclination of the bolt did not increase the joint shear resistance, which is in contradiction to other research findings.

Haas (1981) conducted shear tests on blocks of limestone reinforced with resin-grouted rock bolts and found that no positive effect of bolt pretension could be observed. Similarly, Hibino and Motojima (1981) reported that bolt pretension did not influence the joint shear resistance strength, but only contributed to reduced shear displacement. In contrast, tests by Ferrero (1995) showed bolt pretension influenced

the stress-strain behaviour of the bolt-reinforced joint. Tests on rock bolts carried out by (Aziz *et al.*, 2003) and Jalalifar *et al.* (2006b) showed that the higher the initial bolt pretension load, the greater the shear load at the turning point of the load-displacement curve. In addition, the higher the bolt pretension, the larger the joint shear strength.

For the differences of the rock joint reinforced with grouted or un-grouted cables, Goris *et al.* (1996) carried out laboratory tests and found that the shear resistance of blocks reinforced with grouted cables increased much more rapidly at smaller joint shear displacement than that of rock blocks in which cables were not grouted.

In shear tests performed by Spang and Egger (1990) on fully-bonded bolts, the peak joint shear resistance increased linearly with the bolt cross section while the corresponding displacement was proportional to the bolt diameter.

3.6 Analytical investigation of the shear behaviour of bolted joints

Regarding the shear behaviour of bolted rock joints, there are two load transfer mechanisms involved in the shearing process as shown in Figure 3.5. One refers to the bending section in the close vicinity of the shearing joint plane in which a bolt deforms due to relative slip between joint planes, whilst the other is related to the tensioning section beyond the ‘bending section’ where a bolt is mainly loaded in tension, which is similar to a pull out test. These two load transfer mechanisms jointly determine the ultimate shear resistance and shear displacement of a bolted joint. Both two loading sections and the corresponding load transfer mechanisms need to be studied to understand the shear behaviour of bolted joints.

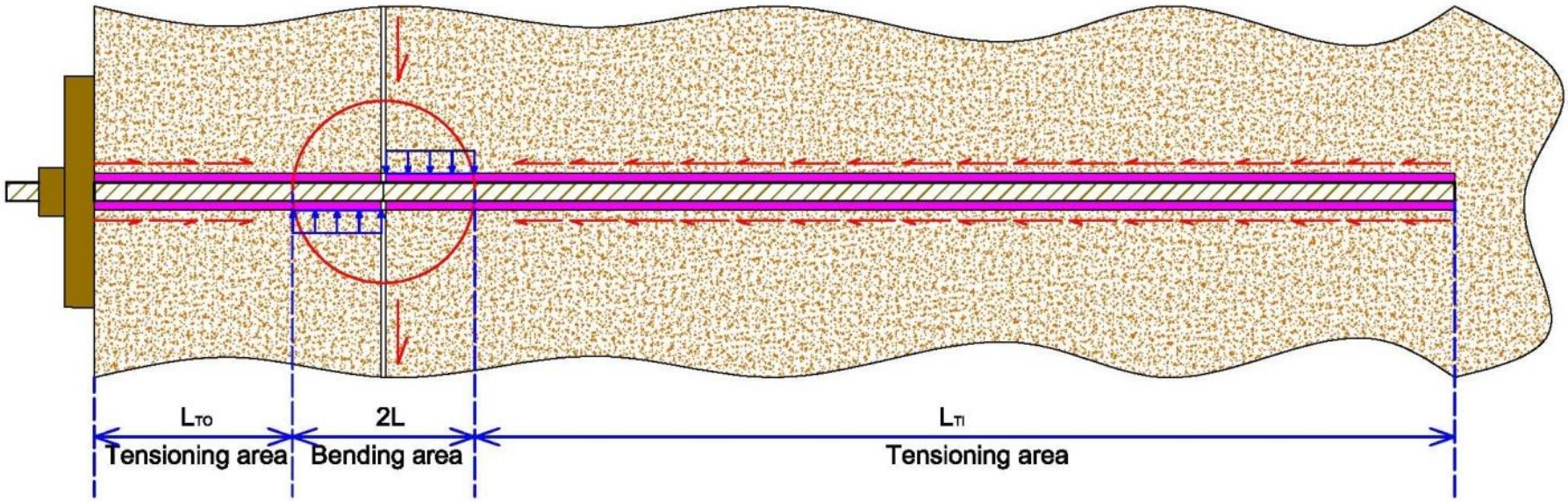

Figure 3.5 Loading state of bolt subjected to lateral shear displacement

In laboratory studies of the bolted rock joint shear behaviour, the *in situ* condition cannot be fully replicated in practice mainly due to the sample dimension. In the laboratory, concrete blocks are normally used to partly simulate the *in situ* condition with suitable boundary conditions. According to the cable strand length and the location of the shearing plane, the shear condition of a bolted joint can be divided into three types. These three shear conditions can be defined by the tensioning length L_{ti} with consideration of the occurrence of bolt de-bonding as shown in Figure 3.5.

When L_{ti} is sufficiently long to provide enough axial friction and interlocking at the cable-grout interface, no obvious axial displacement at the cable inner end can occur. In this case, the shear behaviour of a bolted joint is mainly controlled by the bending section with minimum influence by the tensioning section. This was the widely studied condition in previous investigations. Two methods were used to provide axial resistance of cable strand as shown in Figure 3.6 and Figure 3.7. One is to use a cable strand end restraint assembly, normally the barrel and wedge assembly, to provide sufficient axial resistance. The other is to use long concrete blocks to offer enough axial resistance. Since the shear behaviour is mainly controlled by the bending section, it can be expected that these two methods yield similar results. In practice, since the first method uses small and light concrete blocks, the first method is much easier to work with compared with the second method. Thus the first method is the preferred choice of study by investigators.

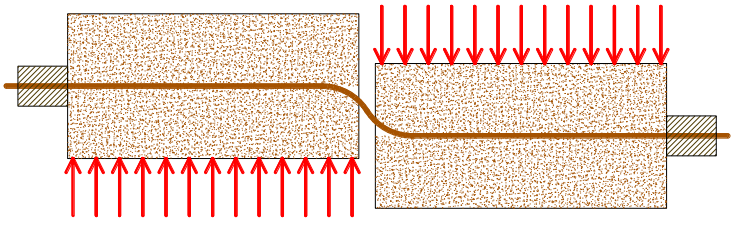

Figure 3.6 Laboratory shear test sample with barrel & wedge assembly to avoid full bolt de-bonding

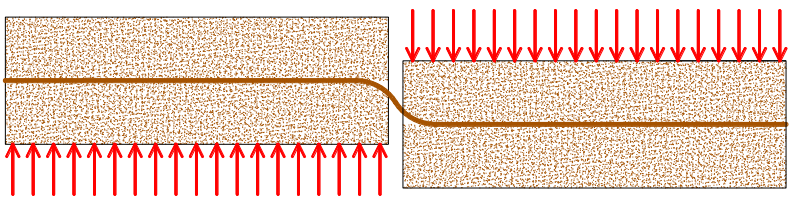

Figure 3.7 Laboratory shear test sample with long anchorage to avoid full bolt de-bonding

The second type as presented in Figure 3.8, shows that L_{ti} is not long enough to prevent cable strand end from slipping along the bolt borehole but long enough to provide axial resistance to allow the occurrence of cable strand failure during the shearing process. In this case, the bending section and the tensioning section equally control the shear behaviour of a bolted joint. The shear system shows the shear behaviour of smaller shear stiffness in this case.

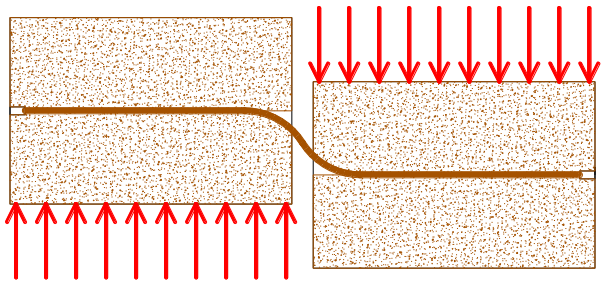

Figure 3.8 Laboratory shear test sample with a suitable anchorage length to allow the occurrence of bolt de-bonding and bolt failure

The third type as presented in Figure 3.9, shows that L_{ti} is too short to offer required axial resistance to avoid the occurrence of full bolt de-bonding and to allow the occurrence of cable strand failure. In this case, the shear behaviour of a bolted joint is controlled by the bending section and the tensioning section. Yet, the shear strength cannot be obtained in this condition.

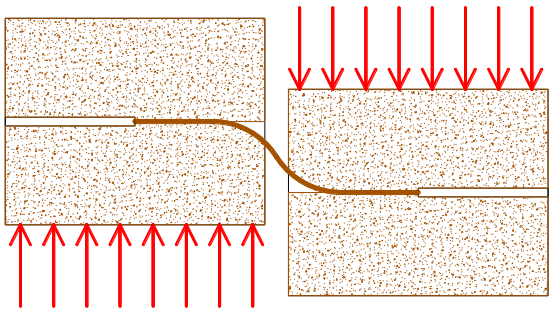

Figure 3.9 Laboratory shear test sample without bolt failure due to full bolt de-bonding

As the relative displacement between the bolt and rock mass is larger in the rock mass close to the excavation than in the rock mass farther from the excavation, the bolt-rock interaction is severer in the bolt section close to the excavation. In addition, field observations by Li (2007, 2010) indicated that bolt failure due to the combined shearing and tensioning loads happened in the bolt section close to the bolt collar.

Thus among these three conditions discussed, the first one was most popular in past studies. In this case, the axial tensile behaviour of the cable strand tensioning section can be ignored in the analysis.

3.6.1 Shear strength of joints

The shear performance of a cable bolt anchored across rock joints is influenced by both the rock mass (concrete) and the cable bolt itself. The friction characteristic of rock joints contributes to the shear strength of a reinforced joint in the shearing process, which needs to be investigated in detail.

The shear strength of planar surfaces and rough surfaces is different. The planar surface is simpler than the latter. Equations used to depict the shear behaviour of planar and rough surfaces are explained in the following section:

Regarding cement-bound planar surfaces, Figure 3.10 shows the loading state of a tested sample, the typical test results and the strength envelope. Based on the Mohr-Coulomb equation, two strength lines are obtained for the peak and residual shear strengths. The peak shear strength envelope is based on the peak shear strength τ_P and the normal stress σ_n, and residual shear strength envelope is based on the residual shear strength τ_r and the normal stress (σ_n). The peak strength line has a slope of the angle of the joint friction (φ) and an intercept of cohesion (c). The residual strength line has a slope of φ. These two strength lines can be represented by the Mohr-Coulomb equations as follows:

$$\tau_P = c + \sigma_n tan\varphi \tag{3.1}$$

$$\tau_r = \sigma_n tan\varphi_r \tag{3.2}$$

Where：

c, is the cohesive strength of the cemented surface;

φ, is the angle of friction;

φ_r, is the residual angle of friction.

Additionally, the residual angle of friction φ_r can be replaced by the basic friction angle φ_b which is generally measured by testing sawn or ground rock surfaces (Hoek, 2007).

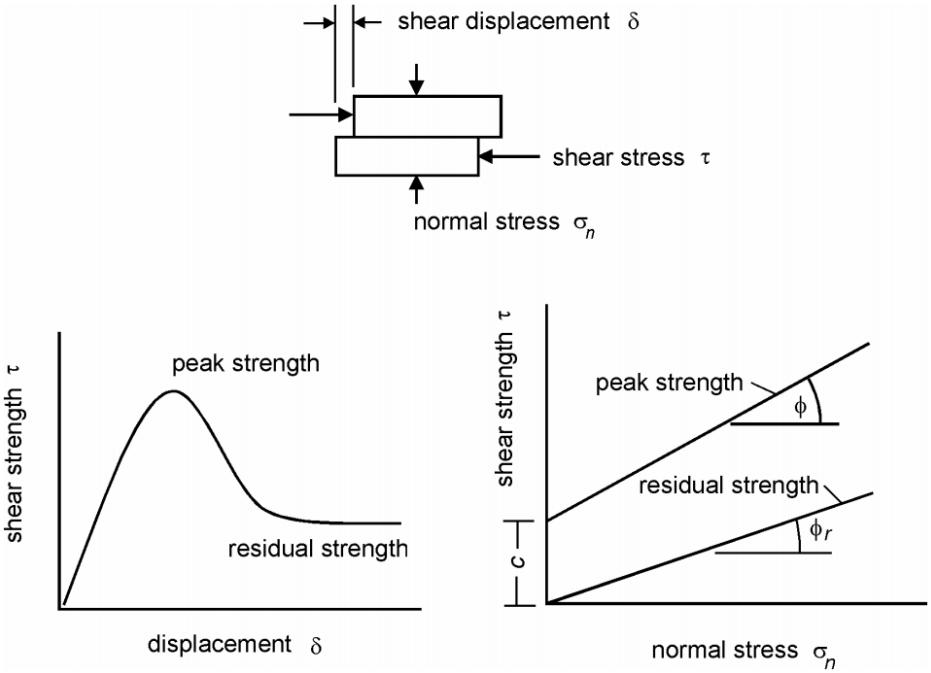

Figure 3.10 Shear testing of discontinuities (Hoek, 2007)

Planes with obvious asperities and undulations behave differently compared with planar planes. Generally, the surface roughness increases the shear strength of a joint surface.

Patton (1966) carried out shear tests on 'saw-tooth' specimens as shown in Figure 3.11, and proposed an equation representing the shear strength and the normal stress relationship as follows:

$$\tau = \sigma_n \tan(\varphi_b + i) \qquad (3.3)$$

Where: i is the angle of the saw-tooth face.

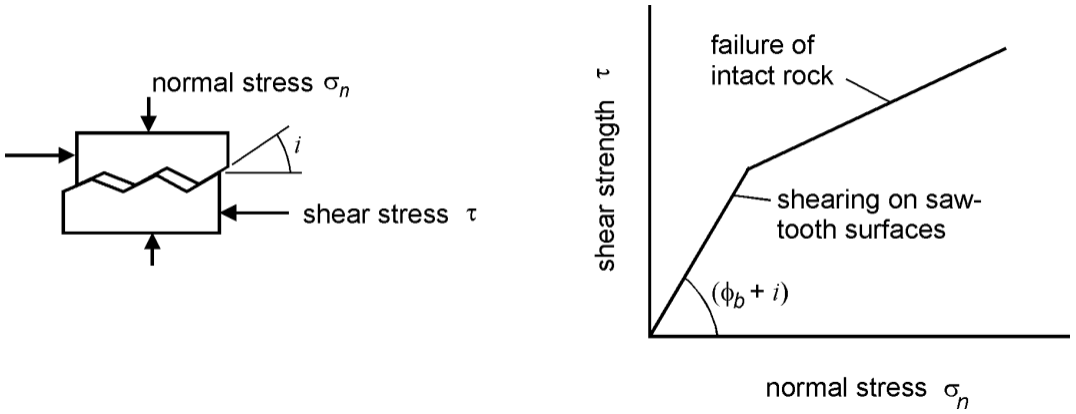

Figure 3.11 Patton's test on the shear strength of saw-tooth specimens (Hoek, 2007)

Patton's equation is invalid at higher normal stresses because the teeth will be damaged since the strength of the intact material is exceeded.

Barton (1976) analysed the behaviour of natural rock surfaces and changed Patton's expression to be:

$$\tau = \sigma_n \tan(\varphi_b + JRC \log_{10}(\frac{JCS}{\sigma_n})) \quad (3.4)$$

Where:

JRC, is the joint roughness coefficient;

JCS, is the joint wall compressive strength.

Additionally, φ_b can also be replaced by φ_r in computational analysis (Barton and Choubey, 1977).

3.6.2 Calculation and prediction of the shear resistance capacity of a bolted joint

Figure 3.12 shows the typical loading state of a bolted concrete joint subject to shearing. Clearly, the contribution of the bolt to the joint shear resistance is attributed to the induced forces in the bolt and on the joint plane. Yet, based on the equilibrium of induced forces on the joint plane, the induced forces on the plane can be derived from the induced forces in the bolt. Thus, the global induced forces at the joint could be determined by the induced forces in the bolt.

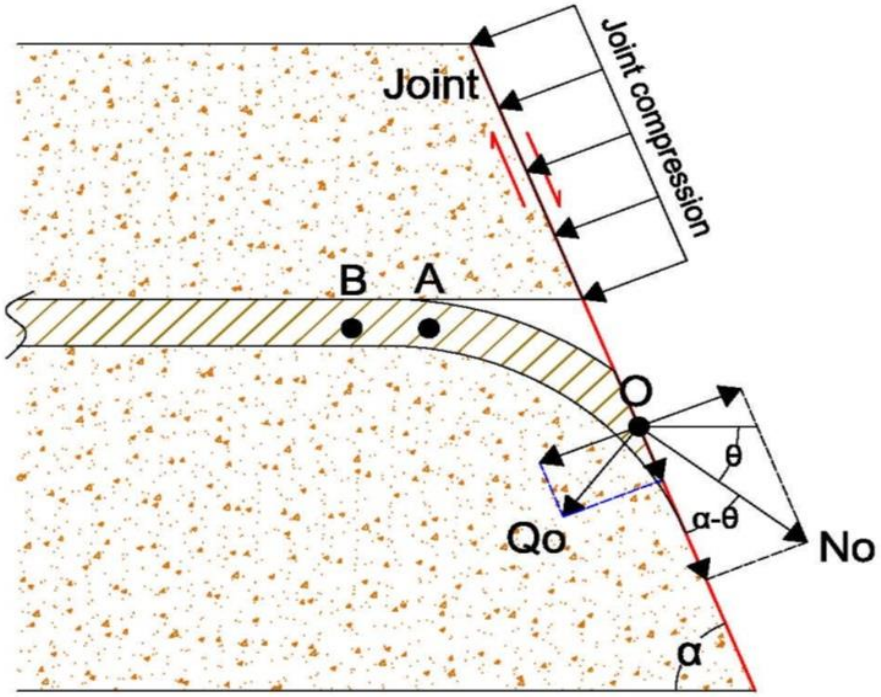

Figure 3.12 Forces induced in a bolt and on the bolted joint plane

The global contribution of a bolt to joint shear strength is calculated in accordance with the following equation:

$$R_b = N_o \cos(\alpha - \theta) + Q_o \sin(\alpha - \theta) + [N_o \sin(\alpha - \theta) - Q_o \cos(\alpha - \theta)]tan\varphi \quad (3.5)$$

Where:

R_b, is the bolt contribution to joint shear strength;

N_o, is the tensile force at the failure location of a bolt;

Q_o, is the shear force at the failure location of a bolt;

α, is the bolt installation angle to joint;

θ, is the bolt deflection angle;

φ, is the joint friction angle.

There are several terms involving the contribution of a bolt to joint shear strength. Different interpretations are given, and some are probably incorrect. Overall, the contribution of a bolt to joint shear resistance related to the above method is calculated based on the following categorised theories (Ferrero, 1995):

- Empirical methods, based on statistical treatment of experimental data (Spang and Egger, 1990);
- Analytical methods based on the equilibrium of the forces acting on the un-deformed reinforcement system (Bjurstrom, 1974);
- Analytical models based on elastic beam theory (Azuar, 1977; El-Ariss, 2007);
- Analytical models based on the formation of two plastic hinges (Dight, 1983; Dulacka, 1972);
- Analytical models based on the equilibrium of the forces acting on the deformed reinforcement system (Ferrero, 1995; Fuller and Cox, 1978; Holmberg and Stille, 1992);

(1) Empirical methods

Spang and Egger (1990) performed laboratory and field tests on joints reinforced by fully cement-encapsulated bolts to study the principal parameters influencing the joint shear resistance capacity and proposed empirical expressions to predict the maximum shear load and the corresponding joint shear displacement, which took into account the most significant parameters including rock deformability, friction angle of joint, bolt inclination angle and joint dilatancy. The contribution of a bolt to the joint shear resistance was expressed as follow:

$$\mathrm{R}_b = P_t \cdot (1 + \Delta T_{A+G}) \cdot m_F \cdot m_R \qquad (3.6)$$

Or

$$\mathrm{R}_b = P_t \cdot [1.55 + 0.011 \cdot EM^{1.5} \cdot sin^2(\alpha + i_d)] \cdot EM^{-0.2}(0.85 + 0.45 \cdot tan\varphi) \qquad (3.7)$$

Or

$$R_b = P_t \cdot [1.55 + 0.011 \cdot {\sigma_c}^{1.07} \cdot sin^2(\alpha + i_d)] \cdot {\sigma_c}^{-0.14}(0.85 + 0.45 \cdot tan\varphi) \quad (3.8)$$

Where:

R_b, is the bolt contribution to the shear resistance of a bolted joint;

P_t, is the maximum tension load of the bolt;

ΔT_{A+G}, is the influence of bolt inclination (installation) angle and joint dilatancy;

m_F, is the influence of rock strength;

m_R, is the influence of joint friction angle;

EM, is the stiffness of mortar and rock;

α, is the bolt inclination angle (installation);

i_d, is the angle of joint dilatancy;

σ_c , is the ultimate compressive strength of rock materials.

In addition, the corresponding joint shear displacement is represented as follow:

$$f(s) = (15.2 - 55.2 \cdot EM^{-0.2} + 56.2 \cdot EM^{-0.4}) \cdot (1 - tan\alpha \cdot (20/EM)^{0.25} \cdot (cos\alpha)^{-0.5}) \quad (3.9)$$

Or

$$f(s) = (15.2 - 55.2 \cdot {\sigma_c}^{-0.14} + 56.2 \cdot {\sigma_c}^{-0.28}) \cdot (1 - tan\alpha \cdot (70/\sigma_c)^{0.125} \cdot (cos\alpha)^{-0.5}) \quad (3.10)$$

Hence, from expressions by Spang and Egger (1990), one can predict the maximum shear load of a bolted joint and the corresponding joint shear displacement provided parameters including joint friction angle, joint dilatancy angle, bolt inclination angle and strength of surrounding rock were known.

Because of the empirical nature of the proposed expressions, their validity is subjected to some conditions as indicated in Spang and Egger's analysis (1990).

(2) The equilibrium of the forces acting on the un-deformed reinforcement system

In the analysis by Bjurstrom (1974), the contribution of a bolt to the shear resistance of reinforced jointed rock mass was dependent on three different effects: a) the friction effect of an initial normal stress and a 'shear-displacement-induced' normal stress, b) a force component of the induced tensile force of the bolt, and c) the dowel effect of the bolt. Actually, the component of the induced tensile force of the bolt was identical to the dowel effect. That is to say, only two effects existed in the shearing process, and Bjurstrom's analysis was probably not correct. Bjurstrom primarily investigated the shear characteristics of rock joints reinforced by grouted un-tensioned bolts. Thus in the calculation of shear resistance the initial cohesion was assumed zero. Additionally, the bolt tension at the peak joint shear resistance was assumed to be equal to the yield limit of the bolt as indicated from the measurement of strain gauges cemented on the bolt. Therefore, only bolt tension was considered in the analytical prediction of joint shear resistance as follows:

$$R_b = N_b(\cos\alpha + \sin\alpha \cdot \mu) \tag{3.11}$$

Where:

R_b, is the reinforcement effect on joint shear resistance due to bolting;

N_b, is the tensile force in the bolt due to shear displacement;

α, is the bolt angle;

μ, is friction coefficient of joint.

Bjurstrom's study was based on testing granite specimens with and without bolt reinforcement. Tests without bolt reinforcement were aimed to investigate the friction properties of shear planes, primarily the friction angle. Based on this equation, the maximum joint shear resistance could be predicted prior to testing, which was conservative compared with the test results. This was due to no consideration of strain-hardening of the bolt or dowel effects, according to Bjurstrom.

Bjurstrom pointed out that aside from the force component of bolt tension force parallel to the joint plane, an additional dowel effect was still in existence. He outlined the expression of this additional dowel effect for both grouted and un-grouted bolts:

The dowel effect of a grouted bolt was,

$$T_{dowel} = d_b^2\sqrt{\frac{\sigma_y\sigma_h}{6\epsilon}} \tag{3.12}$$

The dowel effect of an un-grouted bolt was,

$$T_{dowel} = d_b^2 \cdot 0.67\sqrt{\sigma_y\sigma_c} \tag{3.13}$$

Thus according to Bjurstrom's analysis, the global shear resistance of a grouted bolted concrete joint was:

$$T_f = \mathrm{R}_b + T_{dowel} = N(\cos\alpha + \sin\alpha \cdot \mu) + d_b^2\sqrt{\frac{\sigma_{by}\sigma_h}{6\epsilon}} \tag{3.14}$$

Where:

T_f, is the global shear resistance of a grouted bolted concrete joint;

T_{dowel}, is the joint shear resistance due to dowel effect;

d_b, is the diameter of bolt;

σ_{by}, is the yield stress of bolt;

σ_h, is the average rock strength under bolt compression;

ϵ, constant.

(3) Analytical models based on elastic beam theory

El-Ariss (2007) proposed a new theoretical model to compute the dowel action in reinforced jointed concrete based on the combination of several existing studies. In his study, a comparison was made between experimental results and analytical

results with dowel effect being both considered and neglected. It was revealed that the analytical results with consideration of dowel effect were in agreement with experimental results.

Millard and Johnson (1984) proposed a load-deflection response for dowel bars embedded in concrete as follows:

$$V_d = V_u[1 - \exp(\frac{-k\Delta}{V_u})] \quad (3.15)$$

Where:

V_d, is the dowel force at the shear displacement of Δ at a crack;

V_u, is the ultimate dowel force.

In order to obtain the function of dowel force, parameters including k, Δ, V_u need to be solved.

According to Timoshenko and Lessels (1925), the differential equation for the deflection of a beam on elastic foundation is written as follows:

$$EI\frac{d^4y_b}{dx^4} = -Ky_b \quad (3.16)$$

Where:

K, is the stiffness of the elastic foundation;

y_b, is bolt deflection.

Cut at the crack face, the bar may be treated as a semi-infinite beam as shown in Figure 3.13. The deflection and slope of the dowel at the face of a crack (z in width) can be derived according to the boundary condition as shown in Figure 3.14:

$$y_0 = \frac{V_d}{4\lambda^3 E_s I_s}(2 + \lambda z) \quad (3.17)$$

$$\frac{dy_0}{dx} = \frac{-V_d}{2\lambda^2 E_s I_s}(1 + \lambda z) \quad (3.18)$$

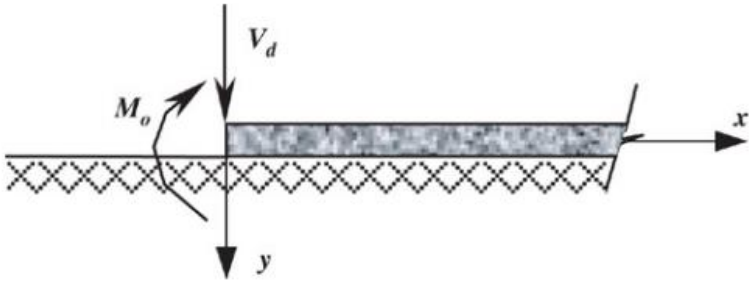

Figure 3.13 Semi-infinite beam on an elastic foundation (El-Ariss, 2007)

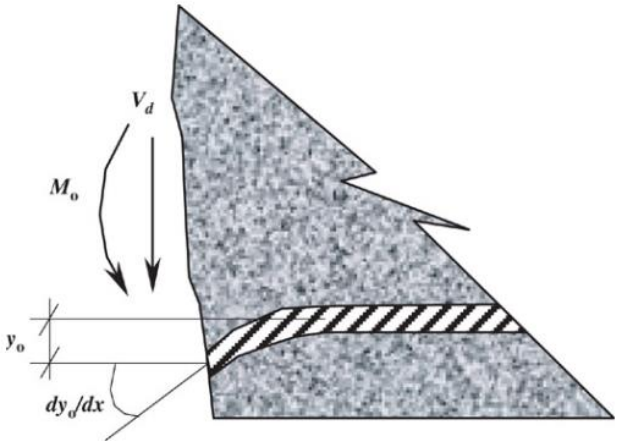

Figure 3.14 Slope and deflection of dowel at the face of the crack (El-Ariss, 2007)

Thus, the dowel displacement Δ is:

$$\Delta = 2\left[y_0 + \left(\frac{dy_0}{dx}\right)\left(\frac{z}{2}\right)\right] \tag{3.19}$$

$$= \frac{V_d}{2\lambda^2 E_s I_s}\left[\frac{(2+\lambda z)}{\lambda} + (1+\lambda z)(z)\right] \tag{3.20}$$

Additionally, Soroushian and Dulacska (1972) have given the estimation of the stiffness of the elastic foundation k and the ultimate dowel force V_u. They are:

$$k = \frac{127 c_1 \sqrt{\sigma_c}}{d_b^{2/3}} \tag{3.21}$$

$$V_u = 1.27 d_b^2 \sqrt{(\sigma_c)(\sigma_y)} \tag{3.22}$$

Where: c_1, is a coefficient ranging from 0.6 for a clear bar spacing of 25 mm to 1.0 for larger bar spacing.

Substituting equations of k, Δ, V_u, in the equation of V_d produces the dowel force of the reinforcing bar:

$$V_d = 1.27 d_b^2 \sqrt{(f_c')(f_y)} \times \left\{ 1 - \exp\left[\frac{-kV_d\left(\frac{2+\lambda z}{\lambda}\right)+(1+\lambda z)(z)}{2.54\lambda^2 E_s I_s d_b^2 \sqrt{(f_c')(f_y)}} \right] \right\} \quad (3.23)$$

(4) Analytical models based on the formation of two plastic hinges

Dulacka (1972) investigated the dowel action of reinforcing element crossing cracks in concrete with two specimen halves being assembled with a gap to eliminate the friction effect. The assembly and its loading state are shown in Figure 3.15. Taking into account the test results, the shear strength of the reinforcement system and the shear displacement were proposed and expressed as:

$$T_f = \rho \mathrm{d}_b^2 \gamma \sigma_y n sin\delta \left[\sqrt{1 + \frac{\sigma_c}{3\rho\gamma^2\sigma_y n sin^2\delta}} - 1 \right] \quad (3.24)$$

$$\Delta_s = \frac{3T}{d_b 10^6} \sqrt{\frac{1}{\sigma_c} tan\left(\frac{T}{T_f}\frac{\pi}{2}\right)} \quad (3.25)$$

Where:

T_f, is the shear force of the shear system at bar failure;

δ, is the bar installation angle;

n, is a coefficient of local compression of concrete;

γ, constant;

$\rho = 1 - N^2/N_y^2$;

N, is the tensile force of bar at bar failure;

N_y, is the tensile force inducing yield in pure tension;

Δ_s, is the slip along the loading direction;

T, is the shear force applied on the shear system.

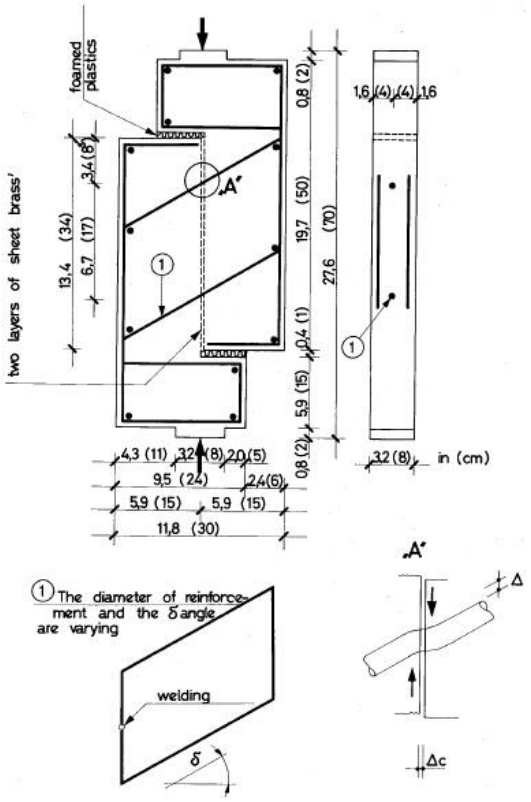

(a)

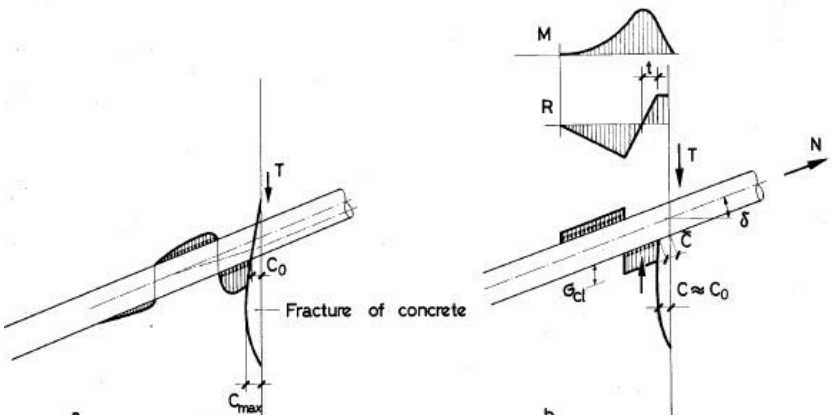

(b) (c)

Figure 3.15 (a) Details of test specimen construction; (b) Probable force distribution; (c) Assumed force distribution along the bar (Dulacka, 1972)

Dight (1983) considered the deformed section of a bar crossing a rock joint between plastic hinges as a rigid body in his analysis based on the load distribution as shown

in Figure 3.16. Two effects of a bar were considered, the dowel effect and the tensile effect as shown in Figure 3.17. The dowel effect referred to the shear force acting in the bar at the joint, while the tensile effect was related to the tensile force induced in the bar.

The derived dowel force related to the direction of shearing was

$$F_{bs} = \frac{F}{cos\theta_\delta} = \frac{d_b^2}{4cos\theta_\delta}\sqrt{1.7\sigma_y p_u \pi(1-(T_{bp}/T_y)^2)} \quad (3.26)$$

Where:

F_{bs}, is the shear force acting in the bar at joint;

p_u, is the bearing capacity of the rock or grout;

T_{bp}, is tension in the bar at plastic moment;

T_y, is yield strength of bar;

θ_δ, is angle between the bar and the normal direction of the joint.

The tensile effect of the bar was

$$T_b = T_y(sin\theta_\delta + cos\theta_\delta \tan(\varphi + i)) \quad (3.27)$$

Where:

φ, is the friction angle of unbolted joint;

i_d, is the dilation angle of joint.

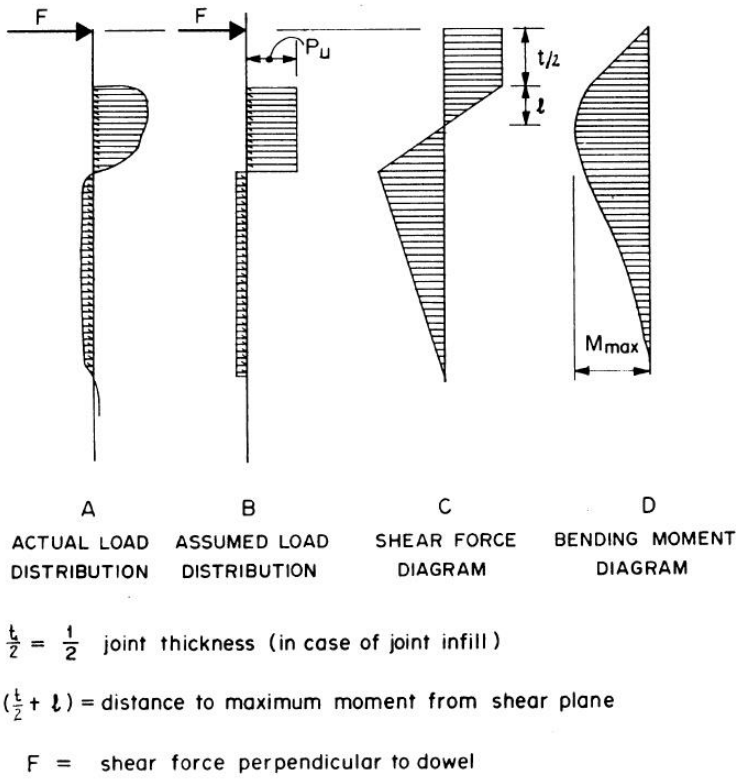

Figure 3.16 Free body diagram for a dowel in shear (Dight, 1983)

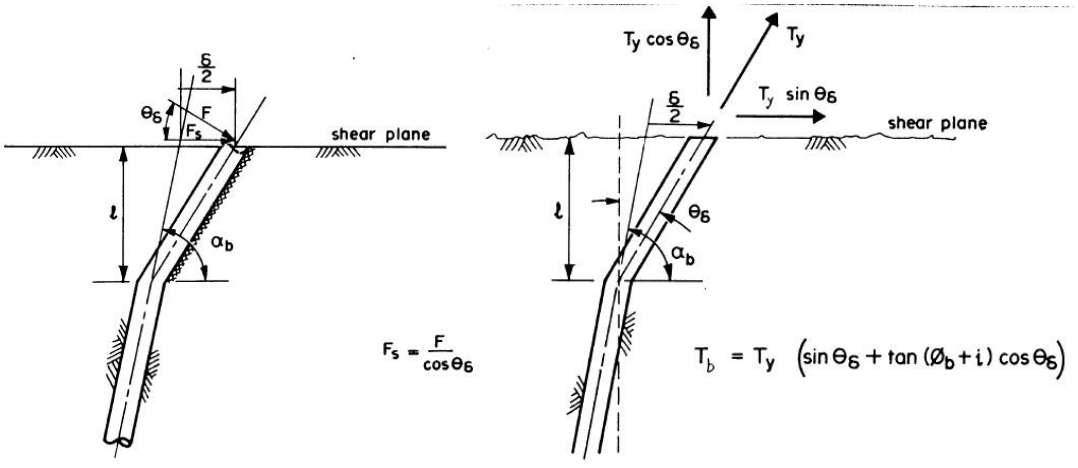

(a) (b)

Figure 3.17 (a) Force distribution for dowel behaviour following displacement δ; (b) Force distribution for tensile behaviour following displacement δ. (Dight, 1983)

(5) Analytical models based on the equilibrium of the forces acting on the deformed reinforcement system

Holmberg and Stille (1992) proposed an analytical mechanical model for predicting the maximum shear resistance and maximum deformation of a bolted joint. Two types of bolt behaviour were described according to rock conditions as shown in Figure 3.18. The first one, mostly observed in hard rocks, was closely related to a shear failure at the bolt-joint intersection. The second, normally observed in weak rocks, was closely related to a failure due to extension strain.

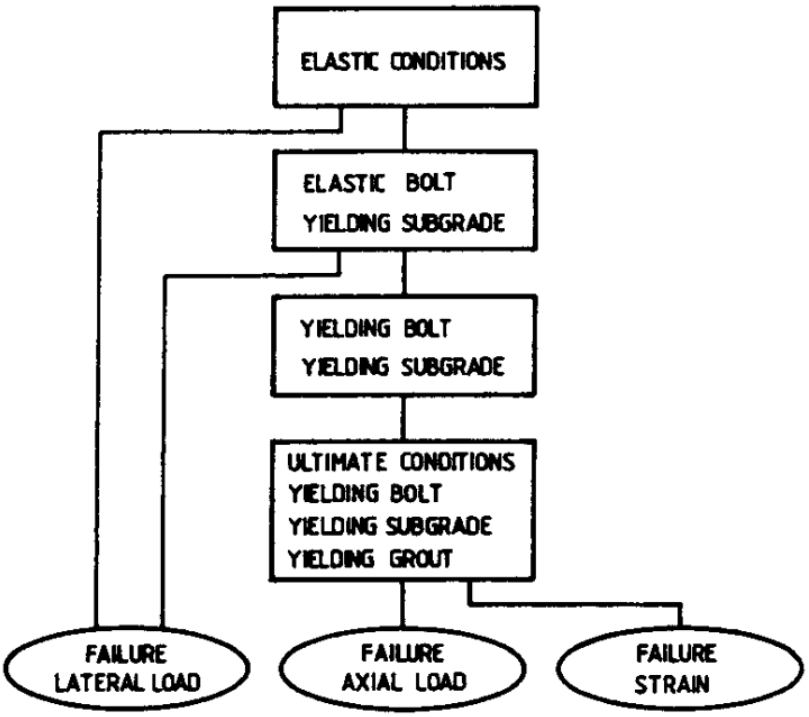

Figure 3.18 Summary of grouted rock bolt performance (Holmberg and Stille, 1992)

(1) Elastic bolt and elastic subgrade

The load condition of the deformed grouted rock bolt is assumed to be according to Figure 3.19.

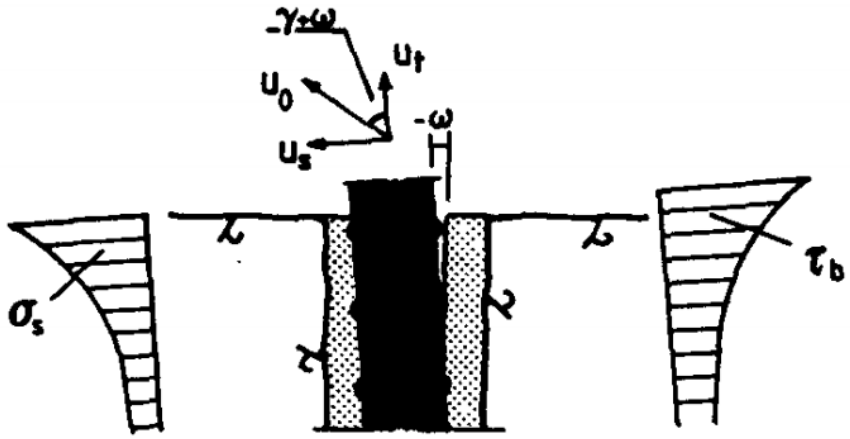

Figure 3.19 Stress state of elastic bolt and subgrade (Holmberg and Stille, 1992)

According to the analyses of Farmer (1975) and Aydan *et al.* (1985), relationships between the axial bolt load, the lateral bolt load and the axial deformation, the lateral deformation of a bolt are as follows:

$$T_t = E\pi r_b^2 \alpha u_t \tag{3.28}$$

$$T_s = \frac{2EI}{l_0^3} u_s \tag{3.29}$$

Where:

$$\alpha = \sqrt{\frac{2k_g}{Er_b}}$$

$$l_0 = \sqrt[4]{\frac{4EI}{k_s d_b}}$$

T_t, is the axial bolt load at the joint intersection;

T_s, is the bolt shear load at the joint intersection;

u_t, is the axial bolt deformation at the joint intersection;

u_s, is the lateral bolt deformation at the joint intersection.

The subgrade (grout and rock compressed by the bolt due to the bolt bending) will be in an elastic condition as long as the subgrade support reaction is less than its yield strength, giving

$$u_s < \frac{nd_b}{300} \tag{3.30}$$

Under elastic state, bolt failure may occur at the bolt-joint intersection due to a combination of the axial force and the shear force in the bolt. Thus substituting T_t, T_s, and the axial load corresponding to the yield strength ,T_{ty}, into the following failure criterion below:

$$\left[\frac{T_t}{T_{ty}}\right]^2 + \left[\frac{2T_s}{T_{ty}}\right]^2 = 1 \tag{3.31}$$

yields a detailed failure criterion as follow.

$$\left[\frac{E\alpha}{\sigma_y}u_t\right]^2 + \left[\frac{Ed_b^2}{4l_0^3\sigma_y}u_s\right]^2 = 1 \tag{3.32}$$

(2) Elastic bolt and yielding subgrade

The load condition of the deformed grouted rock bolt is assumed to be according to Figure 3.20.

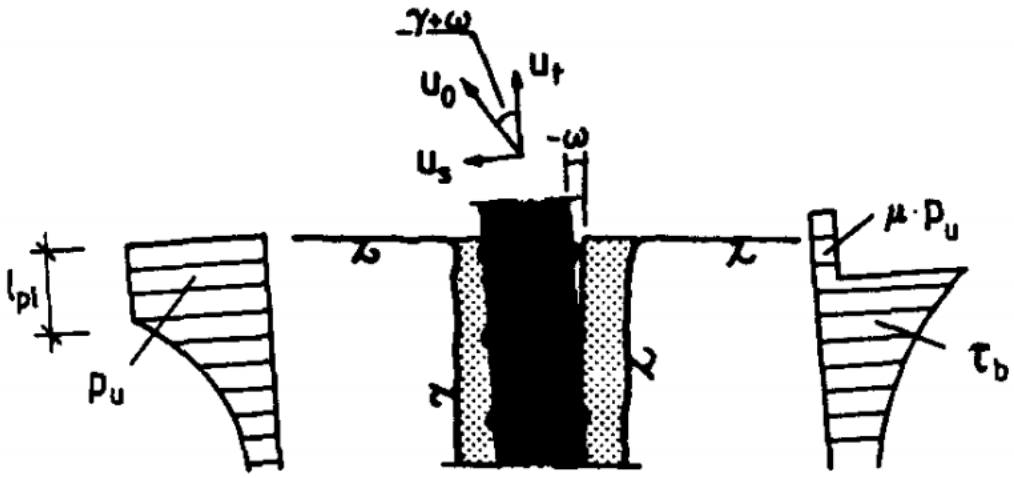

Figure 3.20 Elastic bolt and yielding subgrade

The expressions of lateral load, lateral deformation and axial load under this condition are

$$T_s = \frac{\frac{p_u d_b l_{pl}}{2}(l_{pl}+2l_0)+\frac{2p_u EI}{k_s l_0^2}}{l_0+l_{pl}} \tag{3.33}$$

$$u_s = \frac{T_s l_{pl}}{EI}\left(l_0 l_{pl} + \frac{l_0^2}{2} + \frac{l_{pl}^2}{3}\right) - \frac{p_u d_b l_{pl}^2}{2EI} \cdot \left(l_0 l_{pl} + l_0^2 + \frac{l_{pl}^2}{4}\right) + \frac{p_u}{k_s} \quad (3.34)$$

$$T_t = \mu p_u d_b l_{pl} + E\pi r_b^2 \alpha u_t \quad (3.35)$$

Where:

l_{pl}, is the yielding length of subgrade.

The yield criterion at plastic hinges and the failure criterion at intersection thus are

$$\left[\frac{E\alpha}{\sigma_y} u_t\right]^2 + \left[\frac{2T_s l_{pl} - p_u d_b l_{pl}^2}{2M_{pl}}\right] = 1 \quad (3.36)$$

$$\left[\frac{4\mu p_u l_{pl}}{\pi d_b \sigma_y} + \frac{E\alpha}{\sigma_y} u_t\right]^2 + \left[\frac{8T_s}{\pi d_b^2 \sigma_y}\right]^2 = 1 \quad (3.37)$$

(3) Yielding bolt and yielding subgrade

When the combination of axial load and bending moment exceeds the yield strength of bolt, yield in the bolt appears at the position x = l_{pl}. With the increase of shear displacement, the axial bolt load will increase and yield in the bolt will progress from the initial plastic hinge to the joint intersection.

(4) Ultimate yield condition

This load situation occurs when yield development in the subgrade and yield propagation from the plastic hinge to the bolt-joint intersection both have been accomplished.

By assuming that the bolt behaves as a cable, the following expression can be derived

$$T_t = T_{ty} e^{\mu\varphi} \quad (3.38)$$

It has been assumed that the residual strength of the subgrade is constant and as a result the geometrical shape of the bolt can be described as a parabolic curve. The total deformation (u_0) at the joint intersection for a bolt initially perpendicular to the direction of deformation can be derived as follows:

$$u_0 = \frac{p_u d_b}{2T_{ty}} l_y^2 \tag{3.39}$$

Thus the corresponding slope (ω) of the bolt at the joint intersection is:

$$\omega = -\frac{p_u d_b}{T_{ty}} l_y \tag{3.40}$$

And hence

$$T_t = T_{ty} e^{\mu \frac{p_u d_b}{T_{ty}} l_y} \tag{3.41}$$

Additionally, the mean extension strain is

$$\varepsilon_t = \frac{1}{2}\sqrt{1+\left(\frac{p_u d_b l_y}{T_{ty}}\right)^2} + \frac{T_{ty}}{2p_u d_b l_y} ln\left(\frac{T_{ty}}{p_u d_b l_y} + \sqrt{1+\left(\frac{p_u d_b l_y}{T_{ty}}\right)^2}\right) - 1 \tag{3.42}$$

Failure of the bolt at this stage is considered with two criteria referring to bolt load and strain in the bolt as follow

$$\varepsilon_t = \varepsilon_u \tag{3.43}$$

$$T_t = T_u \tag{3.44}$$

Where:

l_y, is the length of yielding bolt;

ε_u, is the ultimate strain of bolt;

T_u, is the ultimate axial load of bolt.

Pellet *et al.* (1995) and Pellet and Egger (1996) theoretically investigated the contribution of fully grouted rock bolts to the joint shear strength. In their analysis, bolt contribution was divided into additional cohesion effect and additional confining effect, which are related to the parallel force component and the normal force component to the joint. That is:

$$\tau = \left(c_j + \Delta c_b\right) + (\sigma_{n0} + \Delta\sigma_{nb})tan\varphi \quad (3.45)$$

Where:

c_j, is the joint cohesion;

Δc_b, is the additional cohesion provided by the bolt;

σ_{n0}, is the initial confining stress on the joint;

$\Delta\sigma_{nb}$, is the additional confining stress provided by the bolt;

Φ, is the joint friction angle.

The difficulty of this analysis lies in the determination of the intensities and the directions of the forces generated in the bolt during the shearing process.

The deformation of bolts included two stages: elastic stage and plastic stage. The maximum principal stress criterion and the minimum total complementary energy theory were used to derive the bolt yield limit and stress state of the bolt inelastic stage.

$$Q_{oe} = \frac{1}{2}\sqrt{P_u d_b \left(\frac{\pi d_b^2 \sigma_{by}}{4} - N_{oe}\right)} \quad (3.46)$$

$$Q_o = \sqrt[3]{\frac{3N_o P_u^2 \pi^3 tan\beta d_b^2}{1024b}} \quad (3.47)$$

In the plastic stage, the Tresca criterion was used to establish the failure criterion of the bolt.

$$Q_{of} = \frac{\pi d_b^2}{8}\sigma_{bf}\sqrt{1 - 16\left(\frac{N_{of}}{\pi d_b^2 \sigma_{bf}}\right)^2} \quad (3.48)$$

Where:

Q_{oe}, is the shear force acting at point O at bolt yielding stress;

N_{oe}, is the axial force at point O at bolt yielding stress;

Q_{of}, is the shear force at point O at bolt failure;

N_{of}, is the axial force at point O at bolt failure;

σ_{by}, is the bolt yielding strength;

σ_{bf}, is the bolt failure strength.

These yield and failure criterions and the stress state of bolts in shear are presented in Figure 3.21.

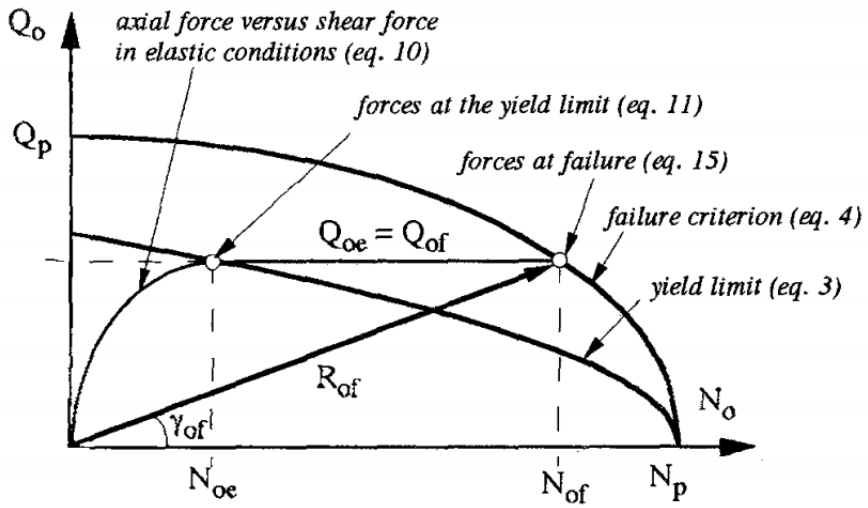

Figure 3.21 Shear force versus axial force in the bolt (Pellet and Egger, 1996)

Experimental and numerical studies by Ferrero (1995) indicated that two different mechanisms of reinforcement failure occurred when varying the rock material property. Theoretical models were proposed to reproduce these two failure mechanisms, one concerning a strong and stiff rock, with bar failure being due to a combination of shear and tensile stresses; and the other involving a weak rock, with bar failure being determined by either the tensile strength or the ultimate elongation of the bar being reached.

The overall shear resistance of a reinforcement system contains two parts: the friction effect and the dowel effect. Both are determined by forces mobilized at the

joint-bar intersection, including the shear force Q normal to the bar axis and the axial tensile force T_r. Thus, the global joint shear resistance can be expressed as:

$$F = T_r cos\alpha_{bj} + Qsin\alpha_{bj} + (T_r sin\alpha_{bj} - Qcos\alpha_{bj})tan\varphi \tag{3.49}$$

Where:

T_r, is the axial tensile force of bolt at intersection;

Q, is the shear force of bolt at intersection;

α_{bj}, is the angle between the bolt axial and the shearing plane.

Figure 3.22shows the loading state of the bar and its element.

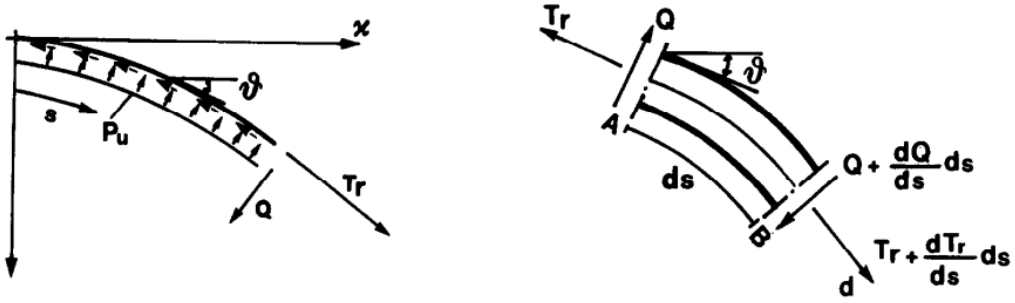

(a) (b)

Figure 3.22 (a) Considered static scheme and (b) forces acting on a bar element (ds) (Ferrero, 1995)

When the surrounding rock behaves in the limit plastic condition, equilibrium equations at both parallel and perpendicular directions to the bar axis can be depicted as:

$$\begin{cases} \frac{dT_r}{ds} = k_{bc}Q + p_u D_b tan\varphi \\ \frac{dQ}{ds} = k_{bc}T_r - p_u D_b \\ Q = -B\mathrm{k}'_{bc} \end{cases} \tag{3.50}$$

Where:

k_{bc}, is the bar curvature;

B, is the static moment on the bar.

With some assumptions, the relationship between the tension force and curvature of the bar can be derived as follows:

$$T_r = \frac{p_u d_b}{k_{bc}} \tag{3.51}$$

The governing differential equation of the bar curvature is:

$$\mathrm{k}_{bc}''' + \frac{\mathrm{k}_{bc}'' \mathrm{k}_{bc}'}{k_{bc}} + \mathrm{k}_{bc}^2 \mathrm{k}_{bc}' + \frac{\mathrm{k}_{bc}'}{k_{bc}} \frac{p_u d_b}{B} = 0 \tag{3.52}$$

An additional assumption of the bar shape at failure is required to solve the general integral of this equation.

For the first yielding mechanism in stiff and strong rock condition, the broken bars were measured and their shapes were approximated with a parabolic equation. Figure 3.23 outlines the forces acting on the bar at failure, and the curvature equation along the bar can be expressed as

$$k_{bc} = \frac{\frac{d^2y}{dx^2}}{\left\{1+\left(\frac{dy}{dx}\right)^2\right\}^{3/2}} == \frac{\frac{2y_o}{x_o^2}}{\left(1+\frac{4y_o^2}{x_o^4}\right)^{3/2}} \tag{3.53}$$

and the tension force is $T_r = p_u d_b \frac{x_o^2}{2y_o}(1 + \frac{4y_o^2}{x_o^2})^{3/2}$.

The global reinforced joint shear resistance can be determined by applying Eq. (3.49).

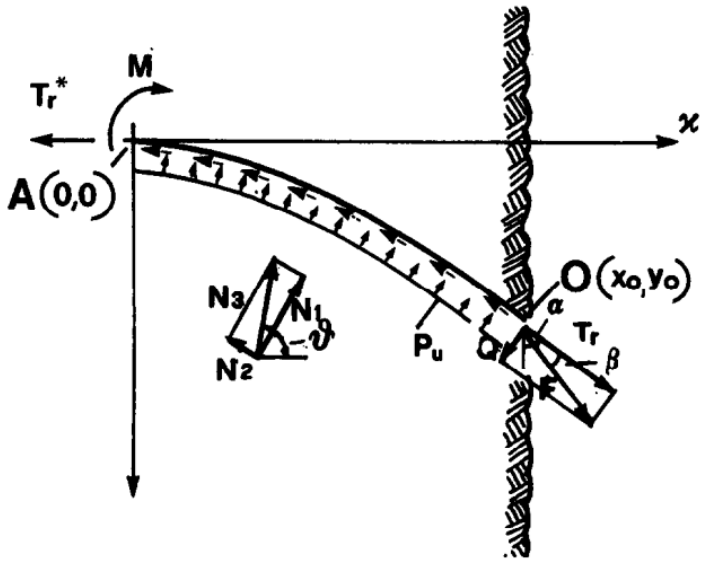

Figure 3.23 Forces acting in the failure mechanism 1 (Ferrero, 1995)

3.6.3 Calculation of bond-slip relationship of a grouted bolt

When a cable bolt is loaded in shear, the generated axial load will propagate along the cable bolt from the shearing plane towards the bolt end. If loaded to failure the cable bolt fails due to the combination of the axial force and the shear force in the vicinity of the shear joint. At the initial stage of loading the axial load in the cable increases and gradually pulls on the cable further away from the joint. With the increase of the shear-induced axial force, a de-bonding zone forms close to the joint and slowly extends further away. This de-bonding will occur when the shear stress at the bolt-grout interface exceeds the bond strength. At any stage of loading, there will be a point along the cable beyond which there is no axial load. As the yielding zone extends, this point moves further away from the shearing joint. The quality of the axial load transfer is important as the further the load transfers from the joint, the less stiff the bolted joint becomes, allowing for greater joint shear displacement for the same load.

3.6.3.1 Load propagation along bolts based on a linear bond-slip model

In tests carried out by Martin *et al.* (2004), an instrumented conventional seven-strands cable bolt was used to study the propagation of axial force along cable bolts. In this study, it was found that the evolvement of axial force was approximately

proportional to the applied load, and an index of load transfer rate, C, was used to denote the ratio of loaded cable length to applied load:

$$C_0 = L_0/P_0 \tag{3.54}$$

Where:

C_0, is the ratio of cable length to applied load;

L_0, is the distance of strain gauge from applied load or point of dilation;

P_0, is the applied load required to initiate bolt deformation at the strain gauge.

In the study by Martin *et al.* (2004), this ratio was about 4.89 mm/kN for a conventional seven-strands cable bolt, while in Milne's tests (Milne *et al.*, 1992) this ratio was roughly 2.28 mm/kN. Moreover, according to Martin, after a strain gauge on the cable bolt started to take load, any additional load will directly increase the strain on the gauge. The increase in load could be obtained from the measured strain based on the cable stiffness K.

Thus, according to Martin's analysis, the axial load of a fully grouted bolt at a specific point is

$$F_p = F - \frac{L_x}{C_0} \tag{3.55}$$

Where:

F_p, is the axial force of bolt at the distance ofL_x;

L_x, is the distance of a specific point from the loaded end.

Based on the analysis of Martin, the bond-slip relationship was derived as shown in Figure 3.24, which is a horizontal line, indicating the bond is a constant.

Figure 3.24 Linear bond-slip model based on test results of Milne *et al.* (1992) and Martin *et al.* (2004)

3.6.3.2 Load propagation along bolts based on a tri-linear bond-slip model

Ren *et al*. (2010) performed the analytical derivation of the grouted bolt full-range behaviour based on a tri-linear bond slip model as shown in Figure 3.25. His tri-linear bond slip model was based on the Yuan (2004) bi-linear model for Fibre Reinforced Plastic (FRP) - concrete joints that was modified by taking the friction effect after de-bonding into account. The tri-linear bond slip model eliminates the plateau behaviour after de-bonding commences, which was shown in Yuan's derivation. Ren *et al*.'s (2010) research was only concerned with the very common de-bonding failure at the bolt-grout interface although there were actually six possible bolt anchorage failure modes, in the three related materials (bolt, grout, rock), at material interfaces (bolt-grout interface or grout-rock interface), and a combination of these failure modes.

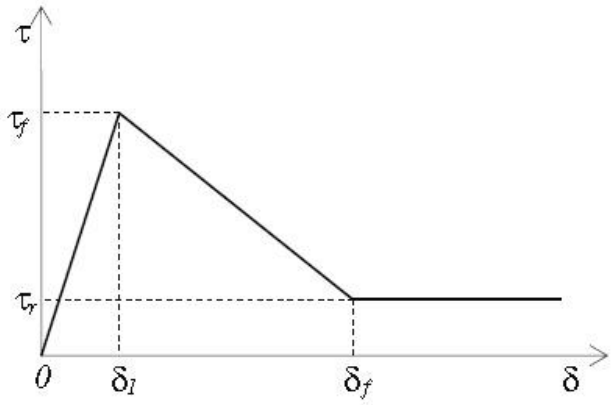

Figure 3.25 Tri-linear bond slip model of bolt-grout interface (Ren *et al.*, 2010)

The tri-linear bond-slip relationship of the bolt-grout interface was mathematically expressed as:

$$\tau(\delta)=\begin{cases}\frac{\tau_f}{\delta_1}\delta & for\ 0\le\delta\le\delta_1\\ \frac{k\tau_f(\delta-\delta_1)+\tau_f(\delta_f-\delta)}{\delta_f-\delta_1} & for\ \delta_1\le\delta\le\delta_f\\ k\tau_f & for\quad \delta\ge\delta_f\end{cases} \tag{3.56}$$

In Ren *et al.*'s analysis, there were totally five loading stages as shown in Figure 3.26, elastic stage, elastic-softening stage, elastic-softening-de-bonding stage, softening-de-bonding stage, and de-bonding stage. For each stage, the load-displacement relationship, the interfacial shear stress distribution and the axial stress of bolt were individually derived. The ultimate load was:

$$P_u=\frac{2\pi r_b\tau_f}{\lambda_2\sqrt{1-k}}\left[\frac{\lambda_2\sqrt{1-k}}{\lambda_1}\sqrt{\cos\left(\lambda_2 a_d\sqrt{1-k}\right)\left[\cos\left(\lambda_2 a_d\sqrt{1-k}\right)-k\right]}+\sin\left(\lambda_2 a_d\sqrt{1-k}\right)\right]+2k\tau_f\pi r_b d_u \tag{3.57}$$

Where:

$$\lambda_1^2=\frac{2\tau_f}{\delta_1 E_b r_b}$$

$$\lambda_2^2=\frac{2\tau_f}{(\delta_f-\delta_1)E_b r_b}$$

$$a_d=\frac{1}{\lambda_2\sqrt{1-k}}\arcsin\left[\frac{\sqrt{\delta_f-\delta_1}\left[\sqrt{\delta_f-k\delta_1-k^2(\delta_f-\delta_1)}-k\sqrt{\delta_1(1-k)}\right]}{\delta_f-k\delta_1}\right]$$

$$d_u=L-a_d-\frac{1}{\lambda_1}\operatorname{arctanh}\left[\sqrt{\frac{\cos(\lambda_2 a_d\sqrt{1-k})-k}{\cos(\lambda_2 a_d\sqrt{1-k})}}\right]$$

When the de-bonding length reached d_u, the displacement at ultimate load was given by:

$$\Delta=$$

$$\frac{\delta_f}{2\lambda_1\lambda_2\sqrt{1-k}}[\lambda_1\left[\lambda_2\sqrt{1-k}(2+kd^2\lambda^2)+2\lambda^2 dsin\left(\lambda_2 a_d\sqrt{1-k}\right)\right]-$$

$$2\lambda^2\lambda_2 a_d\sqrt{1-k}\cos(\lambda_2 a_d\sqrt{1-k})\tanh[\lambda_1(a_d+d-L)]] \quad (3.58)$$

To obtain the analytical result, the four bond-slip model parameters as shown in Figure 3.25 must be known. Calibration needs to be done with control points A, B, C of the experimental load-displacement curve, as shown in Figure 3.26 (b). To get a full-range load-displacement curve the anchorage length should be sufficiently long to experience all five previously mentioned loading stages.

Ren *et al.*'s analysis mainly explained mathematically the full-range behaviour of the grouted rock bolt. There are still limitations in this analysis. Firstly, since the four related parameters are obtained from experimental results, they do not suit the derived solutions when the properties and conditions change in practical applications. Calibration needs to be done for each different condition. Secondly, the snap-back stage shown in Figure 3.26 still exists in the softening-de-bonding stage which could not be recorded in tests. Lastly, a variety of equations need to be considered in each stage, which makes the application of this method very complex and impractical.

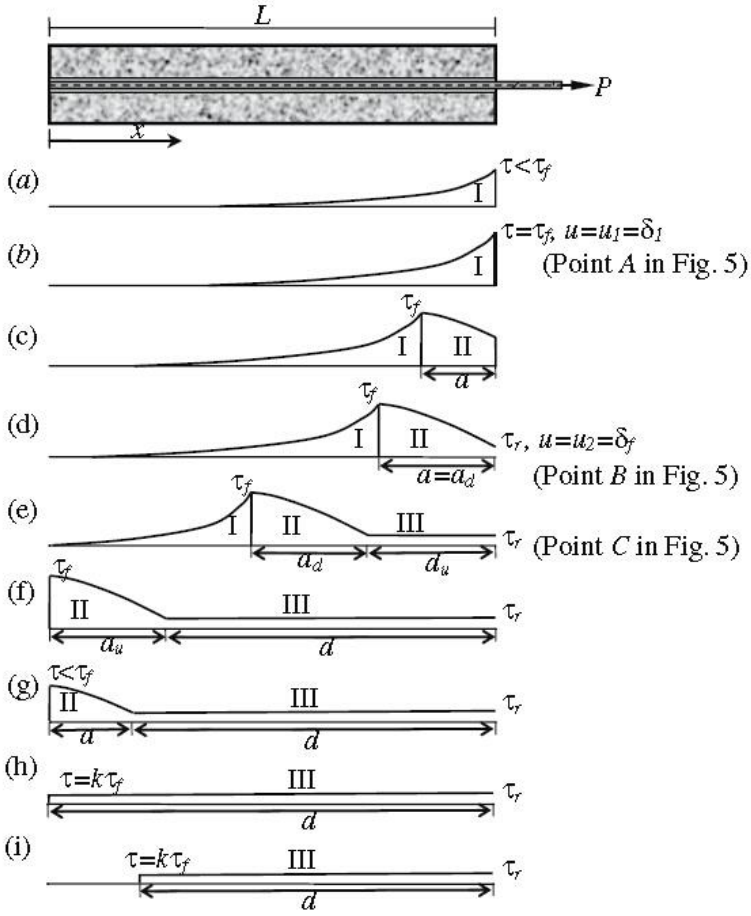

(a)

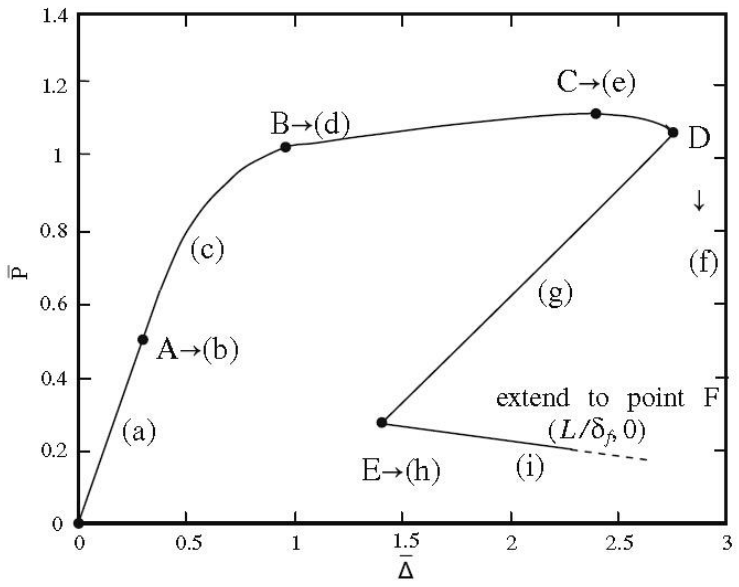

(b)

Figure 3.26 (a) Evolution of interfacial shear stress distribution and propagation of de-bonding; (b) Typical full-range non-dimensional load-displacement curve (after Ren *et al*. 2010)

3.6.3.3 Load propagation along bolts based on a nonlinear bond-slip model

In the area of Externally Bonded Fibre Reinforced Plastics (EB-FRP) joints, researchers performed a variety of pull tests on strain gauged FRP strip to study the bond-slip relationship of the FRP-concrete interface. Based on the experimental results, a simple mathematical function was assumed to represent the distribution of the slip along the bond interface at different loading levels (Zhou *et al.*, 2010). Then based on this assumption, the bond-slip relationship and other related mechanical behaviours were derived. Ma *et al*. (Ma *et al.*, 2013; Ma *et al.*, 2014) used this assumption in the rebar bolting and also gained similar results for both infinite and finite bolt anchorage. The problem in their analysis was that the derivation was based on experimental results, and thus without experimental results all derived equations are not applicable. Their analysis could not predict the bolt tensile behaviour of a general case. After calibrating the control parameters with experimental tests, the loading state of a bolt with different anchorage length under the same condition can be obtained.

Zhou *et al.* (2010) carried out tests and proposed an analytical approach on bond-slip relationship at the EB-FRP-concrete interfaces based on a sole assumption about the distribution of slip along the interface. Based on the same assumption, Ma *et al.* (2013) built an analytical model to study the bonding characteristics of a grouted rock bolt which showed good agreement with their test results. Their analysis indicates that the studies on EB_FRP by Zhou *et al.* (2010) are applicable in bolting research. The analytical model on bond-slip relationship of infinitely long interfaces was compared with the proposed model by Dai *et al*. (2005), which depicted that these two models were generally identical though derived from different directions. However, Zhou *et al.* (2010) advanced this infinite bond length model to a general model of finite bond length, which showed that the former model was a representative case of the latter one.

Analytical solution for EB-FRP joints with an infinite bond length

For a given load P at the loaded end of the FRP strip, there is a corresponding and unique distribution of the internal deformations and stresses at the bond interface, as

shown in Figure 3.27. Based on the equilibrium and deformation compatibility conditions, for a typical segment dx, functions of FRP strain and shear stress along the bond interface can be derived.

$$\varepsilon(x) = \frac{s'(x)}{1+\rho} \tag{3.59}$$

And

$$\tau(x) = \frac{E_f t_f}{1+\rho} s''(x) \tag{3.60}$$

Where:

E_f, is the elastic modulus of FRP strip;

t_f, is the thickness of the FRP strip;

$s(x)$, is the displacement of FRP strip relative to the concrete substrate;

ρ, is the stiffness ratio of the FRP strip to the concrete block calculated by (3.61).

$$\rho = \frac{E_f t_f b_f}{E_c t_c b_c} \tag{3.61}$$

Where:

b_f, is the width of the FRP strip;

E_c, is the elastic modulus of the concrete substrate.

t_c, is the thickness of the concrete substrate.

b_c is the width of the concrete substrate.

The value of ρ is very low and can be neglected for simplicity.

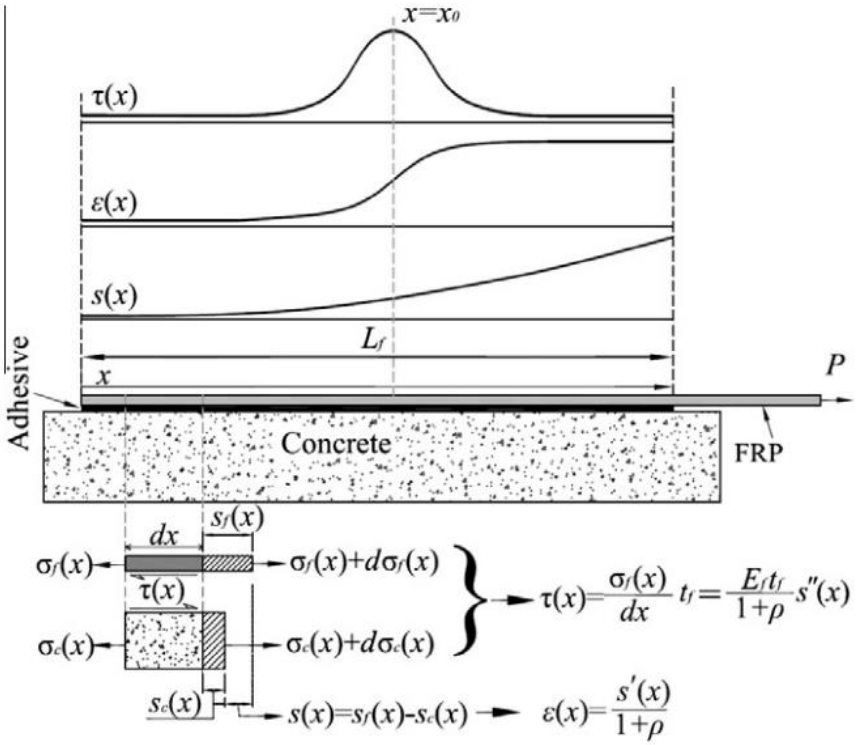

Figure 3.27 Analytical model of EB-FRP joint (Zhou *et al.*, 2010)

Observation of laboratory test results reveals that both the variation and distribution of the slip $s(x)$ along the bond interface at different loading levels are regular, and can be accurately represented by the following function:

$$s(x) = \alpha \ln(1 + e^{\frac{x-x_0}{\beta}}) \tag{3.62}$$

where α, β, and x_0 are coefficients determined from tests. Substituting Eq. (3.62), which is the basic and only assumption of this derivation, into Eqs. (3.59) and (3.60) produces:

$$\varepsilon(x) = \frac{1}{1+\rho} \cdot \frac{\alpha}{\beta} \frac{1}{(1+e^{-\frac{x-x_0}{\beta}})} \tag{3.63}$$

and

$$\tau(x) = \frac{E_f t_f}{1+\rho} \cdot \frac{\alpha}{\beta^2} \frac{e^{-\frac{x-x_0}{\beta}}}{(1+e^{-\frac{x-x_0}{\beta}})^2} \tag{3.64}$$

Rewriting Eq. (3.62) yields

$$e^{\frac{x-x_0}{\beta}} = e^{\frac{s(x)}{\alpha}} - 1 \tag{3.65}$$

Replacing Eq. (3.65) into Eqs. (3.63) and (3.64) leads to

$$\varepsilon(s) = \frac{1}{1+\rho}\frac{\alpha}{\beta}(1 - e^{-\frac{s}{\alpha}}) \tag{3.66}$$

and

$$\tau(s) = \frac{E_f t_f}{1+\rho}\frac{\alpha}{\beta^2}e^{-\frac{s}{\alpha}}(1 - e^{-\frac{s}{\alpha}}) \tag{3.67}$$

Where Eq. (3.66) is the FRP strain-slip relationship and Eq. (3.67) gives the bond-slip relationship. In addition, regression analysis is used to calculate the coefficients α andβ.

Further analysis reveals that the physical meanings of the parameters, α and β, are the turning point of the equivalent bilinear load-slip curve and the reciprocal of the initial slope of the FRP strain versus the slip curve. x_0 is the function of α, β, and P. Shear stress approaches its maximum value at point x_0, which is given by:

$$\tau_{max} = \frac{E_f t_f}{4(1+\rho)}\frac{\alpha}{\beta^2} \tag{3.68}$$

Studies have also pointed out that there exists an effective bond length L_e beyond which the maximum pull load does not increase as the bond length L_f further increases. And the effective length L_e for a typical assembly of FRP and concrete is expressed by:

$$L_e = 2\beta\ln(\frac{1+\delta}{1-\delta}) \tag{3.69}$$

Analytical solution for EB-FRP joints with a finite bond length

For a finite bond length, the strain value determined by Eq. (3.63) is very small, and approaches zero asymptotically and quickly toward the free end for points on the left-hand side of and far away from x_0 (see Figure 3.27). However, the value calculated by Eq. (3.63) is not zero for those points unless x_0 approaches zero, which is unreasonable.

To address this problem to meet the boundary condition of $\varepsilon(0) = 0$, the strain distribution function Eq. (3.63) can be slightly adjusted to:

$$\varepsilon(x) = \frac{1}{1+\rho}\frac{\alpha}{\beta}\frac{x/L_f}{(x/L_f + e^{-\frac{x-x_0}{\beta}})} \tag{3.70}$$

Which always satisfies the boundary condition of $\varepsilon(0) = 0$.

Based on this assumption, the function set of bond-slip relationships can be derived as:

$$\begin{cases} \tau(x) = \frac{E_f t_f}{1+\rho}\frac{\alpha}{\beta^2}\frac{x+\beta}{L_f}\frac{e^{-\frac{x-x_0}{\beta}}}{(x/L_f + e^{-\frac{x-x_0}{\beta}})^2} \\ s(x) = s_0 + \frac{\alpha}{\beta}\int_0^x \frac{t/L_f}{\frac{t}{L_f} + e^{-\frac{x-x_0}{\beta}}} dt \end{cases} \tag{3.71}$$

A single equation describing the relationship of the bond stress to the slip can be obtained by eliminating x_0 from the equation set (3.71). The bond-slip relationship is then not only a function of α and β, but also of x. In other words, the bond-slip relationship is different at different locations of x, which is distinct from the case for an infinite bond length.

From comparison analysis of test results with models of both infinite and finite bond lengths, several conclusions were drawn as indicated in the analysis by Zhou *et al.* (2010).

The derivation process of Ma *et al*.'s theory was similar to Zhou *et al*.'s and the final analytical solutions were also similar. The load-displacement relationship for a bolt of finite length with free end slip is:

$$P = \frac{E\pi d_b^2}{4}\frac{\alpha}{\beta}\sqrt{(1 - e^{-\frac{s_l}{\alpha}})^2 - (1 - e^{-\frac{s_f}{\alpha}})^2} \tag{3.72}$$

When $s_f = 0$, the above expression reduces to the load-displacement relationship for an infinitely long bolt without free end slip as follows:

$$P = \frac{E\pi d_b^2}{4}\frac{\alpha}{\beta}(1 - e^{-\frac{s_l}{\alpha}}) \quad (3.73)$$

As analysed in papers by Ma *et al.* (2013); Ma *et al.* (2014); Zhou *et al.* (2010), the two parameters for the bond-slip model have physical meanings related to the experimental pullout test. In addition, their meanings are different between finite and infinite bolt lengths (Zhou *et al.*, 2010). Nevertheless, their value should remain constant under the same condition no matter whatever length is used. Thus, these parameters can be obtained by short encapsulation pullout test and then used in the condition of long encapsulations.

3.7 Summary

Two load transfer mechanisms are related to bolting, the axial load transfer and the lateral shear load transfer. When subjected to axial loading, only the axial load transfer is involved, whilst when subjected to lateral shear loading, both load transfer mechanisms are involved. Both load transfer mechanisms are reviewed for further analysis of the bolt shear behaviour subjected to lateral shear loading.

Regarding the bond-slip behaviour of bolts, there are two types of test apparatus, the push test and the pull test. Based on the assessment and comparison of existing test apparatuses, a good test apparatus for testing bolt tensioning performance should meet the following requirements:

- Initial confining pressure is available and adjustable to simulate different stress states in the field;
- Rock or concrete samples are required to simulate the grout-rock interface, thereby making the failure at grout-rock interface possible;
- Rock samples should be large enough to avoid size effect;
- Bearing plate size should be suitable to allow all possible failure modes to occur (applying to test method in which a hydraulic tensioner is used);

- The whole test apparatus should be gripped together to prevent the rotation and unwinding of a cable strand sample.

As for the lateral shear behaviour of bolts, the shear apparatuses can be divided into single shear and double shear in general. They differ mainly in the following aspects.

- The consideration of joint friction or not;
- The size of rock or concrete samples;
- The constraint condition of rock or concrete samples;
- The availability of different installation angles of bolts;
- The availability of applying pretension load to bolts;
- The constraint condition of bolt ends.

The interaction of cable bolts and joints is strongly influenced by a great number of factors, such as strength of rock and grout, grout annulus thickness, bolt pretension, grouted or un-grouted conditions, bolt installation angle, joint friction coefficient, loading rate, loading time (creep effect), bolt geometry and bolt strength. These influencing factors have been studied in detail on rock bolts, but few were investigated on cable bolts.

Researchers agree that the combination of tension and shear forces mobilised in bolts causes bolt failure. Whilst some believe that the bolt tensile force plays the critical role in some cases, others argue that shear force is the decisive influencing factor of bolt failure. In addition, at variable stages of laboratory or field tests, bolts may fail due to different mechanisms (tension failure, shear failure or the combination of tension and shear failures) at different parts of their cross-section, especially for cable bolts.

Regarding the contribution of a bolt to joint shear strength, the existing analyses can be divided into the following categories:

- Empirical methods, based on statistical treatment of experimental data;

- Analytical methods based on the equilibrium of the forces acting on the un-deformed reinforcement system;
- Analytical models based on elastic beam theory;
- Analytical models based on the formation of two plastic hinges;
- Analytical models based on the equilibrium of the forces acting on the deformed reinforcement system;

As for the bolt axial tensile behaviour, there are primarily three model types based on different bond-slip model assumptions:

- linear bond-slip model
- trilinear bond-slip model
- non-linear bond-slip model

CHAPTER FOUR
MECHANICAL PROPERTIES OF GROUT, CONCRETE BLOCK AND CABLE BOLT

4.1 Introduction

As discussed in Chapter three, the performance of a cable bolt subjected to shearing is affected by a variety of factors, including the properties of concrete block, grout and cable bolts, the borehole diameter, the bolt pretension, the bolt installation angle and the joint friction angle among others. To deeply understand the contribution of cable bolts to the joint shear performance, these influencing factors must be investigated in detail. Among these factors, the properties of concrete block, grout and cable bolts are basic and necessary parameters in analysis, which are separately studied in this chapter.

Specifically, attention is given to the strength of concrete blocks, the friction angle of concrete joints, the strength of resin and cement grouts, the deformability of grout, the strength and deformability of cable bolts. All these parameters were obtained either in experimental tests conducted in the UOW laboratory, external laboratories or from product manuals provided by suppliers. For some parameters, comparisons were made between laboratory test results and values from product manuals to assess these properties and to ensure the suitable parameters used in the analysis.

4.2 Properties of concrete

4.2.1 Uniaxial compression test

In order to obtain the strength of concrete blocks used in Double Shear Test (DST), cylindrical concrete specimens 100 mm in diameter and 200 mm in height were cast together with DST concrete blocks using the same batch of concrete mixture. Three cylindrical concrete specimens were cast each time using steel moulds as shown in Figure 4.1.

Figure 4.1 Cylindrical concrete samples cast for UCS tests

Figure 4.2 shows the strength variation of cement and concrete tested by Veludo *et al.* (2012). The concrete strength increased steeply at an early curing stage and then remained almost stable after 28 days. Therefore, 28 days old concrete specimens were tested to gain the concrete strength used in the later analysis.

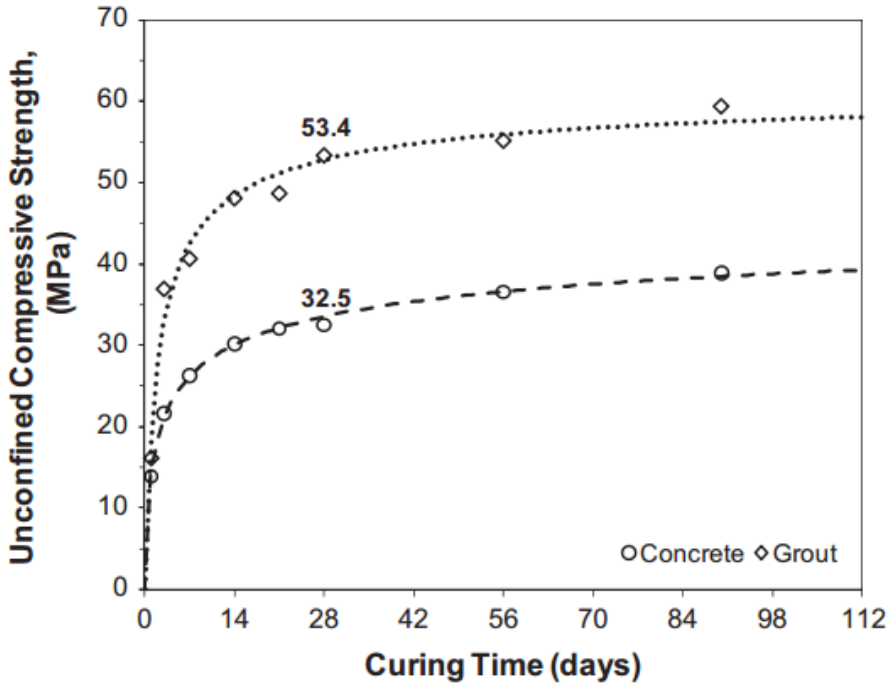

Figure 4.2 Compressive strength of concrete and grout with respect to curing time (Veludo *et al.*, 2012)

Each tested specimen had its rough end plaster-capped prior to testing, which was necessary to avoid stress concentration and premature failure during specimen loading. Specimens were loaded axially to failure in a manually controlled compression machine as shown in Figure 4.3. After each test, the peak load was recorded and the specimen failure surface was photographed and drawn on paper for further analysis.

Figure 4.3 Tested specimen and the testing machine

Table 4.1 lists the peak loads and compressive strength of the first eleven tested concrete specimens. The mixing ratio for 40 MPa concrete was used for the concrete cylinders listed in Table 4.1. When casting these concrete samples, only cement and sand were used and no aggregates were added. The compressive strength of concrete cylinders from the first two mixing batches was much weaker and the ninth batch was much stronger compared with the desired concrete strength. The variation of concrete strength was probably due to unstable vibration and rodding performed to concrete samples. Nevertheless, the other batches produced concrete strength close to 40 MPa. The average strength of the first eleven batches of concrete was 40 MPa with a standard deviation of 6 MPa.

Apart from the first eleven batches of concrete, thirteen more concrete blocks were later cast with the addition of aggregates. For those concrete blocks, three sets were cast using the 60 MPa mixing ratio and all the others were poured using the 40 MPa mixing ratio.

Table 4.1 UCS test results of concrete blocks

Batch No.	Average failure load (kN)	Average strength (MPa)
1	250	32
2	238	30
3	280	36
4	323	41
5	327	42
6	337	43
7	344	44
8	278	35
9	424	54
10	320	41
11	331	42
Average	314	40
S.D.	49	6

The sample cross-sectional area is 0.00785 m^2

After testing, the failure angle of the specimen fracture surface was measured as shown in Figure 4.4. The average failure angle of tested specimens was about 65°. Accordingly, based on the Mohr-Coulomb assumption as shown in Figure 4.5, an equation on the internal frictional angle and failure angle is obtained as follows:

$$\varphi_i = 2\alpha_f - 90° \quad (4.1)$$

Where:

α_f, is the failure angle of concrete specimen;

φ_i, is the internal friction angle of concrete.

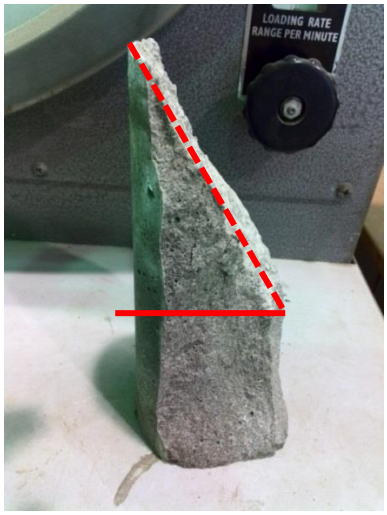

Figure 4.4 Fracture angle of tested concrete specimens

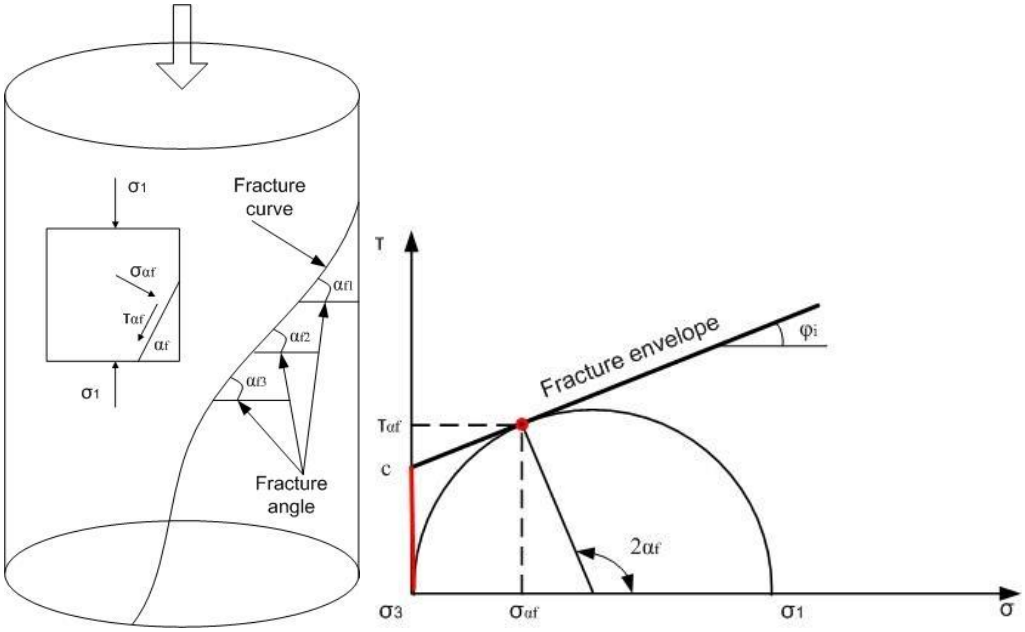

Figure 4.5 Mohr-Coulomb stress state of concrete cylinder in compression

Thus the internal friction angle of concrete was approximately 40°. Additionally, the average concrete cohesion was 9.4 MPa which can be estimated with reference to Eq. (4.2):

$$UCS = \frac{2ccos\varphi_i}{1-sin\varphi_i} \quad (4.2)$$

Where: c, is the cohesion of concrete;

According to the Australian Standard of AS3600 the concrete modulus of elasticity (E) can be calculated based on the compressive strength of tested concrete samples using Eq. (4.3).

$$E_c = 0.043\rho_d{}^{1.5}\sqrt[2]{\sigma_c} \quad (4.3)$$

Where:

E_c, is the modulus of elasticity of concrete, (MPa);

ρ_d, is the concrete density, 2300, (kg/m^3);

σ_c, is the mean strength of concrete samples at a specific age, (MPa).

The mechanical properties of 40 MPa concrete samples used in this study are listed in Table 4.2. The mechanical properties of 60 MPa concrete blocks were not tested.

Table 4.2 Mechanical properties of concrete blocks

UCS(MPa)	40
Elasticity modulus (GPa)	30
Poisson's ratio	0.2*
Cohesion (MPa)	9.4
Internal friction angle (◦)	40

*: Poisson's ratio recommended in Australian Standard AS3600

4.2.2 Concrete joint surface properties

In the shearing process of cable bolted joints, the frictional resistance of joint planes is one of the key factors affecting the overall shear performance of the whole system. Both the shear strength and shear stiffness is increased due to the existence of joint surface friction. To investigate the shear behaviour of a cable bolted joint the shear interface properties must be known. For this reason, a double shear test was conducted on unbolted concrete blocks under four different normal confining pressures. All concrete samples used in the double shear tests in this thesis were cast using the same mould and are expected to have the same joint frictional properties. Thus only one set of concrete blocks was studied.

4.2.2.1 Test procedure

To determine the frictional properties of joint contact interfaces between two side and a central concrete blocks, a set of three concrete blocks were mounted back into the steel moulds and fastened together by four steel bars 22 mm in diameter and two 30 mm thick steel plates as shown in Figure 4.6. A 30 t hydraulic jack was mounted at the end of the concrete block assembly to control and adjust the confining pressure at concrete joints to obtain joint frictional properties at different loading states. A 30 t capacity load cell was installed between concrete block assembly end and the hydraulic jack to monitor the variation of axial loads during the testing procedure. Steel plates of suitable dimensions were placed on the top of the middle concrete block to transfer loads from the compression machine onto the middle concrete block. Steel plates and wood bars were put under the assembly to provide a travel distance for the middle concrete block when the wood bars are removed prior to loading.

Figure 4.6 Double shear assembly without cable bolt reinforcement

When the assembly was ready to test, a forklift machine was used to move and place the double shear assembly on the compression machine as shown in Figure 4.7. Prior to loading, the temporary wood bars underneath the middle block were removed to let the central concrete block be vertically displaced down when loaded. During the loading process, the confining pressure was subsequently altered by the hydraulic jack from 50 kN to 100 kN, 200 kN, and finally 250 kN respectively. The applied

shear load and shear displacement were recorded by a computer connected to the loading machine. After testing, the concrete friction surfaces were examined as shown in Figure 4.8.

Figure 4.7 Double shear assembly placed in the compression machine

Figure 4.8 Concrete friction surface exposed for examination after testing

4.2.2.2 Friction angle of the concrete joints

During the shearing process, the contact surface area between concrete blocks decreased. The confining stress and shear stress of the shear planes were computed on the basis of the effective contact surface area using Eqs. (4.4) and (4.5). The effective confining stresses of four loading stages are presented in Table 4.3.

$$\tau = \frac{F_s}{L_c*(L_c - V_j)} \quad (4.4)$$

$$\sigma_n = \frac{F_n}{L_c*(L_c - V_j)} \quad (4.5)$$

Where:

τ, is the effective shear stress on the joint plane;

σ_n, is the effective confining stress on the joint plane;

F_s, is the shear force of the shear system;

F_n, is the confining force on the joint;

L_c, is the edge dimension of the concrete cross section;

V_j, is the joint shear displacement.

Table 4.3 Confining stress of double shear assembly at different loading stages

Stage	Confining load (kN)	Shear displacement (mm)	Effective confining area (m^2)	Effective confining stress (MPa)
1	50	0	0.09	0.56
		20	0.084	0.60
2	100	20	0.084	1.19
		40	0.078	1.28
3	200	40	0.078	2.56
		55	0.0735	2.72
4	250	55	0.0735	3.40
		70	0.069	3.62

Figure 4.9 shows the variation of vertical shear load versus shear displacement.

According to Mohr-Coulomb failure theory,

$$\tau = c + \sigma_n \tan \varphi \quad (4.6)$$

Since cohesion (c) is zero in the case of pure shear of concrete joints without bonding, hence

$$\tau = \sigma_n \tan \varphi \quad (4.7)$$

Thus,

$$Friction\ coefficient = \tan \varphi = \frac{\tau}{\sigma_n} \quad (4.8)$$

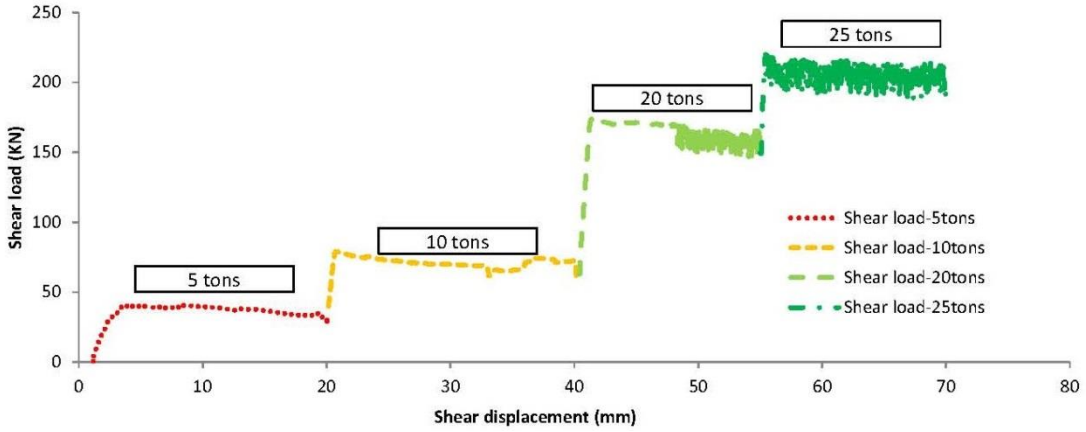

Figure 4.9 Shear load versus shear displacement of unbolted concrete blocks

Based on Eq. (4.8), the variation of joint friction coefficient was obtained as shown in Figure 4.10.

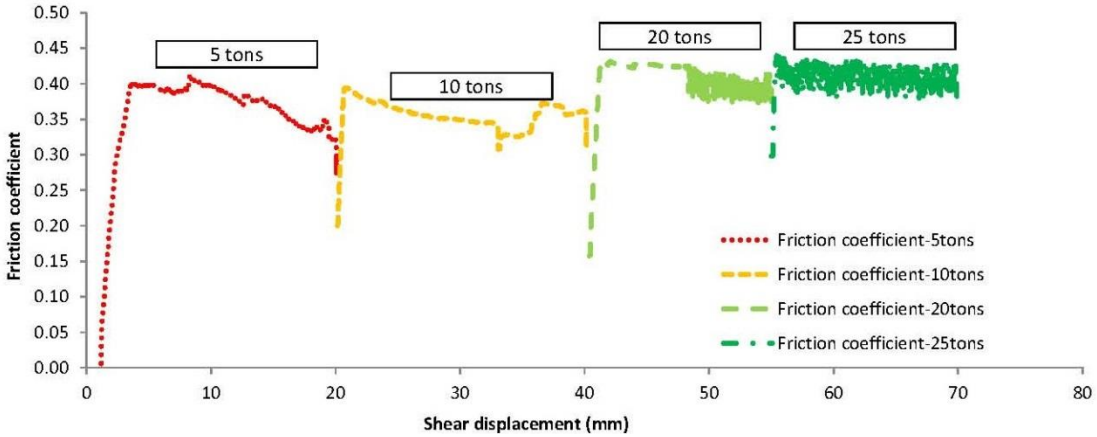

Figure 4.10 Variation of joint friction coefficient versus joint shear displacement

During the first two loading stages, the friction coefficient of joint shear plane remained between 0.35 and 0.4 and the corresponding friction angles were 19° and

22° (converted from the friction coefficient), respectively. In the third loading stage, the range of joint friction coefficient increased to between 0.4 and 0.45 (that was 22° and 24°), which was the stage of maximum value. After this, the joint friction coefficient declined slightly and fluctuated at 0.4 (22°). In addition, from the last part of the third stage onwards, the joint friction coefficient began to experience fluctuation at about 0.4 and the corresponding normal stress started from 2.7 MPa. It is worth mentioning that crashing noises were heard during this period, which indicated the shear failure of unnoticeably small irregularities on the joint shear plane occurred as shown on the joint surface of the tested concrete in Figure 4.8. Thus, the drastic fluctuation of joint friction coefficient may have resulted from the shear failure of small joint surface asperities.

The maximum shear stresses (shear strength of joint) of four loading stages and corresponding normal stresses are extracted and combined to obtain the strength envelope of the tested concrete joints without cable bolt reinforcement as shown in Figure 4.11. It is clearly seen that the regressive result is in close agreement with the previous assumption of joint cohesion (0 MPa) as the regressive cohesion is only 0.02 MPa which is approximately equal to zero. Additionally, the regressive joint friction coefficient of the whole shearing process is around 0.44, and hence the corresponding joint friction angle is 24°.

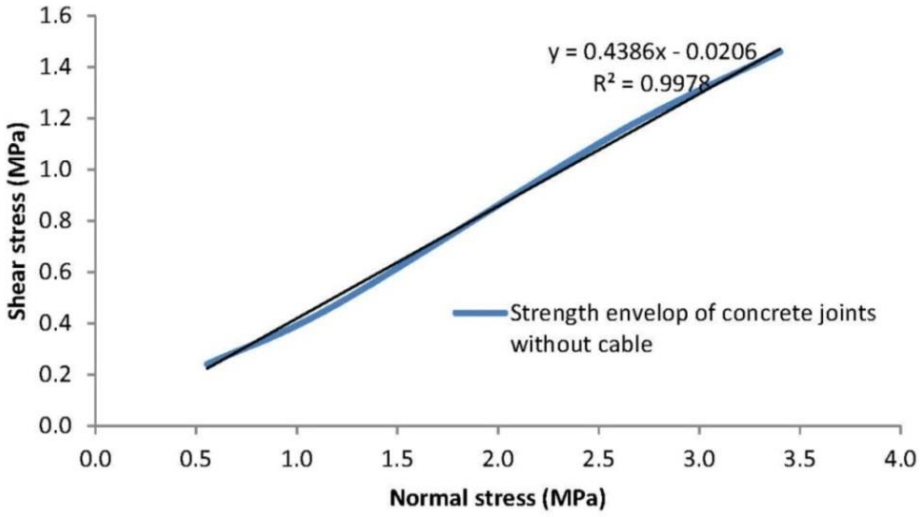

Figure 4.11 Strength envelope of concrete joint without cable bolt reinforcement

4.2.2.3 Joint shear stiffness at different normal stresses

When the concrete blocks were sheared at different normal stresses, the concrete joint surface did not exhibit a stable friction effect immediately. Rather, it took a period for the joint surface friction to increase to its stable stage.

Figure 4.12 gives the shear stress variation at the initial stage of different normal stresses. The joint stiffness in the first stage was only about 0.08 MPa/mm at a normal stress level of 0.56 MPa. Then it continued to increase to 0.43 MPa/mm at 1.19 MPa, 0.78 MPa/mm at 2.56 MPa and 1.34 MPa/mm at 3.4 MPa in the subsequent three stages.

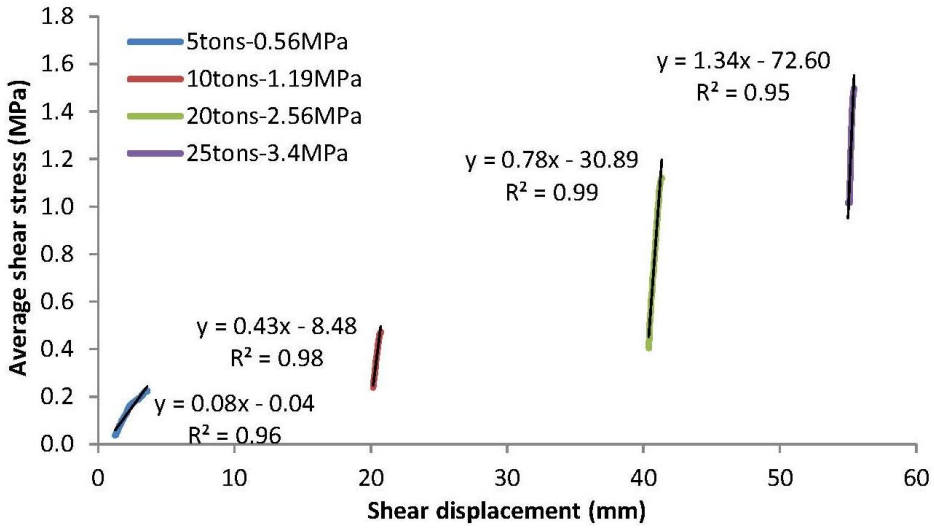

Figure 4.12 Joint shear stiffness at different normal stresses

4.3 Properties of grout material

At present, both resin and cement grouts are extensively used as grout medium in cable and rock bolting. They help to build connection between the reinforcing tendon and the surrounding rock mass to transfer forces between them to stabilise rock strata. Thus grout properties play an important role in the performance of bolts in reinforcing rock strata. In the present thesis, both resin and cement grouts were used in the investigation of cable bolt performance in laboratory tests especially when loaded in shear.

To attain properties of the used resin and cement grouts, a variety of laboratory uniaxial compression tests were conducted on resin and cement samples.

In this study, cube specimens of 40 mm and prisms specimens of 40 mm × 40 mm × 80 mm were tested to investigate the UCS and the elastic deformability of various resin and cement grouts. Figure 4.13 shows specimen moulds of various dimensions used to cast resin and cement samples.

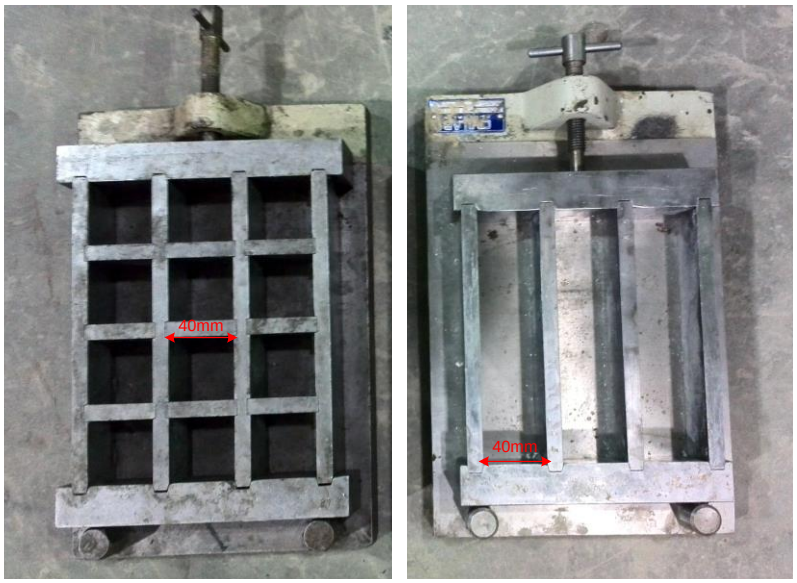

Figure 4.13 Moulds used to cast resin and cement grout samples

The used grout materials are Carbothix, BU100, TD80, FB400 and Stratabinder HS from Jennmar and Minova in Australia. Carbothix is resin grout and all the others are cement grouts. Most grout materials used in Australian coal mines are provided by these two companies.

4.3.1 Uniaxial Compressive Strength (UCS)

Uniaxial compressive tests were performed in laboratory conditions on resin and cement grouts. Grout samples tested in the laboratory included two types. One was cast with the same batch of mixed grouts used in double shear tests as shown in Figure 4.14, and the other was cast using separately mixed grouts as shown in Figure 4.15. All samples were tested at an age of 7 days old. Figure 4.16 shows the grout samples before and after testing. The test results of samples using the same batch of

mixed grouts and the separately mixed grouts are listed in Table 4.4 and Table 4.5 respectively.

Figure 4.14 Sample preparation using the same batch of mixed grouts for double shear tests

Figure 4.15 Sample preparation using separately mixed grouts

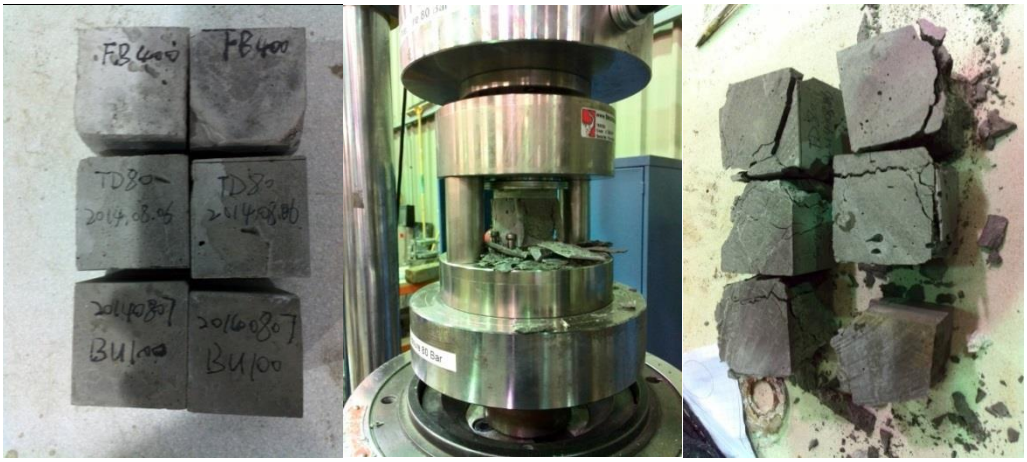

Figure 4.16 Grout samples before and after testing

Table 4.4 UCS of grout samples using the batch of mixed grouts for double shear tests (1st group)

Grout type	Strength (MPa)	Average strength (MPa)
BU100 S1	62.8	63
BU100 S2	63.5	
TD80 S1	59.1	59
TD80 S2	59.2	
FB400 S1	58.3	57
FB400 S2	56.5	
Carbothix S1	38.1	38
Carbothix S2	37.5	

Table 4.5 UCS of grout samples using the separately mixed grouts (2nd group)

Grout type	Cross section (mm^2)	Peak load (kN)	Strength (MPa)	Average (MPa)
TD80 C1	1600	97	61	61
TD80 C2	1600	98	61	
BU100 C1	1600	112	70	66
BU100 C2	1600	99	62	
FB400 C1	1600	45	28	33
FB400 C2	1600	61	38	

As Carbothix in Table 4.4 and FB400 in Table 4.5 were poorly cast, their results were unreasonably small. Therefore, the corresponding results about Carbothix in Table 4.4 and FB400 in Table 4.5 were abandoned. For the well prepared samples, it is observed that test results from Table 4.4 and Table 4.5 were very consistent. This indicates the laboratory results were reliable.

In addition, BU100 and Stratabinder were also systematically investigated with the consideration of curing time of 1, 7, 14, 21, 28 days (Wang, 2015). Strength of grout specimens (7 days old) is given in Table 4.6.

Table 4.6 UCS of BU100 and Stratabinder (3rd group)

Sample	Strength (MPa)	
	BU100	Stratabinder
1	66.24	67.85
2	63.86	67.24
3	63.04	66.56
4	65.87	70.72
5	63.77	68.88
6	65.22	68.69
Average	64.77	68.32

Based on the above test results, it is reasonable to adopt the grout strength listed in Table 4.7 in this thesis. Clearly, the compressive strengths of different grouts were similar and the difference was within 10 MPa. To be simplified, they could be regarded as having the same compressive strength in different double shear tests.

Table 4.7 Summary of grout strength

Type	1st group (MPa)	2nd group (MPa)	3rd group (MPa)	Average(MPa)
BU100	63	66	65	65
TD80	59	61	\	60
FB400	57	\	\	57
Stratabinder HS	\	\	68	68

4.3.2 Deformability and elasticity

Rectangular prismatic specimens with strain gauges were tested in cyclic compressive tests to investigate the deformability of cement grouts used in double shear tests. Samples were cast in steel moulds with a H/D ratio of 4:1 as shown in Figure 4.17. They were then cut into shorter ones with a H/D ratio of 2:1 using a machine cutter. Strain gauges were perpendicularly attached at the centre of the

sample surface to record the axial and radial strain during the test as shown in Figure 4.18. Two samples were tested for each type of cement grout to ensure their consistency.

Figure 4.17 Preparation of cement samples for deformability test

Figure 4.18 Strain gauged samples

Figure 4.19 shows a typical cyclic compressive test result of a rectangular cement specimen. For each sample there were three cyclic loading processes in total. Table 4.8 lists the tangent E value and Poisson's ratio of different cement grouts.

In Table 4.8, the Tangent E and the Poisson's ratio varied for these cement grouts. TD80 exhibited the largest tangent modulus and the smallest Poisson's ratio, whereas FB400 showed the smallest tangent modulus and the largest Poisson's ratio. The tangent modulus of all cement grouts was less than 20 GPa.

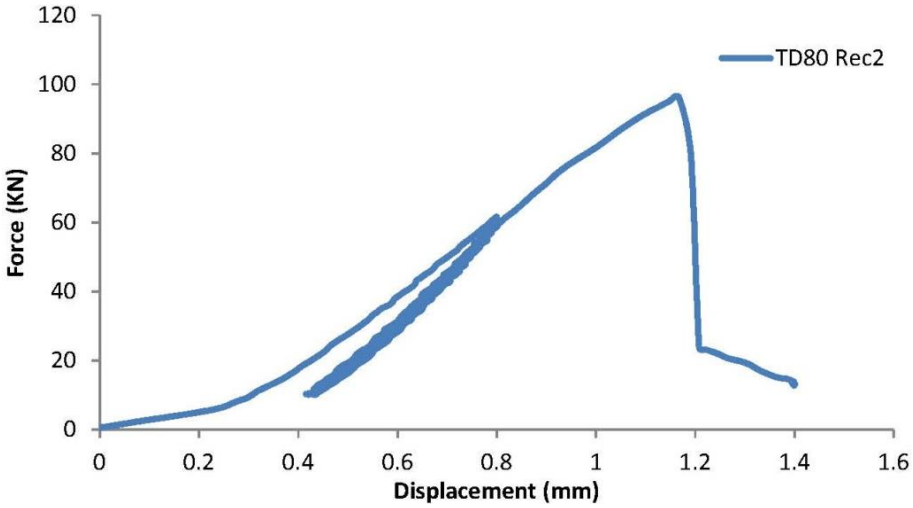

Figure 4.19 Force versus displacement of strain gauged cement specimen (TD80 Rec2)

Table 4.8 Summary of deformability of different cement grouts

Sample No.	Tangent E (GPa)	Average Tangent E (GPa)	Poisson's ratio	Average Poisson's ratio
TD80	15.2	19.6	0.12	0.12
TD80	23.9		0.73/unreasonable	
BU100	19.4	17.5	0.23	0.29
BU100	15.6		0.35	
FB400	9.7	7.2	0.39	0.36
FB400	4.6		0.33	
Stratabinder HS	14.9	17.3	0.29	0.34
Stratabinder HS	19.7		0.39	

4.4 Properties of reinforcing elements

4.4.1 Cable bolt types

A variety of different types of cable bolts were tested in shear under laboratory conditions, including solid and hollow cable bolts. The solid cable bolts consisted of Jennmar's indented/smooth wire Superstrand cable, Jennmar's Garford twin-strand cable and Rio Tinto's smooth wire Superstrand cable which was imported from

China. The hollow cable bolts include Jennmar's indented wire TG, Jennmar's indented/smooth wire SUMO and Minova's SHGC cable of spirally ribbed and smooth wires. They are either widely used in Australia or newly designed for the future market.

Table 4.9 shows the profile and geometrical features of various cable bolts used in double shear tests. The main difference in their structure is the core of cable strand: the hollow steel tube for the groutable cable bolts and the solid steel wire core for the un-groutable cable bolts. The nineteen wires Superstrand cable bolts have a middle layer of thin steel wires, whereas the others do not.

Table 4.9 Summary of cable bolts used in laboratory tests

Cable type	Cross section	Profile	Diameter (mm)	Steel wires
JM indented wire Superstrand cable (JIWS)	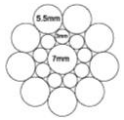		21.8	Nine outer layer indented wires, nine inner layer smooth wires and a smooth king wire
JM smooth wire Superstrand cable (JSWS)	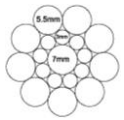		21.8	Nine outer layer smooth wires, nine inner layer smooth wires and a smooth king wire
JM indented wire TG cable (JIWTG)	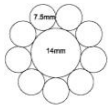		28	Nine outer layer indented wires and a hollow tube
JM indented wire SUMO cable (ISUMO)	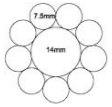		28	Nine outer layer indented wires and a hollow tube
JM smooth wire SUMO cable (SSUMO)	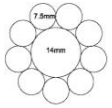		28	Nine outer layer smooth wires and a hollow tube
JM Garford twin-strand cable	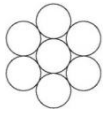		15.2×2	Six outer layer smooth wires and a smooth king wire
Minova's SHGC cable (SHGC)	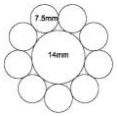		22	Five outer layer smooth wires, four outer layer spirally ribbed wires and a hollow tube
Rio Tinto's smooth wire Superstrand cable (RT)	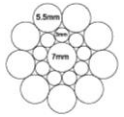		21.8	Nine outer layer smooth wires, nine inner layer smooth wires and a smooth king wire

4.4.2 Cable tensile strength

Cable bolt strengths, including yield strength and failure strength, influence its performance in reinforcing jointed rock mass. Regarding cable bolts used in double shear tests, their mechanical properties are collected from manufacture's product manuals and laboratory tests and are listed in Table 4.10.

Table 4.10 Summary of mechanical properties of cable bolts used in double shear tests

Cable name	Steel area (mm^2)	Yield load (kN)	Yield strength (MPa)	Failure load (kN)	Failure strength (MPa)
Indented JM Superstrand	281.7	472.5	1677	531	1885
Plain JM Superstrand	313	525	1677	590	1885
Indented TG	311.4	504	1618	559	1792
Indented SUMO	311.4	513	1647	573.3	1841
Plain SUMO	346	570	1647	637	1841
Garford twin-strand	143	250	1748	265	1853
SHGC indented wire	38.5	61.6	1600	67.33	1748
SHGC smooth wire	44.2	71.5	1617	80.67	1825
SHGC	\	604	\	673	\
Plain RT wire		519	1659	591	1888
Average		\	1654	\	1840
S.D.		\	44	\	47

Strength of plain JM Superstrand, Garford twin-strand and plain SUMO is from manufacturer's manual. Strength of SHGC and plain RT Superstrand is from laboratory tensile tests. Strength of indented JM Superstrand, indented TG and indented SUMO is 10% off the plain counterparts.

From this table, it is observed that the yield strength and the failure strength of different cable bolts from different manufacturers were very similar irrespective of their wire profile. All cable bolts were made from high tensile strength steel. The average yield strength and failure strength of these cable bolts were about 1654 MPa and 1840 MPa with the standard deviation of 44 MPa and 47 MPa, respectively. For a general cable bolt, the average yield and failure strengths can be used in

calculations to attain results with acceptable precision. Since the failure strength of different cable bolts was similar, the difference of cable failure load was mainly due to the variation of cable cross section area.

4.4.3 Cable bolt deformability

The deformability of cable bolts loaded in tension and in shear plays a significant role in their performance in reinforcing a jointed rock mass. As cable bolts are made of steel wires their main deformation feature is determined by the steel wires. But this does not mean that a cable bolt is exactly the same as its wire component in terms of deformability. Actually, it will be seen in the following analysis that a cable bolt is generally stiffer than its wire component.

4.4.3.1 Cable wire

Normally, an axially tension-loaded steel wire has four typical stages in its stress-strain relationship: elastic stage, yield stage, strain hardening stage, and strain softening stage (necking) as shown in Figure 4.20. A couple of cable strand steel wires were individually tested in tension and their stress-strain relationships were obtained and illustrated in Figure 4.21 and Figure 4.22. The test results of cable steel wires were consistent with the typical relationship shown in Figure 4.20 except for the strain softening stage. This is because tested cable wires did not exhibit an obvious long strain softening stage after the peak load. In Figure 4.21 and Figure 4.22, the yield stage and the strain hardening stage were combined and represented by another strain hardening stage, which simplifies the stress-strain relationship as a linear relationship and is easy to be used in numerical and theoretical analysis with adequate/reasonable accuracy. In addition, the elastic and plastic stages were considered as linearly elastic, yet with different moduli as shown in both Figure 4.21 and Figure 4.22. Thus a bilinear relationship is obtained to represent the steel cable wires. The tensile modulus of the first liner stage is approximately 200 GPa and the second stage is about 4 GPa.

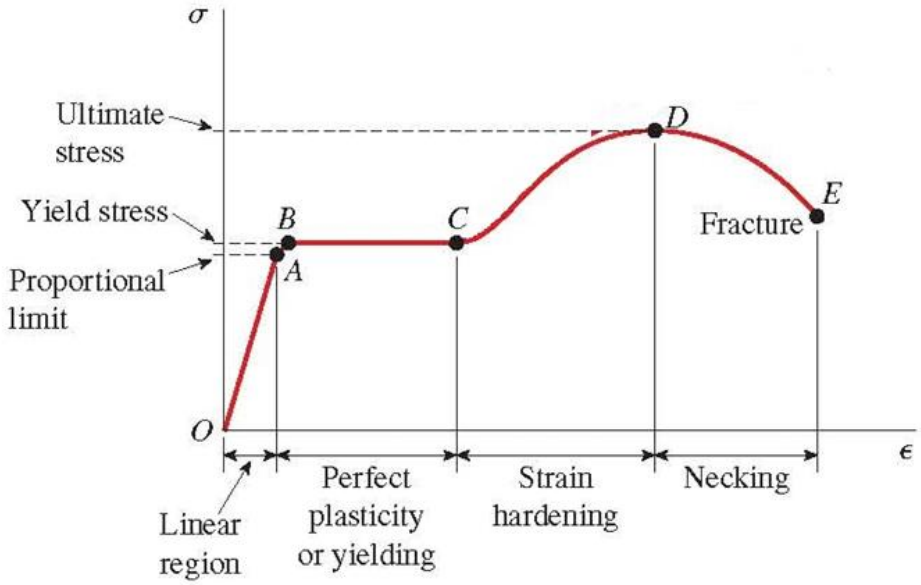

Figure 4.20 Schematic stress-strain relationship of a typical structural steel loaded in tension (not to scale) (Gere and Timoshenko, 1990)

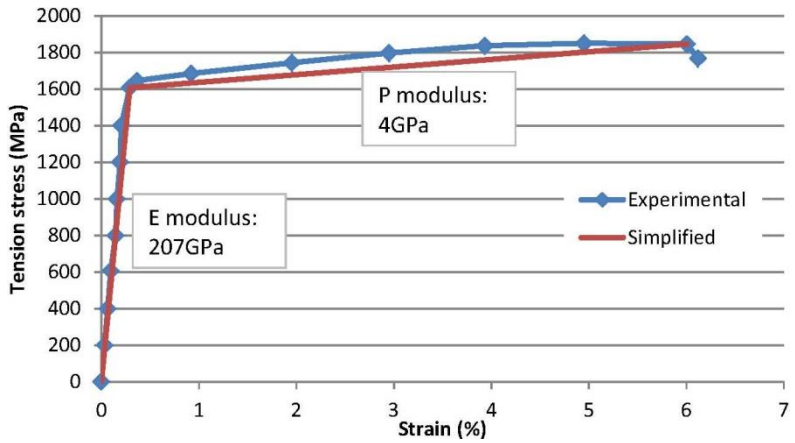

Figure 4.21 Stress-strain relationship of SHGC cable wire: smooth (Orica, 2014)

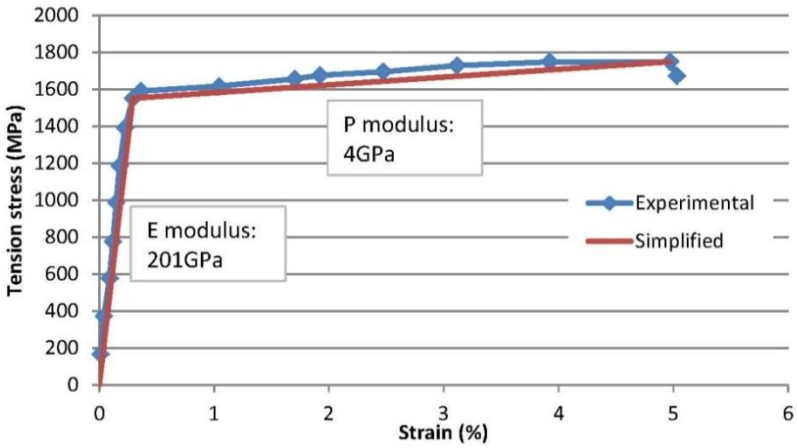

Figure 4.22 Stress-strain relationship of SHGC cable wire: spirally ribbed (Orica, 2014)

4.4.3.2 Cable bolt

A cable bolt comprises multiple steel wires spun around a king wire or a hollow tube. When a cable bolt is loaded in tension, the cable wires tend to fail individually due to stress concentration, especially at the griping point. Thus special attention should be paid to this issue when investigating the strength and deformability of cable bolts.

Tensile tests were conducted in laboratory on the RT Superstrand cable bolt used in this thesis as shown in Figure 4.23. The test result is given in Figure 4.24. Due to the stress concentration causing separate cable wire failure, the average tensile failure load of RT cable tested with traditional barrel and wedge assemblies was only 527 kN. In contrast, the average tensile failure load of RT cable bolt based on the test result of cable wires was about 591 kN (refer to Table 4.10), which was 64 kN higher.

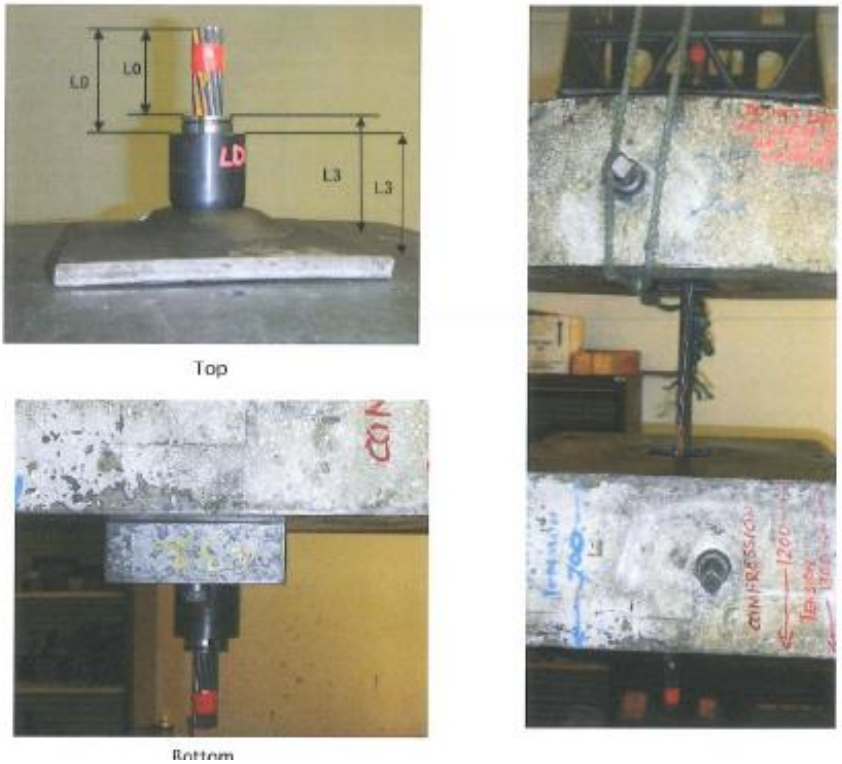

(a) Test setup

(b) Tested cable bolt

Figure 4.23 Tensile test of cable bolt gripped with traditional B/W assemblies

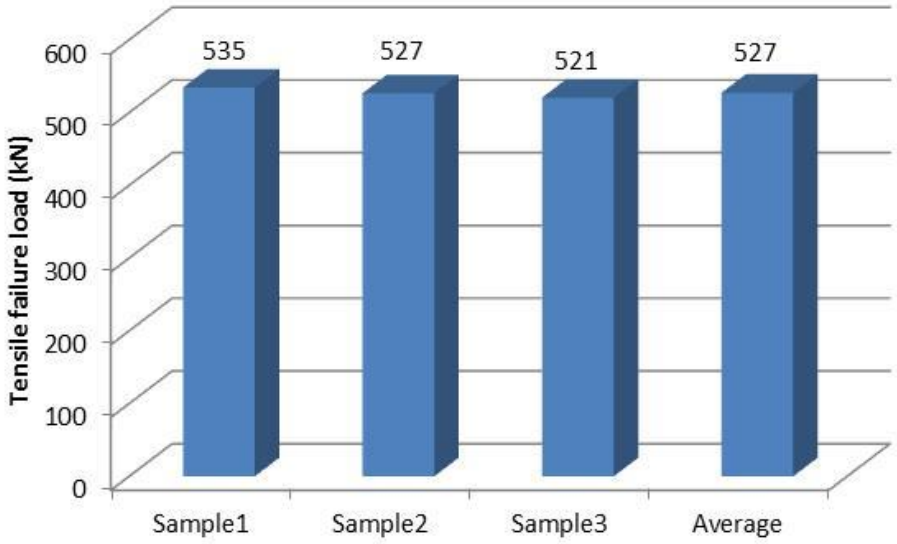

Figure 4.24 Tensile test result of RT Superstrand cable bolt

In order to study the tensile capacity and deformability of cable bolts in tensile tests with anchor assembly, premature cable wire failure due to stress concentration at the anchor assembly should be avoided. Otherwise, the plastic stage of the tested cable bolt could be very short. To solve this problem, Thompson and Villaescusa (2014) developed a custom-designed barrel with two tapered wedges as shown in Figure 4.25. This design allowed wedges to avoid becoming jammed between the barrel and strand, and prevented stress concentration at the B/W assembly. Figure 4.26 shows the test results using both the traditional B/W assembly and the new B/W assembly.

It is seen that one cable bolt with the traditional B/W assembly failed at the end of the linearly elastic stage and the other failed at the early plastic stage. The failure strain of both was less than 1.5%. The third cable bolt with the modified B/W assembly showed a more complete force-strain relationship with the failure strain reaching more than 4%. Clearly, this modified B/W arrangement would permit accurate calculation of the deformability and strength of the cable bolt.

Figure 4.25 Special barrel and wedge assembly for strand testing (Thompson and Villaescusa, 2014)

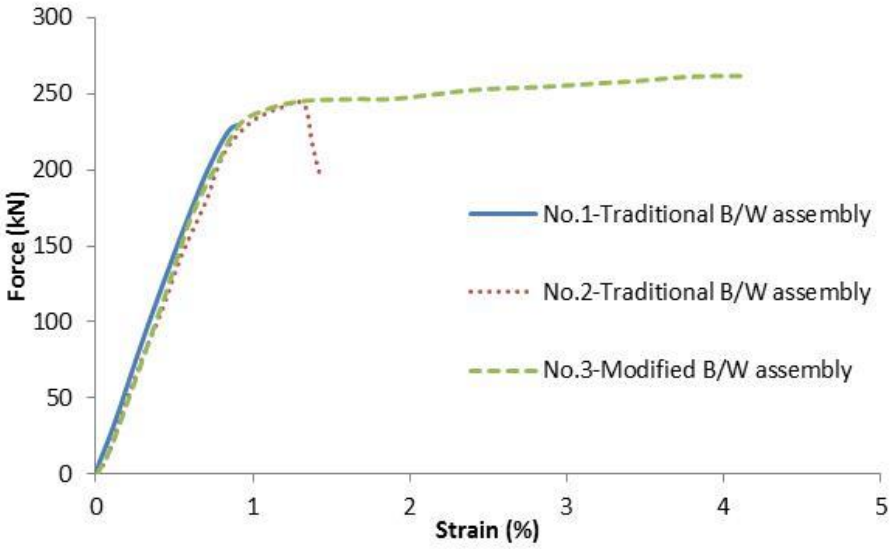

Figure 4.26 Tensile test results of cable bolts gripped by traditional and modified B/W assemblies (Thompson and Villaescusa, 2014)

4.5 Summary

The relevant mechanical properties of the materials used in studying the reinforcing effect of cable bolts are presented, including concrete blocks, grouts and cable bolts. The result can be briefly summarized as follows:

- Three sets of concrete blocks had a strength of 60 MPa and all the others were in general consistent at around 40 MPa. The average friction coefficient of concrete joints was about 0.44 at the stable stage.

- The compressive strength of all cement grouts was around 60 MPa for seven days old samples, whereas the elastic modulus and Poison's ratio tended to vary.

- Several types of cable bolts were used in this study with different diameters (15.2 mm, 22 mm and 28 mm) and strand wire profiles (indented and smooth). The average yield strength and failure strength of these cable bolts were 1654 MPa and 1840 MPa, respectively.

- Steel cable wires had four typical stages in their stress-strain relationships including elastic stage, yielding stage, strain hardening stage, and strain softening stage (necking). And they can be simply represented by two linearly elastic stages of different moduli. A bilinear stress-strain relationship was suitable to represent the steel cable wires. The average moduli of the first and the second linear stages were about 200 GPa and 4 GPa, respectively.

- The strength and deformability of cable bolt were significantly influenced by the test method and the used testing equipment. Normally, the cable strength and modulus in the elastic stage were smaller than that of cable wires. The cable modulus in the plastic stage was either unattainable from the test of cable bolt or excessively larger than that from cable wires.

CHAPTER FIVE
EXPERIMENTAL STUDY ON THE SHEAR PERFORMANCE OF CABLE BOLT-REINFORCED CONCRETE JOINT

5.1 Introduction

In order to study the cable strand contribution to the joint shear strength of concrete (rock) blocks and the axial load propagation in the cable strand, a number of tests were conducted on cable strands with different structures and wire profiles at various pre-tension loads. Different grouts were used to encapsulate cable strands in concrete blocks, including resin grout, BU100 cement, TD80 cement and Stratabinder cement.

In the experimental investigation, the UOW double shear test apparatus was used to study the shear performance of a cable bolt in jointed concrete. The original double shear test apparatus was used to perform shear tests with joint friction. Then the apparatus was modified to be capable of conducting double shear tests without joint friction. The use of both the original and the modified apparatuses helped better investigate the joint shear resistance from the cable bolt and from the joint friction experimentally. Test results from both test apparatuses were analysed and compared in terms of joint shear strength, joint shear stiffness, cable failure mode, cable pre-tension effect and cable wire profile effect.

Single shear tests were also conducted on a number of cable bolts using the British Standard (BS) single shear test apparatus. Results from BS single shear tests were compared with the double shear test results and potential problems of the BS method in testing cable bolt shear performance were discovered and analysed in detail.

5.2 Selection of test method

In order to study the cable shear performance, a laboratory test method should replicate the field condition of cable bolts installed around underground excavations.

The test method also needs to consider the limitation of the laboratory and simplification is necessary for a practical, reproducible and capable test method.

As dicussed in Section 3.6 of Chapter Three, considering the influence of bolt de-bonding in the bolt tensioning section on the bolt shear performance, there are theoretically three possible loading cases based on the relative position of the shearing plane to the bolt free end. In field applications, the cable bolt length is normally 4 to 8 m and the severe loading due to large rock deformation is close to the excavation surfaceas shown in Figure 3.1. Thus, the cable bolt free end is far from the bolt section exposed to severe rock deformation and loading. Therefore, the cable de-bonding does not significantly influence the cable bolt shear performance in field conditions. This is the first loading case discussed in Section 3.6 of Chapter Three. As introduced in Chapter three, in this case, two methods can be used to avoid the occurrence of full cable de-bonding. In this study, the barrel and wedge assembly was used to achieve it.

When a rock discontinuty slides or opens, a cable bolt across it may be loaded in a couple of loading forms, which is determined by the angle between the cable bolt and the discontinuty and the displaceement direction. Figure 5.1 gives all possible loading states of a bolt anchored across a discontinuty caused by the discontinuty opening or sliding. The so called ‘pure shear’ of a cable bolt in Figure 5.1 was considered as a close analogy to this study of shearing across joints but to a limited extent. Actually, the ‘pure shear’ only refers to the initial 90° angle between the bolt and the discontinuty. The ‘pure shear’ does not really exist because the cable bolt is stronger than the rock mass and can crush the rock mass when loaded in shear, which is what occurs in the real shearing process.

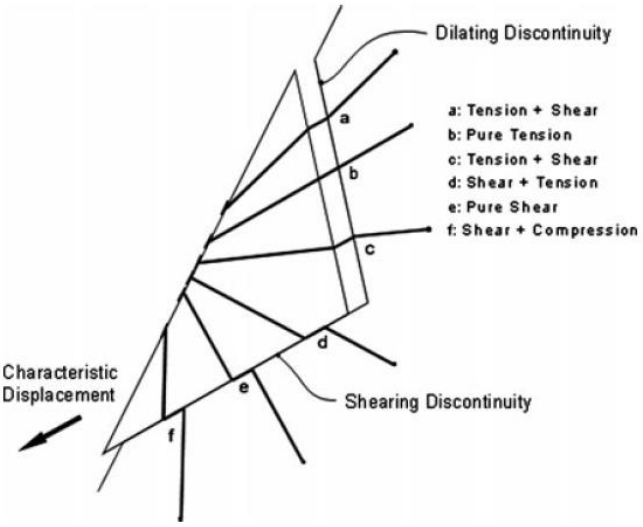

Figure 5.1 Bolt loading state caused by block translations (Thompson *et al.*, 2012)

A cable bolt crossing rock discontinuties can be loaded by the opening or the sliding of the discontinuty. The loading process in the field is expected to be complex. Displacement may occur simutaneously in both directions to load the cable bolt until failure. Displacement may also happen in one direction first then pause at that direction and start in the other. Also possibly, the loading process is a combination of the former two cases,which is much more complex. In this study, the second case was investigated. Only shear displacement was applied on concrete blocks during the loading process, the axial displacement of concrete blocks was maintained zero.

In field conditions, a discontinuty may be an open one or a closed one. In the case of 'pure shear', according to the contact condition of the discontinuty, two sub-cases exist. If friction exists during the shearing process, higher shear strength can be achieved and part of the whole shear resistance comes from the shear plane friction. If friction does not exist, then the whole shear resistance will be attributed to the cable bolt itself. Both cases were investegated using the original and the modified double shear apparatuses which will be introduced in the following section.

5.3 Double shear test with joint friction

The double shear test with joint friction can simulate the shear behaviour of a closed joint reinforced by bolts. The original double shear test apparatus developed in the

University of Wollongong was used to perform the double shear test with joint friction. The testing process involved concrete sample preparison, cable installation and pre-tensioning as well as sample shear loading, which is introduced in the following section.

5.3.1 Experimental procedure

5.3.1.1 Concrete block preparation

Each double shear test sample consists of three concrete blocks with predetermined dimensions. The 300 mm side cubes together with the central rectangular block 450 mm in length, 300 ×300 mm in cross section constitutes the shear system. Sand, aggregates and cement were used to cast the concrete blocks. Figure 5.2 shows the procedure of concrete block preparation.

Figure 5.2 Preparation process of concrete blocks

Concrete blocks used for testing were cast in the steel frame of the double shear test apparatus, which was also used for shear testing of cables later. Prior to casting, a plastic/steel conduit of suitable diameter greased on its surface was placed through the centre of the mould lengthways to create a hole for cable installation in the

concrete blocks. The conduit was wrapped with plastic wire to obtain a borehole with a rifled surface for strong cable anchorage. Once mixed, concrete was poured into each section of the 20 mm thick steel moulds. An electrical hand vibrator was used to drive trapped air out of the concrete to obtain a uniform concrete sample. In addition, several cylindrical concrete samples 200 mm in length, 100 mm in diameter were cast for UCS tests using the same batch mix in steel cylinders. The conduit and the plastic wire were removed when the concretes set. The concrete was left in the moulds for 24 hours to set and then removed and stored in the laboratory with plastic covering and regular showering for about 30 days to cure.

In addition, immediately after concrete casting plastic tubes were inserted into the top part of concrete blocks to make inlet holes for grouting. If no inlet holes were made when casting concrete, grout inlet holes would be drilled later for future grouting.

5.3.1.2 Assembly of double shear test sample

In the initial sets of concrete blocks in which there are no rifled holes left when cast, the central hole was reamed to a specified diameter to form a rifled hole. In addition, vertical grout inlet holes were drilled through the top part of each concrete block for grouting.

To accurately study and monitor the frictional interaction between adjacent joint surfaces, square grids were marked on joint surfaces. After the test, the joint contact variation can be examined.

To set up a sample, the concrete blocks were firstly placed back in the steel moulds. Then a cable bolt of desired length was inserted into the central hole, tensioned and anchored in place using a hydraulic tensioner and two barrel and wedge systems. To monitor the variation of axial loads at the cable ends during the initial cable pre-tensioning and the subsequent shearing stages, two 60 t capacity load cells were installed at the cable ends. To prevent grout from escaping, silicon gel was pasted on adjacent joint shearing surfaces and masking tape and silicon gel were used to fill the annulus gap between the cable bolt and concrete block hole at the concrete end.

Either properly mixed resin or cement grout was poured through the top grout inlet holes using a funnel to fill up the cable-concrete gap and the inlet holes. Before testing, the assembly was left to stand to allow the grout to cure. Most specimens were left for roughly seven days before being tested. Figure 5.3 shows the whole process of assembling the double shear test sample. Figure 5.4 shows a typical assembled cable bolted concrete block sample on a steel carrier base and its components.

Figure 5.3 Procedure of assembling the double shear apparatus

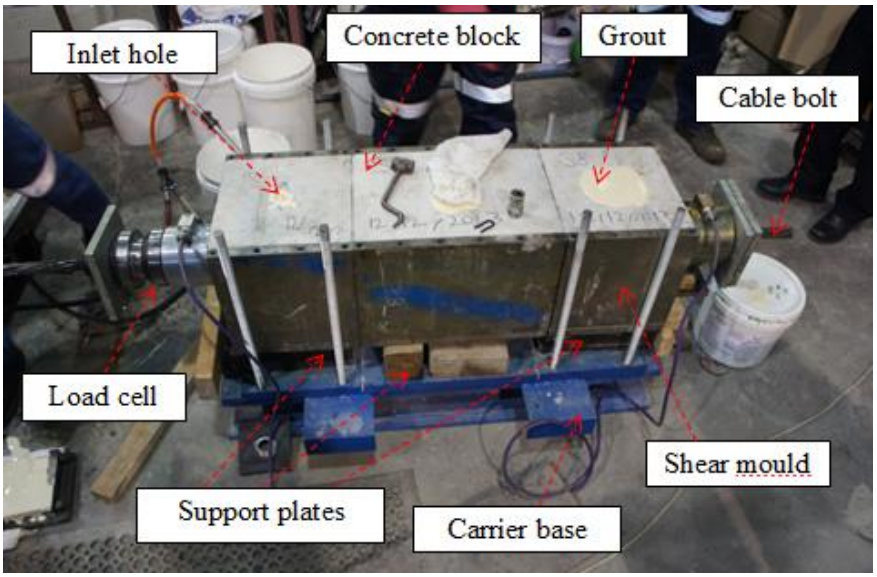

Figure 5.4 Pre-tensioned and grouted DST assembly

5.3.1.3 Testing procedure

When the shear assembly is ready for testing, the whole assembly including the base carrier was moved and placed in position on the 600×600 mm loading platen of the

500 t capacity compression testing machine as shown in Figure 5.5. All three shear boxes were seated on about 110 mm high steel and wooden plates when assembling the concrete blocks. Prior to loading, the wood plates underneath the central block were removed to allow the central block to move vertically downwards during the shearing process. Load on the central block was applied and controlled by displacement at a rate of 1 mm/min. The vertical movement was limited to 100 mm for each test due to the testing machine displacement capacity. The shear load and shear displacement were recorded by the recording system embedded in the compression testing machine, and the axial loads were recorded by a datataker connected to the load cells. During loading, the shear and axial loads and the shear displacement were monitored and simultaneously displayed visually on computer screens.

Figure 5.5 View of double shear test sample under loading

5.3.2 Test specification

As described in Chapter Four, eight types of cable strands (refer to Table 4.9) were tested in various combinations with respect to concrete strength, bolt pretension, grout type, and grouting condition. The specification of each double shear test is given in Table 5.1. All cable bolts were fully encapsulated in these tests except for

T15 and T16. In T15, the cable bolt was anchored only in the middle concrete block. In T16, the cable bolt was anchored in the middle and one side concrete blocks and had no grouting in the other side concrete block. The three grouting conditions of all double shear tests are shown in Figure 5.6.

Table 5.1 Specification of double shear test with joint friction

Test NO.	Cable type	Cable diameter (mm)	Hole diameter (mm)	Grout	Nominal pre-tension (t)	Nominal concrete strength (MPa)
T1-1	Indented JM Superstrand	22	28	Resin	25	40
T1-2	Plain JM Superstrand	22	28	Resin	25	40
T1-3	Indented TG	28	42	TD80	25	40
T1-4	Indented SUMO	28	42	TD80	25	40
T1-5		28	42	TD80	10	40
T1-6	Plain SUMO	28	42	TD80	25	40
T1-7		28	42	TD80	10	40
T1-8	Garford	15.2×2	55	BU100	0	40
T1-9	SHGC	28	42	FB400	25	40
T1-10	SHGC*	28	42	Resin	25	40
T1-11	SHGC	28	42	Resin	10	40
T1-12	Plain RT Superstrand	22	28	SB	10	60
T1-13	Plain RT Superstrand	22	28	SB	10	40
T1-14	Plain RT Superstrand	22	28	SB	0	40
T1-15	Plain RT Superstrand	22	28	SB	0	60
T1-16	Plain RT Superstrand	22	28	SB	0	60

*: strand wires were weakened due to the welding in the manufacturing process. SB: Stratabinder cement. JM: Jennmar. RT: Rio Tinto. SHGC: Secura Hollow Groutable Cable

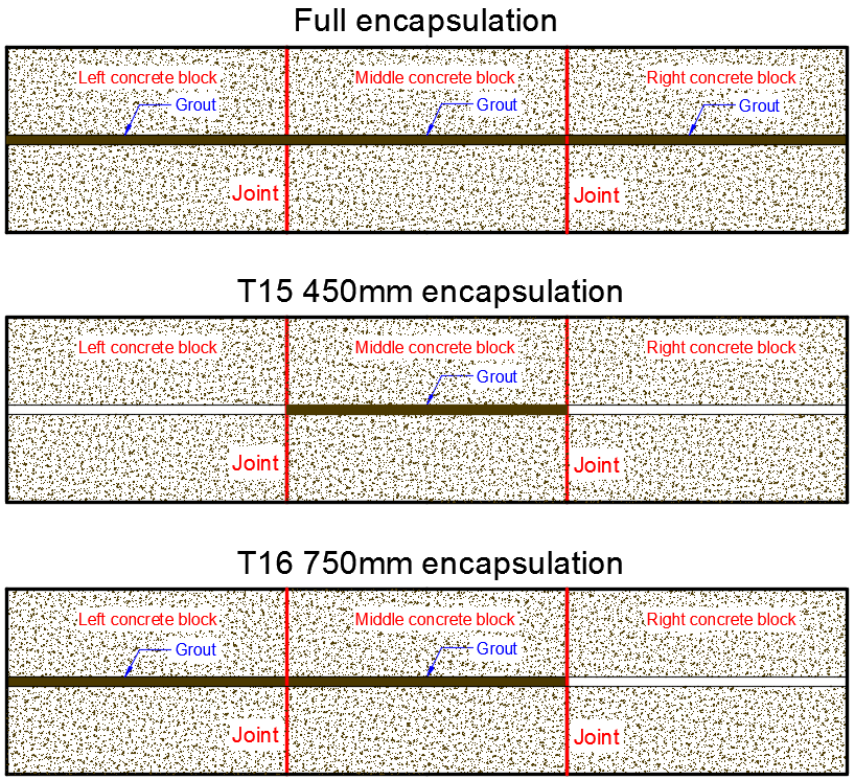

Figure 5.6 Grouting condition of double shear test

5.3.3 Test results

The relationship between the shear force and shear displacement of each tested cable bolt is shown in Appendix A. Table 5.2 summarises the results of double shear tests with joint friction.

Table 5.2 Summary of double shear test results

Test NO.	Cable type	Nominal pre-tension (t)	Shear displacement at maximum shear load (mm)	Maximum shear load (kN)
T1-1	Indented JM Superstrand	25	74.3	1115
T1-2	Plain JM Superstrand	25	65.2	1259
T1-3	Indented TG	25	72.9	1197
T1-4	Indented SUMO	25	32.6	829
T1-5		10	46.0	933
T1-6	Plain SUMO	25	58.8	1424
T1-7		10	78.9	1318
T1-8	Garford	0	82.0	1002
T1-9	SHGC	25	85.3	1601
T1-10	SHGC*	25	63.7	1053
T1-11	SHGC	10	97.6	1544
T1-12	Plain RT Superstrand	10	68.3	1402
T1-13	Plain RT Superstrand	10	69.0	1446
T1-14	Plain RT Superstrand	0	83.4	1291
T1-15	Plain RT Superstrand	0	85.7	1230
T1-16	Plain RT Superstrand	0	90.8	1038

*: Strand wires were weakened due to welding before test.

5.3.4 Result analysis and discussion

5.3.4.1 Typical force-displacement relationship of a double shear test

Figure 5.7 shows a typical shear force – shear displacement profile which was from the test of the indented JM Superstrand cable bolt. From the shear force - shear displacement profiles shown in Appendix A, it can be seen that all cable bolts showed similar force-displacement profiles to the one shown in Figure 5.7 except for T1-15 and T1-16 in which the cable bolts were not fully encapsulated.

In Figure 5.7, it can be seen that a typical double shear test experienced three distinct stages before the occurrence of cable failure during the whole shearing process. In

the first stage, the shear force increased rapidly in an approximately linear manner. The first stage ended normally at a small shear displacement before entering the second stage. In the second stage, the increasing rate of the shear force declined gradually in a steady way. This stage was a transitional stage which is usually related to the shift of cable bolt state from the elastic state to the plastic state. Thus this stage was also called 'elasto-plastic' stage (Jalalifar and Aziz, 2010b). After the transitional stage, the increasing rate of the shear force stayed uniform. Thus the third stage was also approximately linear. The third stage dominated the shear displacement in the whole shearing process until the cable failure.

The shear force – shear displacement profile was dependent upon many factors, including the concrete strength, the concrete joint friction coefficient, the cable properties, the cable pre-tension and many others. Among those, normally the cable's degree of plasticisation was thought as the dominant influencing factor of the typical three – stage profile.

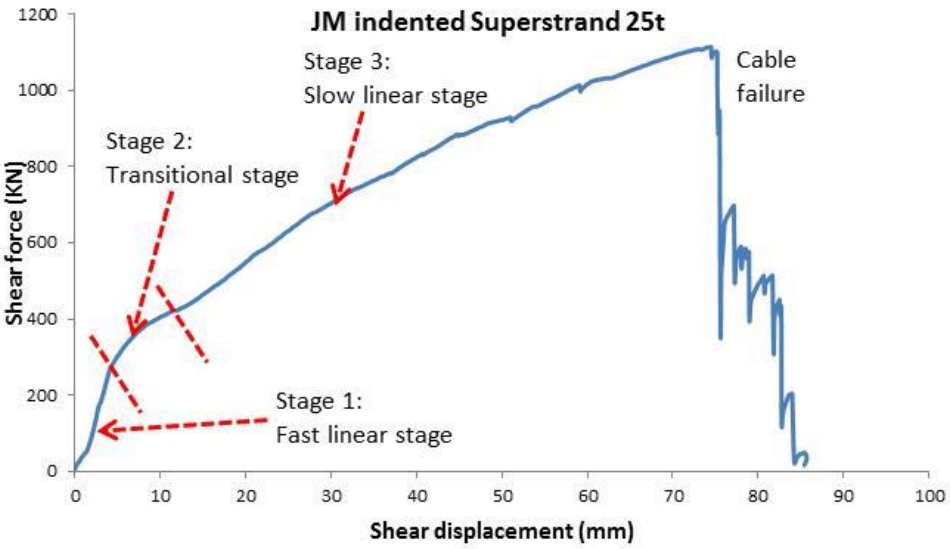

Figure 5.7 A typical shear force – shear displacement profile of the double shear test

5.3.4.2 Cable pre-tension effect

Figure 5.8 and Figure 5.9 compare the joint shear displacement and the joint shear strength at different cable pre-tensions.

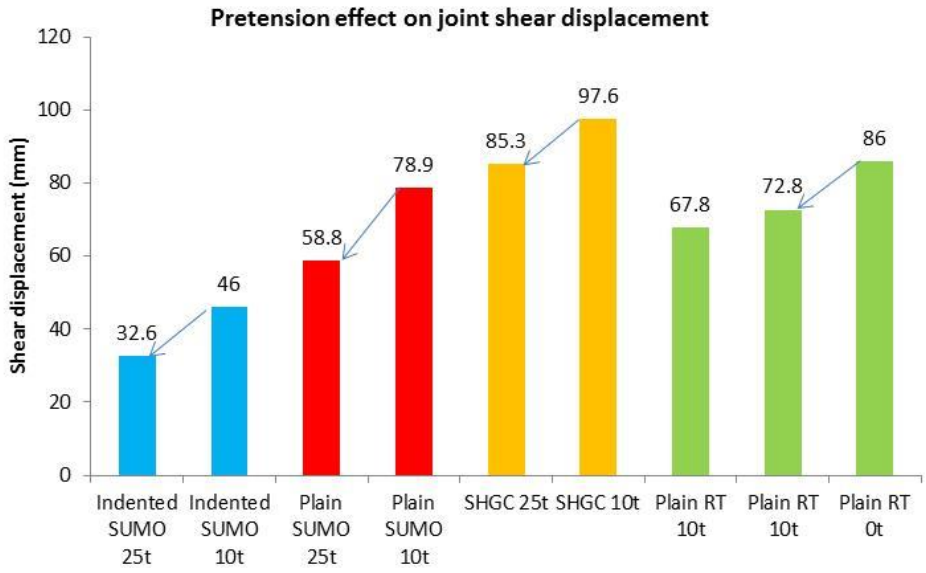

Figure 5.8 Influence of cable strand pretension on the joint shear displacement at cable failure

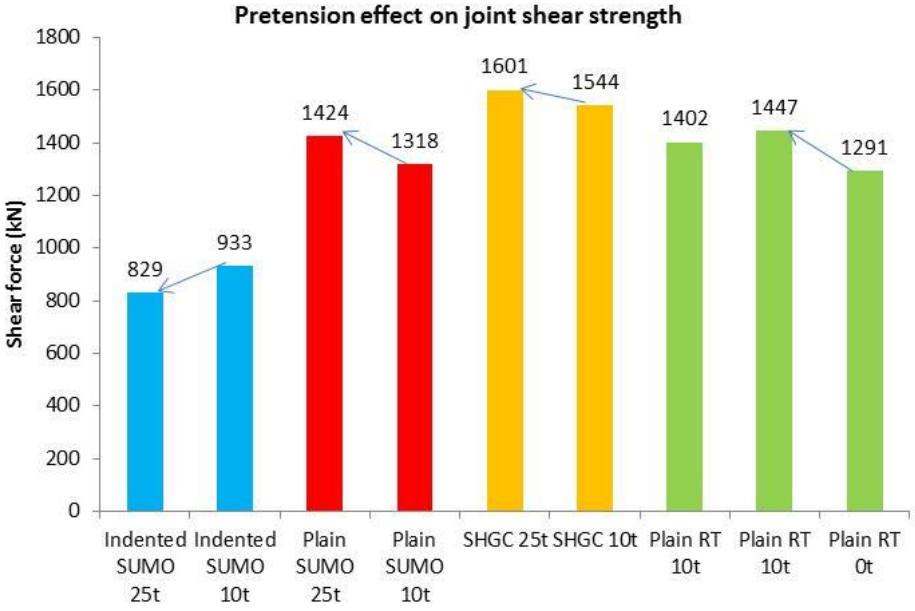

Figure 5.9 Influence of cable strand pretension on the joint shear strength

As shown in Figure 5.8, regarding the influence of cable strand pre-tension on joint shear displacement at cable failure, the test results were very consistent for all tested cable strands. The larger the cable pre-tension, the smaller the joint shear displacement at cable strand failure.

As for the influence of cable pre-tension on the joint shear strength, the test results were consistent for all tested cable strands except the indented SUMO cable strand. Cable pre-tension increased the shear strength of joints reinforced by cable strands consisting of smooth wires (plain SUMO, plain RT) or a combination of both smooth and spirally ribbed wires (SHGC). However, for the indented SUMO cable strands, cable pre-tension decreased the joint shear strength. That is to say, the cable pre-tension appeared to have different influence on cable bolted joint shear strength for indented and plain cable bolts.

Figure 5.10 shows the influence of cable strand pre-tension on the overall average shear stiffness of cable bolted joints in the pre-peak stage. Pre-tension increased the overall average shear stiffness of joints reinforced by all types of cable strands, including indented and plain SUMO, SHGC and plain RT cable strands.

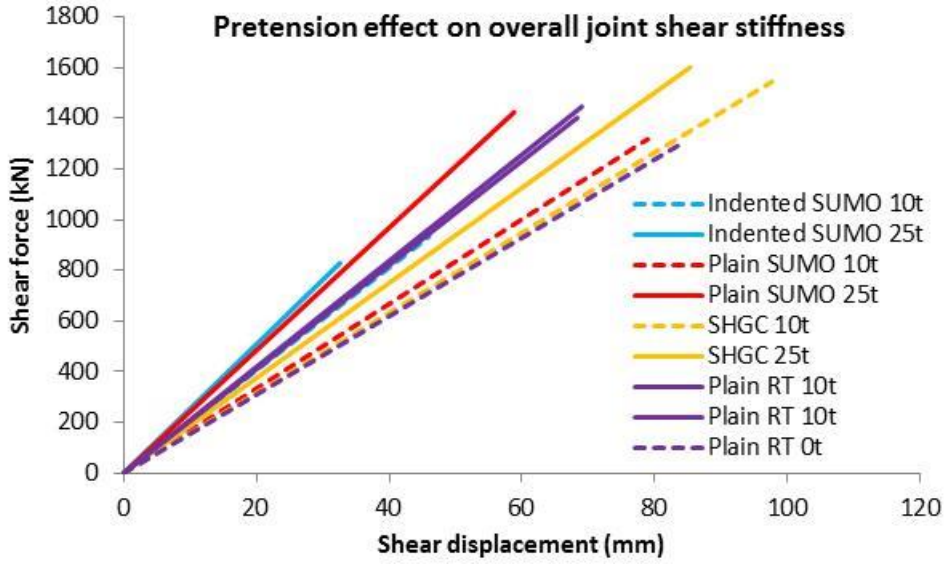

Figure 5.10 The overall joint shear stiffness of concrete joints reinforced by SUMO, SHGC and RT cable bolts

5.3.4.3 Cable strand wire profile effect

Figure 5.11 and Figure 5.12 compare the shear strength and shear displacement of concrete joints reinforced with cable bolts of different strand wire surface profiles.

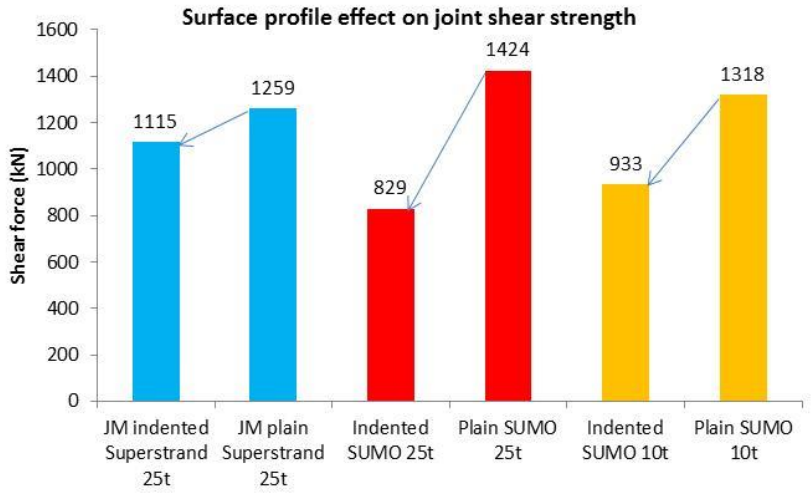

Figure 5.11 Influence of cable wire surface profile on the joint shear strength

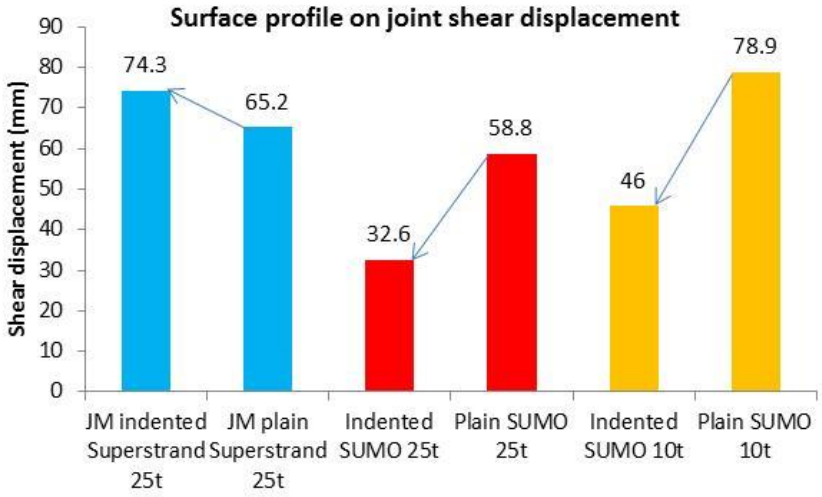

Figure 5.12 Influence of cable wire surface profile on the joint shear displacement at cable failure

As for the influence of cable wire surface profile on the joint shear strength, test results were very consistent for all tested cable strands. Concrete joints reinforced by cable bolts with indented steel wire surface produced smaller joint shear strength.

Regarding the influence of cable wire surface profile on the joint shear displacement, the test results showed a difference between the solid and hollow cable strands. For hollow SUMO cable strands, as expected, the indented cable bolt failed at smaller joint shear displacements than the counterpart of smooth wires at pre-tensions of both 10 t and 25 t. However, for the solid Superstrand cable strands, the indented cable bolts failed at larger shear displacements than the counterpart of smooth wires.

The solid Superstrand cable strands produced results which are opposite to what is expected. More tests are required in the future to prove if this is just an abnormality.

Figure 5.13 shows the influence of cable wire surface profile on the overall average shear stiffness of cable bolted joints in the pre-peak stage. Similar to the strand wire profile effect on the joint shear strength, difference was observed between hollow and solid cable bolts. For hollow SUMO cable strands, indented wire surface increased the overall average joint shear stiffness at pre-tensions of both 10 t and 25 t. However, for solid Superstrand, indented wire surface decreased the overall average joint shear stiffness.

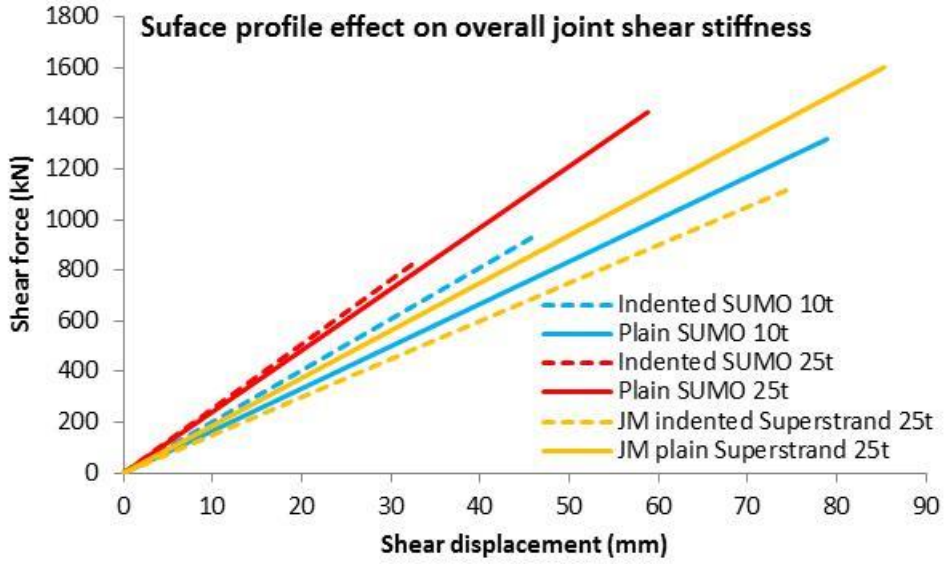

Figure 5.13 Average joint shear stiffness reinforced with SUMO and Superstrand cable bolts

5.3.4.4 Axial load development

Figure 5.14 illustrates schematically the development of the bolt axial stress along the cable bolt and the normal force across concrete joint plane during the shearing process.

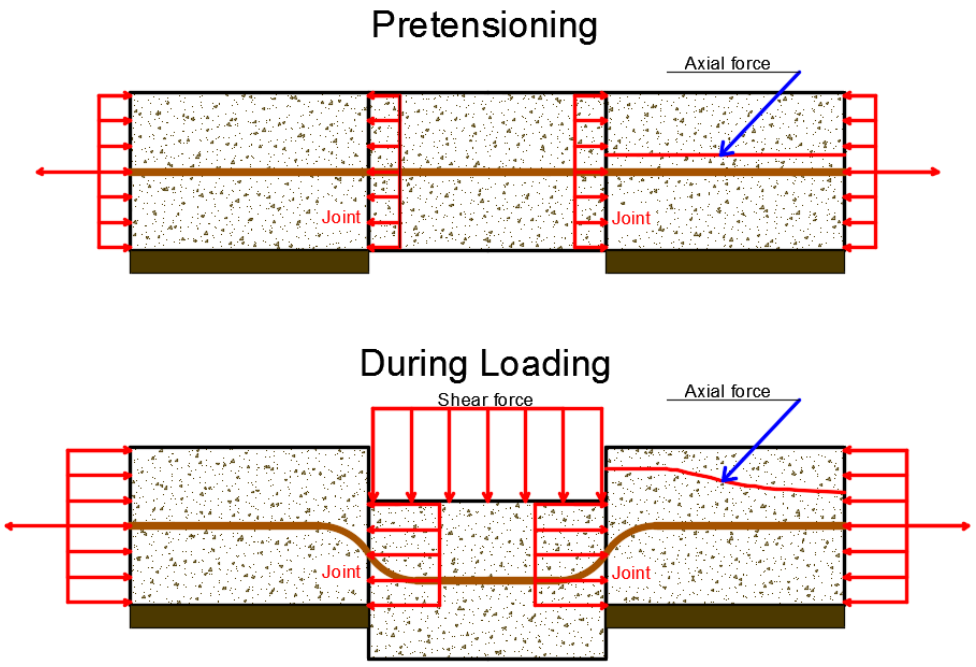

Figure 5.14 Schematic stress state of the shear system

When assembling the double shear test sample and prior to grouting, the cable strand was pre-tensioned. Before the centre block was loaded, there was no frictional effect between the cable bolt and surrounding grout encapsulation. Thus, the axial tensile force in the cable bolt was identical at each cross section of the cable strand. The confining force across each concrete joint surface was equal to the axial force in the cable strand.

During the shearing process, the cable strand bent at the joints, generating shear force and additional axial force in the cable strand near the shearing joints. The axial force in the cable strand began to increase and propagate along the cable axis from the joint to the cable ends. The axial force recorded by load cells at the cable ends began to increase when the shear-induced axial force reached the cable bolt ends from the shearing joints. Then as the central concrete block was further loaded, the axial force in the entire cable strand continued increasing. The horizontal confining force on the joint plane was larger than the reading of load cells at the cable ends due to the existence of the frictional resistance at the bolt-grout interface along the cable bolt.

Figure 5.15 shows the relationship between the shear force and the axial force increment of the first double shear test with indented JM Superstrand cable bolt. The relationships of all other cable bolts except for the SHGC cable in T1-10 and the RT Superstrand cable bolts in T1-15 and T1-16 are given in Appendix B.

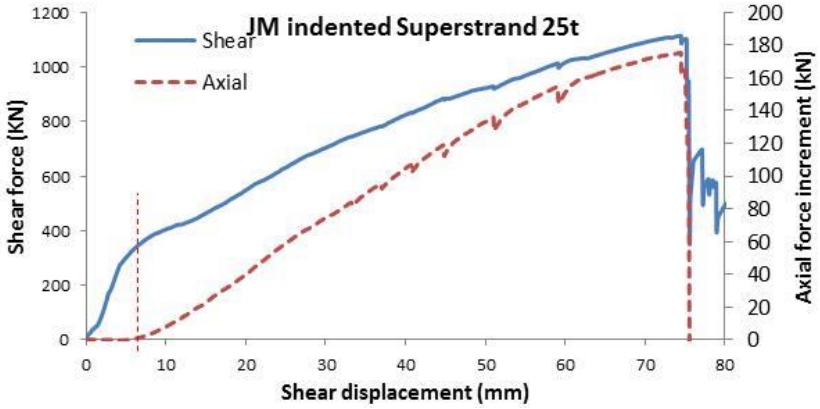

Figure 5.15 Relationship between the shear force and the axial force increment

In Figure 5.15, it is obvious that the axial force remained almost constant before the turning stage of shear force which is normally regarded as the transition of cable bolt from the elastic state to the plastic state. Beyond this elasto-plastic stage, the axial force started to increase noticeably and approximately in a linear manner. This indicated the shear-induced axial force reached the load cell at the cable strand end after the elasto-plastic stage. In addition, during the plastic stage the shear force also experienced an approximately linear increase. According to Pellet and Egger's (1996) analysis, the axial force in the bolt section between two plastic hinges beside the shearing plane would increase approximately in a linear manner in the bolt plastic stage.

Figure 5.16 summarises the joint shear force at which the axial load began to show an obvious increase. Two conclusions can be drawn:

- The cable pre-tension has influenced the relationship between the shear force and axial force at the initial shear loading stage. The higher the cable pre-tension load, the larger the shear force at which the axial load started to increase.

- The surface profile of cable wires had almost no influence on the shear force corresponding to the start of axial force increase. For both SUMO and JM Superstrand cable bolts, when the axial force started to increase, the joint shear force reinforced by the plain cable was similar to the joint shear force reinforced by the indented cable.

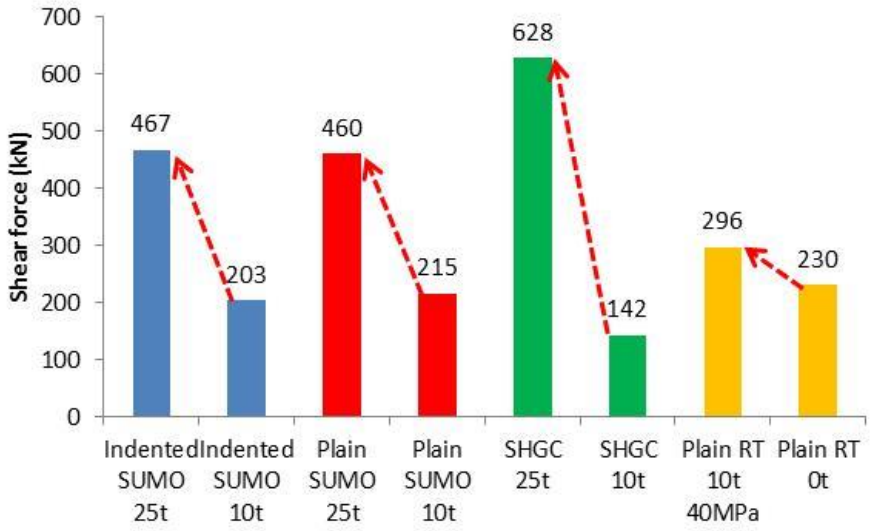

(a) Influence of cable pre-tension

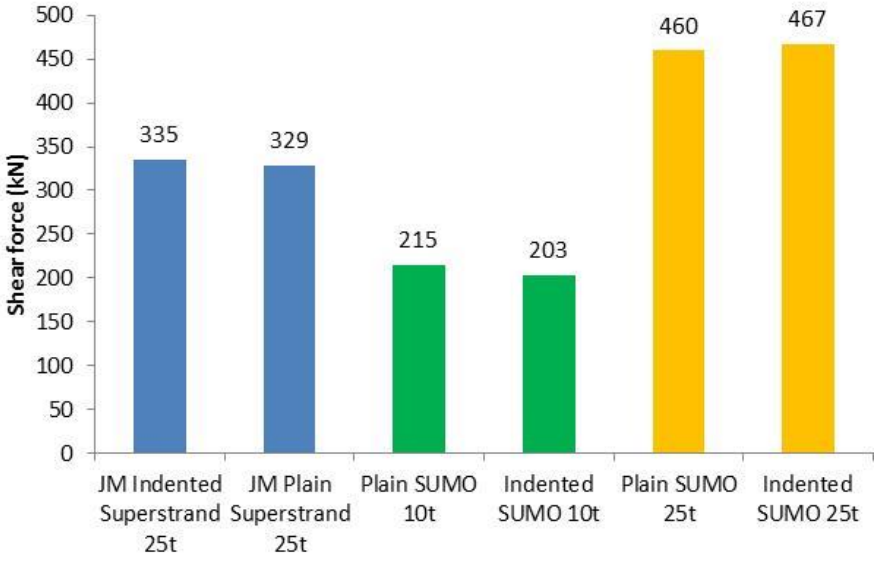

(b) Influence of cable wire surface profile

Figure 5.16 Shear force at the start of axial force increment at cable end

Table 5.3 and Table 5.4 summarise the peak axial force in double shear tests on the cable bolted joint.

Table 5.3 Influence of cable pre-tension on the peak axial force

Test	Cable structure	Average peak axial force (kN)
Indented SUMO 25t	Hollow	284
Indented SUMO 10t		293
Plain SUMO 25t		391
Plain SUMO 10t		409
SHGC 25t		462
SHGC 10t		488
Plain RT 10t	Solid	411
Plain RT 10t		\
Plain RT 0t		380

Table 5.4 Influence of cable wire profile on the peak axial force

Test	Average peak axial force (kN)
Indented JM Superstrand 25t	400
Plain JM Superstrand 25t	430
Indented SUMO 25t	284
Plain SUMO 25t	391
Indented SUMO 10t	293
Plain SUMO 10t	409

In Table 5.3, solid and hollow cable bolts experienced difference in terms of the cable pre-tension influence on the peak axial force. For the hollow cable strands, the higher the bolt pre-tension, the lower the peak axial force in general. However for the solid cable bolts, the higher the bolt pretension, the larger the peak axial force.

In Table 5.4, the cable wire surface profile also influenced the peak axial force at cable end. Since the indented wire surface provided more resistance at the cable-

grout interface, load cells installed at the cable ends recorded lower peak axial force in indented cable strands than in the plain cable strands of smooth wires.

5.3.4.5 Direct cable contribution to the joint shear strength

The cable contribution to the joint shear strength depends upon the rock/concrete strength, grout strength, bond strength of the interfaces, mechanical properties of cable bolts, joint friction characteristics and cable pre-tension (Jalalifar and Aziz, 2010b). The direct cable strand contribution to the joint shear strength can be evaluated using the following expression:

$$T_c = \frac{F_s - 2N\tan\varphi}{2F_{max}} \quad (5.1)$$

Where:

T_c, is the direct cable contribution to joint shear strength;

F_s, is the shear force of the whole double shear system;

N, is the normal force on joint shearing surface, hypothetically equal to axial load at bolt end (reading of load cells);

F_{max}, is the tensile failure load (strength) of cable bolt;

φ, is the friction angle of concrete block joint surface.

In the double shear tests, F_s, φ and F_{max}can be easily obtained, while the normal force (N) acting on the shearing joint were not recorded. The load cell reading at cable strand ends might be thought to be equal to the normal force at the joint shearing plane, which is obviously incorrect due to the frictional resistance at the cable-grout interface as discussed in the previous section (5.3.4.4).

Prior to and after grouting, the axial tensile force acting on all cross sections of the cable bolt was identical. Then during the grout curing stage, the axial tensile force might fall slightly at different cross sections due to the possible relaxing of the cable wires. When the double shear assembly was mounted in the compression machine,

the axial load in the cable strand at the joint was still equal to the reading of load cells at the cable end. Thus prior to testing, according to the equilibrium of forces at the joint the normal confining force on the concrete joint plane remained equal to the cable axial force at the joint plane and other cross sections.

During the first 1 mm to 2 mm joint shear displacement, the cable strand deformation was very small. It is reasonable to assume that the normal confining force at the joint did not vary much during this period. Thus the friction force on the concrete joint varied only due to the variation of the joint friction coefficient as discussed in Section 4.2.2 of Chapter Four. Considering that the shear force of the shear system was a combination of the joint friction and the cable dowel force, the shear force of the bolted system should be larger than the unbolted double shear system as described in Section 4.2.2. All shear force-displacement curves of bolted concrete blocks should lie above the shear force-displacement curves obtained from the test on the unbolted concrete joint at the same shear displacement.

Figure 5.17 shows the relationship between the shear force and shear displacement of double shear tests, with and without the reinforcement of cable bolts. It is observed that all curves of concretes blocks reinforced with cable strands were below the curve of the unbolted concrete blocks at the same pre-tension load. There were two possible reasons for this. One is that the normal force at the joint had fallen in all tested samples prior to loading. The other is that with the potential relative separation of concrete blocks, the confining stress on joint surfaces was reduced, which lowered the required shear force to press down the middle concrete block. The occurrence of the concrete block separation was previously reported and investigated by Song (2003) and Jia *et al.* (2007). They termed this behaviour as the ‘rail’ effect of bolt in reinforcing discontinuous rock mass. It was emphasised that this ‘rail’ effect would weaken the shear strength of the discontinuous rock mass.

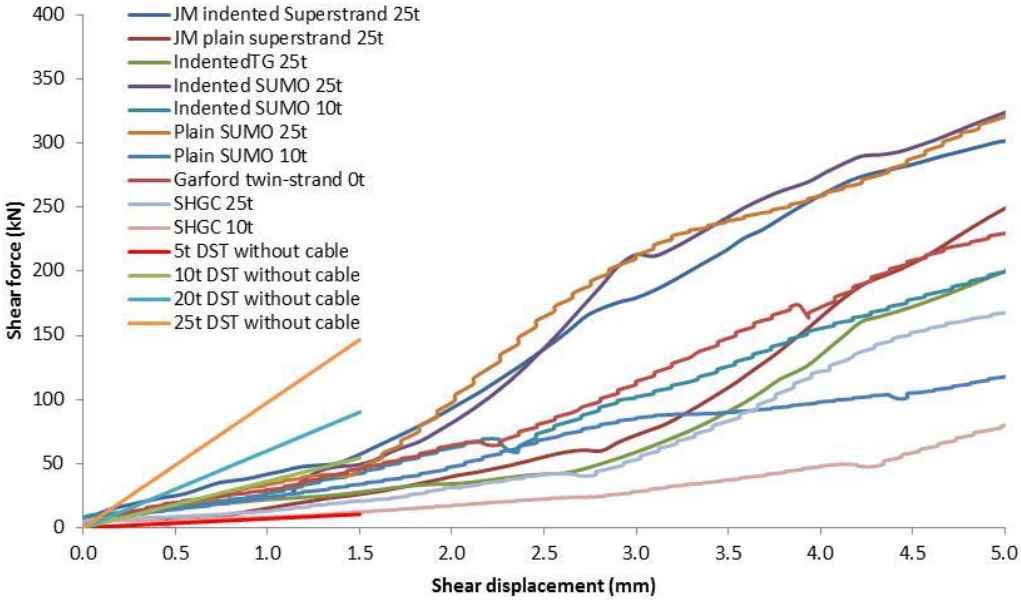

Figure 5.17 Shear force - shear displacement relationships of double shear tests with and with cable reinforcement at the initial loading stage

Figure 5.18 shows the direct cable bolt contribution to the joint shear strength calculated in accordance with Eq. (5.1). The shear force and the joint shear displacement were standardized by the cable bolt tensile strength and the cable bolt diameter respectively.

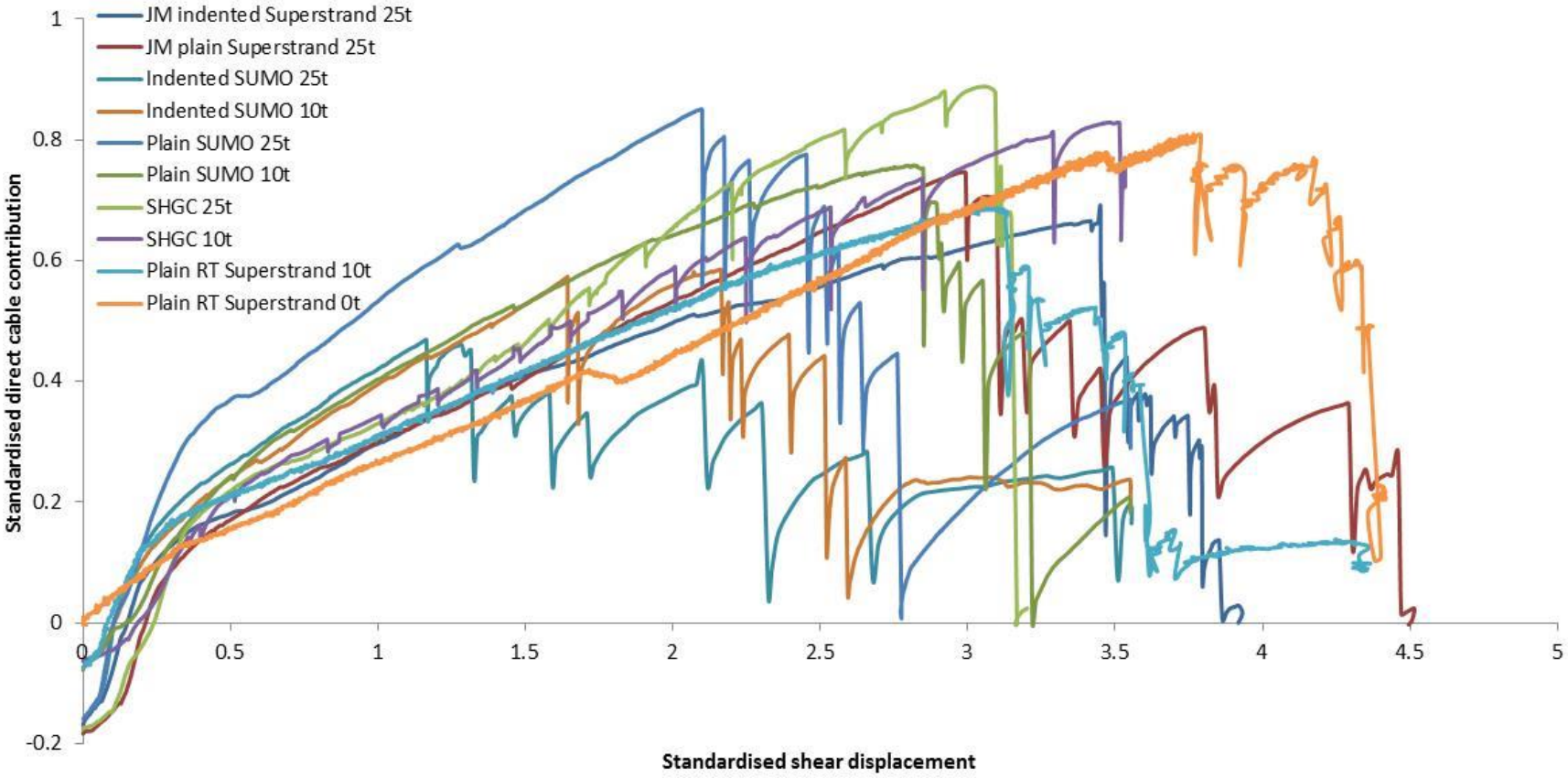

Figure 5.18 Relationship between the direct cable bolt contribution to joint shear strength and the joint shear displacement

It is seen that in the initial loading stage the direct cable contribution was negative in Figure 5.18. Several factors could contribute to this. According to Eq. (5.1), all factors increasing the joint confining stress (N) and the joint friction coefficient would contribute to this negative direct cable–joint contribution. Firstly, the two factors leading to the results shown in Figure 5.17 also contributed to the results shown in Figure 5.18. Secondly, the joint friction coefficient used in the calculation was 0.44 which was obtained in the stable stage, whilst the true friction coefficient in the initial stage increased from zero to about 0.44 as presented in Section 4.2.2 of Chapter Four. Another possible reason was shown in Figure 5.19. In Eq. (5.1), the joint confining stress (N) was N_{joint} in Figure 5.19. According to the equilibrium of forces at the joint, N_{joint} equals the horizontal component (N_{oh}) of axial force at point O (N_o). Due to the deflection of the cable bolt and the weak friction of grout, the axial force at point O (N_o) was slightly larger than the axial force at point A (N_A). Point A was the demarcation point of the cable deflecting section and the cable straight section. Because of the grout resistance in the section AB, the cable axial force at point A (N_A) was larger than that at point B (N_B). $N_B$was equal to the reading of load cells. Based on the above force relations from point O to point B, the exact relationship between N_{joint} and $N_B$was not attainable. Nevertheless, N_{joint} and N_B were thought to be equal for simplification in past research (Grasselli, 2005; Jalalifar and Aziz, 2010b). If N_{joint} was smaller than N_B, the used joint confining force in Eq. (5.1) would be larger than the true joint confining force, which led to a negative direct cable contribution in the calculation.

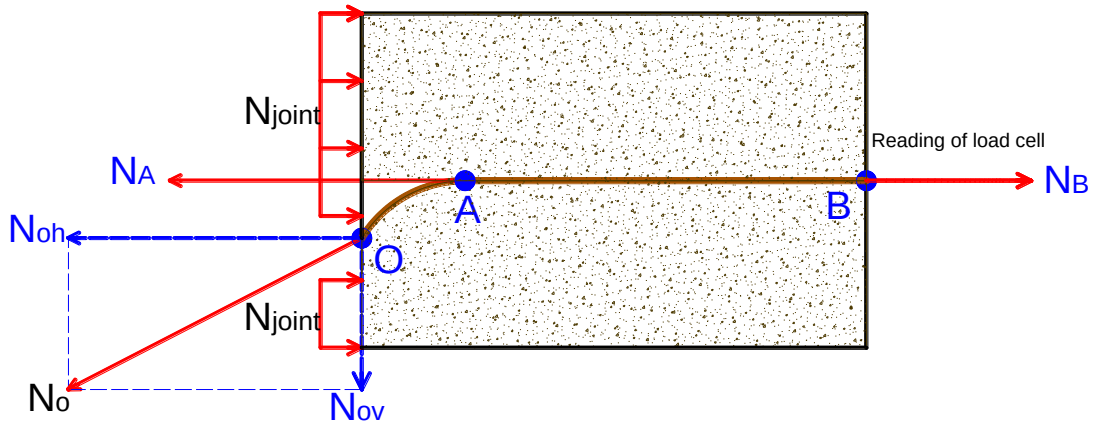

Figure 5.19 Relationship between the joint confining force and the load cell reading

Figure 5.20 shows the cable pre-tension effect on the direct cable-joint contribution. The cable pre-tension effect on the direct cable-joint contribution was not consistent between smooth and indented cable strands. The direct cable-joint contribution increased with cable pre-tension increasing for smooth cable bolts (Plain SUMO and SHGC), but it was exactly opposite for indented SUMO cable strands.

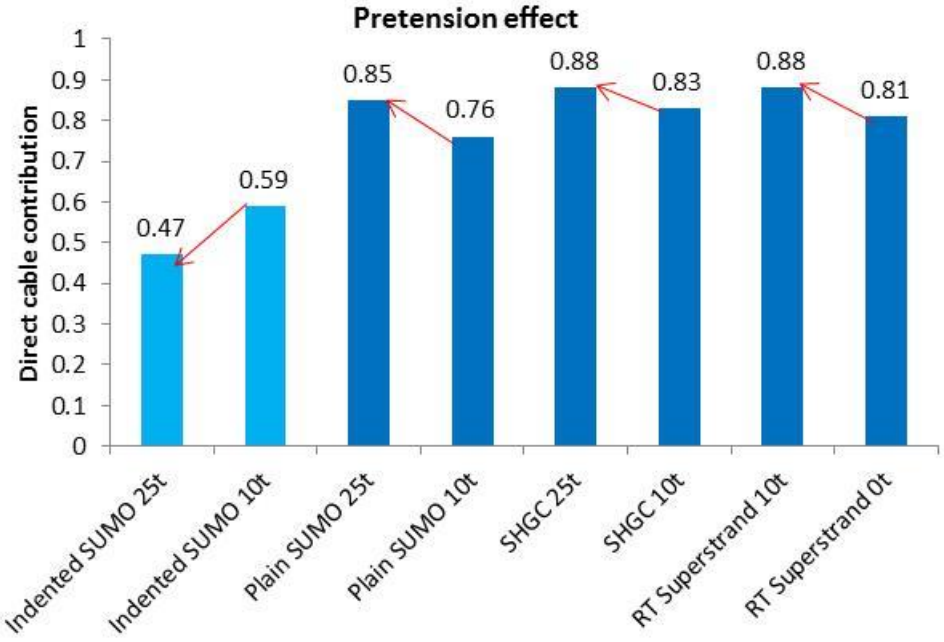

Figure 5.20 Pretension effect on direct cable-joint contribution

Figure 5.21 shows the cable wire profile effect on the direct cable-joint contribution. Cable wire profile effect on the cable-joint contribution was consistent among all tested cable strands irrespective of cable strand type and pre-tension load. Specifically, the maximum direct cable-joint contribution decreased from 0.75, 0.85 and 0.76 to 0.69, 0.47 and 0.59 for JM Superstrand 25 t, SUMO 25 t and SUMO 10 t, respectively.

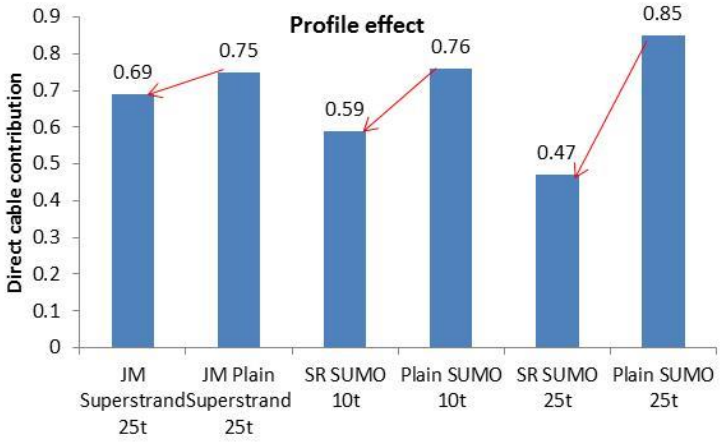

Figure 5.21 Profile effect on direct cable-joint contribution

5.3.4.6 Relationship between the shear and normal forces and stresses

Figure 5.22 illustrates the relationship between the shear force and normal force of the double shear tests on different cable bolted jointed concrete blocks.

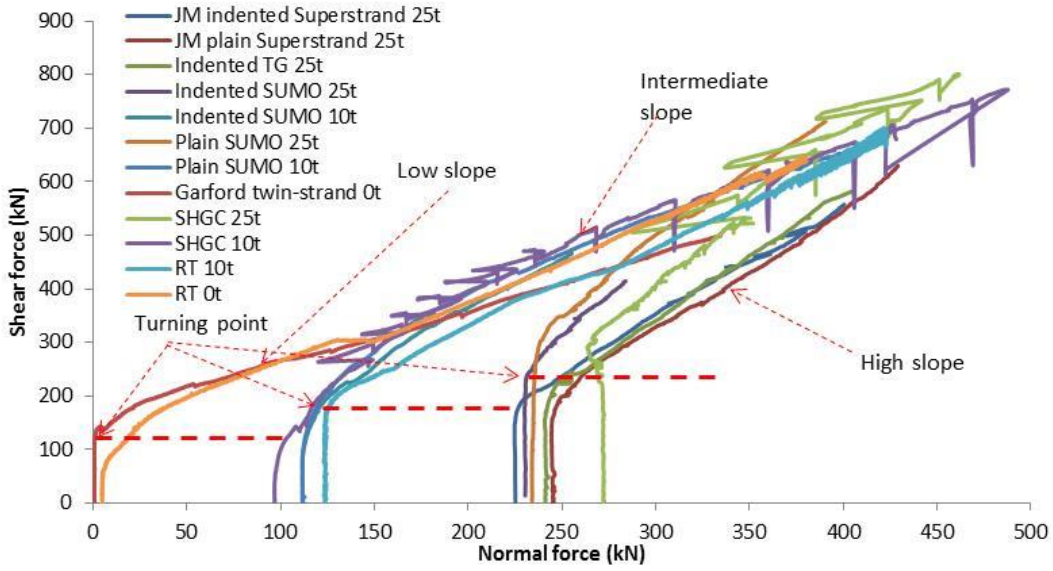

Figure 5.22 Relationship between the shear forceandthe normal force of cable bolted jointed concrete blocks

Since the concrete joint contact surface area varied during the shearing process, the accurate contact area was practically unobtainable in the test. Thus it is impossible to attain the accurate shear and normal stresses at the concrete joint based on the recorded shear and normal forces. If it is assumed that the concrete joint surfaces were in full contact with each other during shearing (this is not the real situation), the

shear and normal stresses can be obtained. Based on the recorded shear and axial forces and the joint shear displacement, the corresponding shear and axial stresses can be gained using the following equations:

$$\tau = \frac{F_s}{0.3(0.3-S)} \tag{5.2}$$

$$\sigma_n = \frac{F_n}{0.3(0.3-S)} \tag{5.3}$$

Where:

F_s, is the shear force of the shear system;

F_n, is the normal force on joint plane;

τ, is the shear stress of the system;

σ_n, is the normal stress calculated based on the reading of load cells;

S, is the joint shear displacement.

The relationship between the shear and normal stresses based on the above equations is shown in Figure 5.23.

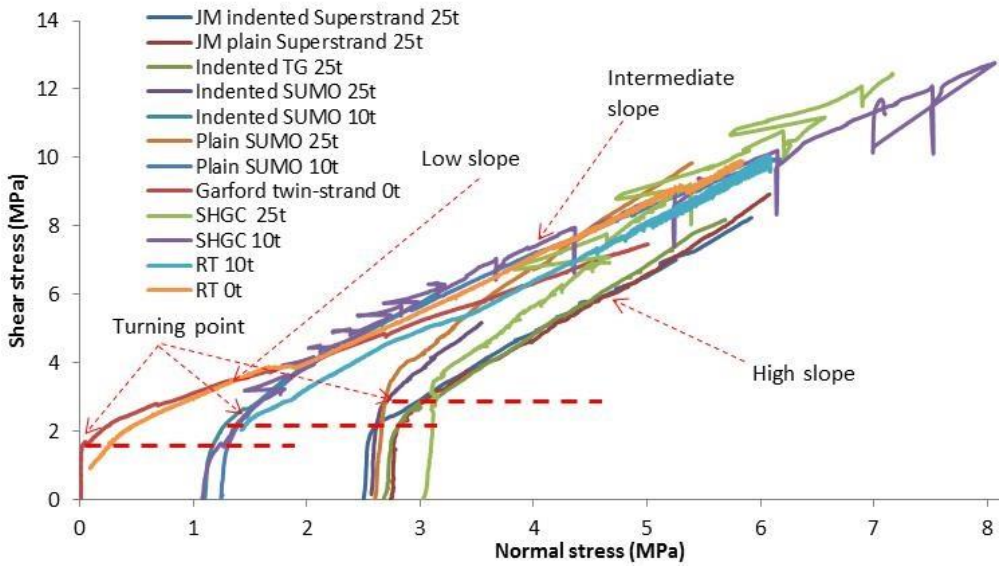

Figure 5.23 Relationship between the shear stress and normal stress

In a typical shear force-shear displacement profile, there are two obviously different stages separated by a turning point (or a transition section) which is ordinarily related to the plasticization of cable bolts. Considering the axial force of cable bolts (normal force action on the joint plane), two Mohr-Coulomb criteria could be established for the cable bolted joint. One is for the stage before the turning point and the other is for the stage after the turning point. Since the normal force was recorded by load cells at the end of the cable strands, the reading of load cells did not vary (see Figure 5.22) until the shear-induced axial force propagated to the load cell. Thus, the Mohr-Coulomb criterion for the first stage before the turning point cannot be achieved experimentally. Analytical result of the normal force at the joint is required for the first stage. Here, the Mohr-Coulomb criterion for the second stage is analysed based on the test results.

The shear force and normal force of the second stage are extracted and best linearly fitted and listed in Appendix C. The stress relationship is fitted and listed in Appendix D.

The relationship obtained from the regression analysis can be expressed as follows:

$$F_s = aF_n + b \tag{5.4}$$

$$\tau = a'\sigma_n + b' \tag{5.5}$$

Where: a, b, a', b', are the regression coefficients.

From the regressed equations between the shear stress and normal stress, the slope and intercept of the second stage can be obtained. The slope of the stress profile represents the friction coefficient of the bolted concrete joint. However, the obtained intercept from the stress regression analysis was not the real cohesion because the axial force loss due to the friction resistance at the cable-grout interface and the cable pre-tension were not considered in the above regression.

The slope of the force and stress profiles of all tested cable bolts is summarized and listed in Table 5.5.

Table 5.5 Summary of Slopes of force and stress profiles

Test	Slope of force relationship	Slope of stress relationship
Indented JM Superstrand 25 t	2.07	1.80
Plain JM Superstrand 25 t	2.26	1.95
TG 25t	2.37	2.06
Indented SUMO 25 t	3.27	2.73
Indented SUMO 10 t	2.06	2.03
Plain SUMO 25 t	2.60	2.35
Plain SUMO 10 t	1.49	1.52
Garford twin-strand 0 t	1.00	1.09
SHGC 25 t	2.72	2.35
SHGC 10 t	1.44	1.48
RT Superstrand10 t	1.62	1.62
RT Superstrand 0 t	1.40	1.46

From the above figures and tables, the following conclusions can be drawn:

- As shown in Figure 5.22 and Figure 5.23, the turning point between the shear and normal forces of the cable bolted joint was influenced profoundly by the cable pre-tension force. Generally, the higher the pre-tension, the larger the shear force at the turning point. This was the same as the tests on rock bolts conducted by Aziz *et al.* (2003).

- As shown in Table 5.5, the cable pre-tension had a great influence on the friction coefficient of the shear system in general. The higher the cable pre-tension, the larger the friction coefficient of the bolted concrete joint.

- As shown in Table 5.5, the influence of cable wire surface profile on the joint friction coefficient was different. For the solid cable strand (JM Superstrand), the indented wire surface lowered the joint friction coefficient slightly. However, for the hollow cable strands (SUMO), the indented wire surface increased the joint friction coefficient significantly.

- The slopes of the force relationship and stress relationship were not exactly the same. This was due to the decrease in the joint contact surface area. If the concrete joint contact area remained constant during the shearing process, the slope of the regressed force and stress relationships would be the same.

- The cohesion of the cable bolted concrete system cannot be obtained because the accurate axial load loss along the cable strand was not known.

5.3.4.7 Failure modes and patterns of cable wires

When subjected to lateral shearing displacement, cable bolt wires tended to fail individually in different failure modes. The cable wire failure mode could be compared with the recorded loads to study the loading state and failure process of the cable bolt. Following each double shear test, the failure mode of all cable wires was examined and recorded for further analysis. The wire failure modes of the first sixteen cable bolt in double shear tests with joint friction are listed in Appendix E. Table 5.6 summarises the number of different failure modes of the snapped cable strand wires.

Table 5.6 Statistics of cable wire failure mode

Test NO.	Profile	Failure mode			Comment
		In tension	In shear	Total failure	
T1-1	Indented	6	13	19	40 MPa concrete blocks without aggregates
T1-2	Plain	17	2	19	
T1-3	Indented	0	9	9	
T1-4	Indented	0	12	12	
T1-5	Indented	5	4	9	
T1-6	Plain	9	0	9	
T1-7	Plain	9	0	9	
T1-8	Plain	10	5	15	
T1-9*	SR	3	0	3	
	Plain	4	1	5	
T1-11	SR	4	0	4	
	Plain	5	0	5	
SR (percentage)		18 (32%)	38 (68%)	56	\
Plain (percentage)		54 (87%)	8 (13%)	62	
Sum (percentage)		72 (61%)	46 (39%)	118	
T1-13	Plain	10	9	19	40 MPa concrete blocks with aggregates
T1-14	Plain	8	8	16	
Plain (percentage)		18 (51%)	17 (49%)	35	\
T1-12	Plain	8	11	19	60 MPa concrete blocks with aggregates
T1-15	Plain	5	12	17	
T1-16	Plain	4	9	13	
Plain (percentage)		17 (35%)	32 (65%)	49	\

*: One cable wire failing in a combination of tension and shear was not considered; SR is short for spirally ribbed. SR cable wires are regarded as indented wires in the following analysis.

The statistics in Table 5.6 clearly demonstrate some characteristics of the failure mode of cable wires. The statistics can be divided in general into two groups with respect to the aggregate inclusion, the tests in concrete blocks without aggregates and the tests in concrete blocks with aggregates. Considering all tested plain and

indented cable strands (T1-1 to T1-11) in concrete blocks without aggregates, tension failure of cable wires was the main failure mode accounting for roughly 61%, and the remaining 39% of failure was in shear. In addition, it is shown that indented and plain cable wires failed differently. Most plain wires failed in tension (87%), but an opposite result for the indented cable wires of which 68% were failure in shear.

Yet, the result of tests in concrete blocks with aggregates showed some difference compared to that without aggregates. The two tests (T1-13and T1-14) on plain cable bolts in concrete blocks with aggregates showed that 49% of failures were in shear compared to only 13% in tests without aggregates. This indicated the significant influence of concrete/rock ingredient on the cable wire failure mode.

Additionally, the concrete blocks in T1-12, T1-15 and T1-16 were stronger (60 MPa) than in T1-13 and T1-14. More cable wire failures in shear occurred in the strong concrete blocks than in the weak. The former witnessed 65% failure in shear compared to 49% failure in shear of the latter.

Based on the above analysis, the following conclusions can be drawn:

- The aggregates in concrete blocks affected the cable wire failure mode. The inclusion of aggregates in concrete blocks caused more cable wire failures in shear;

- The cable wire profile affected the cable wire failure mode. More failures in shear were witnessed in indented cable bolts than in plain cable bolts.

- Strong concrete blocks caused more cable wire failures in shear than the weak concrete blocks.

5.4 Double shear test without joint friction

When bolted fractured rock strata slide along the rock discontinuities, the induced friction force on the sliding plane is one of the main sources of the rock joint shear resistance. The presence of friction on the rock fracture plane significantly enhances

the shear resistance of the rock joint shear plane. Besides the friction contribution to the rock joint shear resistance, the direct bolt contribution (also called 'dowel' effect) is the other main contribution. To fully understand the joint-reinforcing behaviour of bolts, it is necessary to separate these two contributions in analysis. However, in laboratory study, it is difficult to separate the joint friction contribution from the total. This is mainly due to the variation of the joint friction coefficient and the difficulty in measuring the confining force on the shearing joint plane during the shearing process as discussed previously. Performing tests on bolted rock joints without joint friction helps avoid the presence of the joint friction contribution and the total shear resistance is attributed to the bolt dowel effect. This helps understand the bolt dowel effect and in turn, also facilitates the understanding of the joint friction contribution through the comparison with shear test with joint friction.

5.4.1 Test apparatus

To eliminate the joint friction effect, there are two methods in principle: reducing the joint friction coefficient to zero or making a gap at the shearing joint. The former is impossible in practice. The latter method was used in this study as the main technique to eliminate the joint friction effect. The test apparatus used in the double shear test with joint friction was also used in the double shear test without joint friction. When setting up the double shear test assembly, a gap could be kept at the joint using the original double shear test apparatus. Yet, the gap would disappear when the concrete sample was pre-tensioned or when the side concrete blocks were pulled towards the middle block during the loading process. Additional devices are required to maintain the joint gap during the process of pre-tensioning and shearing. A steel frame was designed to realize this, as shown in Figure 5.24. The frame comprised two 30 mm thick steel plates, four long steel bars and a number of washers and bolts for connection. The specific dimensions of each frame component are given in Table 5.7.

The assembly procedure was similar to that without the external steel frame. After the concrete blocks were positioned in the double shear mould, a 10 mm thick rubber ring of suitable dimension was placed and held by a steel wire at the concrete joint in

line with the concrete central hole. The rubber ring was used to bridge the central hole between the side and the middle concrete blocks for grouting. Then a cable bolt with a desired length was inserted into the concrete central hole and the rubber rings. After the cable bolt was installed, the steel wires used to hold the rubber rings were removed. The side concrete blocks were pushed towards the central block to press the rubber rings from both sides and also to make a small gap of equal width at the shearing joint. The rubber rings allowed the grout to flow between the middle and side concrete holes without leaking. The side concrete blocks were sealed at their outer end around the cable to prevent grout leaking. The side steel plates of the external frame shown in Figure 5.24 were then installed at the ends of the concrete sample with the cable bolt through the central hole of the plates. After that, the four arm bars were put beside the concrete sample and bolted together with the two side steel plates. Thereafter, the installation of load cells, washers and barrel, wedge assemblies and other components was the same as the test with joint friction presented previously. The double shear test assembly with the external steel frame is shown in Figure 5.25.

After assembling the sample, the remaining procedure of pre-tensioning and shearing was exactly the same as the double shear test with joint friction. The specific process is not introduced here.

Figure 5.24 Main components of the steel frame used to maintain the joint gap

Table 5.7 Dimension of the frame components

Name	Length (mm)	Width (mm)	Height (mm)
Steel plate	520	350	30
Arm bar	1050	100	40
Washer	100	40	3
Bolt	70	\	\

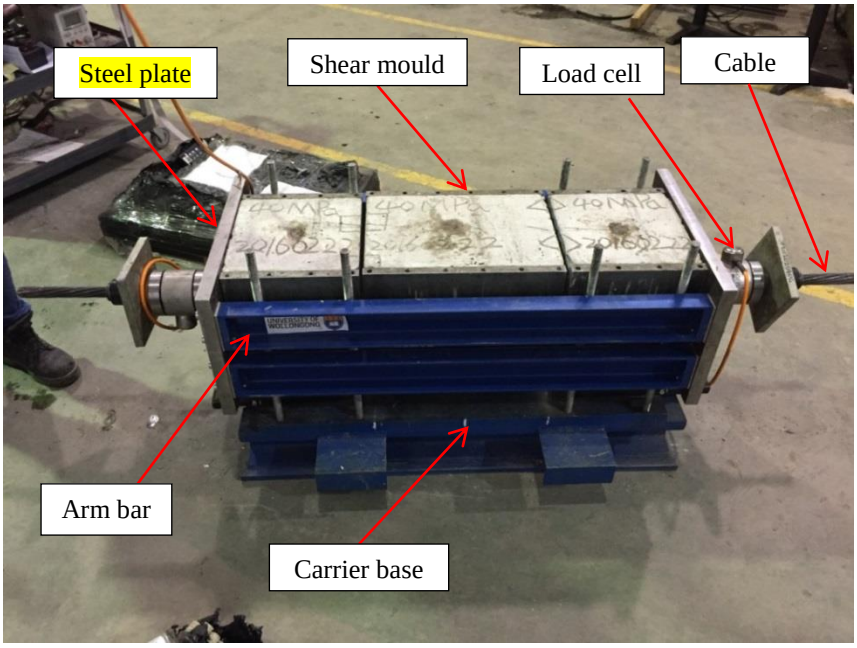

Figure 5.25 Double shear test assembly with the external frame to maintain the gap at joints

5.4.2 Test specification

Eight cable bolts in total were tested using the modified double shear test apparatus, including four plain Rio Tinto Superstrand cable bolts, two plain Sumo cable bolts and two indented Sumo cable bolts. The specific configuration of each double shear test is given in Table 5.8.

Table 5.8 Specification of double shear test with joint friction

Test NO.	Cable type	Cable diameter (mm)	Hole diameter (mm)	Grout	Nominal pre-tension (t)	Nominal concrete strength (MPa)
T2-1	Plain RT Superstrand	22	28	SB	15	40
T2-2					0	
T2-3					10	
T2-4					0	
T2-5	Plain SUMO	28	42		15	
T2-6					0	
T2-7	Indented SUMO				15	
T2-8					0	

SB: Stratabinder cement

It should be noted that though there were four plain RT cable bolts in the double shear test without joint friction as shown in Table 5.8, it was not reasonable to compare the first two cable bolts with the second two. This was because the setup of the test sample was different. As mentioned previously, ring rubbers were used to bridge the concrete hole at the shearing joint. Yet, this technique was used from the third test on, but not for the first two tests. When assembling tests T2-1 and T2-2, the concrete hole was enlarged irregularly by hammering and PVC pipes were inserted into the hole as a bridge tunnel at the joint. Figure 5.26 schematically shows how the concrete hole was connected at the joint. Since the cable bolt mainly deformed in a short section close to the joint during the shearing process, the use of the PVC pipes and the presence of the irregularly enlarged section around the concrete hole could significantly weaken the reactive compression of grout and concrete especially in the initial loading stage. The cable bolt could easily deform to fit the irregular concrete hole and the shear performance of the bolted concrete joint would be accordingly different. Thus, in the analysis section, tests T2-1 and T2-2 and tests T2-3 and T2-4 were separately analysed.

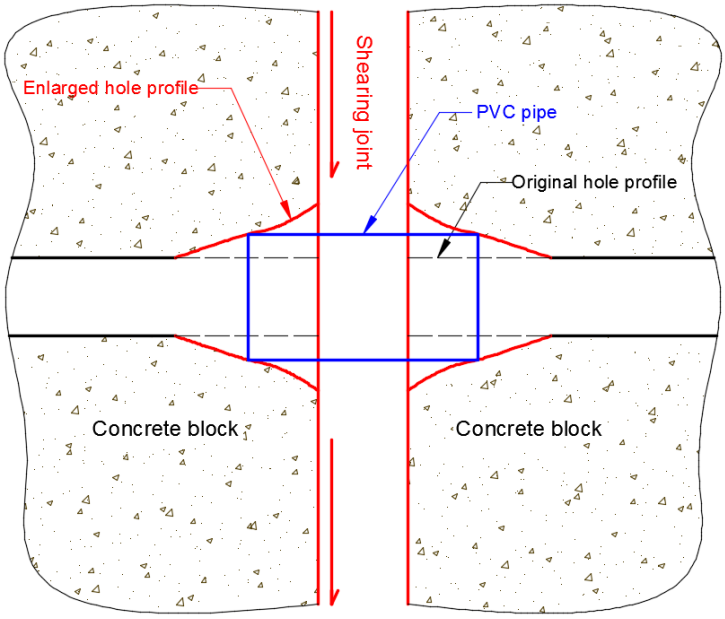

Figure 5.26 Schematic of the concrete hole connection with PVC pipe

5.4.3 Test result

Similar to the previous double shear tests with joint friction, the shear force, the joint shear displacement and the axial force were recorded during the shearing process. These recorded loads are given in Figure 5.27. The maximum shear force and the corresponding joint shear displacement are summarised in Table 5.9.

Table 5.9 Specification of double shear test with joint friction

Test NO.	Cable type	Nominal pre-tension (t)	Nominal concrete strength (MPa)	Maximum shear force (kN)	Shear displacement (mm)
T2-1	Plain RT Superstrand	15	40	774	85.2
T2-2		0		884	95.3
T2-3		10		738	89.7
T2-4		0		761	95.4
T2-5	Plain SUMO	15		852	88.2
T2-6		0		886	105
T2-7	Indented SUMO	15		767	85.7
T2-8		0		815	93.4

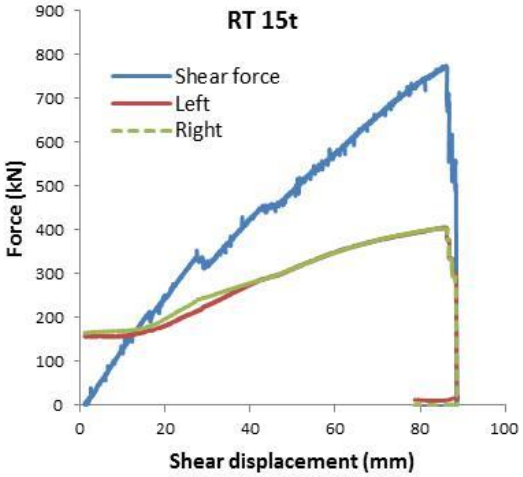

(a) T2-1

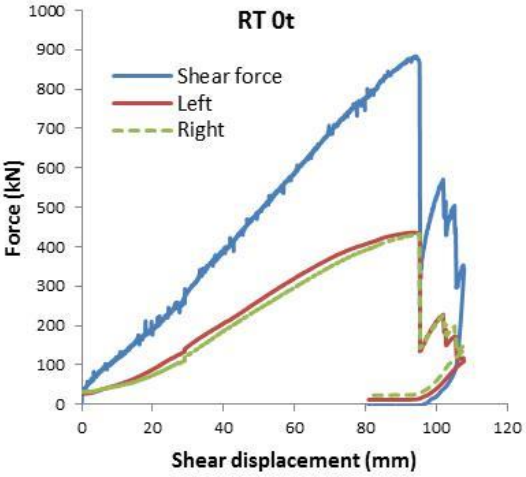

(b) T2-2

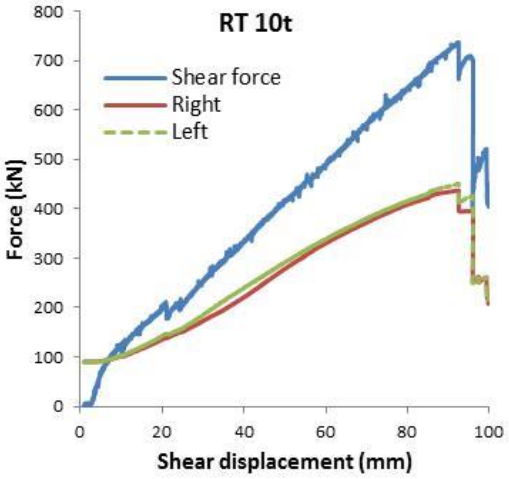

(c) T2-3

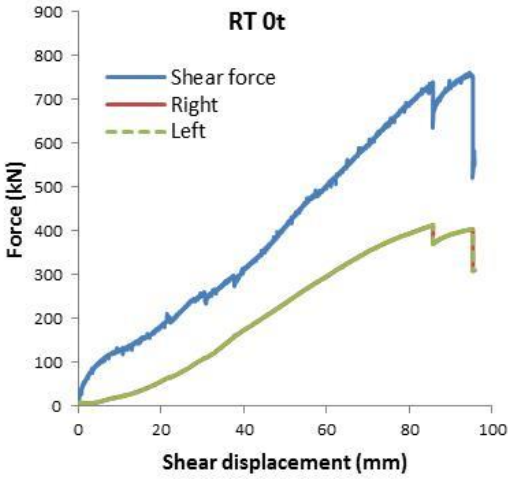

(d) T2-4

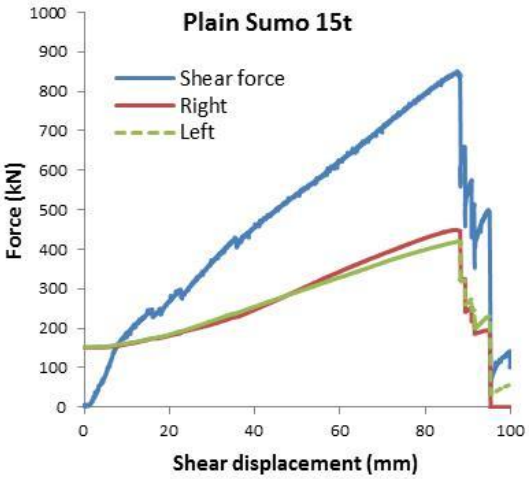

(e) T2-5

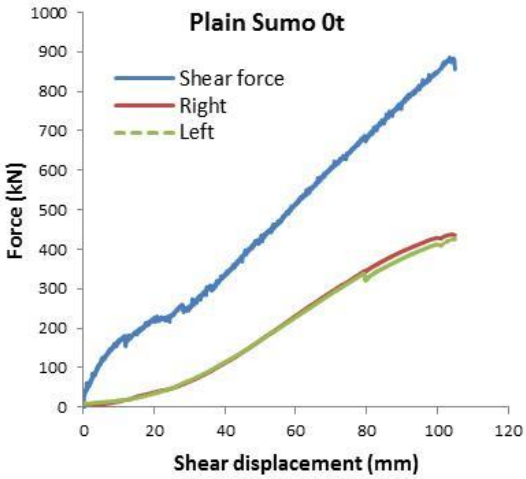

(f) T2-6

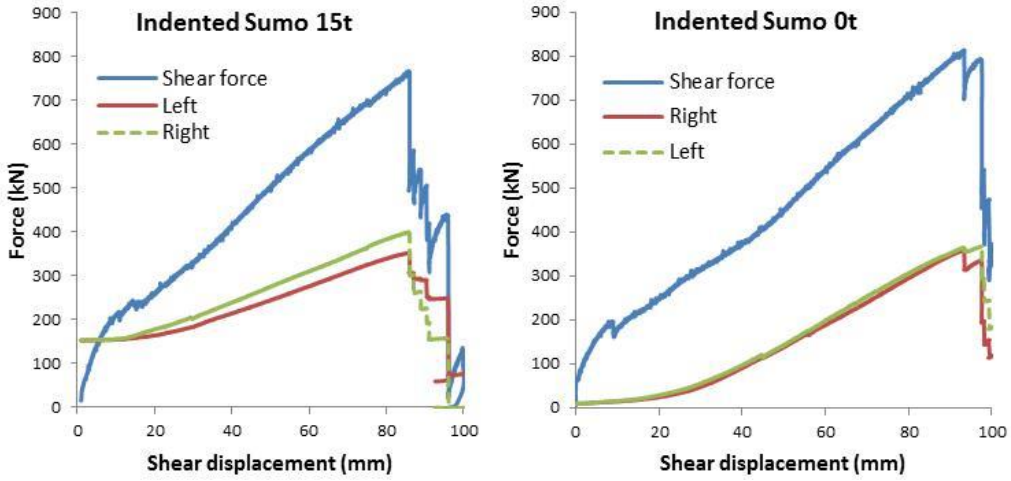

(g) T2-7 (h) T2-8

Figure 5.27 Double shear test results of all cable bolted concrete samples

5.4.4 Result analysis and discussion

5.4.4.1 Cable pre-tension effect

To study the influence of cable pre-tension on the shear performance of bolted concrete blocks, varied pre-tensions were applied. The maximum shear force and the corresponding joint shear displacement are given in Figure 5.28 and Figure 5.29.

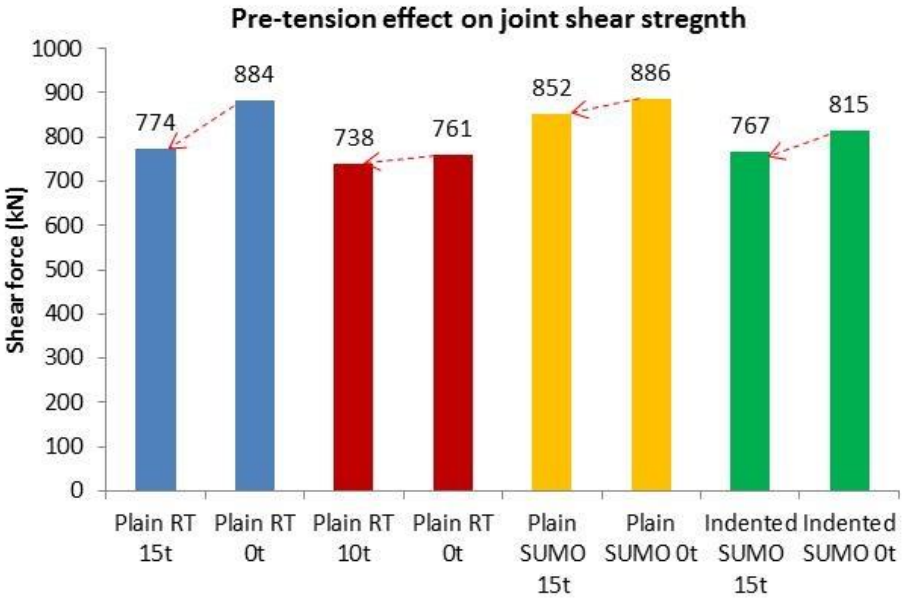

Figure 5.28 Influence of cable pre-tension on the joint shear strength

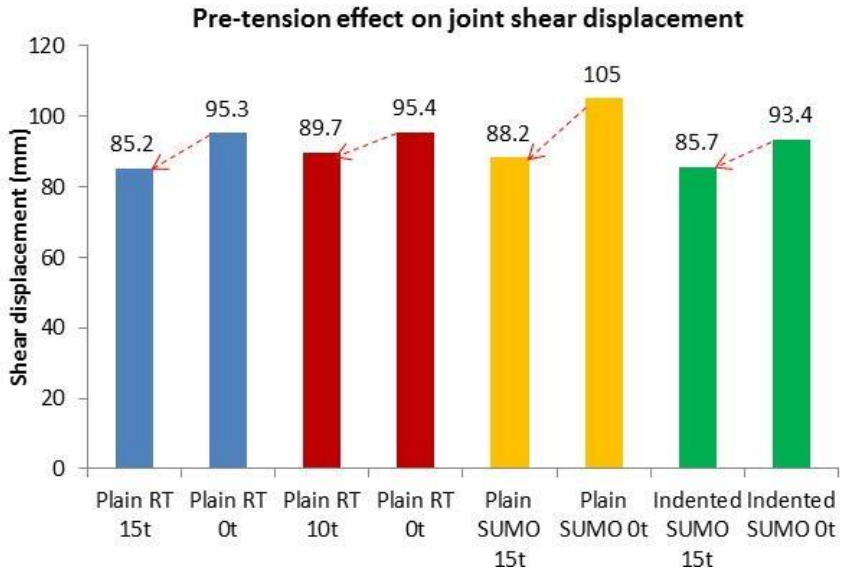

Figure 5.29 Influence of cable pre-tension on the joint shear displacement at cable failure

As shown in Figure 5.28 and Figure 5.29, in the shear tests with open joints, the influences of cable pre-tension on the maximum shear force and the corresponding joint shear displacement were both consistent. As expected, when increasing the cable pre-tension, the cable bolt reached its strength more easily at a smaller shear force and shear displacement.

5.4.4.2 Cable wire profile effect

In double shear tests without joint friction, smooth-wire cable bolts and indented-wire cable bolts were both tested. The influence of cable wire profile on the joint shear strength and the joint shear displacement are shown in Figure 5.30 and Figure 5.31.

The influence of cable wire profile on the shear performance of the bolted concrete blocks was consistent. Specifically, higher shear force and larger joint shear displacement were seen in tests with smooth cable wires than with indented cable wires at both 0 t pre-tension and 15 t pre-tension. Since the indented cable bolt was carved and lost about 10% of its cross section area, the indented-wire cable bolt had a tensile strength 10% less than the smooth-wire cable bolt. The double shear test results in Figure 5.30 showed that the increase of joint shear strength was

approximately proportional to the increase of the cable bolt tensile strength. To be specific, the indented SUMO 15 t test produced a shear strength accounting for 90% of the Plain SUMO 15 t test. The indented SUMO 0 t test yielded 92% shear strength of the Plain SUMO 0 t test.

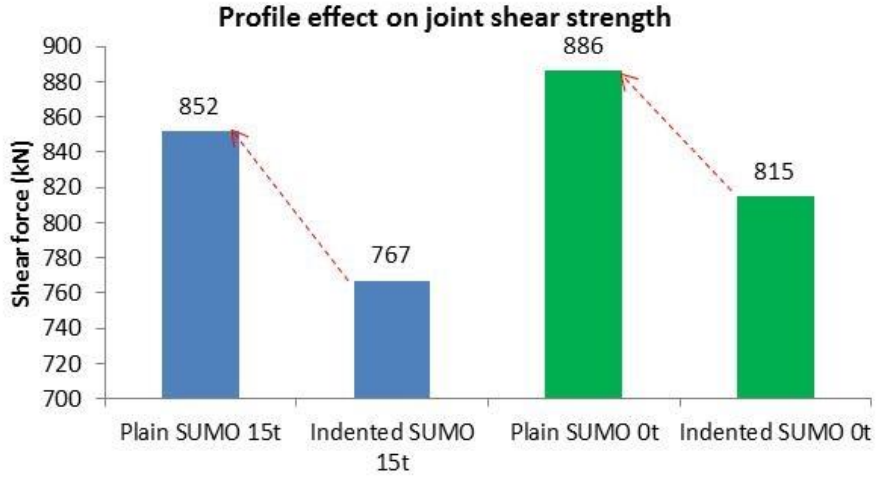

Figure 5.30 Influence of cable wire profile on the joint shear strength

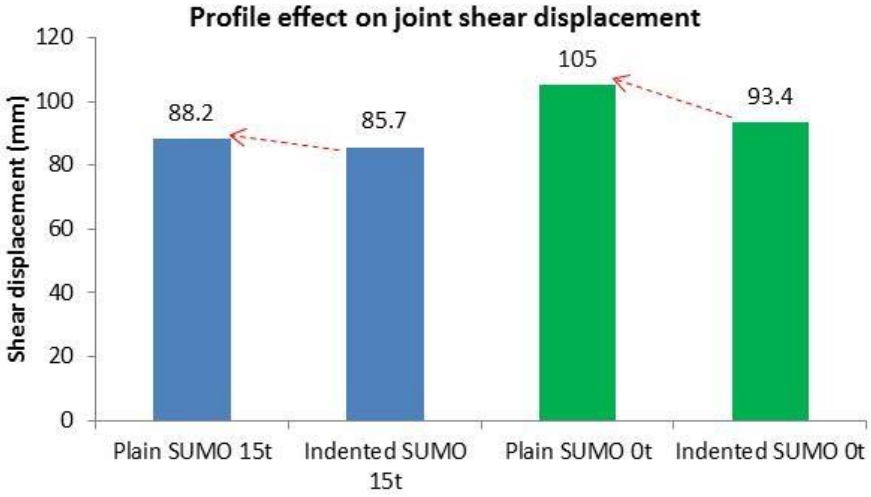

Figure 5.31 Influence of cable pre-tension on the joint shear displacement at cable failure

5.4.4.3 Failure modes and patterns of cable wires

The failure modes of all the eight cable bolts in double shear tests without joint friction are listed in Appendix F. The number of wire failure modes in each test was summarised in the form of tension and shear as shown in Table 5.10.

Table 5.10 Statistics of cable wire failure mode

Test NO.	Profile	Failure mode		
		In tension	In shear	Total failure
T2-1	Plain	11	8	19
T2-2	Plain	15	0	15
T2-3	Plain	6	2	8
T2-4	Plain	2	1	3
T2-5	Plain	8	1	9
T2-6	Plain	6	0	6
T2-7	Indented	8	1	9
T2-8	Indented	4	2	6
Plain		48 (80%)	12 (20%)	60
Indented		12 (80%)	3 (20%)	15
Sum		60 (80%)	15 (20%)	75

In Appendix E, the failure condition of each cable bolt at two shearing joints showed a visible phenomenon that almost all the cable bolts except the one in test T2-8 failed at only one joint and the cable bolt section at the other joint was intact. This was different from the double shear tests with joint friction in which most cable bolts failed at two shearing joints after testing. The reason was possibly that the presence of a gap at the shearing joint made the middle concrete block to adjust more easily than the test without joint gaps during the shearing process. One joint tended to carry more shear load than the other.

In Table 5.10, the statistics of cable wire failure mode showed that most cable wire failed in tension and few failed in shear irrespective of the cable wire profile. In addition, more cable wires failed in tension in double shear tests without joint friction than with joint friction. The tension failure in double shear tests without joint friction accounted for 80% wire failures on average, whereas the tension failure in double shear tests with joint friction accounted for less than 60% total wire failures (refer to Table 5.6).

5.5 Comparison of tests with and without joint friction

Double shear tests both with and without joint friction were performed in this study. Since the shear resistance was attributed to the joint friction and the cable dowel effects, the comparison between the two types of tests can help better understand these two effects in the shearing process.

From the test results shown in Appendix A and Figure 5.27, it was observed that the shear force-shear displacement relationship was similar in both types of tests. All the tests exhibited the typical load profile as shown in Figure 5.7, including the elastic stage, the transitional stage, the plastic stage and the failure stage. They mainly differed in the shear force and shear displacement at cable failure.

Sumo cable bolts were tested using both test methods, and the test results are given in Table 5.11.

In Table 5.11, it is seen that the influence of cable pre-tension on the joint shear displacement was consistent in double shear tests with and without joint friction. Higher cable pre-tension produced smaller joint shear displacement. Also, tests without joint friction yielded larger joint shear displacement than with joint friction due to the presence of a joint gap in tests without joint friction. When it comes to the shear force, the cable pre-tension showed a negative influence on the shear force in all tests except T1-6 and T1-7 in terms of both the whole shear force and the cable dowel effect.

Table 5.11 Double shear test results of Sumo cable bolts

Test	Cable profile	Cable pre-tension (t)	Shear displacement (mm)	Peak shear force (kN)	Joint friction coefficient	Average axial load per joint (kN)	Friction component per joint (kN)	Cable component (Dowel) (kN)
T1-4	Indented	25	32.6	829	0.44	284	125	579
T1-5	Indented	10	46	933	0.44	293	129	675
T1-6	Plain	25	58.8	1424	0.44	391	172	1080
T1-7	Plain	10	78.9	1318	0.44	409	180	958
T2-5	Plain	15	88.2	852	\	\	\	852
T2-6	Plain	0	105	886	\	\	\	886
T2-7	Indented	15	85.7	767	\	\	\	767
T2-8	Indented	0	93.4	815	\	\	\	815

5.6 Comparison of double shear test and single shear test results

Besides the double shear test method, the single shear test is another method of experimentally investigating the shear performance of cable bolts in reinforcing rock strata. The single shear test apparatus of the British Standard (BS 7861-2) is commonly used in laboratory tests. In this section, four different cable bolts were tested using the British Standard Single Shear Test (BSSST) apparatus. The BSSST results were compared with the double shear test results. The comparison helped to learn the influence of test methods on cable bolt shear performance.

5.6.1 British standard single shear test

The single shear test apparatus used in this study had the same structure and similar dimensions to the British standard (British Standard Institution, 2009), as shown in Figure 5.32. The only difference was the length of the steel shear tube. The British standard was 450 mm in length of a shear tube, whereas the one used in this study was 500 mm.

To prepare the shear test sample, cable bolts were cut into sections with the desired length to anchor into the shear tubes. To anchor the cable section into the steel tubes, one end of the steel tube was blanked off with strong adhesive tape to inhibit cement escaping. After cement grout was poured into the steel tube, the cable bolt was inserted into the tube centrally and held vertically to permit the grout to harden. The cable bolt was left to set for one day, and then the other half of the cable was anchored into another steel tube in the same way. The whole shear sample was allowed to cure for more than one week before testing.

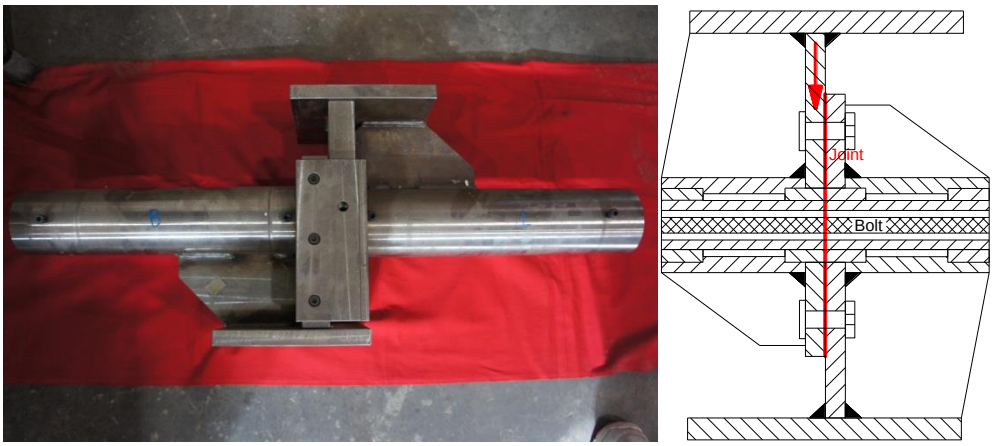

Figure 5.32 Apparatus used in British single shear test (Adjusted from BS 7861-2)

When the grout cured, the steel shear tube with the anchored cable bolt was placed in position into the single shear apparatus. The contact interface of two steel tubes was exactly overlapping to the shear plane of the single shear apparatus to make sure the cable bolt was sheared at the desired cross section. The single shear apparatus was loaded at 1 mm/min until cable failure on a compression machine as shown in Figure 5.33.

Figure 5.33 A British single shear test assembly loaded by an INSTRON testing machine

5.6.2 Single shear test result

Four single shear tests were conducted on different cable bolts, including plain JM Superstrand, indented JM Superstrand, plain Sumo and indented Sumo. No pre-

tension load was applied to the cable bolts in these tests. The single shear test results are given in Figure 5.34 and Figure 5.35.

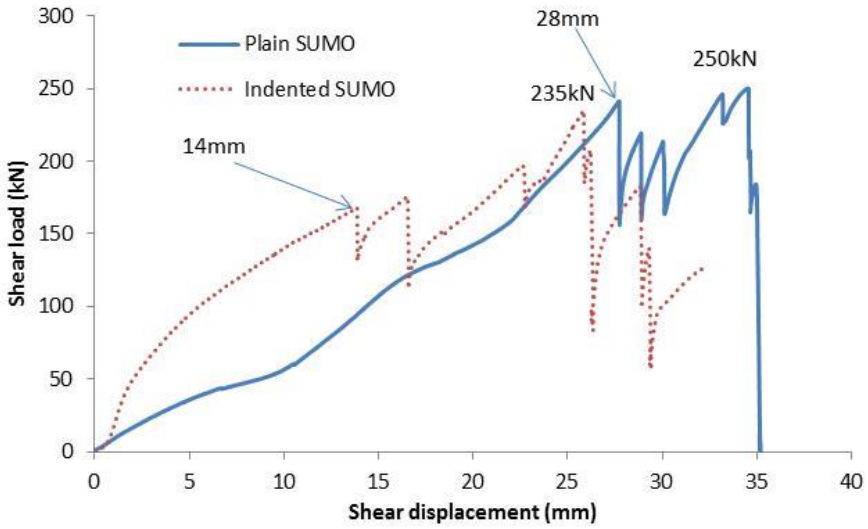

Figure 5.34 Single shear test results of Sumo cable bolts

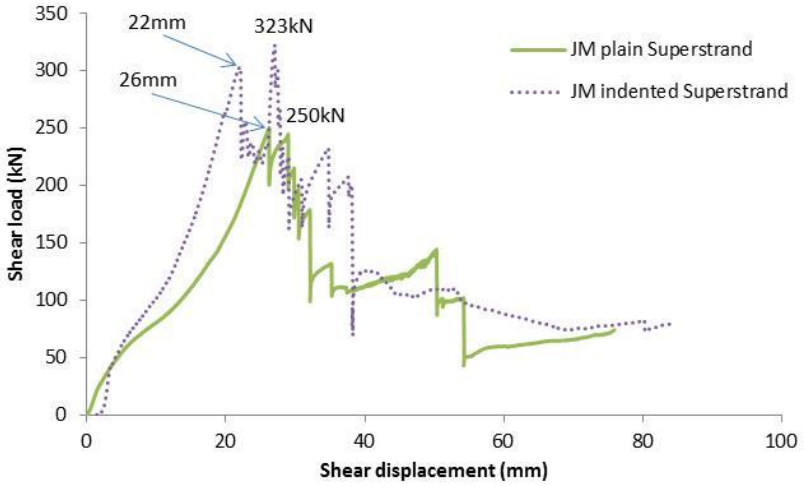

Figure 5.35 Single shear test results of Superstrand cable bolts

5.6.3 Comparison of single shear and double shear test results

As presented previously, the Sumo and JM Superstrand cable bolts were also investigated in the double shear tests. Sumo cable bolts were tested using the shear apparatus both with and without joint friction, while JM Superstrand cable bolts were tested using only the shear apparatus with joint friction. The test results of

Sumo and JM Superstrand cable bolts using different shear test apparatuses are given in Figure 5.36 and Figure 5.37.

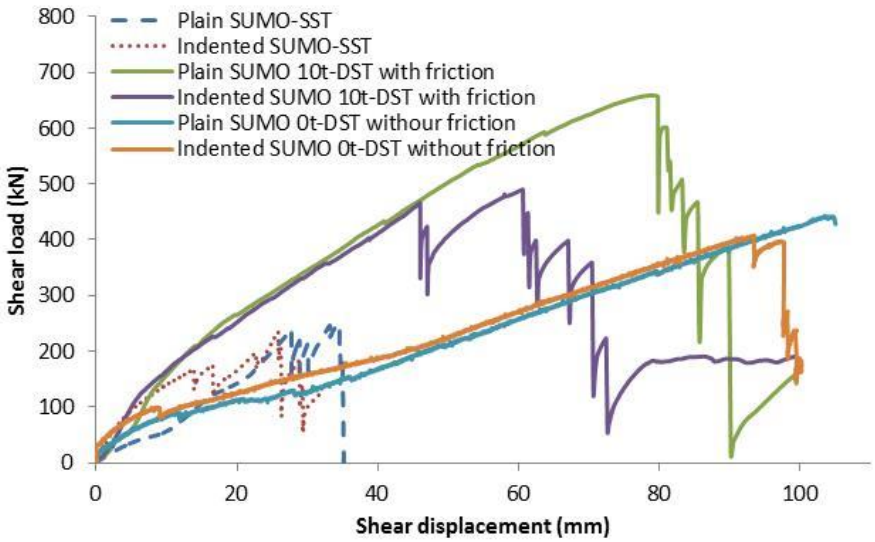

Figure 5.36 Relationship between shear force and shear displacement of Sumo cable bolts in different shear tests (The shear force of double shear test was for one shearing plane.)

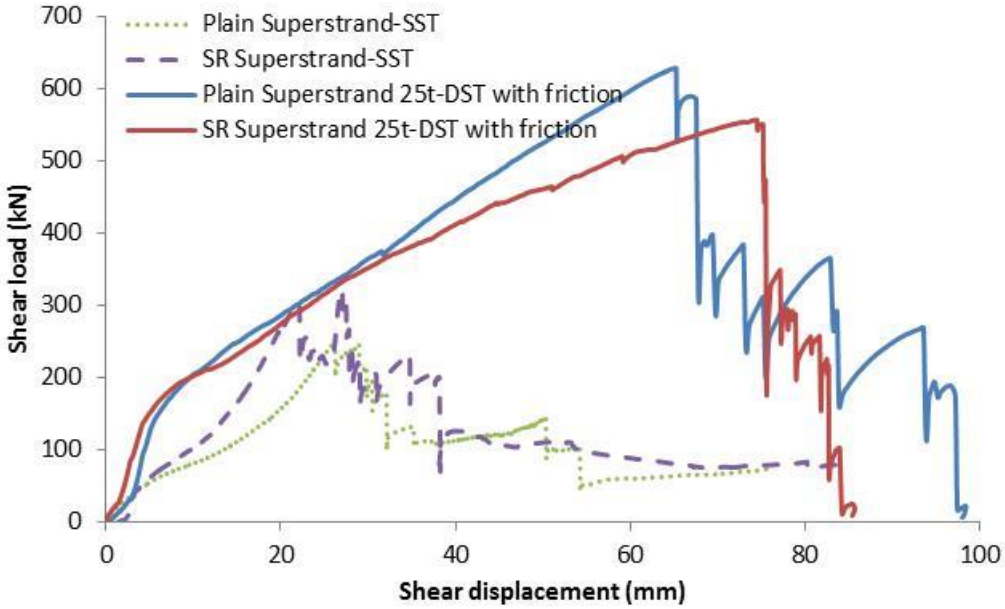

Figure 5.37 Relationship between shear force and shear displacement of Superstrand cable bolts in different shear tests (The shear force of double shear test was for one shearing plane.)

From Figure 5.36 and Figure 5.37, it was observed that the shear performance of cable bolted concrete blocks was different when the three different shear apparatuses

were used. The difference between different double shear tests has been discussed in previous sections. Here, the single shear test result was compared with the double shear test results. The peak shear force of both Sumo and Superstrand cable bolts in the single shear test was approximately half of the peak shear force in the double shear test with joint friction and a little more than half of the peak shear force in the double shear test without joint friction. In addition, the shear displacement at cable failure in the single shear test was much smaller than in the double shear test. The obvious difference of the single shear test indicated that the cable bolt probably behaved in a different way in the single shear test.

After testing, the cable bolt failure mode was also examined in the single shear test as shown in Figure 5.38. Unlike the cable wire failure mode in the double shear test, it is observed that all cable wires failed in shear in the single shear test. In addition, cable bolts got in contact with the steel shear tube and obvious contact compression/shearing marks were left on the steel shear tube. From the failure mode, it can be inferred that the cable failure was caused by the stiff contact between the cable bolt and the steel shear tube, which induced severe stress concentration. The inappropriate shear tube size was the main reason for the poor shear performance of cable bolts in the single shear tests.

Figure 5.38 Cable wire failure mode in single shear test

In addition, cable de-bonding was observed at the cable end in all single shear tests. This de-bonding allowed cable bolts to move more easily at the shearing plane. Hence, the cable bolt got into contact with the shear tube more easily.

To obtain the complete shear performance of cable bolts in the single shear test, the steel shear tube and the whole shear apparatus must be enlarged to avoid the cable-mould contact in the testing process. Moreover, the cable bolt can be welded to the end of the shear tube to prevent the occurrence of cable de-bonding.

Figure 5.39 shows the cross section of the shear tube of the single shear test apparatus and the shear box of the double shear test apparatus. When an assembly is loaded laterally, the cable bolt bends, compresses and crushes into the surrounding grout and concrete. With the increase of joint shear displacement, the cable bolt further crushes into the surrounding concrete. More tension force and shear force are generated until the cable bolt reaches its strength at a certain point. However, if a cable bolt gets into contact with the steel mould prior to cable failure, severe stress concentration will be induced at the contact point. This stress concentration could significantly advance the cable bolt reaching its strength and thus cable failure occurs prematurely, at smaller joint shear displacement and smaller shear force. This is exactly what happened in the single shear tests. The diametrical difference of the cable bolt and the mould should be sufficiently large to avoid their direct contact and interaction. How much should the diametrical difference be? The answer is related to the possible concrete joint shear displacement at cable failure. The joint shear displacement at cable failure was influenced by a variety of factors (Aziz *et al.*, 2015a; Aziz *et al.*, 2014; Aziz *et al.*, 2015b; Craig and Aziz, 2010; Li *et al.*, 2016; Li *et al.*, 2015; McKenzie and King, 2015). For commonly used cable bolts tested in concrete blocks of normal strength (more or less of 40 MPa) using the presented double shear test apparatus and other double or single shear test apparatuses, the joint shear displacement at cable failure were approximately in the range of 40 ~ 100 mm which depended on the particular test condition and cable type. The deflection of the cable bolt at the concrete joint shear plane, which was half of the joint shear displacement at cable failure, was thus in the range of 20 ~ 50 mm. So the radial difference should be more than this range to avoid the cable-mould contact during

the loading process. In the presented tests, if all the cable bolts were anchored exactly at the center of the concrete borehole, the diametrical difference would be 6 mm and 136 mm for the BSSST and the DST respectively according to their dimensions. Obviously, the radial difference of BSSST was too small compared to the required shear deflection (20 ~ 50 mm). Thus, the diameter of the BSSST shear tube should be increased to avoid the occurrence of cable-mould contact during the shearing process.

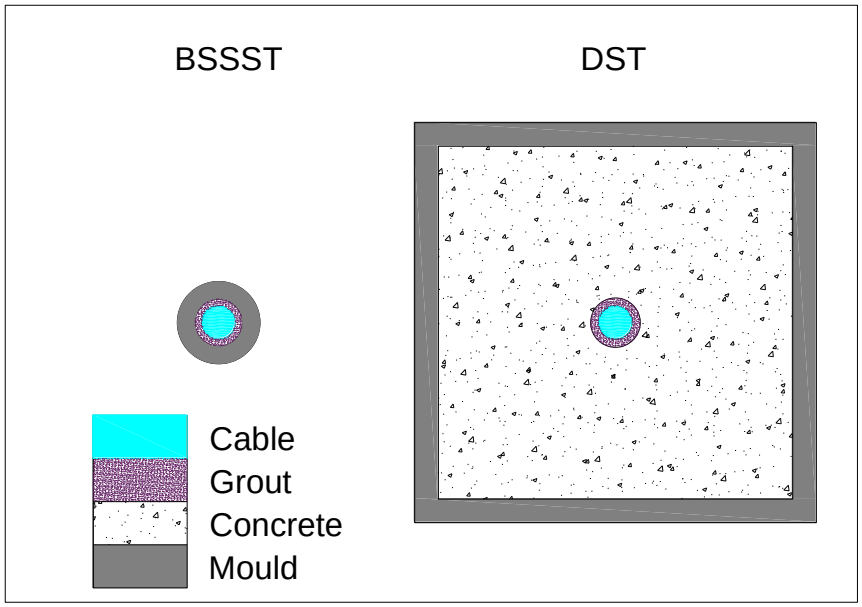

Figure 5.39 Cross section of the shear test apparatuses (drawn in scale)

5.7 Summary

In this chapter, double shear tests carried out on different cable bolts were introduced with regard to the preparation, the assembly and the test procedure. These double shear tests were divided into two groups: with joint friction and without joint friction. Based on the recorded shear-induced forces and displacements, test results were analysed and compared between double shear tests with and without joint friction. The analyses included the joint shear strength, the pre-tension and cable wire surface profile effect, the cable axial force propagation, the direct cable-joint contribution (cable dowel effect), the relationship between shear and normal forces and the failure modes of cable wires. Also, a number of BSSSTs were performed and

the results were compared with the double shear test results. The following conclusions were drawn from the experimental study:

Double shear test with joint friction:

- Regarding the influence of cable pre-tension on the joint shear strength, the test results were consistent for all tested cable strands except the indented cable strand. As for the influence of cable pre-tension on joint shear displacement, consistent results were observed: the larger the cable pre-tension, the smaller the joint shear displacement at cable strand failure. The cable pre-tension increased the overall shear stiffness of bolted joints for all tested cable strands, including indented and plain SUMO, SHGC and plain RT cable strands.

- As for the cable wire surface profile effect, the indented cable wire surface profile decreased the cable bolted joint shear strength. However the influence of cable wire surface profile on the joint shear displacement at failure and the overall joint shear stiffness was different between the solid and hollow cable strands.

- The relationship coefficient between the shear force and normal force was different from the relationship coefficient between the shear stress and normal stress. In general, higher cable pre-tension loads produced a larger relationship coefficient of the shear and normal loads.

- The aggregates in concrete blocks affected the cable wire failure mode. The inclusion of aggregates in concrete blocks caused more cable wire failures in shear. The cable wire profile affected the cable wire failure mode. More failures in shear were witnessed in indented cable bolts than in plain cable bolts. Strong concrete blocks caused more cable wire failure in shear than the weak concrete blocks.

Double shear test without joint friction:

- The influences of cable pre-tension on the maximum shear force and the corresponding joint shear displacement were both consistent. The increase of the cable pre-tension decreased both the bolted joint shear strength and the joint shear displacement.

- The influence of cable wire profile on the shear performance of the bolted concrete blocks was also consistent. Higher shear force and larger joint shear displacement were observed in tests with smooth cable wires at both 0 t pre-tension and 15 t pre-tension. The increase of cable bolted joint shear strength was approximately proportional to the increase of the cable bolt tensile strength due to the cable cross section area variation.

- Most cable wires failed in tension and few failed in shear irrespective of the cable wire profile. In addition, more cable wires failed in tension in double shear tests without joint friction than with joint friction.

Comparison between tests with and without joint friction:

- In general, the cable bolt pre-tension had a negative influence on the cable dowel component.

- The cable pre-tension influence on the joint shear displacement was consistent. All cable bolts with a larger pre-tension failed at a smaller shear displacement.

- Due to the presence of joint gap in the double shear test without joint friction, the joint shear displacement was obviously larger in the double shear test without joint friction than with joint friction.

Comparison between double and single shear test results:

- The shear strength of cable bolts in the British Standard single shear test was much smaller than that in the double shear test.

- The contact between the cable and the shear tube due to the small tube size and the cable de-bonding mainly affected the cable shear performance in the single shear test. To obtain the complete cable shear performance, the steel shear tube should be enlarged and the cable bolt should be welded to the tube end.

- Due to the contact between the shear tube and the cable bolt, all cable bolt wires failed in shear.

CHAPTER SIX
PERFORMANCE COMPARISON OF CABLE BOLTS AND OTHER BOLTS LOADED IN SHEAR

6.1 Introduction

FG bolts, steel rebar bolts (RB) and cable bolts have been widely used in rock reinforcement. FG bolts and steel rebar bolts are both single straight tendons, while cable bolts are flexible tendons composed of multi-wire strand (Hutchinson and Diederichs, 1996). Unlike the currently used steel rebar bolts and cable bolts which are made of steel, FG bolts are made of inorganic nonmetallic glass fibres. Each of them also contains a variety of bolt types differing primarily in structures and dimensions, such as bolt diameter, rib spacing, rib height and surface profile. All these designs are aimed to improve the bolt strength and load transfer between bolts and rock masses when bolts are loaded in tension.

Tensile properties of bolts, including the strength and deformation modulus, are the important characteristics of bolts in ground support. They influence the bolt performance in reinforcing rock strata. From the simple uniaxial tensile test, elastic modulus, plastic modulus (modulus in the strain hardening stage), yielding strength and tensile strength can be obtained.

Due to the difference of FG bolts, steel rebar bolts and cable bolts in strength, deformation modulus and structure, their shear behaviour is expected to be different.

Based on the experimental studies on the cable shear performance in reinforcing concrete block joints presented in the previous chapter and the existing research on the shear performance of steel rebar bolts and FG bolts, these bolts can be compared to study their features in reinforcing jointed rock mass.

This chapter focuses on the influence of bolt strength and bolt deformation modulus on the bolted joint shear strength, joint shear stiffness and bolt failure mode for FG bolts, steel rebar bolts and cable bolts.

6.2 Tensile behaviour of different bolts

Figure 6.1 shows the setup of a tensile test of FG bolts. The stress-strain relationships of FG bolts, steel rebar bolts, and cable bolts (Faulkner, 2012; Faulkner *et al.*, 2013) are given in Figure 6.2.

Figure 6.1 Tensile test of FG bolt

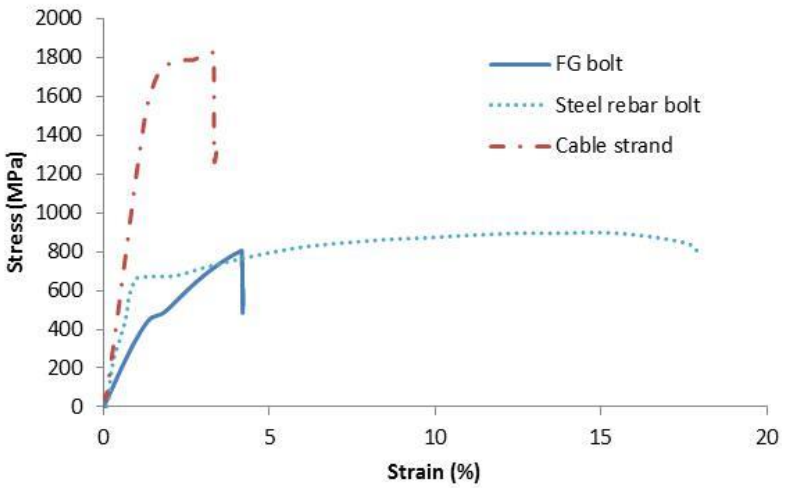

Figure 6.2 Stress-strain relationship of different bolts (relationship of cable bolt is from Faulkner 2012, all the others are from tests conducted in the CME laboratory of UOW)

From Figure 6.2, it can be seen that all the stress-strain curves were different. For FG bolts, the stress-strain relationship was very close to a line at the beginning and then its stiffness decreased slightly with the increase of elongation until the final failure. Overall, its tensile modulus did not change much before final failure. When it comes to steel rebar bolts, there were obviously two different stages during the tensioning process, the first elastic stage and the second plastic stage. The tensile modulus was much larger in the elastic stage than in the plastic stage. The failure strain of steel rebar bolts was normally at the range of 10%~20%. In comparison, a cable strand had a similar deformation modulus in the elastic stage as steel rebar bolt, but was higher in the plastic stage. Cable bolts in tension failed at a small strain which was less than 5%. In general, cable bolts had higher tensile strength than steel rebar bolts and FG bolts.

6.3 Failure criterion of bolt under combined loads

A bolt used to reinforce jointed rock mass takes both tensile and shear forces due to the axial and lateral movement of the rock mass. Thus, the bolt failure is attributed to the combination of tensile and shear forces (Dight, 1983; Jalalifar and Aziz, 2010a; Pellet and Egger, 1996). An equation developed to predict the failure load which takes into account contributions of both tensile and shear forces (Dight, 1983) is:

$$\left(\frac{N_o}{N_f}\right)^2 + \left(\frac{Q_o}{Q_f}\right)^2 = 1 \qquad (6.1)$$

Where:

N_o and Q_o, are the tensile and shear forces respectively at failure of a bolt;

N_f, is the ultimate tensile strength of a bolt (equal to $A_b\sigma_{bf}$);

Q_f, is the ultimate shear strength of a bolt (equal to $A_b\tau_{bf}$);

A_b, is the bolt cross section area;

σ_{bf} and τ_{bf}, are the failure strengths of bolt loaded in pure tension and pure shear, respectively.

Regarding Eq. (6.1), When τ_f is equal to $\frac{\sigma_{bf}}{2}$, the equation represents the Tresca criterion in the plane stress state. When τ_f is equal to $\frac{\sigma_{bf}}{\sqrt{3}}$, the equation becomes the Von Mises criterion in the plane stress state. In this study, the Tresca criterion is used. For steel rebar bolts and cable bolts, it is suitable to use the Tresca criterion. However, there is currently no existing failure criterion for FG bolts. Nevertheless, the potential criterion for FG bolts should also be limited by the shear strength and tensile strength and thus have a shape similar to the Tresca criterion or the Von Mises criterion. Therefore a similar criterion based on the tensile and shear strength of FG bolts is to be used to qualitatively describe the FG bolt failure behaviour.

From the form of the failure criterion in Eq. (6.1), when N_f is not equal to Q_f, the failure equation takes the form of an ellipse, which is the normal case for all currently used bolts. If both steel rebar bolts and cable bolts are assumed as a Tresca material (Dight, 1983),the relationship will exists between N_f and Q_f in the form of $Q_f = 0.5N_f$. However, there is not a constant relationship betweenN_f and Q_f for different FG bolts. Accordingly, punch tests were carried out to obtain the shear strength of FG bolts using a punch shear apparatus as shown in Figure 6.3. Table 6.1 gives the punch test results of FG bolts (Gilbert *et al.*, 2015). By considering the tensile strength of FG bolts shown in Figure 6.2, then the relationship for FG bolts is roughly $Q_f = 0.13N_f$.

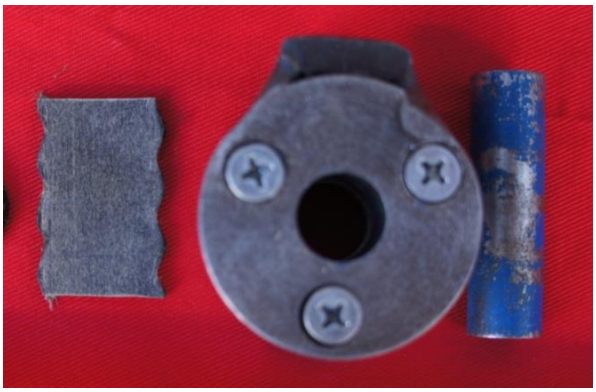

Figure 6.3 FG plate and punch shear test device

Table 6.1 Punch shear test results of FG bolt

Sample	MN	T (m)	D (m)	MPa
A	0.012	0.00297	0.0128	102.22
B	0.012	0.00302	0.0127	102.30
C	0.013	0.00302	0.0129	107.50
Average				104.01

Based on Eq. (6.1), the failure criteria of FG bolts, steel rebar bolts and cable bolts are shown in Figure 6.4 in the form of $\frac{N_o}{N_f}$ and $\frac{Q_o}{N_f}$. If the bolt deflection is considered constant and joint friction is ignored in the calculation of bolted joint shear strength provisionally, clearly, the larger the summation of tensile force and shear force in bolts, the higher the joint shear strength. It can be seen from Figure 6.4 that, in general, the summation of tensile force and shear force increases with the decrease of shear force. This is mainly due to the different change rates of tensile and shear forces as shown in Figure 6.4. Since the tensile force increases much more rapidly than the shear force decreases, the summation of tensile and shear forces at bolt failure increases with the decrease of shear force. Besides, the influence of shear force is greater in FG bolts than in steel rebar bolts and cable bolts due to the small shear strength of FG bolts. That is to say the increase of shear force in FG bolts is more detrimental than in steel rebar bolts and cable bolts. Considering the deformation moduli of three different bolts shown in Figure 6.2, the shear force in steel rebar bolts and cable bolts loaded laterally increases faster than in FG bolts prior to yielding. However, the shear force in FG bolts increases much faster after the initial elastic stage of steel rebar bolts and cable bolts since FG bolts do not have an obvious plastic stage. Thus at increased shear displacement FG bolts tend to fail at small tensile force due to their constant deformation modulus and low shear strength.

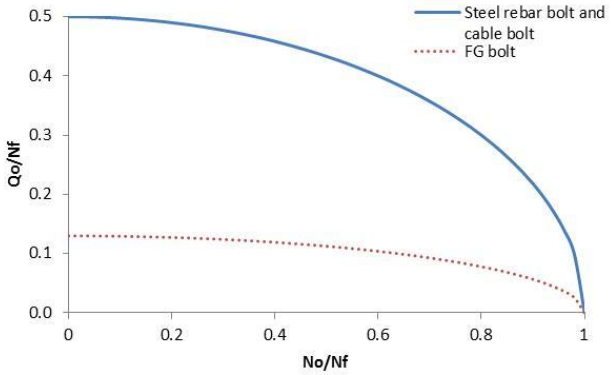

Figure 6.4 Relationship between tensile force and shear force of FG bolts, steel rebar bolts and cable bolts

6.4 Bolt types

The shear performance of different cable bolts in reinforcing concrete blocks has been investigated previously using the UOW double shear test apparatus. Besides this, a great number of double shear tests were also carried out in the past on different steel rebar bolts and FG bolts using another set of UOW double shear test apparatus of smaller dimensions (Gilbert *et al.*, 2015; Jalalifar, 2006; Jalalifar and Aziz, 2010a, 2010b). Here, these bolts are combined to make a comparison about their shear performance. In physical appearance these bolts differ mainly in diameter and surface profile as detailed in Figure 6.5 and in Table 6.2.

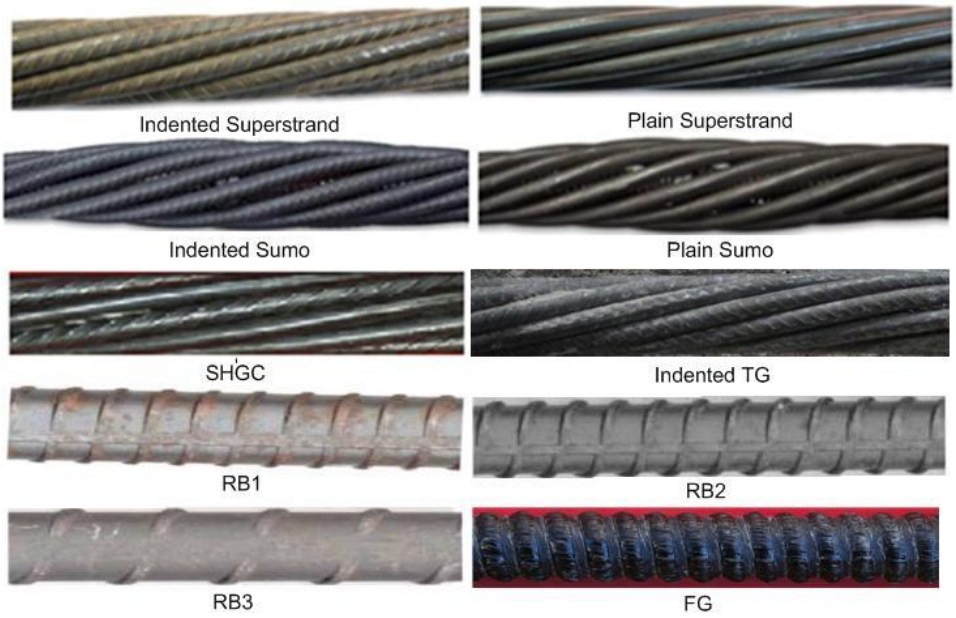

Figure 6.5 Bolt types tested in double shear tests

Table 6.2 Specification of tested bolts

Bolt type	Diameter (mm)	Surface profile		Cross section	Structure feature	Tensile strength (kN)
		Thread or rib spacing	Profile			
FG	22	10	\	Solid	\	307
RB1	22	11.5	\	Solid	\	328
RB2	22	12	\	Solid	\	342
RB3	22	24	\	Solid	\	358
Indented JM Superstrand	22	\	Indented	Solid	\	531
Plain JM Superstrand	22	\	Smooth	Solid	\	590
Indented TG	28	\	Indented	Hollow	\	558
Indented Sumo	28	\	Indented	Hollow	Bird cage	573
Plain Sumo	28	\	Smooth	Hollow	Bird cage	637
SHGC	28	\	Smooth+ SR	Hollow	\	673

SR: spirally ribbed cable wires

6.5 Bolt test results

Thirty one bolts were compared in total in this study, including five FG bolts, nine cable bolts and seventeen steel rebar bolts. Except for eleven steel rebar bolts, all the other twenty bolts were shear-loaded to failure. Considering the field application of different bolts, different pretension loads were applied to FG bolts, steel rebar bolts and cable bolts. Table 6.3 summarizes test results of these twenty bolts which were loaded to failure.

From Table 6.3, it can be seen that FG bolted joints failed at small shear displacement and shear force. In general, the joint shear displacement at steel rebar bolt failure was similar to that at cable bolt failure, but the shear strength of steel rebar bolted joints was much lower than the cable bolt counterpart. In addition, bolt

pretension had a positive effect on the peak shear force, but a negative effect on the joint shear displacement.

Table 6.3 Test results of 20 bolts which were shear-loaded to failure

Bolt type	Concrete strength (MPa)	Pretension (kN)	Joint shear displacement at bolt failure (mm)	Peak shear force (kN)
FG	40	2.5	22	164
FG	40	4.5	22	183
FG	40	5	36	205
FG	40	15	18	220
FG	40	20	16	258
Average			23	/
Indented JM Superstrand T1	40	250	74	1115
Plain JM Superstrand T2	40	250	65	1259
Indented TG T3	40	250	73	1210
Indented Sumo T4	40	250	33	829
Indented Sumo T5	40	100	46	933
Plain Sumo T6	40	250	59	1424
Plain Sumo T7	40	100	79	1318
SHGC T9	40	250	85	1601
SHGC T11	40	100	98	1544
Average			68	/
RB1	20	20	92	762
RB1	20	20	81	813
RB1	20	20	86	821
RB1	20	20	75	756
Average			84	/
RB1	100	20	70	770
RB1	100	80	54	799
Average			62	/

6.6 Joint shear stiffness with bolt reinforcement

Figure 6.6 shows typical shear load-displacement curves of three double shear tests on FG bolts, steel rebar bolts and cable bolts and the schematic relationship as well.

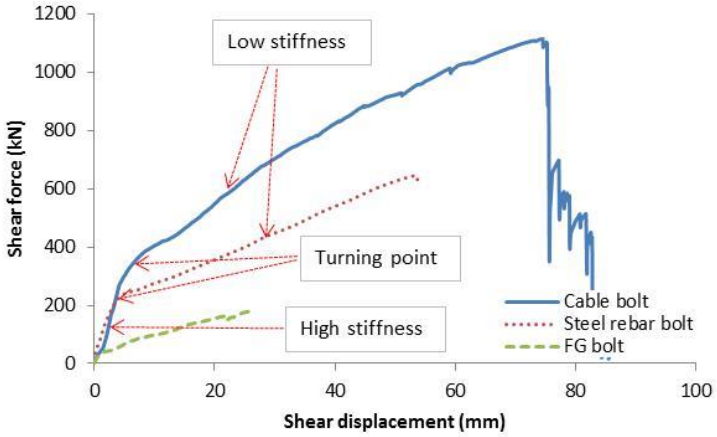

(a) Real test results

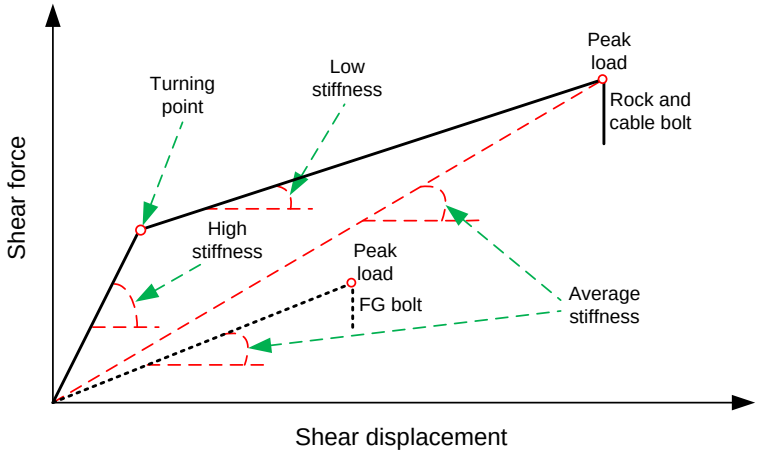

(b) Schematic

Figure 6.6 Shear force vs shear displacement of FG bolts, steel rebar bolts and cable bolts

The shear load-displacement curves of steel rebar bolts and cable bolts were similar, but they were different from the FG bolts. For steel rebar bolts and cable bolts, obviously, the shear process could be divided into two stages before bolt failure, the high stiffness stage and the low stiffness stage. In a specific shear test, the shear stiffness was controlled by a variety of influencing factors, such as the bolt modulus, bolt deformation, concrete strength and variation of joint friction coefficient.

Normally, the variation of bolted joint shear stiffness was mainly attributed to the variation of bolt modulus (Jalalifar, 2006; Pellet and Egger, 1996). Thus for steel rebar bolts and cable bolts, the high stiffness stage was normally related to the elastic state and the low stiffness stage was related to the plastic state of bolts. Unlike steel rebar bolts and cable bolts, FG bolts did not obviously exhibit two different stages. Instead, similar as FG bolts loaded in tension, their shear stiffness decreased gradually with the increase of joint shear displacement until bolt failure.

Based on the shear behaviour of joints reinforced by FG bolts, steel rebar bolts and cable bolts, they can be represented by a linear and a bilinear relationship. Table 6.4 and Table 6.5 summarize the joint shear stiffness of steel rebar bolts and cable bolts, respectively. Both high stiffness and low stiffness stages were calculated and listed in these two tables. Since steel rebar bolts listed in Table 6.5 were not loaded to failure, their average shear stiffness cannot be compared with cable bolts. Therefore, the average shear stiffness of rock bolts and cable bolts was not summarized in Table 6.4 and Table 6.5. Table 6.6 shows the average shear stiffness of FG bolted joints before the peak load.

Table 6.4 Shear stiffness of cable bolted joints (bolts were loaded to failure)

Bolt type	Pretension (kN)	Average shear stiffness (kN/mm)		Low/High
		High	Low	
Indented JM Superstrand	250	25.7	5.7	0.22
Plain JM Superstrand	250	22.6	7.8	0.35
Indented TG	250	19.9	6.8	0.34
Indented Sumo	250	29.9	8.6	0.29
Indented Sumo	100	20.0	8.7	0.44
Plain Sumo	250	23.7	8.2	0.35
Plain Sumo	100	15.3	7.1	0.46
SHGC	250	19.4	7.7	0.39
SHGC	100	13.2	7.2	0.54
Average		21.1	7.5	0.38

Table 6.5 Shear stiffness of steel rebar bolted joints (bolts were not loaded to failure)

Bolt type	Pretension (kN)	Average shear stiffness (kN/mm)		Low/High
		High	Low	
RB1	0	12.6	1.7	0.13
RB1	20	26.2	3.9	0.15
RB1	50	24.4	4.7	0.19
RB1	80	32.6	5.7	0.18
RB2	0	15.7	1.4	0.09
RB2	20	20.7	5.2	0.25
RB2	50	24.5	4.6	0.19
RB2	80	25.0	5.4	0.21
RB3	0	14.5	1.0	0.07
RB3	20	32.4	4.7	0.15
RB3	50	38.5	3.6	0.09
Average		24.3	3.8	0.15

Table 6.6 Shear stiffness of FG bolted joints (bolts were loaded to failure)

Bolt type	Pretension (kN)	Average shear stiffness (kN/mm)
FG	2.5	7.5
FG	4.5	8.3
FG	5	5.7
FG	15	12.6
FG	20	15.7

From Table 6.4 to Table 6.6, the following conclusions can be drawn:

- In the high joint shear stiffness stage, the joint shear stiffness was influenced by the pretension for both cable bolts and steel rebar bolts. The larger the bolt pretension, the greater the joint shear stiffness. In addition, steel rebar bolted joints had similar average shear stiffness to cable bolted joints in this stage.

- In the low joint shear stiffness stage, the joint shear stiffness of cable bolted joints was not noticeably influenced by pretension. The influence of pretension on steel rebar bolted joints was not very consistent. The joint shear stiffness of steel rebar bolted joints was similar with different pretension loads, while it was very small without pretension. Additionally, the average shear stiffness of cable bolted joints doubled that of steel rebar bolted joint. This was consistent with the larger plastic modulus of cable bolts compared to steel rebar bolts as shown in Figure 6.2.

- The low-high stiffness ratio was also different when comparing the steel rebar bolted and cable bolted joints. The average ratio of cable bolted joint was 0.38, while the steel rebar bolted joint was only 0.15.

- For FG bolted joints, the joint shear stiffness also increased with the increase of bolt pretension.

6.7 Bolt contribution to joint shear strength

There have been various analytical and experimental investigations undertaken looking at bolts and their contribution to joint shear strength (Ferrero, 1995; Grasselli, 2005; Jalalifar and Aziz, 2010b; Pellet and Egger, 1996). These studies suggested that two types of contribution, the frictional effect and the dowel effect, were made by a bolt to the joint shear strength. Figure 6.7 shows the typical loading state of a bolt-reinforced joint.

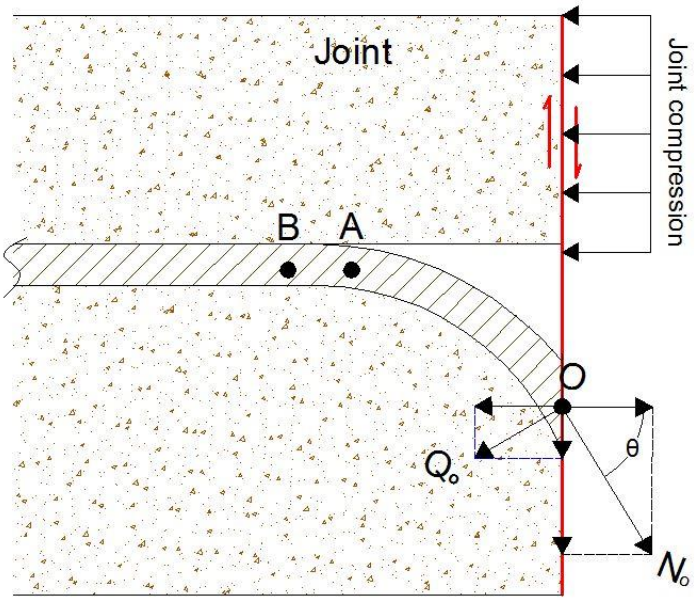

Figure 6.7 Loads induced on joint and in tendon (Li *et al.*, 2015)

The bolt contribution to the joint shear strength is:

$$R = N_o \sin\theta + Q_o \cos\theta + [N_o \cos\theta - Q_o \sin\theta] tan\varphi \quad (6.2)$$

In the experimental analysis, there is another definition of the bolt contribution to joint shear strength, based on recorded loads (Grasselli, 2005; Jalalifar and Aziz, 2010b).

$$R = F_s - 2N tan\varphi \quad (6.3)$$

Where:

F_s, is joint shear force;

N, is the externally applied normal force at the joint surface.

To compare bolts with different dimensions, the bolt contribution is normally standardized by the maximum tensile failure force of bolts as follow:

$$T_{nbc} = \frac{R}{2N_f} \quad (6.4)$$

Where:

T_{nbc}, is the normalized bolt contribution to joint shear strength;

N_f, is the bolt tensile strength.

Figure 6.8 shows the loading state of the bolt-reinforced jointed rock mass in the field after the bolt installation. This field condition is always simplified in the laboratory to study the reinforcing effect of bolts. Figure 6.9 shows the overall loading state of a typical shear system in the normal direction. Primarily two stages are included, the initial stage and the shear loading stage. In the initial stage, the normal force at the joint contains the bolt pretension and the initial external confining force:

$$N_{joint} = N_{pretension} + N_e \tag{6.5}$$

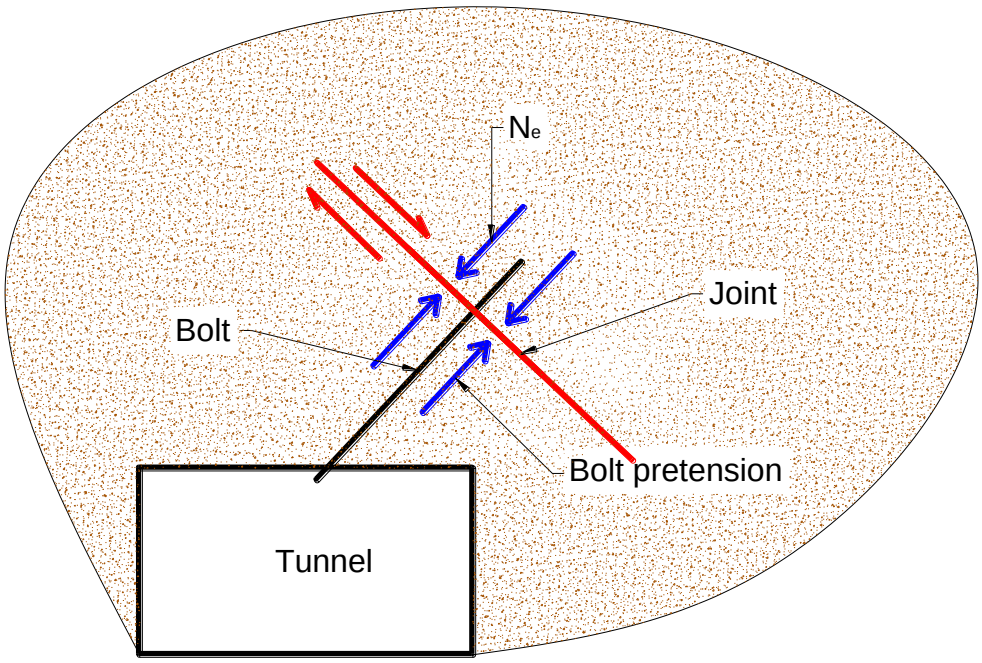

Figure 6.8 Loading state of a bolt-reinforced jointed rock mass in the field

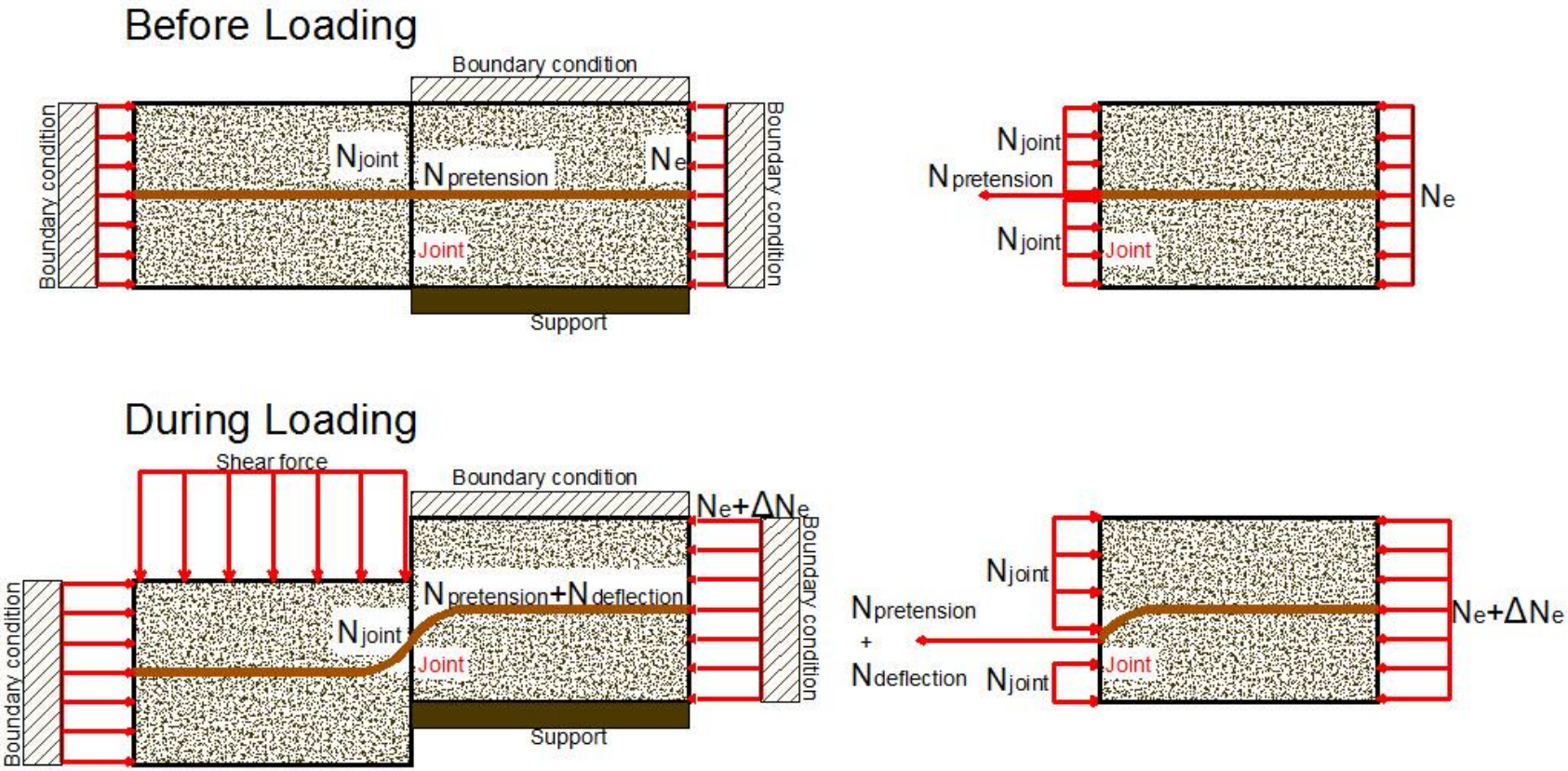

Figure 6.9 Loading state of a simplified laboratory shear system in the normal direction

In the loading stage, besides the bolt pretension and the initial external normal force, the normal force at the joint also contains the normal force induced from bolt deflection as well ($N_{deflection} + \Delta N_e$). The induced normal force is attributed to the additional normal component of the bolt force at the joint ($N_{deflection}$) and the additional external normal force (ΔN_e). The additional external normal force is dominated by the boundary condition of the shear system. Thus the total normal force at the joint during the shearing process is:

$$N_{joint} = N_{pretension} + N_{deflection} + N_e + \Delta N_e \quad (6.6)$$

Where:

N_{joint}, is the total normal force on the joint plane;

$N_{pretension}$, is the normal force induced by pre-tension on the joint plane;

$N_{deflection}$, is the normal force induced by bolt deflection on the joint plane;

N_e, is the normal force on the joint plane caused by initial external confining stress;

ΔN_e, is the additional external confining stress.

Regarding the normal confining force (N) at joints in Eq.(6.3), there are two types of forces as shown in Figure 6.9. One is related to the initial normal confining force applied on the concrete end surface before testing (Srivastava and Singh, 2015), N_e, and the other is related to the additional normal force induced from bolt deflection and boundary confinement, ΔN_e. They can be simply named the initial external normal force and the induced external normal force, respectively. To attain the bolt contribution to joint shear strength, the bolt pretension ($N_{pretension}$) and the induced external normal force (ΔN_e) should be considered as part of this contribution. Thus in Eq. (6.3), N refers to the initial external normal force at joints, N_e, rather than the combination of the initial (N_e) and induced (ΔN_e) external normal forces and the bolt pretension ($N_{pretension}$). If no initial external normal force (N_e) is applied, then N is

equal to zero in Eq. (6.3). For all the tests presented in this paper, there was no initial external normal force, thus N is equal to zero.

The contribution of FG bolts, steel rebar bolts and cable bolts was normalized by their tensile strength and listed in Table 6.7 to Table 6.9, respectively. All bolts listed in Table 6.7 to Table 6.9 were loaded to failure during the testing process.

Table 6.7 Normalized FG bolt contribution to joint shear strength (bolts were loaded to failure)

Concrete strength (MPa)	Pretension (kN)	Tensile strength (kN)	Failure shear force (kN)	Normalized bolt contribution
40	2.5	307	164	0.27
40	4.5	307	183	0.30
40	5	307	205	0.33
40	15	307	220	0.36
40	20	307	258	0.42
Average				0.34

Table 6.8 Normalized steel rebar bolt contribution to joint shear strength (RB1) (bolts were loaded to failure)

Concrete strength (MPa)	Pretension (kN)	Tensile strength (kN)	Failure shear force (kN)	Normalized bolt contribution
20	20	328	762	1.16
20	20	328	813	1.24
20	20	328	821	1.25
20	20	328	756	1.15
100	20	328	770	1.17
100	80	328	799	1.22
Average				1.20

Table 6.9 Normalized cable bolt contribution to joint shear strength (bolts were loaded to failure)

Cable type	Concrete strength (MPa)	Pretension (kN)	Tensile strength (kN)	Failure shear force (kN)	Normalized bolt contribution
Indented JM Superstrand	40	250	531	1115	1.05
Plain JM Superstrand	40	250	590	1259	1.07
Indented TG	40	250	558	1197	1.07
Indented Sumo	40	250	573	829	0.72
Indented Sumo	40	100	573	933	0.81
Plain Sumo	40	250	637	1424	1.12
Plain Sumo	40	100	637	1318	1.03
SHGC	40	250	673	1601	1.19
SHGC	40	100	673	1544	1.15
Average					1.02

From Table 6.7 to Table 6.9, it can be seen that the bolt contribution to joint shear strength was different for FG bolts, steel rebar bolts and cable bolts. Firstly, the contribution of FG bolts was extremely small, and the average contribution was just 0.33 times its tensile strength. In contrast, the contribution of a steel rebar bolt was higher than its tensile strength and the average contribution was 1.20 times its tensile strength. Similar to the steel rebar bolt, the cable bolt contribution was normally larger than its tensile strength, but slightly lower than the normalised contribution of steel rebar bolts.

In addition, for FG bolts, steel rebar bolts and cable bolts, their contribution to joint shear strength all increased with the increase of bolt pretension except the hollow indented Sumo cable. Indented Sumo was a cable bolt with indented cable wires, which exhibited a different pretension effect compared to FG bolts, steel rebar bolts and other cable bolts.

Looking back at the calculation of bolt contribution to joint shear strength in Eq. (6.2), it is known that the bolt contribution is attributed to two parts, the direct contribution (dowel effect) and the indirect contribution (friction effect) of bolt axial and shear forces. When the loading state of a bolt remains stable, the larger the bolt force component perpendicular to a joint, the lower the joint shear capacity. This is due to the contribution of perpendicular force component being weakened by the friction coefficient which is less than one in these tests.

For FG bolts, steel rebar bolts and cable bolts, their shear strength is much lower than their tensile strength. In order to achieve higher shear strength of a bolted joint, it is better to reach bolt failure at higher axial force rather than higher shear force. In a perpendicularly-bolted joint, the larger the joint shear displacement at bolt failure, the higher the axial force in the bolt with the joint shear strength being higher as well. The deformation modulus of a bolt also influences the loading state of the bolt. Bolts with higher deformation modulus have higher capacity to take both shear and axial forces at a specific deformation.

Considering the tensile behaviour of FG bolts, steel rebar bolts and cable bolts as shown in Figure 6.2, it is clear why the FG bolt contribution to joint shear strength was so small. Due to the approximate invariability of FG bolt modulus before final failure, force increment was almost constantly proportional to bolt deformation. Thus the shear force accounted for a larger portion of the total force in FG bolts at failure than in steel rebar bolts and cable bolts while axial force was far from its tensile strength. FG bolt failure was primarily due to the approach of bolt shear force to the bolt shear strength rather than the approach of the bolt axial tensile force to the bolt tensile strength compared with steel rebar bolt and cable bolt as shown in Figure 6.10. FG bolts tended to fail at smaller shear displacement with smaller axial tensile force and larger shear force, which accordingly yielded lower joint shear strength.

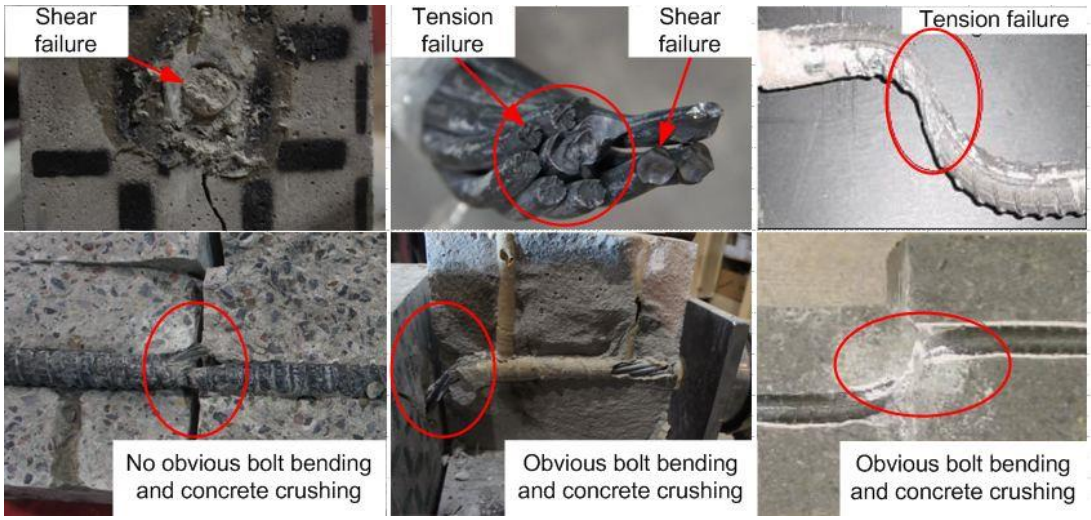

Figure 6.10 Failure modes of FG bolt, steel rebar bolt and cable bolt in reinforcing 40 MPa concrete joints

Generally, rock and cable bolts have high strength to carry loads both in tension and in shear, while FG bolts have only high tensile strength but considerably low shear strength. Even though FG bolts cannot carry high load in shear, they are still widely used in reinforcing coal ribs in underground coal mines because the shear displacement in coal ribs is not severe.

6.8 The direct bolt contribution to joint shear strength

From Eq. (6.2), it is known that the joint shear strength is attributed to two parts, the direct contribution and the indirect contribution of bolts. The direct contribution is related to the parallel component of axial and shear forces to the joint, while the indirect contribution is related to the perpendicular component of axial and shear forces to the joint. The bolt direct contribution corresponds to the bolted joint shear strength with perfectly smooth joint surface contact or without joint surface contact. From the direct contribution of a bolt to a rough joint, the bolt contribution to a smooth or a detached joint can to some degree be assessed as well.

Table 6.10 shows the bolt direct contribution to joint shear strength with reinforcement of FG bolts, steel rebar bolts and cable bolts, respectively. Eq. (6.3) was used in this calculation. The shear strength (40 kN) of FG bolts was obtained

from punch tests on thin plates cut from FG bolts (Gilbert *et al.*, 2015), and the half tensile strength of steel rebar bolts and cable bolts was used as their shear strength.

It should be noted that in the calculation of the bolt direct contribution in Table 6.10 the reading of load cells at the cable end was considered as the same as the normal force at the joint. This was not very accurate because the consumption of axial force in bolts between joints and load cells was ignored. Since Plain Sumo and indented Sumo were bird-caged cable bolts, this axial force consumption of axial force was very large. Thus they were neglected in Table 6.10.

From Table 6.10, it can be seen that the direct contribution of FG bolts was different from steel rebar bolts and cable bolts. The increase in shear strength of FG bolts ranged roughly between 0.73 and 1.8 times bolt shear strength. The shear strength increase of FG bolts was improved by bolt pretension. In comparison, the increase in shear strength of steel rebar bolts and cable bolts fell in the range of about 0.4 to 0.8 times their shear strength and their pretension effect was the same as FG bolts. Thus the increase in joint shear strength of FG bolts was much higher than the steel rebar bolts and cable bolts counterparts. This was mainly due to the small shear strength of FG bolts.

Table 6.10 Direct contribution of different bolts to joint shear strength (bolts were loaded to failure)

Bolt type	Pretension (kN)	Average peak axial force (kN)	Peak shear force (kN)	Joint friction coefficient	Direct contribution (kN)	Bolt shear strength (kN)	Increase in shear strength
FG	2.5	29	164	0.44	69	40	0.73
FG	4.5	43	183	0.44	73	40	0.81
FG	5	62	205	0.44	75	40	0.88
FG	15	31	220	0.44	96	40	1.41
FG	20	40	258	0.44	111	40	1.79
RB1	20	227	762	0.6	245	164	0.49
RB1	20	196	813	0.6	289	164	0.76
RB1	20	219	821	0.6	279	164	0.70
RB1	20	210	756	0.6	252	164	0.54
Indented JM Superstrand	250	400	1115	0.44	382	265.5	0.44
Plain JM Superstrand	250	430	1259	0.44	440	295	0.49
Indented TG	250	410	1197	0.44	418	279	0.50
SHGC	250	462	1601	0.44	597	336.5	0.77
SHGC	100	488	1544	0.44	557	336.5	0.66

The shear strength of FG bolt was obtained by punch shearing the FG plates in the direction perpendicular to the bolt axis.

6.9 Summary

By experimentally comparing the reinforcing effect of FG bolts, steel rebar bolts and cable bolts with consideration of their tensile properties, the following conclusions were drawn:

- The shear force of an FG bolted joint increased gradually from the beginning to end, while the shear force of joints reinforced by either steel rebar bolt or cable bolt increased bi-linearly, which was clearly consistent with their tensile deformation modulus.

- The joint shear stiffness was highly influenced by the bolt pretension in the high stiffness stage, but not in the low stiffness stage for both steel rebar bolts and cable bolts.

- The steel rebar bolt contribution to joint shear strength standardised by the tensile strength was the largest, followed by cable bolts, then FG bolts.

- Steel rebar bolts and cable bolts tended to fail in tension at large shear displacements, while FG bolts in shear at small shear displacements due to its low shear strength and constant deformation modulus.

- The direct contribution of FG bolts to the joint shear strength ranged from 0.73 to 1.8 times its shear strength, while it was between 0.4 and 0.8 times their shear strength for steel rebar bolts and cable bolts.

CHAPTER SEVEN
ANALYTICAL APPROACH FOR A GROUTED CABLE BOLT SUBJECTED TO SHEARING

7.1 Basic state of a grouted cable bolt loaded laterally

Similar to a rock bolt, a grouted cable strand bends at joints of concrete blocks when loaded laterally, and at the same time the surrounding media provide a reaction to the cable strand due to mutual compression (Pellet and Egger, 1996). The cable strand thus bears a combination of an axial force, a shear force and a bending moment. With the increase of the shear load and shear displacement at joints, two types of singular points form in the cable bolt, one at the cable –joint intersection with zero bending moment and the other at the point of maximum bending moment on both side of the joint with zero shear force. From beginning to end, a cable strand undergoes the elastic stage, the yielding stage and the failure stage resulted from the stress increase in cable wires. Based on the beam theory, the normal stress in a bent cable strand is contributed to a superimposing of a uniformly distributed stress yielded by an axial force and a linearly varying stress generated by the bending moment along the cable axis. Since the stress induced by a bending moment is centrosymmetrical, the normal stress is thus strengthened on one side and weakened on the other when a cable strand is pre-tensioned. Figure 7.1 shows the loading state of a grouted cable strand with the formation of a plastic hinge. The stress state at a certain cross section of a laterally loaded cable is as follows:

$$\sigma = \frac{N}{A} \pm \frac{My_n}{I} \tag{7.1}$$

$$\tau = \frac{Q}{A_b} \tag{7.2}$$

$$A_b = \frac{\pi d_b^2}{4} \tag{7.3}$$

$$I = \frac{\pi d_b^4}{64} \tag{7.4}$$

Where:

A_b, is the cross section area of a cable strand;

I, is the inertia moment of a cable strand;

M, is the bending moment at a cross section of a cable strand;

y_n, is the distance from the neutral axis of the cable strand;

In the cable strand, the axial load N may contain two parts, the shearing-induced axial force and the cable pre-tension if the cable bolt is pre-tensioned.

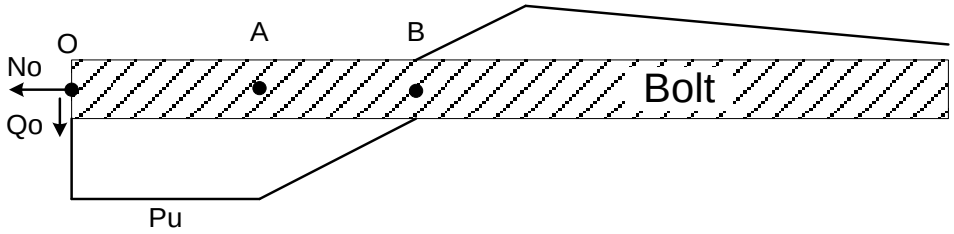

Figure 7.1 Schematic loading state of a cable strand subjected to shearing

7.2 Basic equation for a grouted cable bolt subjected to shearing

7.2.1 Cable bolt

7.2.1.1 Loading and deformation along a cable bolt

Researchers introduced the theory of Beam on Elastic Foundation (BEF) to investigate the behaviour of a tendon in reinforcing joints (El-Ariss, 2007; Friberg, 1940; Jalalifar, 2006; Tanaka and Murakoshi, 2011; Timoshenko, 1940). The governing differential equation for the deflected beam is written as follows:

$$EI\frac{d^4y_{bd}}{dx^4} = -Ky_{bd} \tag{7.5}$$

Where:

E, is the elastic modulus of the cable strand;

K, is the elastic modulus of the foundation;

y_{bd}, is the deflection of the cable strand;

The solution to this differential equation is given by:

$$y_{bd} = e^{\lambda x}(Acos\lambda x + Bsin\lambda x) + e^{-\lambda x}(Ccos\lambda x + Dsin\lambda x) \quad (7.6)$$

$$\lambda = \sqrt[4]{\frac{k}{4EI}} \quad (7.7)$$

Where: A, B, C, D, are constants, determined from the boundary conditions for a particular problem.

And the slope and bending moment of the beam is thus obtained as follows:

$$\theta = y'_{bd} \quad (7.8)$$

$$M = -EIy''_{bd} \quad (7.9)$$

According to the above equations, a laterally loaded cable strand bearing the reaction of the surrounding material is schematically shown in Figure 7.2.

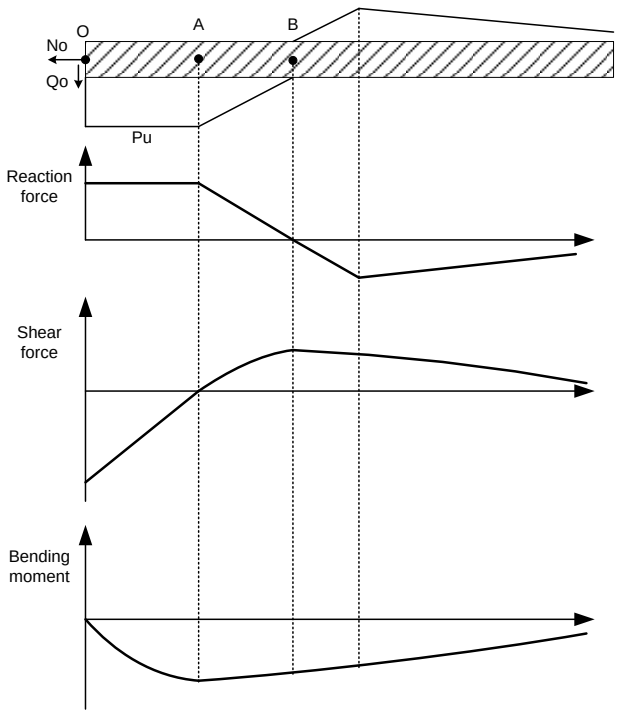

Figure 7.2 Schematic load distribution of a grouted cable strand subjected to shearing

7.2.1.2 Elastic state

When a cable strand is loaded axially or laterally or by a bending moment, it undergoes elastic deformation before the normal or shear stresses exceed its tensile or shear yield strength. If only the axial load or the shear load is applied to a cable strand, the elastic condition of a cable strand is maintained as long as the following expressions are satisfied:

$$N < N_{yield} \tag{7.10}$$

$$Q < Q_{yield} \tag{7.11}$$

$$M < M_{yield} \tag{7.12}$$

Where:

N_{yield}, is the tensile yield strength of a cable strand, equal to $A_b\sigma_{yield}$;

Q_{yield}, is the yield strength in shear of a cable strand, equal to $A_b\tau_{yield}$;

M_{yield}, is the yield bending moment, equal to $\frac{\pi d_b^3}{32}\sigma_{yield}$;

In addition, a relationship exists between the tensile yield strength σ_{yield} and the shear yield strength τ_{yield} for a Tresca material, as $\sigma_{yield} = 2\tau_{yield}$.

7.2.1.3 Yield criteria

For the occurrence of yielding, two typical positions are considered, including the bolt-joint intersection and the plastic hinge. Prior to the occurrence of yielding at these two positions, no yielding occurs at any other position since they carry the maximum shear force and the bending moment of a laterally loaded cable strand.

For the yielding at the bolt-joint intersection due to a combination of axial load and shear load, the cable yielding is determined by the following expression (Neal, 1977; Pellet, 1994):

$$\left(\frac{N_o}{N_{yield}}\right)^2 + \left(\frac{Q_o}{Q_{yield}}\right)^2 = 1 \quad (7.13)$$

For the yielding condition at the maximum bending moment position due to a combination of axial load and bending moment, the following expressions are used (Holmberg and Stille, 1992; Neal, 1977; Pellet, 1994):

$$\frac{N_A}{A} + \frac{M_A y}{I} = \sigma_{yield} \quad (7.14)$$

$$\left(\frac{N_A}{N_{yield}}\right)^2 + \left(\frac{M_A}{M_{pl}}\right)^2 = 1 \quad (7.15)$$

Note that, Eqs. (7.14) and (7.15) correspond to the onset of yielding of the outermost layer of a cable bolt and the formation of a fully plasticised cable cross section respectively. For Eq. (7.14), since the plastic hinge has not formed, thus there is still shear force at this point, which is neglected in Eq. (7.14) as a simplification considering that the shear force is very small at this moment.

7.2.1.4 Failure criteria

With the increase in shear displacement, loads in the cable section between plastic hinges will increase, resulting in the development of yielding. Failure normally occurs either at the bolt-joint intersection or at the plastic hinge position finally when one of the following expressions is satisfied:

$$\left(\frac{N_o}{N_f}\right)^2 + \left(\frac{Q_o}{Q_f}\right)^2 = 1 \quad (7.16)$$

$$\left(\frac{N_A}{N_f}\right)^2 + \left(\frac{M_A}{M_{pl}}\right)^2 = 1 \quad (7.17)$$

Where:

N_f, is the ultimate tensile strength of a cable strand, equal to $A_b\sigma_{bf}$;

Q_f, is the ultimate shear strength of a cable strand, equal to $A_b\tau_{bf}$;

M_{pl}, is the plastic bending moment, equal to $\frac{1.69\pi d_b^3}{32}\sigma_{yield}$;

In addition, a relationship also exists between the ultimate tensile strength σ_{bf} and the ultimate shear strength τ_{bf} for a Tresca material, as $\sigma_{bf} = 2\tau_{bf}$.

7.2.2 Grout and concrete

7.2.2.1 Elastic state

With the deflection of a cable strand loaded in shear, the host grout and concrete provide a reaction force to prevent this deformation. This reaction force is proportional to the compression deformation of grout and concrete. A half-empirical expression was given according to a discussion of the modulus of support material reaction and on properties of rock materials (Lambe and Whitman, 2008; Terzaghi, 1955). This expression is written as:

$$p = K_m u = \frac{E_m}{1.35 d_b} u = \frac{300\sigma_c u}{d_b} \tag{7.18}$$

Where:

p, is the support reaction;

K_m, is the lateral stiffness of support material;

E_m, is the modulus of elasticity of support material;

u, is the lateral deformation of support material.

7.2.2.2 Yield state

The host material begins to yield when the reaction stress exceeds its yield strength. Theoretically, this occurs initially at the bolt-joint intersection. With the increase of the cable strand deflection, the yielding propagates from the joint plane towards the plastic hinge positions. The yield criterion is expressed as (Holmberg and Stille, 1992):

$$\frac{300\sigma_c u_l}{d_b} = p_u \tag{7.19}$$

Where:

u_l is the compression displacement of surrounding materials at which the cable yielding occurs;

p_u is the yield strength of the support host materials.

It is assumed that the residual strength of the support material is constant and equal to the yield strength, since a bolt crushed into the support material when additional displacement occurs (Holmberg and Stille, 1992).

For the calculation of the yield strength, Pellet (1996) gave the following expression as an approximation.

$$p_u = \sigma_c d_b \tag{7.20}$$

7.3 Cable plastic hinge location

7.3.1 Initiation of plastic hinge

For the grout and concrete on the compression side, it is assumed they are in a plastic state and the reaction force is constant from the yield position to the joint plane. Thus based on the force equilibrium equation in the lateral direction of the cable strand, the shear force at the bolt-joint intersection can be obtained from:

$$\sum F_y = 0$$

$$Q_{oy} = p_u l_y + Q_{Ay} \tag{7.21}$$

Where:

Q_{oy}, is the shear force at bolt-joint intersection when a cable starts to yield;

l_y, is the distance from the start position of the cable yielding to the joint plane;

Q_{Ay}, is the cable shear force at yielding location when the cable yielding starts.

According to the bending moment equilibrium at point A (See Figure 7.2), the bending moment at point A is:

$$\sum M_A = 0$$

$$M_A = Q_{oy} l_y - \frac{p_u {l_y}^2}{2} \tag{7.22}$$

Combining Eqs. (7.21) and(7.22) yields,

$$M_A = Q_{Ay} l_y + \frac{p_u {l_y}^2}{2} \tag{7.23}$$

Then, the start positon of cable yielding can be acquired by substituting Eqs. (7.3), (7.4), (7.23) into the yield criterion Eq. (7.14) as follows:

$$\frac{p_u}{2} {l_y}^2 + Q_{Ay} l_y + \frac{N_A d_b}{8} - \frac{\pi d_b^3}{32} \sigma_y = 0 \tag{7.24}$$

$$l_y = \frac{-Q_{Ay} + \sqrt{Q_{Ay}^2 - \frac{p_u}{4}(N_A d_b - \frac{\pi d_b^3}{4} \sigma_y)}}{p_u} \tag{7.25}$$

If let Q_{Ay} equals zero, the plastic distance degenerates to be identical to Jalalifar's derivation (Jalalifar, 2006).

$$l_y = \sqrt{\frac{1}{4p_u}(\frac{\pi d_b^3}{4} \sigma_y - N_A d_b)} \tag{7.26}$$

7.3.2 Formation of plastic hinge

The cable yielding initiates at the maximum bending moment point in the outermost fibre of a cable strand, and develops across the cross section to form a fully plasticized cross section - plastic hinge. The shear force at the plastic hinge point disappears when the plastic hinge forms completely. A combination of the axial force and bending moment leads to the presence of a plastic hinge.

Based on Eqs. (7.15) and (7.23), replacing the tensile yield strength and plastic bending moment produces the following relation:

$$\frac{32 p_u l_{pl}^2}{3.38 \pi d_b^3 \sigma_{yield}} + (\frac{4N_A}{\pi d_b^2 \sigma_{yield}})^2 = 1 \tag{7.27}$$

Then by simplification, the fully plasticized hinge point distance is obtained as:

$$l_{pl} = \sqrt{\frac{3.38(\pi^2 d_b^4 \sigma_y^2 - 16N_A^2)}{32 p_u \pi d_b \sigma_y}} \tag{7.28}$$

$$l_{pl} = \sqrt{\frac{3.38(\pi^2 d_b^4 \sigma_y^2 - 16N_A^2)}{32 \sigma_c \pi d_b^2 \sigma_y}} \tag{7.29}$$

In Eq. (7.29), it can be seen that the plastic hinge distance is mainly influenced by bolt diameter, yield strength of bolt, strength of support material and axial load at the plastic hinge. The influence of these four factors on this distance is also very clear. As expected, the plastic hinge distance increases with the increase of bolt diameter, d_b, and bolt tensile yield strength, σ_y. However, the distance decreases with the increase of support material strength, σ_c, and axial load of the cable strand, N_A. Especially regarding the influence of the axial load, since the additional shearing-induced axial load is very small at the initiation of the plastic hinge, it is negligible in the analysis of the plastic hinge distance (Jalalifar, 2006). Thus the distance is mainly affected by the cable pre-tension in terms of the axial load, N_A, in Eq. (7.29).

7.3.3 Relationship between plastic hinge distances

As discussed previously, cable plasticization occurs and propagates from the outermost section to the centre at an identical cross section for an un-pre-tensioned cable and from the tensile side to the compressive side for a pre-tensioned cable. Since the initiation point of plastic hinge and the fully plasticized hinge are at the same cross section, the yield distance l_y and l_{pl} should be equal. Thus, by combining Eqs. (7.24) and (7.29), the expression of shear force at plastic hinge point, Q_{Ay}, can be obtained.

7.4 Contribution of a bolt to joint shear strength

There have been various analytical and experimental investigations undertaken looking at the cable and rock bolts and their contribution to joint shear strength (Ferrero, 1995; Grasselli, 2005; Jalalifar and Aziz, 2010b; Pellet and Egger, 1996). These studies suggested that two types of contribution, the frictional effect and the dowel effect, were made by a bolt to the joint shear strength. The typical loading state of a bolt-reinforced joint is shown in Figure 3.12.

The bolt contribution to the joint shear strength is as follows:

$$R_b = N_o \cos(\alpha - \theta) + Q_o \sin(\alpha - \theta) + [N_o \sin(\alpha - \theta) - Q_o \cos(\alpha - \theta)] tan\emptyset \quad (7.30)$$

There are two different definitions about the dowel effect. One is related to the combination of the parallel components of the axial and shear forces of the bolt to the joint (Grasselli, 2005; Jalalifar and Aziz, 2010b; Pellet and Egger, 1996), and the expression is as follows:

$$R_{dowel} = N_o \cos(\alpha - \theta) + Q_o \sin(\alpha - \theta) \quad (7.31)$$

The other one is connected to only the bolt shear force itself, including the normal component and the parallel component of the shear force to the joint which produce indirect and direct contributions respectively to the joint shear strength (Ferrero, 1995). The expression is as follows:

$$R_{dowel} = Q_o \sin(\alpha - \theta) - Q_o \cos(\alpha - \theta)\, tan\emptyset \quad (7.32)$$

In this thesis, the direct contribution of both axial and shear forces is considered as the dowel effect, thus Eq. (7.31) was used.

7.5 Mechanical model

As previously discussed, when a grouted rock bolt or cable strand in rock is subjected to shearing, the bolt deforms and plastic hinges form at both sides of the joint plane. Reaction forces in the host material (grout and rock) are mobilized accordingly to control the deformation of the bolt and loads are transferred between the host material and the bolt. In the shearing process, both the bolt and the host material experience the elastic stage and plastic stage successively.

During loading, the reinforcement bolt and the host material progress from the elastic stage to the plastic stage. In the elastic stage of the host material, the host material reaction force is approximately proportional to its compression displacement as discussed previously in Eq. (7.18) (Lambe and Whitman, 2008; Terzaghi, 1955). According to Ferrero's (1995) study, the shape of the bolt

deflecting section can be approximated with a parabolic equation. Thus it is reasonable to assume the reaction force distribution exhibits the same shape in the elastic stage. In the plastic stage of the host material, the host material reaction force remains constant since the bolt crushes into the host material (Holmberg and Stille, 1992). Thus a constant uniform distribution of the reaction force is assumed for the host material in its plastic stage.

During shear loading, the bolt moduli decrease from the perfectly elastic state to the fully plastic state along the bolt deflecting section between plastic hinges, and the host material reaction force varies from a parabolic distribution to a constant distribution.

According to the analysis of the plastic hinge formation, the distance from joint plane to plastic hinge is normally less than 3~ 4 times the bolt diameter for most commonly used bolts. In the tests reported by Jalalifar and Aziz (2010b) on steel rebar bolts, this length was normally less than 60 mm, which was less than three times the bolt diameter. In addition, when a bolt deflects due to shearing, the tension and compression forces between bolt and the host material are produced on the top and bottom side respectively. Since the cohesion between the host material and the bolt is very small, the grout on the tension side can easily detach from the bolt surface. After the grout and rock yields within the compressive zone, the host material is crushed and unable to bear higher compressive load. Based on the above analysis, the frictional effect between the host material and bolt is negligible as reported in several previous studies (Jalalifar, 2006; Pellet and Egger, 1996).

An assumption is made here that the deflecting section of a bolt between two plastic hinges is statically indeterminate with two fixed ends. Two different mechanical models with elastic reaction and plastic reaction of the host material are shown in Figure 7.3, respectively.

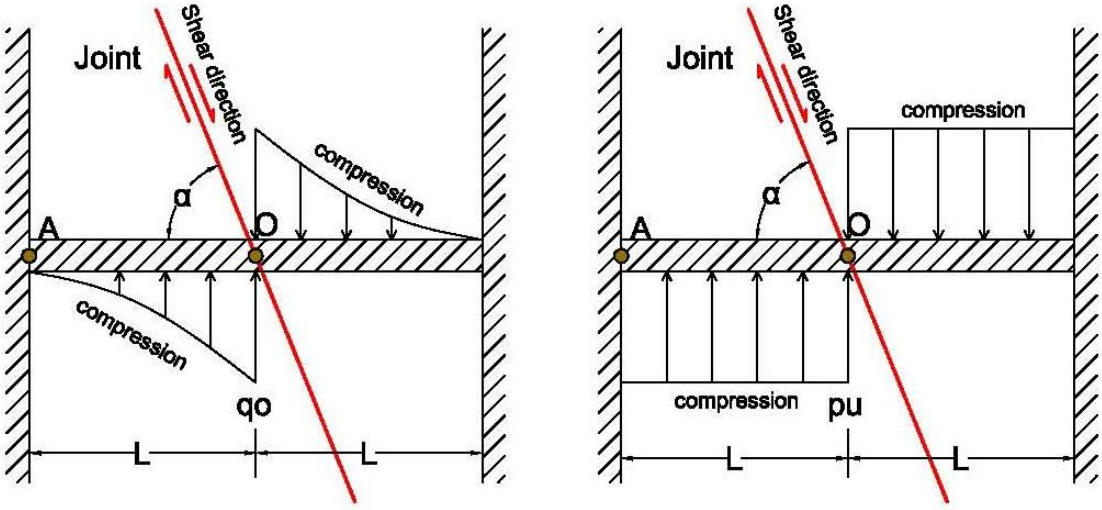

Figure 7.3 Simplified mechanical models of a bolt subjected to shearing both in elastic and plastic stages of host material

7.6 Elastic stage of the host material

To solve a statically indeterminate beam problem, first one needs to transform the original problem into to a statically determinate beam by removing all redundant reactions (Hibbeler *et al.*, 2006). In this problem, there are three redundant reactions that can be removed. Considering half of the beam, a combination of axial force R_1, shear force R_2, and bending moment R_3 can be used to represent the restraint of the other half as shown in Figure 7.4.

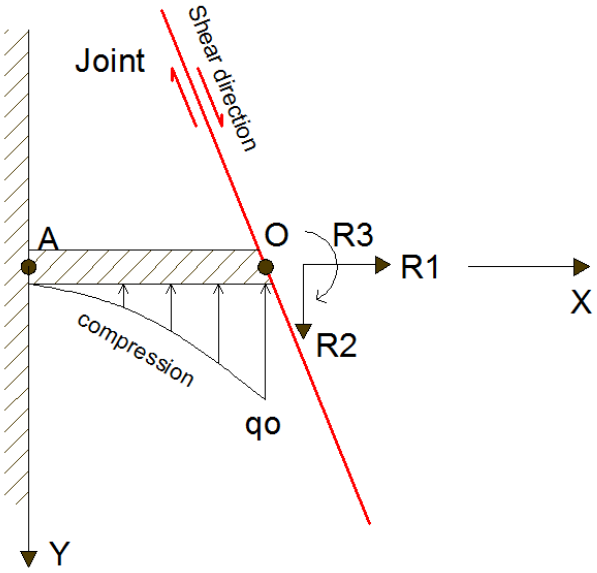

Figure 7.4 Loading state of a statically determinate beam

Thus, based on the force method of statically indeterminate structures, three compatibility equations can be written as follows:

$$\begin{cases} f_{11}R_1 + f_{12}R_2 + f_{13}R_3 + \Delta_{1q} = \Delta_1 \\ f_{21}R_1 + f_{22}R_2 + f_{23}R_3 + \Delta_{2q} = \Delta_2 \\ f_{31}R_1 + f_{32}R_2 + f_{33}R_3 + \Delta_{3q} = \Delta_3 \end{cases} \tag{7.33}$$

Or in a matrix form,

$$\begin{bmatrix} f_{11} & f_{12} & f_{13} \\ f_{21} & f_{22} & f_{23} \\ f_{31} & f_{32} & f_{33} \end{bmatrix} \begin{bmatrix} R_1 \\ R_2 \\ R_3 \end{bmatrix} + \begin{bmatrix} \Delta_{1q} \\ \Delta_{2q} \\ \Delta_{3q} \end{bmatrix} = \begin{bmatrix} \Delta_1 \\ \Delta_2 \\ \Delta_3 \end{bmatrix} \tag{7.34}$$

Or simply

$$\boldsymbol{fR} + \Delta_{\boldsymbol{q}} = \Delta \tag{7.35}$$

Where:

f_{ij}, is the displacement along the direction of R_i caused by the unit of R_j, also known as flexibility coefficient;

Δ_{iq}, is the displacement along the R_i direction caused by the grout reaction force;

Δ_i, $i = 1,2,3$, is the axial extension, the lateral deflection and the deflection angle of bolt at point O.

According to the loading state in the elastic stage, the influence of the grout reaction force is:

$$q(x) = \frac{q_o}{L^2}x^2 \tag{7.36}$$

$$Q(x) = \frac{q_o}{3L^2}x^3 \tag{7.37}$$

$$M(x) = \frac{q_o}{12L^2}x^4 \tag{7.38}$$

$$v(x) = \frac{1}{EI} \cdot \frac{q_o}{360L^2}x^6 \tag{7.39}$$

Thus, the flexibility matrix and the deformation matrix induced by external loads can be obtained based on beam theory as:

$$\boldsymbol{f} = \begin{bmatrix} \frac{L}{EA} & 0 & 0 \\ 0 & \frac{L^3}{3EI} + \frac{kL}{GA} & \frac{L^2}{2EI} \\ 0 & \frac{L^2}{2EI} & \frac{L}{EI} \end{bmatrix} \tag{7.40}$$

$$\Delta_q = \begin{bmatrix} 0 \\ -(\frac{q_o L^4}{360EI} + \frac{k q_o L^2}{12GA}) \\ -\frac{q_o L^3}{60EI} \end{bmatrix} \tag{7.41}$$

Where:

L, is the plastic hinge distance from the joint plane to hinges, refer to Eq. (7.26);

k, is a concentration coefficient of the shear stress distribution at the cable cross section, which is equal to 4/3 for a solid cross section and is determined using the inner and outer radii for a hollow cross section (Gere and Timoshenko, 1990).

Because of the symmetry of the deflecting beam, it is reasonable to assume $R_3 = 0$ (Pellet and Egger, 1996). Thus, substituting Eqs. (7.40) and (7.41) into Eq. (7.34) yields:

$$\begin{bmatrix} \frac{L}{EA} R_1 \\ \left(\frac{L^3}{3EI} + \frac{kL}{GA}\right) R_2 - (\frac{q_o L^4}{360EI} + \frac{k q_o L^2}{12GA}) \\ \frac{L^2}{2EI} R_2 - \frac{q_o L^3}{60EI} \end{bmatrix} = \begin{bmatrix} \Delta_1 \\ \Delta_2 \\ \Delta_3 \end{bmatrix} \tag{7.42}$$

Solving Eq. (7.42)in reference to Δ produces:

$$R_1 = \frac{EA}{L} \Delta_1 \tag{7.43}$$

$$R_2 = \frac{(2GAEIL^2 + 60kE^2I^2)\Delta_3 - 12GAEIL\Delta_2}{18EIkL^2 - 3GAL^4} \tag{7.44}$$

$$q_o = \frac{(80GAEIL^2 + 240kE^2I^2)\Delta_3 - 120GAEIL\Delta_2}{6EIkL^3 - GAL^5} \tag{7.45}$$

Based on Eq. (7.37), the shear force at point O can be obtained:

$$R_2 = \frac{q_o L}{3} \tag{7.46}$$

Thus combining Eqs. (7.44), (7.45), (7.46) gives the relationship between Δ_2 and Δ_3 as follows:

$$\Delta_3 = \frac{18GAL}{13GAL^2+30kEI} \cdot \Delta_2 \tag{7.47}$$

Substituting Eq. (7.47) into (7.44)and (7.45) yields:

$$R_2 = \frac{240kGAE^2I^2-40G^2A^2EIL^2}{(6EIkL-GAL^3)(13GAL^2+30kEI)} \cdot \Delta_2 \tag{7.48}$$

$$q_o = \frac{720kGAE^2I^2-120G^2A^2EIL^2}{(6EIkL^2-GAL^4)(13GAL^2+30kEI)} \cdot \Delta_2 \tag{7.49}$$

According to the deformation relationship shown in Figure 7.5, the following equation exists:

$$\frac{\Delta_2}{\Delta_1} = \frac{sin\alpha}{\cos(\alpha-\theta)} = \frac{sin\alpha}{\cos\alpha\cos\theta+\sin\alpha\sin\theta} \tag{7.50}$$

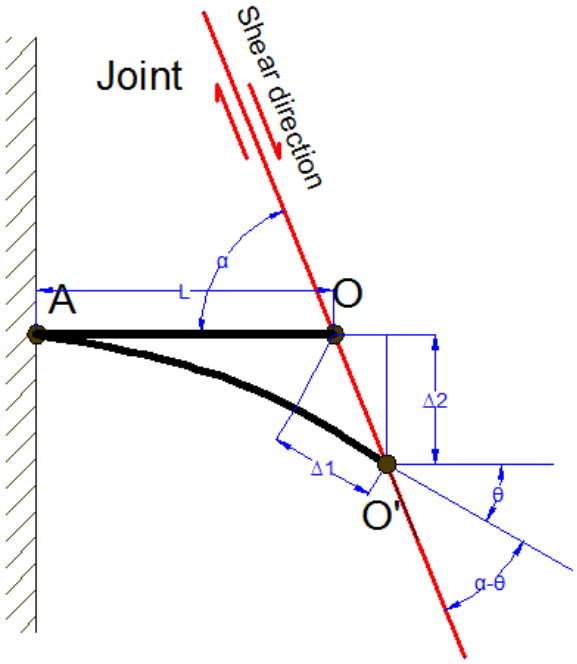

Figure 7.5 Deformation compatibility condition at bolt-joint intersection

Since θ, equal to Δ_3, is very small in the elastic stage, one can get:

$$\Delta_1 = \frac{\cos\alpha + \sin\alpha \cdot \Delta_3}{sin\alpha} \cdot \Delta_2 \tag{7.51}$$

Thus combining Eqs. (7.43), (7.48), (7.49) and (7.51), the bolt loading state with the increase of the shear displacement can be obtained and then the occurrence of the plastic hinges formation in the elastic stage can be checked using Eqs. (7.14) and (7.15). To further simplify these calculations, it is sufficient to only check the state with the load density (q_o) being equal to the maximum concrete reaction, p_u, equal to $\sigma_c d_b$ (Pellet and Egger, 1996).

7.7 Plastic stage of the host material

When the shear deformation of a grouted bolt increases, the host medium reaction force increases as well. The host medium plasticisation starts after the reaction force exceeds its yield strength, and from then on, the reaction force in the plastic zone remains constant. Thus, a new loading state appears as shown in Figure 7.3.

It should be noted that the elastic stage in the host material transforms into the plastic stage in a plasticisation process. In this process plasticisation in the host medium propagates from the joint surface plane inwards to the plastic hinges. Finally, the whole length between the joint surface and plastic hinges behaves in the plastic manner. In this study, this transition stage is not considered.

In a similar manner to the elastic stage, the redundant reactions can be written as follows:

$$R_1 = \frac{EA}{L}\Delta_1 \tag{7.52}$$

$$R_2 = \frac{\Delta_2 + \frac{p_u L^4}{8EI} + \frac{k p_u L^2}{2GA}}{\frac{L^3}{3EI} + \frac{KL}{GA}} \tag{7.53}$$

$$R_2 = \frac{\Delta_3 + \frac{p_u L^3}{6EI}}{\frac{L^2}{2EI}} \tag{7.54}$$

Since the bolt deflection angle is very small in the elastic stage of the host material, in the plastic stage the deflection angle is assumed to start from zero. Thus the deformation compatibility relationship in the plastic stage is the same as in the elastic stage.

$$k_1 = \frac{\Delta_2}{\Delta_1} = \frac{sin\alpha}{\cos(\alpha-\theta)} \tag{7.55}$$

Combining Eqs. (7.52), (7.53) and (7.55) produces:

$$R_1 = k_2 \cdot R_2 + k_3 \tag{7.56}$$

Where:

$$k_2 = \frac{\frac{AL^2}{3I} + \frac{kE}{G}}{k_1}$$

$$k_3 = -\frac{\frac{p_u AL^2}{8I} + \frac{kp_u EL}{2G}}{k_1}$$

When the axial force and shear force at point O satisfy the failure criteria (7.16), then the cable breaks. Thus, the axial and shear forces at point O when the cable failure occurs can be obtained from Eqs. (7.16) and (7.56).

After obtaining the axial and shear forces at point O, substituting them into Eq.(7.30)yields the bolt contribution to the joint shear resistance capacity.

7.8 Joint shear displacement and bolt deformation at failure

The final deformation curve of a bolt at failure subjected to shearing consists of two parts, the host medium reaction and the bolt shear force. With the shear force (Q_o) derived from Eqs. (7.16) and (7.56), and the host medium reaction strength (p_u), the corresponding contributions can be described as follows:

$$V_{Q_o} = \frac{Q_o}{6EI}(3Lx^2 - x^3) + \frac{kQ_o}{GA}x \tag{7.57}$$

$$V_{p_u} = \frac{p_u}{24EI}(x^4 - 4Lx^3 - 4L^2x^2) + \frac{kp_u}{2GA}x^2 \tag{7.58}$$

Then, the actual deformation curve at failure is given by:

$$V(x) = V_{Q_o} - V_{p_u} \tag{7.59}$$

For the case when $x = L$, the bolt shear displacement ($V(L)$) at point O is equal to one half of the total joint shear displacement since Eq. (7.59) represents a half space only (see Figure 7.3).

7.9 Parametric investigation

In the derivation of the bolt contribution to joint shear strength, a variety of related factors are taken into account. All these factors together determine the bolt performance subjected to shearing. Accordingly, in view of cable bolts, four of these influencing factors are investigated in detail, including bolt pre-tension, joint friction angle (coefficient), concrete strength (the host medium), and bolt installation angle.

7.9.1 Cable pre-tension

Pre-tension is an important influencing factor in a cable-reinforced jointed concrete system. Many variables are influenced by pre-tension during shearing, such as the plastic hinge distance, the ultimate joint shear failure displacement, the shear and axial forces of a cable strand at failure. Thus the cable bolt contribution to joint shear strength is also impacted. In simple terms, the greater the cable bolt pre-tension, the smaller the plastic hinge distance and the ultimate (final)joint shear displacement at cable failure. Though the influence of cable bolt pre-tension on some variables is clear, its impact on the joint shear resistance capacity is not apparent since these variables can also influence each other. To clarify the effect of cable bolt pre-tension on the joint shear strength, these pertinent variables need to be considered simultaneously.

Figure 7.6 shows the relationship between the shear force and the axial force at different cable pre-tensions, and a specific case of cable bolt failure ($E = 4GPa$, $G = 1.6GPa$). The other parameters involved in this section are $\varphi = 24°$,$d_b = 0.022m$. Solutions for other cases are listed in Table 7.1 to Table 7.3.

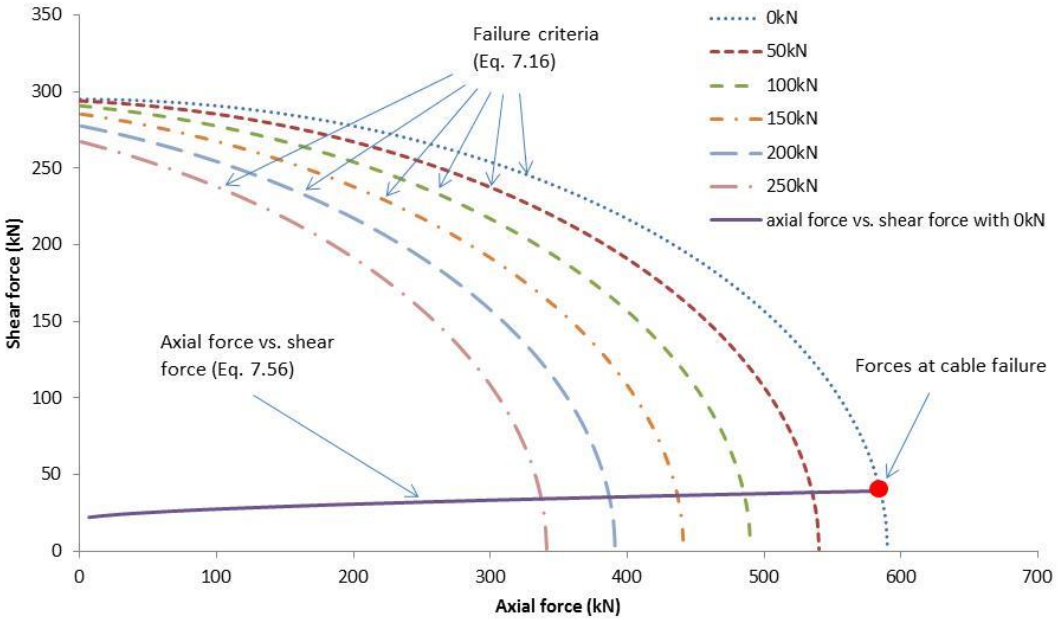

Figure 7.6 Shear force versus axial force in the cable bolt

Table 7.1 Cable bolt contribution to joint shear strength at various cable pre-tensions

Pre-tension effect (E=2 GPa, G=0.8 GPa)						
Pre-tension (kN)	0	50	100	150	200	250
θ (radian)	1.54	1.41	1.296	1.184	1.08	0.98
No (kN)	587	586	588	587	587	587
Qo (kN)	35.7	34.8	34.2	33.5	33.0	32.6
R_{No} (kN)	595	620	636	641	639	631
R_{Qo} (kN)	-15	-10	-5	-1	3	6
R (kN)	580	610	631	640	642	638

Table 7.2 Cable bolt contribution to joint shear strength at various cable pre-tensions

Pre-tension effect ($E_{average}$=4 GPa, $G_{average}$=1.6 GPa)						
Pre-tension (kN)	0	50	100	150	200	250
θ (radian)	0.929	0.873	0.818	0.760	0.705	0.646
No (kN)	587	584	585	582	586	586
Qo (kN)	39.3	39.0	38.7	38.5	38.5	38.5
R_{No} (kN)	625	613	603	587	576	559
R_{Qo} (kN)	10	12	14	16	18	21
R (kN)	634	625	617	603	594	579

Table 7.3 Cable bolt contribution to joint shear strength at various cable pre-tensions

Pre-tension effect (E=10 GPa, G=4 GPa)						
Pre-tension (kN)	0	50	100	150	200	250
θ (radian)	0.544	0.516	0.486	0.456	0.424	0.389
No (kN)	581	584	582	583	583	581
Qo (kN)	49.0	49.3	49.5	49.9	50.3	50.8
R_{No} (kN)	519	512	498	487	474	457
R_{Qo} (kN)	31	32	34	35	37	39
R (kN)	550	544	532	522	510	495

Theoretically, when cable bolt failure occurs at the bolt-joint intersection, the entire cable deflecting section between the plastic hinges should be in the plastic state. Thus the cable plastic stage moduli should be used in the calculation. During the cable strain hardening, cable moduli vary from the maximum to a minimum. From the laboratory tensile tests carried out on cable wires (refer to Chapter 4) (Orica, 2014), the averages of cable wire plastic moduli are $E_{average} = 4\ GPa$, $G_{average} = 1.6\ GPa$. Here in Table 7.1 to Table 7.3, a range of cable bolt plastic moduli are used, including the average one, a smaller one and a larger one.

From Table 7.1 to Table 7.3 it can be seen that the cable pre-tension has two different effects on the joint shear strength. For a cable failing at the smaller moduli, the greater the cable pre-tension, the more contribution the cable makes. In contrast, an exactly opposite trend takes place for a cable failing at the average or higher moduli.

Figure 7.7 shows the double shear test results of SUMO cables and the test apparatus. This figure offers the shear displacement and shear force at failure and the average shear stiffness of the shear system rather than real loading-displacement curves. Compared with the experimental results analysed in Chapter 5 and shown in Figure 7.7, it is clear that the cable bolt pre-tension effect in this analysis is consistent with the experimental tests. Specifically, the cable bolt pre-tension decreased the shear strength of joints reinforced with indented SUMO cable strands which normally failed at much smaller shear displacements than the plain cable bolt.

This corresponds to the cable bolt pre-tension effect shown in Table 7.2 and Table 7.3. However, the cable bolt pre-tension increased the shear strength of joints strengthened with plain SUMO cable bolts which normally failed at much larger shear displacements. Thus, this corresponds to the cable bolt pre-tension effect shown in Table 7.1.

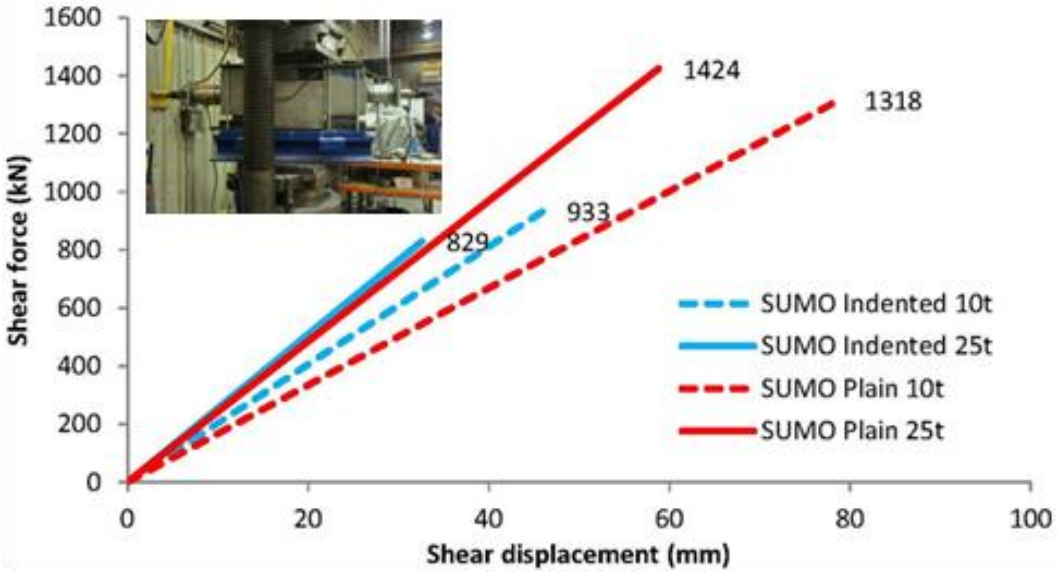

Figure 7.7 Pre-tension effect on joint shear resistance capacity

In the above analysis, there are two different cable pre-tension effects on the bolted joint shear strength. Going back to check the cable contribution to joint shear strength described in Eq. (7.30), since the bolt installation angle and the joint friction angle are constant the cable contribution was found to be influenced by two parameters, the cable loading state (the axial force and shear force) and the cable deflection angle. Therefore, theoretically the cable pre-tension affects the joint shear strength by changing these two parameters. Checking data in Table 7.1 to Table 7.3, it can be clearly seen that both the axial and shear forces obtained at various cable pre-tensions do scarcely vary. Thus the joint shear strength variation is mainly due to the cable deflection angle. Since the cable strand pre-tension has two different effects, the cable deflection angle should correspondingly have two effects on the joint shear strength as well.

There is a maximum joint shear strength point (turning point) when the cable deflection angle changes. In Table 7.1 to Table 7.3, the joint shear strength increases

with the increase of cable deflection angle when the cable deflection angle is less than approximately one radian (57°) and decreases when the cable deflection angle exceeds one radian. Therefore one radian is the turning point of the cable pre-tension effect on joint shear strength in the studied case.

Why is it one radian? Is it always one radian for all cases or just a special case? Since the joint shear strength is ultimately determined by the cable loading state and the joint friction angle (Eq. (7.30)), the turning point of cable deflection angle (where the maximum joint shear strength occurs) should be determined by them as well.

Figure 7.8 and Figure 7.9 show the influences of the axial load and the joint friction coefficient respectively on the turning point of cable deflection angle for a perpendicularly reinforced joint.

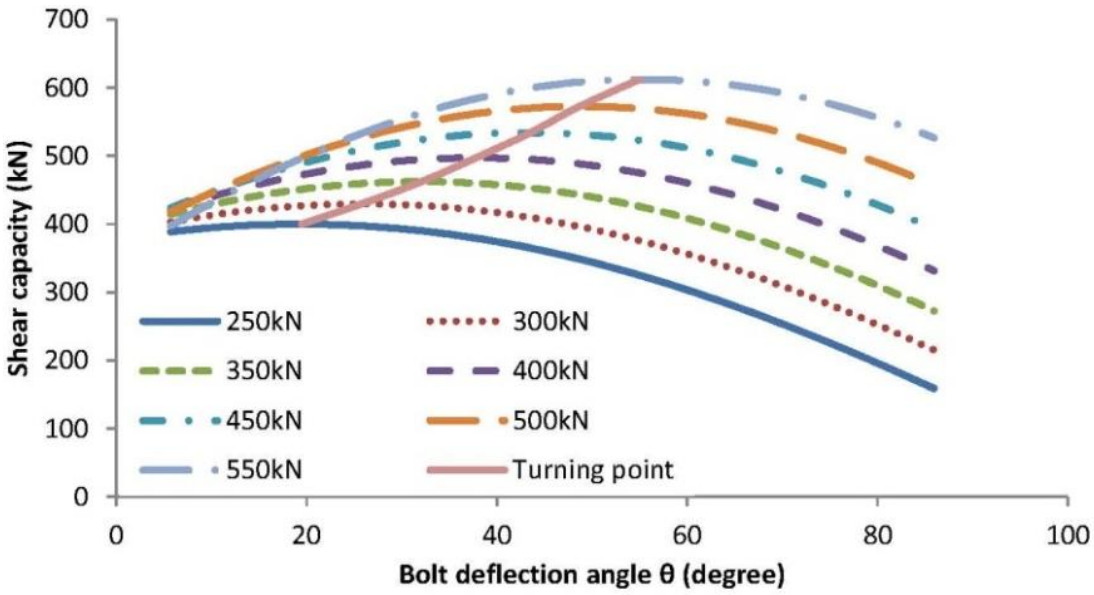

Figure 7.8 Influence of axial load at failure on the turning point of joint shear strength with the joint friction coefficient of 0.44.

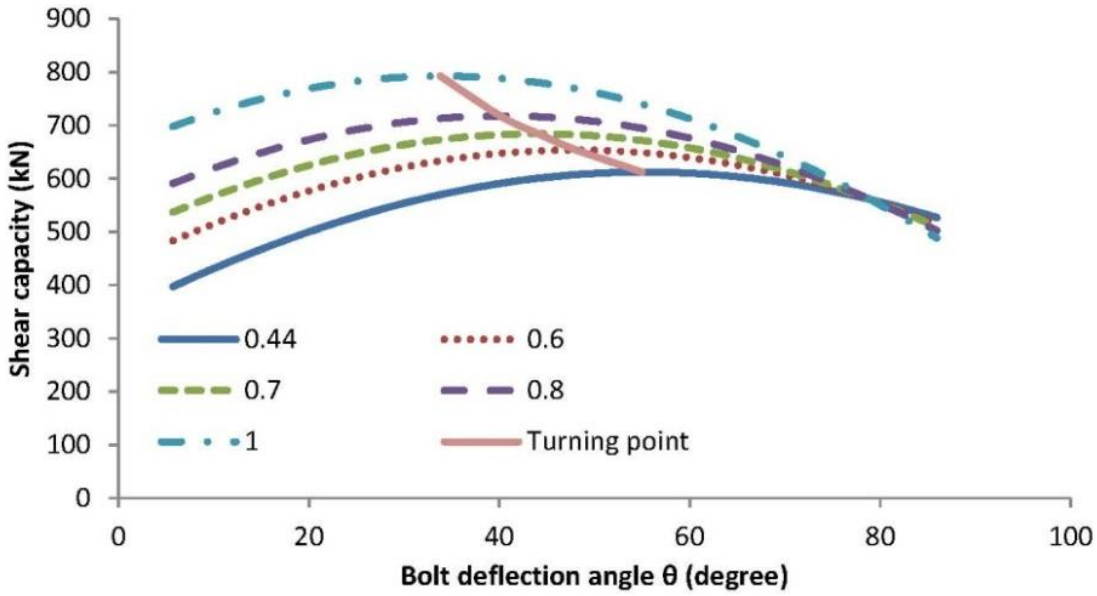

Figure 7.9 Influence of the joint friction coefficient on the turning point of joint shear strength with the axial load of 550 kN

In Figure 7.8, the turning point of bolt deflection angle has a very clear increasing trend with the increase in axial load. Specifically, the turning point increases from 19° to 55° with the axial load ascending from 250 kN to 550 kN. However, in Figure 7.9, the turning point decreases with the increase of joint friction coefficient. While the turning point is located at 55° with a friction coefficient of 0.44, it drops to only about 34° with a joint friction coefficient of 1. Thus, the turning point of cable deflection angle is not fixed and it changes with the variation of the cable loading state and the joint friction angle. The calculated cable deflection turning point of one radian in Table 7.1 to Table 7.3 is for a specific case ($tan\emptyset = 0.44, \alpha = 90°, N_o \approx 580\ kN$).

7.9.2 Joint friction angle/coefficient

Since the joint friction angle appeared only in the calculation of cable contribution to joint shear strength (refer to Eq. (7.30)), it only affects the joint shear strength but not the final loading state of cable bolts at failure. The influence of the joint friction angle has been given in Figure 7.9 and its effect on the turning point of cable deflection angle has been discussed as well. In addition to this, the joint friction angle effect on joint shear strength weakens with the increase of the cable deflection angle and there is almost no difference when the cable deflection angle approaches

80° as shown in Figure 7.9 and Figure 7.10. The large deflection angle normally occurs in the case of weak concrete and small cable pre-tension. And thus the joint friction angle effect is much more evident in the opposite situation (strong concrete and large cable pretension) as shown in Figure 7.10. Also as expected, a higher friction angle produces higher joint shear strength.

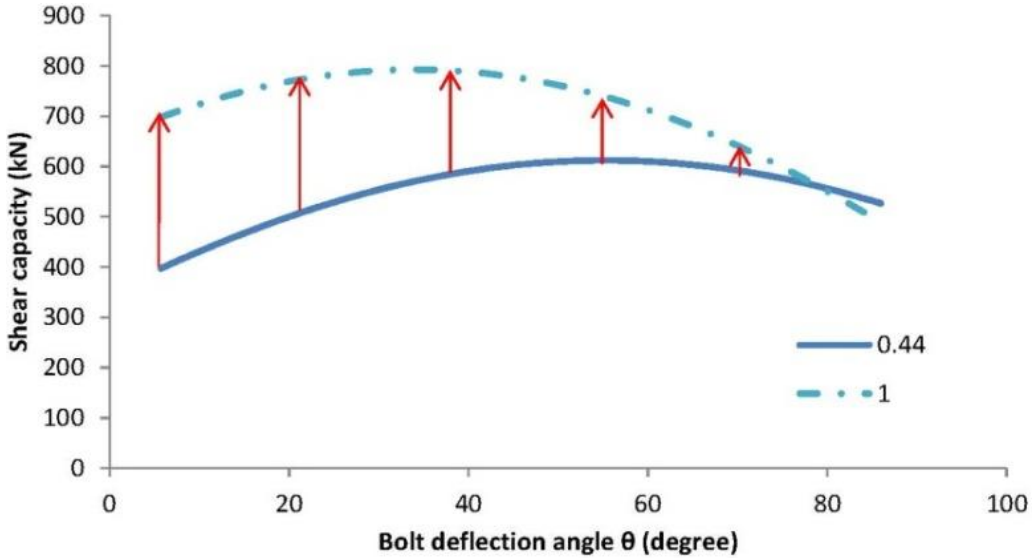

Figure 7.10 Influence of the joint friction coefficient on the joint shear strength at varied cable deflection angles for the axial load of 550 kN

7.9.3 Concrete strength

The strength of concrete and grout material has a significant influence on the cable bolt deformation and the shear strength of a reinforced joint (Aziz *et al.*, 2003; Craig and Aziz, 2010; Ferrero, 1995; Jalalifar *et al.*, 2006b; Spang and Egger, 1990). It is reasonable to make an assumption that the shear displacement increases with the decrease of the surrounding concrete strength. Past studies (Aziz *et al.*, 2003; Jalalifar *et al.*, 2006b) also supported this assumption as shown in Figure 7.11. Thus it is also credible that the tensile strain of cable bolts anchored in soft concrete progresses further than in hard concrete. Hence, the cable bolt moduli at failure are assumed to increase with the increase of concrete strength in Table 7.4. The theoretically calculated results of cable bolts installed in concrete of varied strengths are given in Table 7.4.

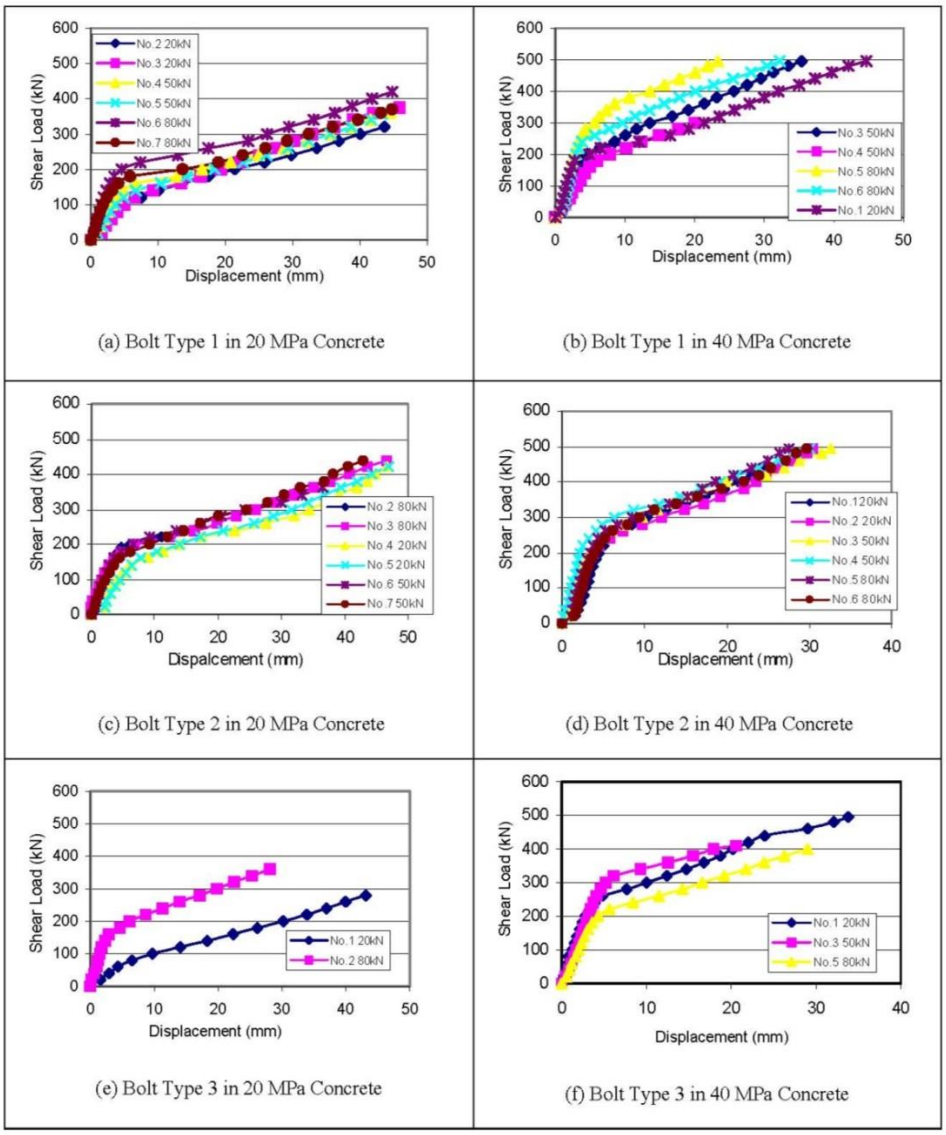

Figure 7.11 Shear load and shear displacement of bolts tested in both 20 MPa and 40 MPa strength concrete under different loading conditions (Aziz *et al.*, 2003)

Table 7.4 Cable loading state at failure with varied concrete strengths

Concrete strength (MPa)	Shear failure load per joint (kN)	Cable modulus at failure (GPa)	Joint shear displacement (mm)	Axial force component at bolt-joint intersection (kN)	Shear force component at bolt-joint intersection (kN)
20	641	3	119	588	23
40	631	4	73	584	39
60	611	5	53	579	56
80	592	6	42	572	72

Similar to the past experimental tests carried out by other researchers (Ferrero, 1995; Spang and Egger, 1990), the weaker the concrete, the larger the shear strength of cable bolted joints. The joint shear displacement is very large when the concrete is very soft, but it cannot further increase since the concrete will collapse prior to the cable bolt failure. When the concrete is very strong, the cable failure will be similar to a guillotine shear test since the shear force will increase and the axial force will decrease. The calculated values in Table 7.4 indicate that as the concrete strength increases the cable bolt shear force increases at a greater rate than the decrease in axial force. This is consistent with the experimental results in this study and also in a previous study (Ferrero, 1995) that showed more tensile failures were witnessed in weak concrete while more tensile-shear combined failures were seen in hard concrete.

7.9.4 Cable installation/inclination angle

In practical application, cable bolts may be anchored at any angle to joints and therefore for each case they will behave differently. Shear tests have been carried out on concrete/rock joints reinforced with bolts at various bolt installation angles to study their influence and experimental conclusions have been drawn in several papers by other researchers (Azuar, 1977; Bjurstrom, 1974; Egger and Fernandes, 1983; Grasselli, 2005; Haas, 1981; Hibino and Motojima, 1981; Spang and Egger, 1990). In these studies, the bolt installation angle across the joint was found to influence the bolt failure mode, the shear strength and the deformation stiffness of a bolted joint.

Based on the analytical method, the influence of bolt installation angle on the joint shear strength is analysed here with consideration of the joint friction angle variation as shown in Figure 7.12. The relevant parameters are $E = 4\,GPa$, $G = 1.6\,GPa$, $d_b = 0.022\,m$, $\sigma_{yield} = 1677\,MPa$, $\sigma_f = 1885\,MPa$.

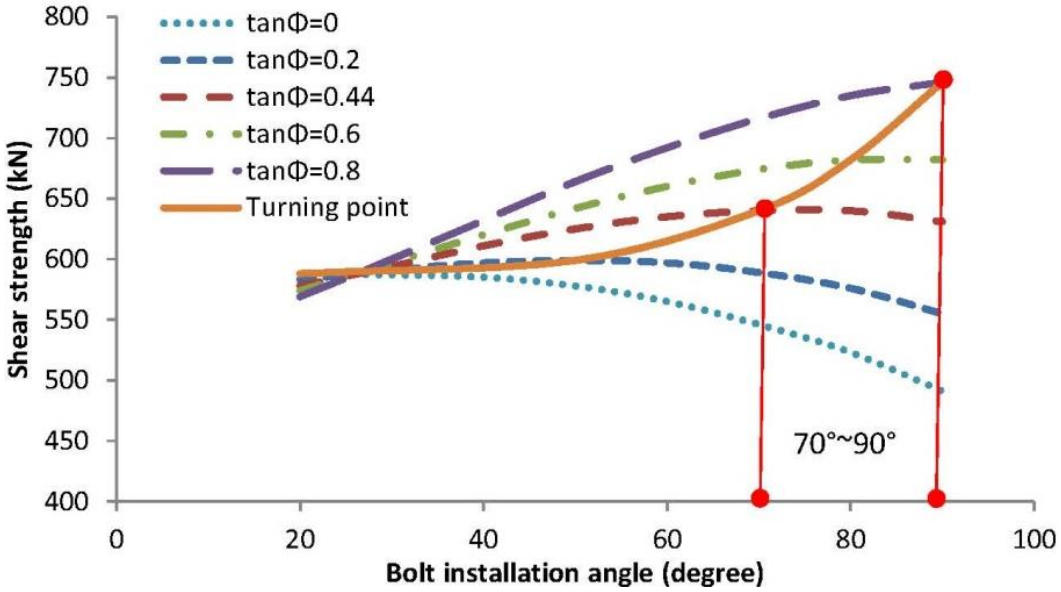

Figure 7.12 Influence of bolt inclination angle on the joint shear strength with varied joint friction coefficients

Clearly, the bolt installation angle influences joint shear strength magnitudes which are further modified by the joint friction angle as shown in Figure 7.12. Under the above given conditions, for the extreme case of the joint friction coefficient of 0, the joint shear strength continuously decreases with the increase of bolt installation angle, whereas for a joint friction coefficient of 0.8, the joint shear strength continues to increase. The case of high joint friction angle partly agrees with Spang and Egger's (1990) conclusion. For the friction angle between these two cases, the joint shear strength increases for lower installation angles, reaching a maximum and then decreases. This maximum versus the bolt installation angle is described by the "turning point" line as shown in Figure 7.12. Thus, there is a maximum joint shear strength for each joint friction angle, and a turning point of bolt installation angle. In detail, the turning point of bolt installation angle ascends roughly from 50°, to 70° and 80° when the joint friction coefficient increases from 0.2, to 0.44 and 0.6, respectively. For practical purposes it can be assumed that in most cases the rock joint coefficient of friction would be higher than approximately 0.4 which is the concrete joint friction coefficient used in this study. Thus, it can be inferred that the maximum joint shear strength will occur mostly within the bolt installation angle of 70°-90° as shown in Figure 7.12.

7.10 Comparison of analytical and experimental results

To validate this analytical method, the results of the method were compared to the double shear tests carried out on commonly used cable bolts tested in the University of Wollongong laboratory.

To compare the analytical model with the double shear experimental study, the same dimensions and required parameters were used for calculations. Parameters include the diameter of cable bolt, the yield and failure strength of cable bolt, the compressive strength of concrete block, the cable installation angle to the joint, the friction angle of the joint, the tensile and the shear modulus of the deflecting cable bolt section at failure. Although the cable moduli for both the elastic and plastic stages could be obtained from the laboratory tests, it appeared to be impossible to accurately predict the average moduli of the deflecting cable section between plastic hinges at failure when subjected to shearing. This is because the cable moduli vary during the shearing process from the initial elastic state to the final plastic state. In addition, a cable bolt may break earlier due to special factors contributing to cable weakening or concrete strengthening. Yet, without these local cable weakening and concrete strengthening, the cable bolt will continue to yield until failure. The specific moduli for each cable are determined by the degree of cable plasticisation at failure. It is reasonable to assume that for a constant plastic hinge length, the larger the joint shear displacement, the smaller the cable moduli.

To predict the joint shear resistance and shear displacement at failure, larger moduli can be applied to cable bolts failing normally at smaller shear displacements and smaller moduli can be applied to cable bolts failing at larger shear displacements. However, it is still not easy to specify suitable moduli to an individual specific condition since the shear displacement is affected by many factors. Generally, larger moduli apply to cable bolts with surface indentation and/or high pretension, while smaller moduli apply to cable bolts with smooth surface and/or low pretension.

To validate the analytical model, cable bolt moduli at failure were determined according to the actual shear displacements obtained in experiments. The joint shear capacities of the analytical method and the experimental tests were then compared.

Table 7.5 lists the specific moduli of each test calculated according to the actual joint shear displacement and Eq. (7.59). Figure 7.13 illustrates the joint shear resistance of different cable strands tested at varied pre-tensions from both the analytical model and experiments. Figure 7.14 shows the strength difference between the analytical and experimental results. Only results of double shear tests with joint friction were compared with the analytical model.

Table 7.5 Moduli calculated according to the actual shear displacement

Cable type	Pre-tension (t)	E (GPa)	Joint shear displacement (mm)	Concrete strength (MPa)
Indented JM Superstrand	25	1.3	74.3	36
Plain JM Superstrand	25	2	65.2	41
Indented TG	25	4	62.9	30
Indented SUMO	25	15	32.6	32
Indented SUMO	10	12	46	42
Plain SUMO	25	2	58.8	41
Plain SUMO	10	2	78.9	43
Plain Garford	0	2	82	42
SHGC	25	2.1	85.3	44
SHGC	10	2.2	97.6	54
Plain RT Superstrand	10	2.35	68.3	60
Plain RT Superstrand	10	3.15	69	40
Plain RT Superstrand	0	3.15	83.4	40

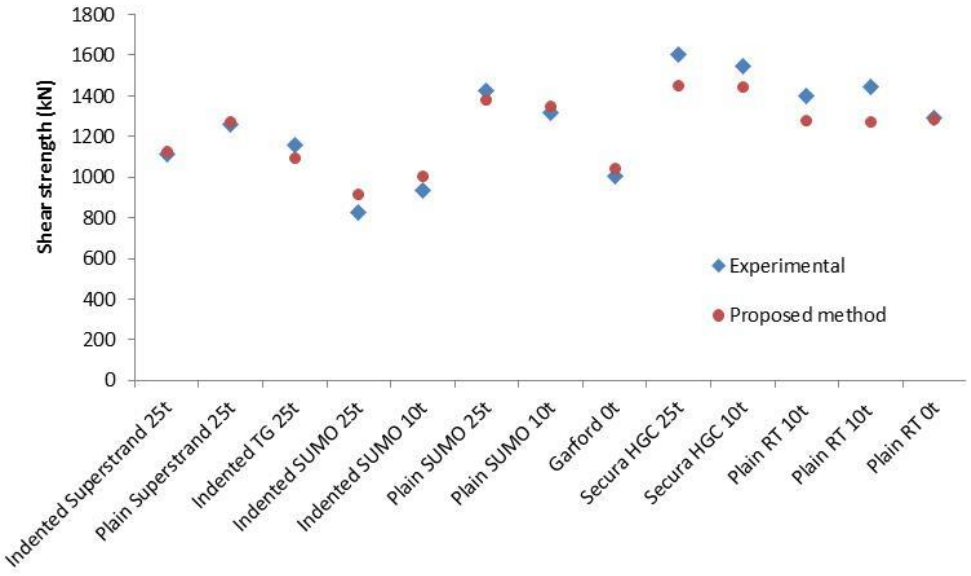

Figure 7.13 Reinforced joint shear resistance obtained from experimental tests and computed with the proposed analytical method

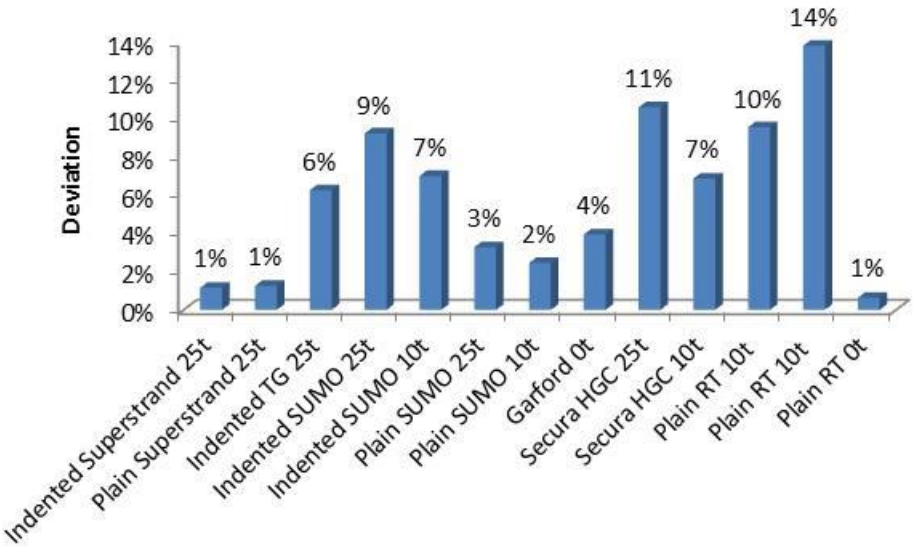

Figure 7.14 Deviation between the experimental and the analytical results

In Figure 7.13, it is obvious that the analytical model agrees closely with the experimental test results where the derived moduli were based on the actual joint shear displacement. As shown in Figure 7.14, the differences between the experimental results and analytical model are small and not more than 14%. Thus the proposed method is acceptable from the view of predicting the joint shear strength with experimentally obtained joint shear displacements.

It is seen from Table 7.5 that the moduli of the cable plastic hinge section at failure are in close relationship with their surface profiles. Except the indented JM Superstrand 25 t cable strand, all the other indented cable bolts showed larger moduli than the plain cable bolts. This indicates the feasibility of determining the cable strand moduli at failure based on the cable bolt surface profile. The smaller moduli of the indented JM Superstrand 25 t cable due to its larger shear displacement seem unreasonable when compared with its plain counterpart. The reason of this behaviour may be that the weaker concrete allowed more shear displacement, leading to its late failure at the slightly smaller moduli (see Table 7.5). Unlike the cable bolt surface profile effect, the cable pre-tension effect on the cable bolt moduli is not very obvious.

7.11 Summary

The derived analytical model that enables realistic calculations of cable bolted concrete joint shear reinforcement is detailed here.

The work mainly involves the derivation of the maximum joint shear resistance and corresponding joint shear displacement with cable reinforcement, and the analysis of four influencing factors for cable bolts with the aim to provide an effective method to design and assess a cable bolted reinforcement system.

Based on the loading state and the deformation of cable bolt and rock material, an assumption is made that the bolt deflecting section between plastic hinges is statically indeterminate with two fixed ends. According to the force method for the statically indeterminate problem and some basic conclusions from other existing research, the bolt contribution to joint shear strength and the bolt deformation are derived.

Parametric investigations were conducted on four related influencing factors, and conclusions were drawn as follows:

- Cable pre-tension affects the joint shear strength in two different ways. For cables failing at smaller plastic moduli with large cable deflection angles, the pre-tension increases the cable contribution to joint shear strength. Decrease

in joint shear strength is experienced for cables failing at the average or larger plastic moduli with small deflection angles.

- The turning point of cable deflection angle decreases with the increase of joint friction angle. The joint friction angle affects the joint shear capacity. This effect diminishes with the increase in cable deflection angle and there is almost no difference when the cable deflection angle approaches 80°.

- Hard concrete/rock provides lower joint shear strength and smaller shear displacements. Cable shear failures tend to occur in hard concrete/rock due to the increase in shear force generated in the cable, while tension failures usually occur in soft concrete/rock.

- The effect of bolt installation angle on joint shear strength is affected by the joint friction angle. For the extreme case of the friction coefficient of 0, the joint shear strength continuously decreases with the increase of bolt installation angle, whereas for a friction coefficient of 0.8, the joint shear strength increases. For practical purposes it can be assumed that in most cases the joint friction coefficient would be higher than approximately 0.4. Thus, it can be inferred that the maximum joint shear strength will occur mostly within the bolt installation angle ranging 70°-90°.

The analytical model when compared with the experimental test results with the derived moduli based on the actual joint shear displacements, showed close agreement. The cable surface profile showed a significant influence on the cable moduli at failure while the cable pre-tension did not.

CHAPTER EIGHT
CONCLUSIONS AND RECOMMENDATIONS

8.1 Conclusions

8.1.1 General

Bolts installed in the fractured rock mass around excavations normally bear combined tensile and shear loads due to the opening and sliding of rock fractures. Direct shear restraint and induced high normal stress are applied by the bolt to the fracture surfaces to minimise their displacements. This mechanism allows the excavation surfaces to stabilise and makes them self-supporting. In the interactive process of rock mass and bolt, two load transfer mechanisms are involved: the axial tensioning (bolt-resin-rock shear load transfer) and the lateral bolt shearing. Axial tensioning was the common focus in past studies, whereas lateral shearing is attracting more attention at present. The strength of the bolt when subjected to both shear and tensile loads is less than that of bolt under pure tension. Thus, ignoring the shear load in bolting design would potentially lead to a higher safety factor which is detrimental to support design.

It is inferred based on the review of existing test methods that joint friction, bolt de-bonding, boundary conditions, bolt installation angle, contact condition between bolt and steel mould and loading mode are significant factors for designing an effective and versatile shear test apparatus/method.

Bolt shear behaviour involves both the bolt bending section and the bolt tensioning section. The existing theories in relation to the bolt bending section can be divided into five categorises, whilst most theories in relation to the bolt tensioning section (elongation and de-bonding) can be generally placed into three categories.

8.1.2 Experiments

Basic mechanical properties of grout, concrete blocks and cable bolts were obtained for the experimental and theoretic analysis of bolt shear behaviour. The strength of

used concrete blocks was 40 MPa and 60 MPa, which allowed to investigate the concrete strength effect. The average friction coefficient of concrete shear surface was about 0.44, with which the joint friction effect and the bolt direct contribution were investigated. The grout used for various experiments had consistent strength of 60 MPa and hence did not produce new variables that may influence the overall double shear results.

The various tensile tests on cable bolt and cable wires showed that their average yield strength and failure strength were about 1650 MPa and 1815 MPa, respectively. A bilinear stress-strain relationship was found to be suitable to represent the steel cable wires. The average moduli of the first and the second simplified linear stages of the bilinear model were about 200 GPa and 4 GPa, respectively. This bilinear model and the cable properties were used in the analytical study.

It was found from double shear tests with joint friction that increasing pre-tension helped to improve the shear strength and stiffness of the bolted shear plane, which in turn undesirably caused the ultimate cable failure at smaller shear displacement. The indented cable bolts produced smaller shear strength than the smooth counterparts due to the reduction of bolt cross sectional area. The inclusion of aggregates in concrete blocks, the cable wire profile and concrete strength appeared to affect the modes of cable wire failure in the statistical analysis. The barrel and wedge assemblies helped to prevent the cable bolt from fully de-bonding.

The comparison between double shear tests with and without joint friction indicated that the cable pretension had a negative influence on the cable direct contribution to joint shear strength and the cable failure displacement. The presence of joint gap in tests without joint friction substantially increased the cable bolt failure displacement, which indicated the significant influence of joint gap.

The shear strength value produced from the British Standard single shear tests were lower than that obtained from the double shear tests. This was due to the occurrence of cable de-bonding and the contact between the cable and steel shear tubes in the

testing process. The possible solution is to enlarge the diameter of the steel shear tubes and/or to weld cable ends to the shear tubes.

Because of the different structures and composition of Fibre Glass bolts, steel rebar bolts and cable bolts, which caused different mechanical properties, their behaviour in ground strata reinforcement were different. In particular, the shear force of a Fibre Glass bolt reinforced joint increased gradually throughout testing, while the shear force of joints reinforced by either steel rebar bolt or cable bolt increased bi-linearly, which was clearly consistent with their tensile deformation modulus.

8.1.3 Theory and Modelling

An analytical model was proposed and compared with the double shear test results with the derived moduli based on the actual joint shear displacements, which showed close agreement. Parametric investigations were performed on four influencing factors, including cable pre-tension, joint friction coefficient, concrete strength and cable installation angle. Conclusions drawn from the parametric investigations were as follows:

- The cable bolt pre-tension affected the joint shear strength in two different ways. As for cables failing at smaller plastic moduli with large cable deflection angles, cable pre-tension increased its contribution to joint shear strength. A decrease in joint shear strength was experienced for cables failing at the average or larger plastic moduli with small deflection angles.

- The turning point of cable deflection angle decreased with the increase of joint friction angle. The joint friction angle affected the joint shear capacity. This effect diminished with the increase in cable deflection angle and there was almost no difference when the cable deflection angle approached 80°.

- Hard concrete/rock provided lower joint shear strength and smaller shear displacements. Failures in shear tended to occur in hard concrete/rock due to the increase in shear force generated in the cable, while failures in tension usually occurred in soft concrete/rock.

- The effect of bolt installation angle on the joint shear strength was affected by the joint friction angle. For the extreme case of the zero friction coefficient, the joint shear strength continuously decreased with the increase of bolt installation angle, whereas for a friction coefficient of 0.8, the joint shear strength kept increasing. For practical purposes it can be assumed that in most cases the joint friction coefficient would be higher than approximately 0.4. Thus, it can be inferred that the maximum joint shear strength will occur within the bolt installation angle ranging 70°-90°.

8.2 Recommendations

Further theoretical and experimental studies are required to enhance the understanding of the cable shear behaviour as follows:

- Due to the spiral structure of cable bolts, the stress distribution in cable wires is unclear especially when loaded in shear. In general, a stress distribution pattern similar to that of solid rock bolts was assumed for cable bolts in both existing analytical and experimental investigations. Since cable wires fail individually when loaded in shear, it is essential to determine the basic stress distribution on the cross section of each cable wire. Shear tests on cable bolts with closely spaced strain gauges or similar monitoring systems, such as optical fibre, being attached on cable wires is a possible way to obtain the stress distribution. Strain gauge protection is a significant issue in the testing process.

- The loading mode in the shear and the axial directions is expected to affect the cable shear performance. In both directions, the loading mode can be a combination of force and displacement. Yet, no studies were undertaken about this case in the past. To study this, a shear testing apparatus that is capable of adjusting the loading methods separately in both directions at the same time is required.

- An analytical model that combines the joint shear force and the bolt axial force development is necessary. This model can help predict the shear loading state by monitoring the axial load at the bolt end in field applications.

- Cable de-bonding is also an important factor influencing the cable reinforcing effect on joints. When shearing occurs at a position close to the cable inner end or when rock mass is crushed at the cable outer end to allow cable to move axially, cable de-bonding can possibly occur during the shearing process. If cable de-bonding occurs, it can be expected that the shear stiffness at the shearing plane will decrease and the shear strength will change as well. Yet, experimental and analytical investigations are required to quantitatively study this de-bonding effect.

- Though the mode of cable wire failure was categorised as "broken in tension" and "broken in shear", they normally occurred more or less in the form of a combination of both modes as often observed. A detailed and systematic analysis of cable wire failure should be performed with regard to the position of cable wires within the testing apparatus and the loading condition during different phases.

- The cable failure displacement from the double shear tests was much smaller than that from the Megabolt single shear tests (McKenzie and King, 2015). The double shear test employed a rectangular mould which could provide little and non-uniform confinement, whereas the Megabolt single shear test used circular moulds which could provide uniform but small confinement. It is thought that this confinement probably played an important role in the cable failure displacement, which should be investigated.

REFERENCES

Aydan, O. (1989). The stabilisation of rock engineering structures by rockbolts. Ph.D. thesis, Nagoya University, Nagoya.

Aydan, O., Ichikawa, Y., & Kawamoto, T. (1985). Load bearing capacity and stress distributions in along rockbolts within elastic behaviour of interfaces. *In: Proceedings of the International Conference on Numerical Methods in Geomechanics*, Balkema, Rotterdam, 1281-1292.

Ayres, N., & Gardner, L. (2014). Testing tendon support units under a combination loading scenario. Journal of the Southern African Institute of Mining and Metallurgy, 114(10), 829-834. URL: http://www.scielo.org.za/scielo.php?pid=S0038-223X2014001000012&script=sci_arttext&tlng=en

Aziz, N. (2004). An update of roof bolt research at the University of Wollongong. *In: Proceedings of the 5th Coal Operators' Conference*, Wollongong, NSW, Australia, 215-224. URL: http://ro.uow.edu.au/coal/147/

Aziz, N., Damian, P., & Richard, W. (2003). Double shear testing of bolts. *In: Proceedings of the 4th Coal Operators' Conference*, Wollongong, NSW, Australia, 154-161. URL: http://ro.uow.edu.au/coal/172/

Aziz, N., Hawker, R., Mirzaghorbanali, A., Nemcik, J., Li, X., & Rasekh, H. (2015a). Strength characteristics of secura hollow groutable cable bolts. *In: Proceedings of the 15th Coal Operator' Conference*, Wollongong, NSW, Australia, 160-167. URL: http://ro.uow.edu.au/coal/560/

Aziz, N., Jalalifar, H., & Concalves, J. (2006). Bolt surface configurations and load transfer mechanism. *In: Proceedings of the 7th Coal Operators' Conference*, Wollongong, NSW, Australia, 236-244. URL: http://ro.uow.edu.au/coal/51/

Aziz, N., Kay, H., Nemcik, J., & Stefan, M. (2014). Shear strength properties of Hilti plain and indented strand cable bolts. *In: Proceedings of the 14th Coal Operators' Conference*, Wollongong, NSW, Australia, 156-162. URL: http://ro.uow.edu.au/coal/509/

Aziz, N., Mirzaghorbanali, A., Nemcik, J., Heemann, K., & Mayer, S. (2015b). Shear strength properties of plain and spirally profiled cable bolts. *Canadian Geotechnical Journal*, 52(999), 1-6. doi:dx.doi.org/10.1139/cgj-2014-0504

Azuar, J. J. (1977). Stabilization de massifs rocheux fissures par barres dacier scellees (73). Report of research, LPC.

Barton, N. (1976). The shear strength of rock and rock joints. *International Journal of Rock Mechanics and Mining Sciences & Geomechanics Abstracts*, 13(9), 255-279. doi:10.1016/0148-9062(76)90003-6

Barton, N., & Choubey, V. (1977). The shear strength of rock joints in theory and practice. *Rock Mechanics*, 10(1-2), 1-54. doi:10.1007/bf01261801

Bawden, W., Dube, S., & Hyett, A. J. (1994). A laboratory study on the capacity of fully grouted cable bolts subjected to combined axial and lateral loads. Report to URIF, Kingston, Ontario, Canada, 1-11.

Bjurstrom, S. (1974). Shear strength of hard rock joint reinforced by grouted untensioned bolts. *In: Proceedings of the International Congress of Rock Mechanics*, Denver, 1194-1199.

British Standard Institution. (2009). Strata reinforcement support system components used in coal mines Specification for flexible systems for roof reinforcement.

Craig, P., & Aziz, N. (2010). Shear testing of 28mm hollow strand TG cable bolt. *In: Proceedings of the 10th Coal Operators' Conference*, Wollongong, NSW, Australia, 171-179. URL: http://ro.uow.edu.au/coal/303/

Dai, J. G., Ueda, T., & Sato, Y. (2005). Development of the nonlinear bond stress-slip model of fiber reinforced plastics sheet-concrete interfaces with a simple method. *Journal of Composite and Construction*, 9(1), 52-62. doi:10.1061/(ASCE)1090-0268(2005)9:1(52)

Dight, P. M. (1982). A case study of the behaviour of a rock slope reinforced with fully grouted rock bolts. *In: Proceedings of the International Symposium on Rock bolting*, Abisko, Sweden, 523-538.

Dight, P. M. (1983). Improvements to the stability of rock walls in open pit mines. Ph.D. thesis, Monash University, Melbourne.

Dolinar, D. R., Tadolini, S. C., & Blackwell, D. V. (1996). High horizontal movements in longwall gate roads controlled by cable support systems. *In: Proceedings of the 15th International Conference on Ground Control in Mining*, Morgantown, 497-509. URL: http://icgcm.conferenceacademy.com/papers/detail.aspx?subdomain=icgcm&iid=1097

Dulacka, H. (1972). Dowel action of reinforcing crossing cracks in concrete. *American Concrete Institute Journal*, 754-757.

Egger, P., & Fernandes, H. (1983). A novel triaxial press - study of achored jointed models. *In: Proceedings of the International Congress on Rock Mechanics*, Melbourne, 171-175.

El-Ariss, B. (2007). Behavior of beams with dowel action. *Engineering Structures*, 29(6), 899-903. doi:10.1016/j.engstruct.2006.07.008

Fabjanczyk, M., & Tarrant, G. (1992). Load transfer mechanisms in reinforcing tendons. *In: Proceedings of* the 11th International Conference on Ground Control in Mining. URL: http://icgcm.conferenceacademy.com/papers/detail.aspx?subdomain=icgcm&iid=1993

Farmer, I. W. (1975). Stress distribution along a resin grouted rock anchor. *International Journal of Rock Mechanics and Mining Sciences & Geomechanics Abstracts*, 12(11), 347-351. doi:10.1016/0148-9062(75)90168-0

Faulkner, D. D. (2012). The development and application of polyurethane injectable cable bolts. *In: Proceedings of the 31st International Conference of Ground Control in Mining*, Morgantown, WV, 1-5. URL: http://icgcm.conferenceacademy.com/papers/detail.aspx?subdomain=icgcm&iid=1002

Faulkner, D. D., Cook, T. M., & Stankus, J. C. (2013). A comprehensive analysis of cable bolt anchorage characteristics. *In: Proceedings of the 32nd International Conference on Ground Control in Mining*, Morgantown, WV, 1-8. URL: http://icgcm.conferenceacademy.com/papers/detail.aspx?subdomain=icgcm&iid=1384

Ferrero, A. M. (1995). The shear strength of reinforced rock joints. *International Journal of Rock Mechanics and Mining Sciences & Geomechanics Abstracts*, 32, 595-605. doi:10.1016/0148-9062(95)00002-X

Friberg, B. F. (1940). Design of dowel in transverse joints of concrete pavements. *Transactions of the American Society of Civil Engineers*, 195(1), 1076-1095.

Fuller, P. G., & Cox, R. H. T. (1978). Rock reinforcement design based on control of joint displacement - a new concept. *In: Proceedings of the Australia Tunnelling Congress*, Sydney, 28-35.

Gao, J., Shi, B., Zhang, W., Zhu, H., Xu, H., & Zhang, D. (2005). Experimental study on monitoring of stress for prestressed anchorage cable using distributed fiber optic sensor. *Chinese Journal of Rock Mechanics and Engineering*, 24(S2), 5604-5609. URL: http://en.cnki.com.cn/Article_en/CJFDTotal-YSLX2005S2059.htm

Garford Pty Ltd. (1990). An improved economical method for rock stabilisation. Unpublished work, Garford Pty Ltd, Perth, WA, Australia.

Ge, X., & Liu, J. (1988). Study on the shear resistance behaviour of bolted rock joints. *Chinese Jounal of Geotechnical Engineering*, 10(1), 8-19. URL: http://en.cnki.com.cn/Article_en/CJFDTotal-YSLX2005S2059.htm

Gere, J. M., & Timoshenko, S. P. (1990). *Mechanics of materials*. Amsterdam: KENT Publishing Company.

Gilbert, D., Mirzaghorbanali, A., Li, X., Rasekh, H., Aziz, N., & Nemcik, J. (2015). Strength properties of fibre glass dowels used for strata reinforcement in coal mines. *In: Proceedings of the 15th Coal Operator' Conference*, Wollongong, NSW, Australia, 365-375. URL: http://ro.uow.edu.au/coal/586/

Goris, J. M. (1990). Laboratory evaluation of cable bolt supports: evaluation of supports using conventional cables (RI9308). Report of investigations, Bureau of Mines, USA, 1-23.

Goris, J. M., Martin, L. A., & Curtin, R. P. (1996). Shear behaviour of cable bolt supports in horizontal bedded deposits. *Cim Bulletin*, 89(1001), 124-128. URL: http://www.osti.gov/scitech/biblio/405595

Grasselli, G. (2005). 3D behaviour of bolted rock joints: experimental and numerical study. *International Journal of Rock Mechanics and Mining Sciences*, 42(1), 13-24. doi:10.1016/j.ijrmms.2004.06.003

Haas, C. J. (1981). Analysis of rock bolting to prevent shear movement in fractured ground. *Journal of Mining Engineering*, 698-704.

Hagan, P., Chen, J., & Saydam, S. (2014). The load transfer mechanism of fully grouted cable bolts under laboratory tests. *In: Proceedings of the 14th Coal Operators' Conference*, Wollongong, NSW, Australia, 137-146. URL: http://ro.uow.edu.au/coal/507/

Hagan, P., Chen, J. H., Hebblewhite, B., Saydam, S., & Mitra, R. (2015). Optimising the selection of fully grouted cable bolts in varying geotechnical environments (C22010). ACARP project report.

Haile, A., Jager, A., & Wojno, L. (1995). Strata control in tunnels and an evaluation of support units and systems currently used with a view to improving the effectiveness of support stability and safety of tunnels (GAP 026). Project report.

Hibbeler, R. C., Tan, K.-H., & Nolan, B. (2006). *Structural analysis*. Upper Saddle River, New Jersey: Pearson Prentice Hall.

Hibino, S., & Motojima, M. (1981). Effects of rock bolting in jointed rocks. *In: Proceedings of the International Symposium of Weak Rock*, Tokyo, 1052-1062.

Hoek, E. (2007). Practical rock engineering. Online source, retrieved from https://www.rocscience.com/learning/hoek-s-corner/books.

Holmberg, M., & Stille, H. (1992). The mechanical behaviour of a single grouted bolt. *In: Proceedings of the International Symposium on Rock Support*, Rotterdam, 473-481. doi:10.1016/0148-9062(94)92631-X

Hutchins, W., Bywater, S., Thompson, A., & Windsor, C. (1990). A versatile grouted cable dowel reinforcing system for rock. *In: Proceedings of the The AusIMM Proceedings*, 25-29.

Hutchinson, D. J., & Diederichs, M. S. (1996). *Cable bolting in underground mines*. Richmond, British Columbia: BiTech Publishers.

Hyett, A., Bawden, W., Lausch, P., Moosavi, M., Ruest, M., & Pahkala, M. (1997). The SMART cable bolt: an instrument for the determination of tension in 7-wire strand cable bolts. *In: Proceedings of the International Symposium on Rock Support–Applied Solutions for Underground Structures*, 1-16. URL: https://www.researchgate.net/publication/237481700_THE_SMAR_T_CABLE_BOLT_AN_INSTRUMENT_FOR_THE_DETERMINATION_OF_TENSION_IN_7WIRE_STRAND_CABLE_BOLTS

Ito, F., Nakahara, F., Kawano, R., Kang, S. S., & Obara, Y. (2001). Visualization of failure in a pull-out test of cable bolts using X-ray CT. *Construction and Building Materials*, 15(5-6), 263-270. doi:10.1016/s0950-0618(00)00075-1

Jalalifar, H. (2006). A new approach in determining the load transfer mechanism in fully grouted bolts. Ph.D. thesis, University of Wollongong, Wollongong.

Jalalifar, H., & Aziz, N. (2010a). Analytical Behaviour of Bolt–Joint Intersection Under Lateral Loading Conditions. *Rock Mechanics and Rock Engineering*, 43(1), 89-94. doi:10.1007/s00603-009-0032-6

Jalalifar, H., & Aziz, N. (2010b). Experimental and 3D numerical simulation of reinforced shear joints. *Rock Mechanics and Rock Engineering*, 43(1), 95-103. doi:10.1007/s00603-009-0031-7

Jalalifar, H., Aziz, N., & Hadi, M. (2006a). An assessment of load transfer mechanism using the instrumented bolts. *In: Proceedings of the 7th Coal Operators' Conference*, Wollongong, NSW, 255-265. URL: http://ro.uow.edu.au/coal/53/

Jalalifar, H., Aziz, N., & Hadi, M. (2006b). The effect of surface profile, rock strength and pretension load on bending behaviour of fully grouted bolts. *Geotechnical and Geological Engineering*, 24(5), 1203-1227. doi:10.1007/s10706-005-1340-6

Jia, Y.-x., Song, H.-w., & Duan, Y.-y. (2007). Physical simulation study on railway effect of bolt in discontinuous rock mass. *Journal of China University Of Mining And Technology-Chinese Edition*, 36(5), 614-617. URL: http://en.cnki.com.cn/Article_en/CJFDTOTAL-ZGKD200705011.htm

Jirovec, P. (1978). Wechselwirkung zwischen anker und gebirge. *Rock Mechanics*, 7, 139-155. doi:10.1007/978-3-7091-8529-2_11

Karabin, G., & Debevec, W. J. (1976). Comparative evaluation of conventional and resin bolting systems. Research report, Mining Enforcement and Safety Administration, Pittsburgh, PA (USA).

Kharchafi, M., Grasselli, G., & Egger, P. (1999). 3D behaviour of bolted rock joints: experimental and numerical study. *In: Proceedings of the Symposium of Mechanics of Jointed and Faulted Rock*, Balkema, Sweden, 299-304.

Lambe, T. W., & Whitman, R. V. (2008). *Soil mechanics*: John Wiley & Sons.

Lewis, M., Rimas, P., & Doug, M. (2002). Determination of physical properties of cable bolts in cement grout pull tests using instrument King Wires. *In: Proceedings of the Canadian Institute of Mining Annual Conference*, Vancouver, 1-8.

Li, C. C. (2006). Rock support design based on the concept of pressure arch. *International Journal of Rock Mechanics and Mining Sciences*, 43(7), 1083-1090. doi:http://dx.doi.org/10.1016/j.ijrmms.2006.02.007

Li, C. C. (2007). A practical problem with threaded rebar bolts in reinforcing largely deformed rock masses. *Rock Mechanics and Rock Engineering*, 40(5), 519-524. doi:10.1007/s00603-006-0094-7

Li, C. C. (2010). Field observations of rock bolts in high stress rock masses. *Rock Mechanics and Rock Engineering*, 43(4), 491-496. doi:10.1007/s00603-009-0067-8

Li, L., Hagan, P., & Saydam, S. (2014). Tensile stress mobilization along a rockbolt under shear load. *In: Proceedings of the Transitional Development in Rock Mechanics: Recognition, Thinking and Innovation*, Xi'an China, 275-279.

Li, X., Aziz, N., Mirzaghorbanali, A., & Nemcik, J. (2016). Behavior of fiber glass bolts, rock bolts and cable bolts in shear. *Rock Mechanics and Rock Engineering*, 49(7), 2723–2735. doi:10.1007/s00603-015-0907-7

Li, X., Nemcik, J., Mirzaghorbanali, A., Aziz, N., & Rasekh, H. (2015). Analytical model of shear behaviour of a fully grouted cable bolt subjected to shearing. *International Journal of Rock Mechanics and Mining Sciences*, 80, 31-39. doi:10.1016/j.ijrmms.2015.09.005

Ludvig, B. (1983). Shear tests on rock bolts. *In: Proceedings of the International Symposium on Rock Bolting*, Abisko, Sweden, 193-203.

Ma, S. Q., Nemcik, J., & Aziz, N. (2013). An analytical model of fully grouted rock bolts subjected to tensile load. *Construction and Building Materials*, 49(0), 519-526. doi:http://dx.doi.org/10.1016/j.conbuildmat.2013.08.084

Ma, S. Q., Nemcik, J., Aziz, N., & Zhang, Z. Y. (2014). Analytical model for rock bolts reaching free end slip. *Construction and Building Materials*, 57(0), 30-37. doi:10.1016/j.conbuildmat.2014.01.057

Martin, L., Milne, D., Ruest, M., & Pakalnis, R. (2004). Evaluation of instrumented cable bolts in cement grout to determine physical and numerical modeling properties (RI9662). Report of investigations, National Institute for Occupational Safety and Health, USA, 1-14.

Matthews, S., Tillmann, V., & Worotnicki, G. (1983). A modified cable bolt system for the support of underground openings. *In: Proceedings of the Proceedings of AusIMM annual conference*, Broken Hill, Melbourne, 243-255.

McHugh, E., & Signer, S. (1999). Roof bolt response to shear stress: laboratory analysis. *In: Proceedings of the 18th International Conference on Ground Control in Mining*, Morgantown, WV, 232-238. URL: http://icgcm.conferenceacademy.com/papers/detail.aspx?subdomain=icgcm&iid=835

McKenzie, R., & King, B. (2015). Megabolt shear testing program. *Presented at the NSW Underground Geotechnical Society Preliminary Program*, Sydney, NSW, Australia.

Millard, S. G., & Johnson, R. P. (1984). Shear transfer across cracks in reinforced concrete due to aggregate interlock and to dowel action. *Magazine of Concrete Research*, 36, 9-21. URL: http://www.icevirtuallibrary.com/content/article/10.1680/macr.1984.36.126.9

Milne, D., Gendron, A., & Hamilton, R. (1992). Cable bolt research summary report. Internal report, Noranda Technology Centre, Montreal, Quebec.

Neal, B. G. (1977). *The plastic methods of structural analysis*. New York: John Wiley & Sons.

Nemcik, J., Porter, I., Baafi, E. Y., & Lukey, C. A. (2009). Geotechnical assessment of skin reinforcement in underground mines. *In: Proceedings of the 28th International Conference on Ground Control in Mining*, West Virginia University, Morgantown, WV, 1-5. URL: http://icgcm.conferenceacademy.com/papers/detail.aspx?subdomain=icgcm&iid=230

Orica. (2014). Mechanical property test report. Unpublished technical report.

Patton, F. D. (1966). Multiple modes of shear failure in rock. *In: Proceedings of the 1st International Society of Rock Mechanics Congress*, Lisbon, Portugal, 509-513. URL: https://www.onepetro.org/conference-paper/ISRM-1CONGRESS-1966-087

Pellet, F. (1994). Strength and deformability of jointed rock masses reinforced by rock bolts. Ph.D. thesis, Swiss Federal Institute of Technology, Lausane, Swiss.

Pellet, F., & Egger, P. (1996). Analytical model for the mechanical behaviour of bolted rock joints subjected to shearing. *International Journal of Rock Mechanics and Rock Engineering*, 29(2), 73-97. doi:10.1007/BF01079755

Pellet, F., Egger, P., & Fernandes, H. (1995). Contribution of fully bonded rock bolts to the shear strength of joints: analytical and experimental evaluation. *In: Proceedings of the International Conference on Mechanics of Jointed and Faulted Rock*, Vienna, Austria, 873-878.

Ren, F. F., Yang, Z. J., Chen, J. F., & Chen, W. W. (2010). An analytical analysis of the full-range behaviour of grouted rock bolts based on a tri-linear bond-slip model. *Construction and Building Materials*, 24(3), 361-370. doi:10.1016/j.conbuildmat.2009.08.021

Schmuck, C. (1979). Cable bolting at the Homestake gold mine. *Mining Engineering*, 31(12), 1677-1681.

Signer, S. P., Cox, D., & Johnston, J. (1997). A method for the selection of rock support based on bolt loading measurements. *In: Proceedings of the International Symposium on Rock Support: Applied Solutions for Underground Structures*, Lillehammer, Norway, 1-12.

Song, H. (2003). New study on transverse effect of rock bolts in discontinuous rock mass. *Journal of China University of Mining and Technology*, 32(2), 161-164. URL: http://en.cnki.com.cn/Article_en/CJFDTOTAL-ZGKD200302016.htm

Spang, K., & Egger, P. (1990). Action of fully-grouted bolts in jointed rock and factors of influence. *Rock Mechanics and Rock Engineering*, 23, 201-229. doi:10.1007/BF01022954

Srivastava, L., & Singh, M. (2015). Effect of fully grouted passive bolts on joint shear strength parameters in a blocky mass. *Rock Mechanics and Rock Engineering*, 48(3), 1197-1206. doi:10.1007/s00603-014-0615-8

Stillborg, S. (1984). Experimental investigation of steel cables for rock reinforcement in hard rock. Ph.D. thesis, Lulea University of Technology, Lulea, Sweden.

Tanaka, Y., & Murakoshi, J. (2011). Reexamination of dowel behavior of steel bars embedded in concrete. *ACI Structural Journal*, 108(6), 659-668, 634-644. URL: https://trid.trb.org/view.aspx?id=1131107

Terzaghi, K. (1955). Evaluation of coefficients of subgrade reaction. *Geotechnique*, 5(4), 297-326. doi:10.1680/geot.1955.5.4.297

Thomas, R. (2012). The load transfer properties of post–groutable cable bolts used in Australia coal industry. *In: Proceedings of the 31st International Conference on Ground Control in Mining*, Morgantown, WV, 1-10. URL: http://icgcm.conferenceacademy.com/papers/detail.aspx?subdomain=icgcm&iid=1011

Thompson, A. G., & Villaescusa, E. (2014). Case studies of rock reinforcement components and systems testing. *Rock Mechanics and Rock Engineering*, 47(5), 1589-1602. doi:10.1007/s00603-014-0583-z

Thompson, A. G., Villaescusa, E., & Windsor, C. R. (2012). Ground support terminology and classification: an update. *Geotechnical and Geological Engineering*, 30(3), 553-580. doi:10.1007/s10706-012-9495-4

Timoshenko, S. (1940). *Strength of materials* (Vol. 1): D. Van Nostrand Company, inc.

Timoshenko, S., & Lessels, J. (1925). *Applied elasticity*. Pennsylvania: Westinghouse Technical Night School Press.

Veludo, J., Júlio, E. N. B. S., & Dias-da-Costa, D. (2012). Compressive strength of micropile-to-grout connections. *Construction and Building Materials*, 26(1), 172-179. doi: 10.1016/j.conbuildmat.2011.06.007

Wang, Y. (2015). Grout properties for strata reinforcement in coal mine. Undergraduate thesis, University of Wollongong, Wollongong, NSW.

Windsor, C. (1990). Ferruled strand. Unpublished memorandum. Perth: CSIRO.

Windsor, C. R. (1992). Invited lecture: cable bolting for underground and surface excavations. Rock support in mining and underground construction, 349-366.

Windsor, C. R. (1997). Rock reinforcement systems. *International Journal of Rock Mechanics and Mining Sciences*, 34(6), 919-951. doi:10.1016/S1365-1609(97)80004-4

Windsor, C. R. (1999). Rock reinforcement practice. Unpublished training material.

Windsor, C., & Thompson, A. (1996). Terminology in rock reinforced practice. *In: Proceedings of the 2nd North American Rock Mechanics Conference*, Montréal, Québec, Canada, 225-232.

Yuan, H., Teng, J. G., Seracino, R., Wu, Z. S., & Yao, J. (2004). Full-range behavior of FRP-to-concrete bonded joints. *Engineering Structures*, 26(5), 553-565. doi:10.1016/j.engstruct.2003.11.006

Zhou, Y., Wu, Y., & Yun, Y. (2010). Analytical modeling of the bond–slip relationship at FRP-concrete interfaces for adhesively-bonded joints. *Composites Part B: Engineering*, 41(6), 423-433. doi:10.1016/j.compositesb.2010.06.004

APPENDIX A

The following lists the results of cable bolts in double shear tests with joint friction: In tests T9 and T11, only one axial load was given because one load cell did not work properly.

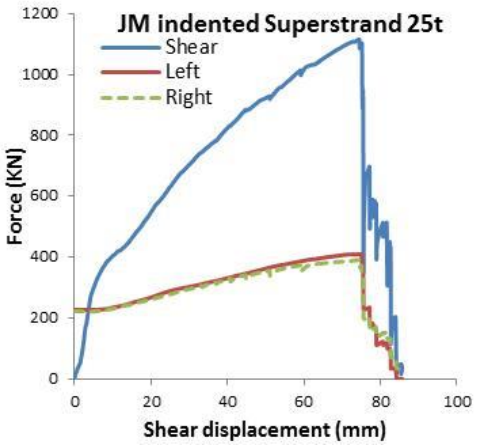

(a) T1-1

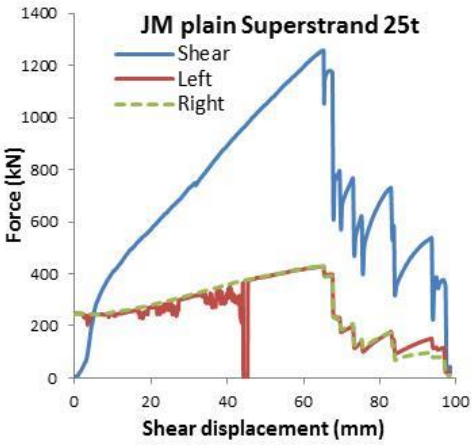

(b) T1-2

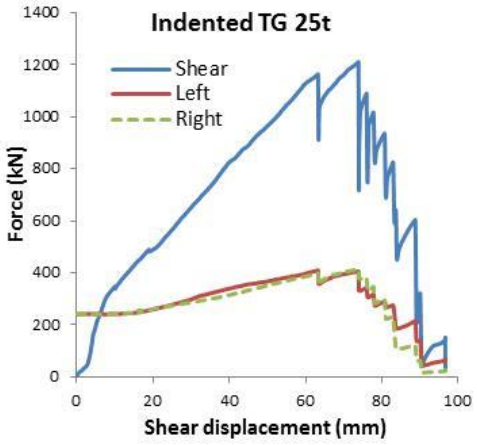

(c) T1-3

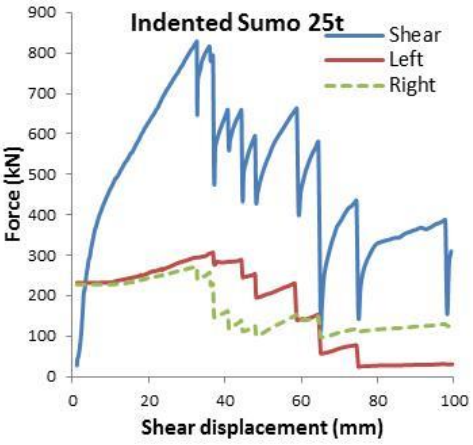

(d) T1-4

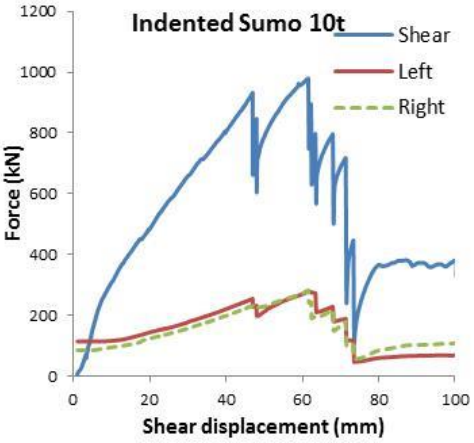

(e) T1-5

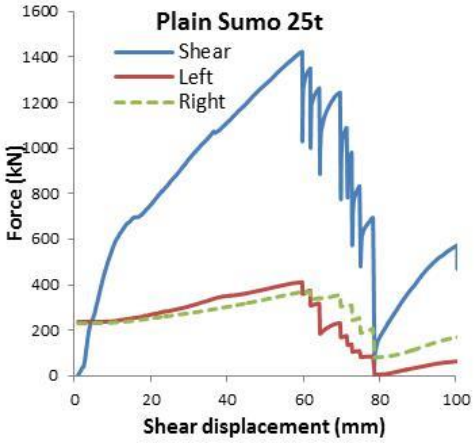

(f) T1-6

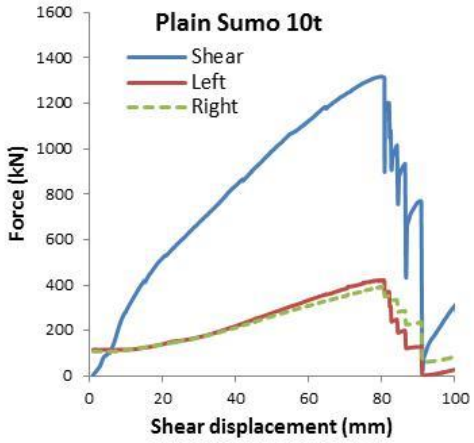

(g) T1-7

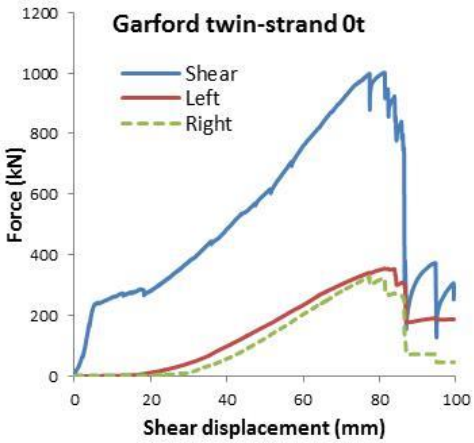

(h) T1-8

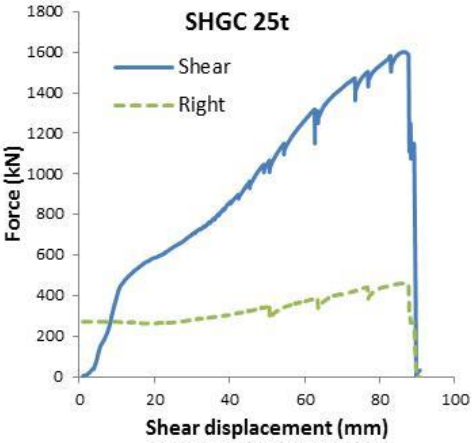

(i) T1-9

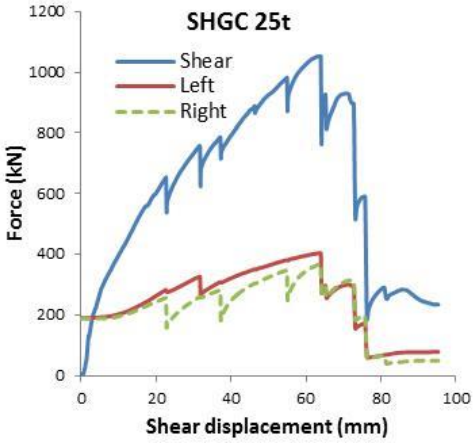

(j) T1-10

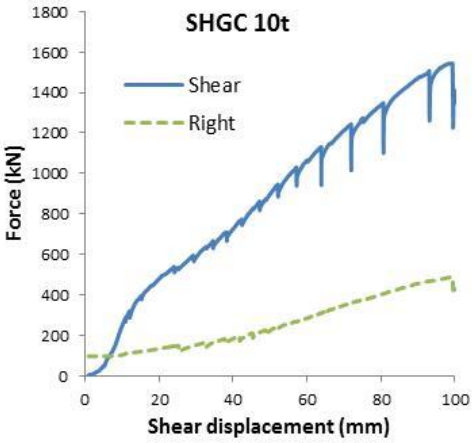

(k) T1-11

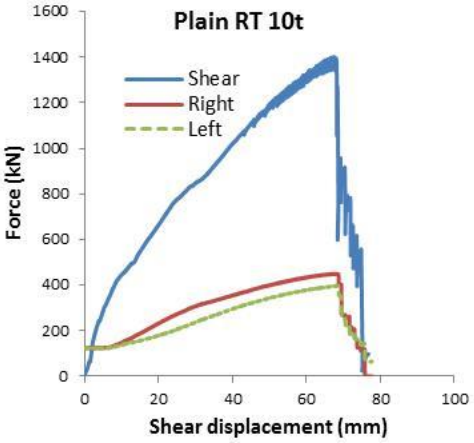

(l) T1-12

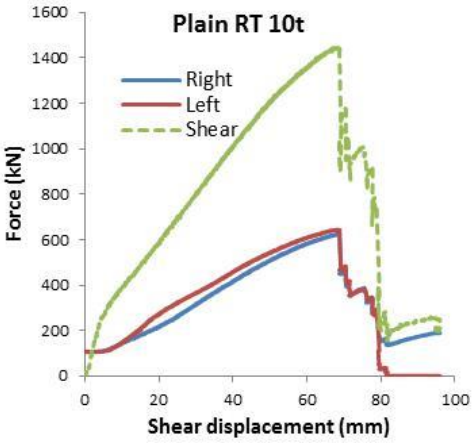

(m) T1-13

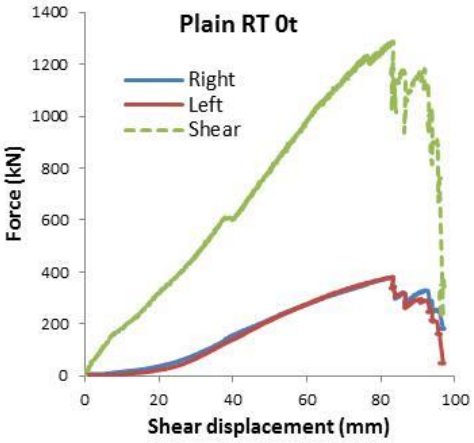

(n) T1-14

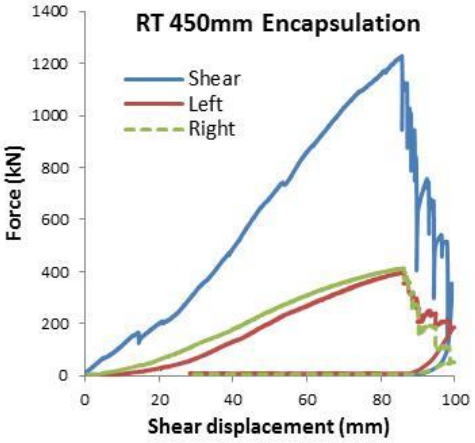

(o) T1-15

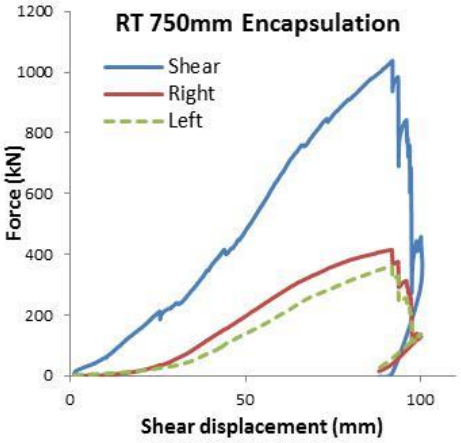

(p) T1-16

APPENDIX B

The following lists the relationship between the shear force and the axial force increment of different cable bolts in double shear tests with joint friction.

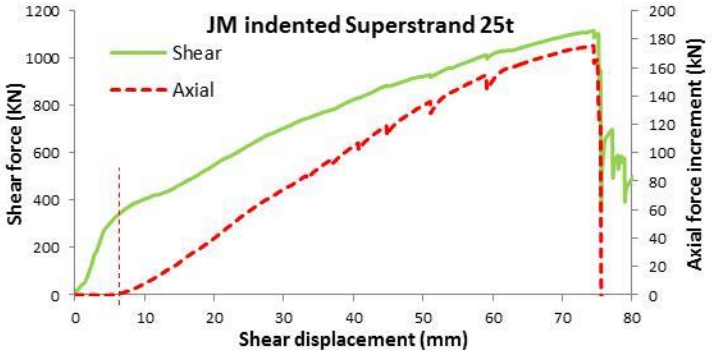

(a) T1-1

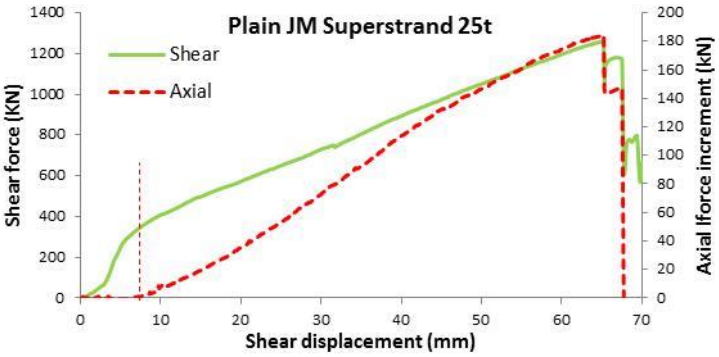

(b) T1-2

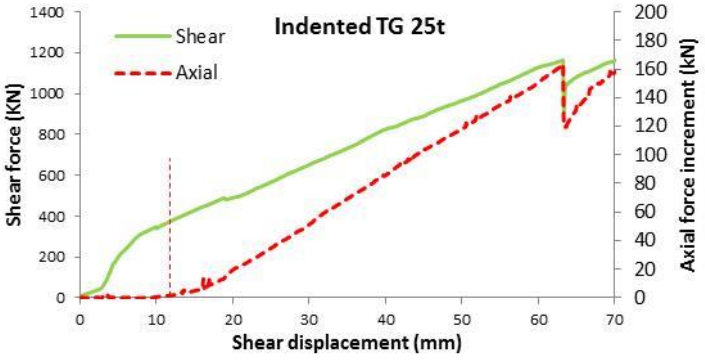

(c) T1-3

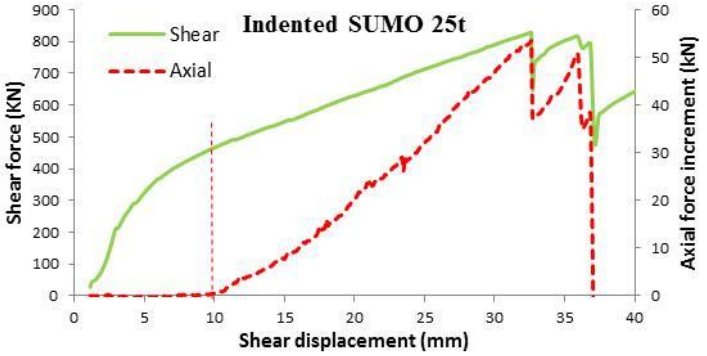

(d) T1-4

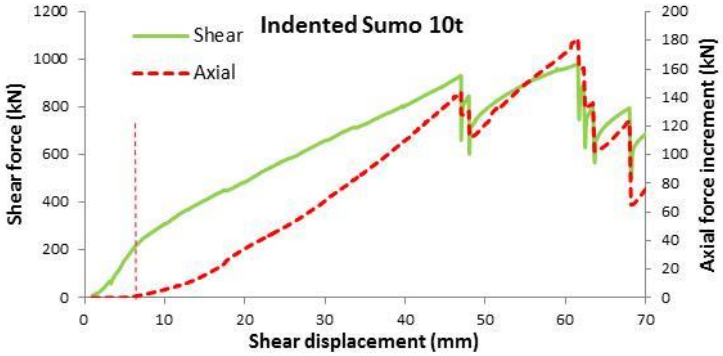

(e) T1-5

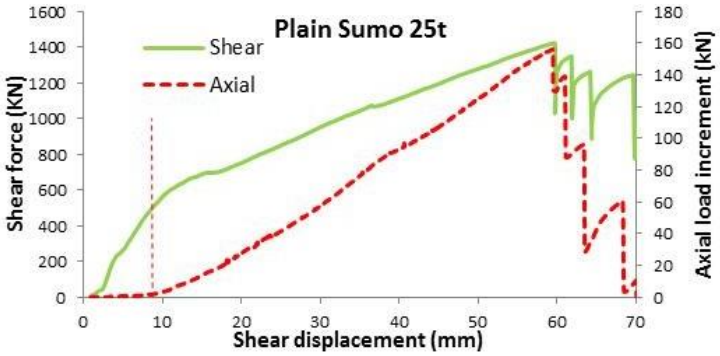

(f) T1-6

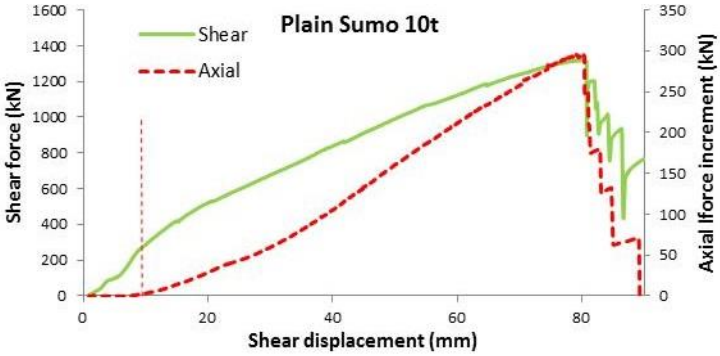

(g) T1-7

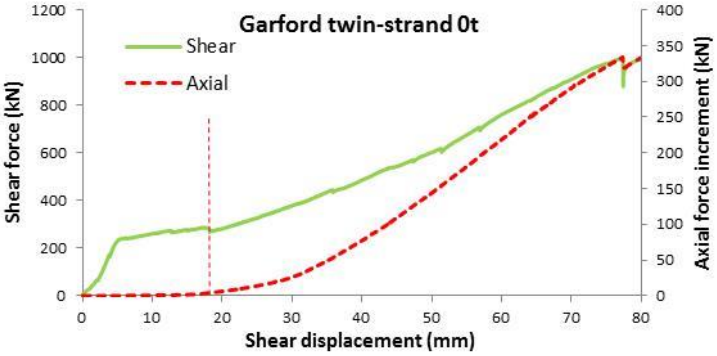

(h) T1-8

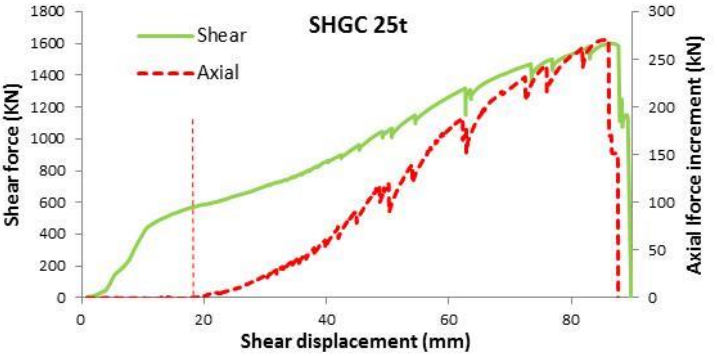

(i) T1-9

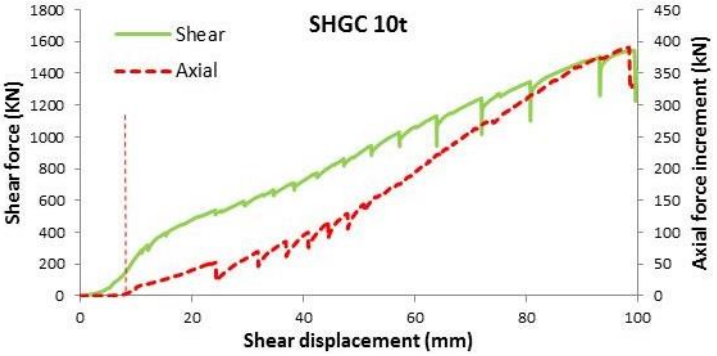

(j) T1-11

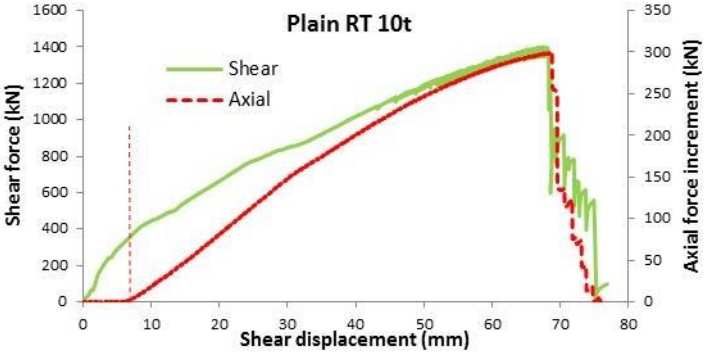

(k) T1-12

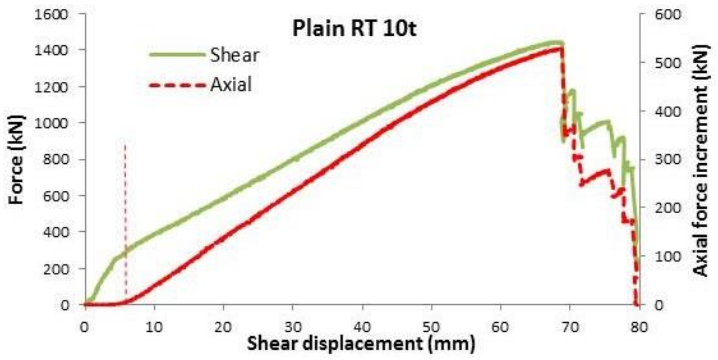
Plain RT 10t
Shear
Axial
Force (kN)
Axial force increment (kN)
Shear displacement (mm)
0
200
400
600
800
1000
1200
1400
1600
100
300
500
0
10
20
30
40
50
60
70
80

(l) T1-13

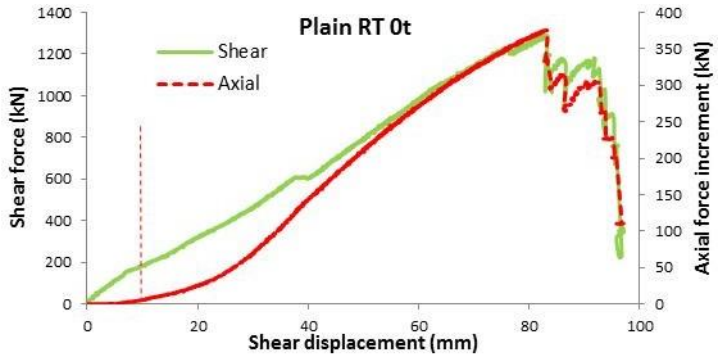
Plain RT 0t
Shear
Axial
Shear force (kN)
Axial force increment (kN)
Shear displacement (mm)
0
200
400
600
800
1000
1200
1400
50
100
150
200
250
300
350
400
0
20
40
60
80
100

(m) T1-14

APPENDIX C

The following lists the relationship between the shear force and normal force for various cable bolts with initial pre-tension load of 0 t, 10 t and 25 t.

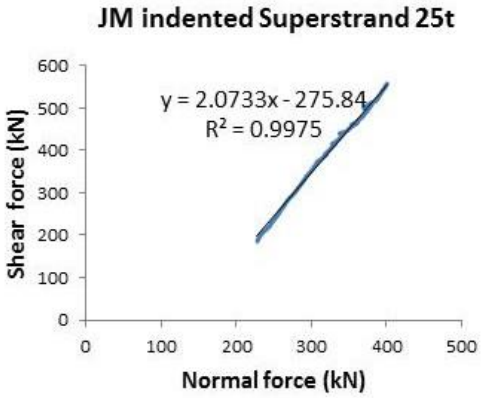

(a) T1-1

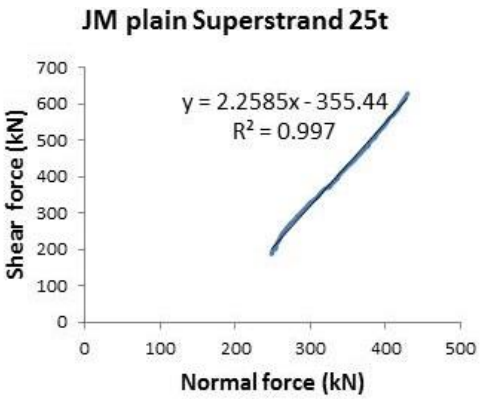

(b) T1-2

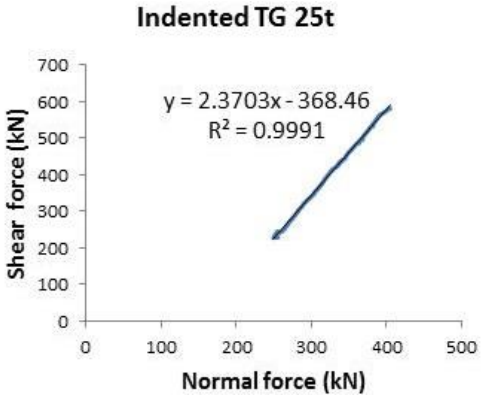

(c) T1-3

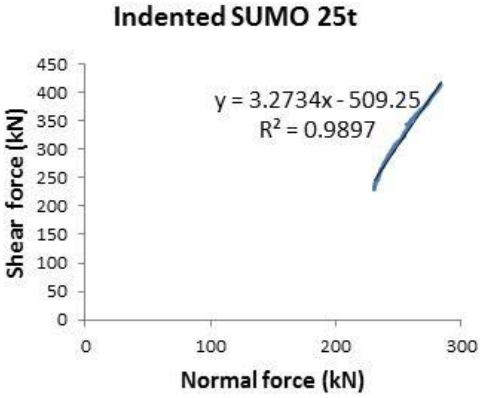

(d) T1-4

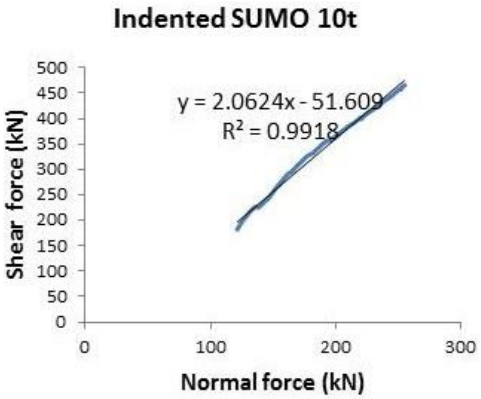

(e) T1-5

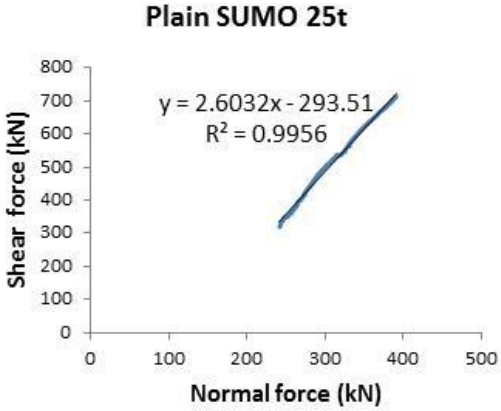

(f) T1-6

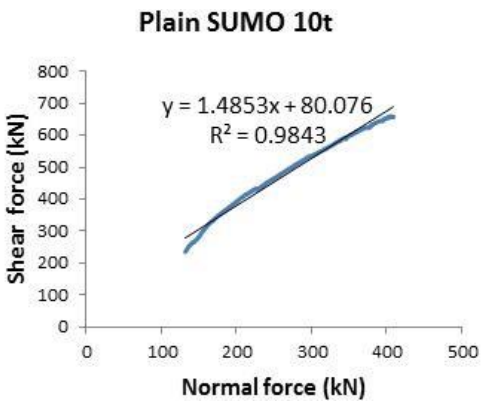

(g) T1-7

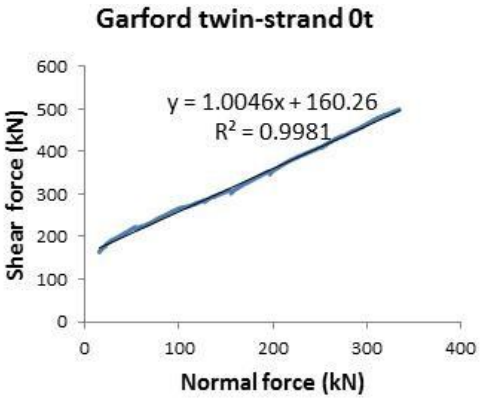

(h) T1-8

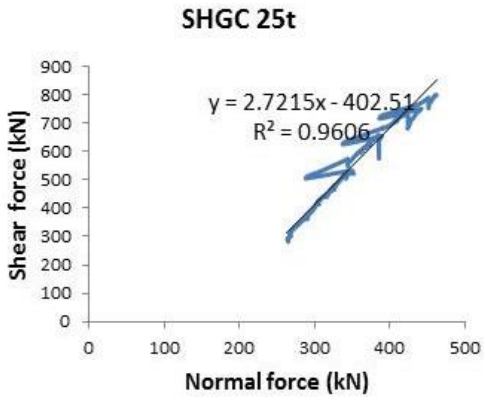

(i) T1-9

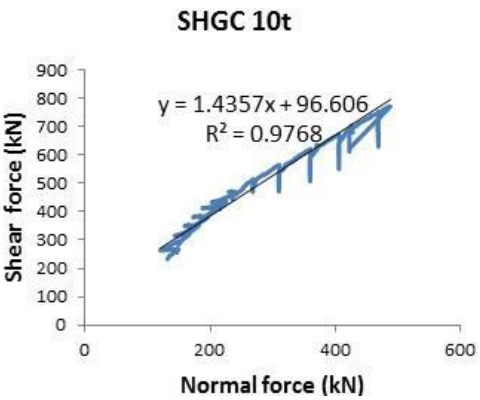

(j) T1-11

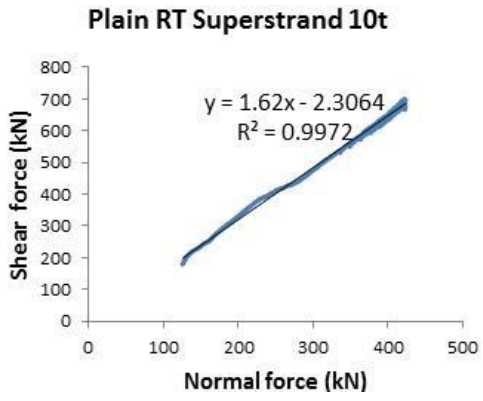

(k) T1-13

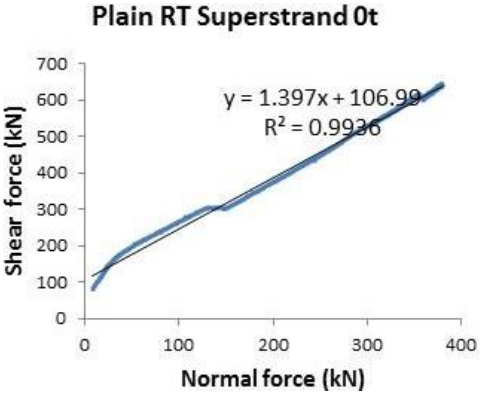

(l) T1-14

APPENDIX D

The following lists the relationship between the shear stress and normal stress for various cable bolts with initial pre-tension load of 0 t, 10 t and 25 t.

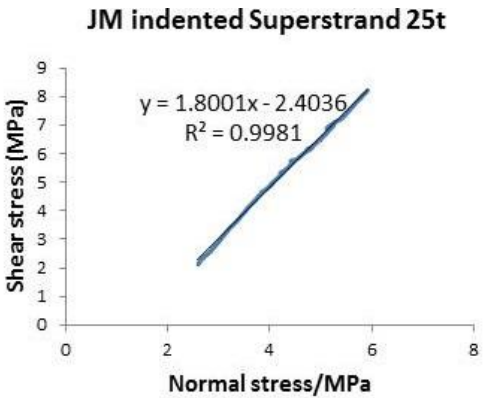

(a) T1-1

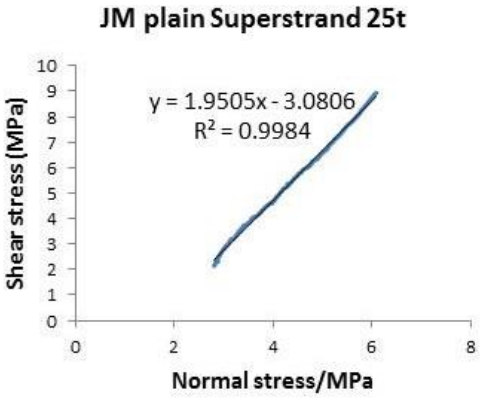

(b) T1-2

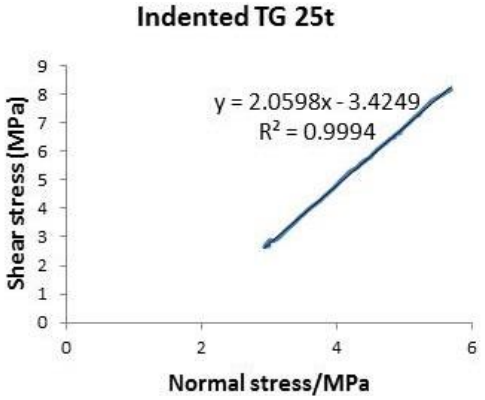

(c) T1-3

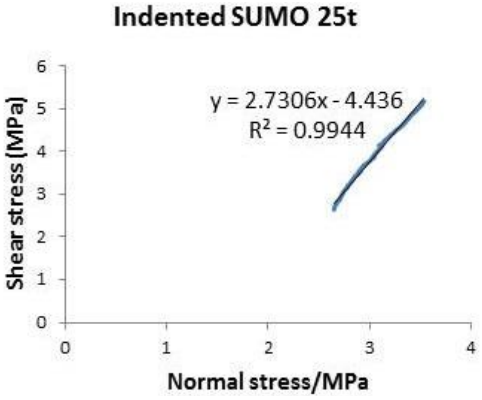

(d) T1-4

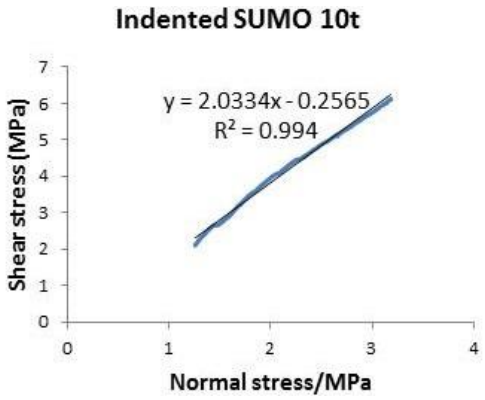

(e) T1-5

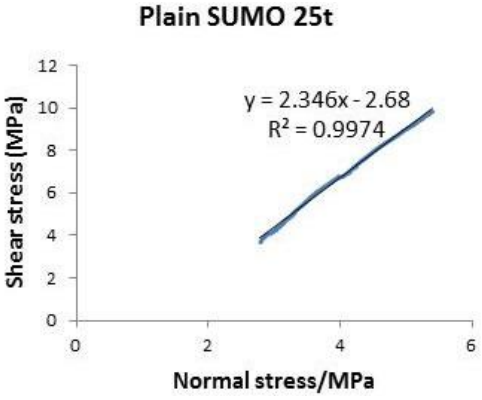

(f) T1-6

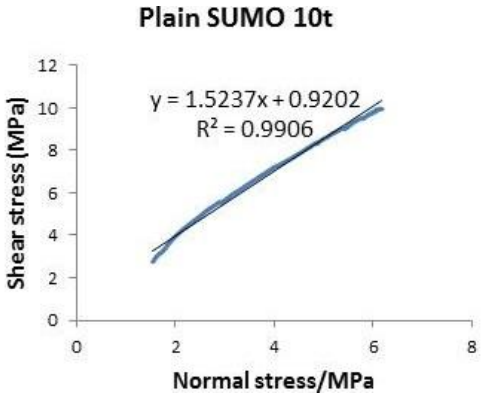

(g) T1-7

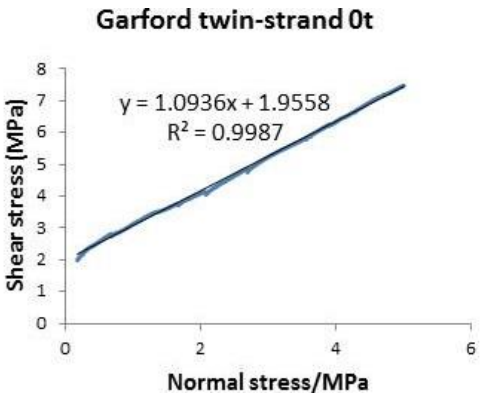

(h) T1-8

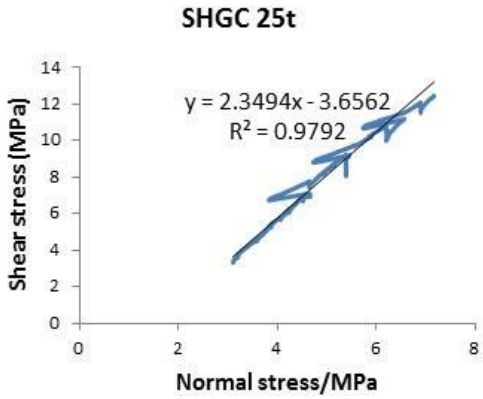

(i) T1-9

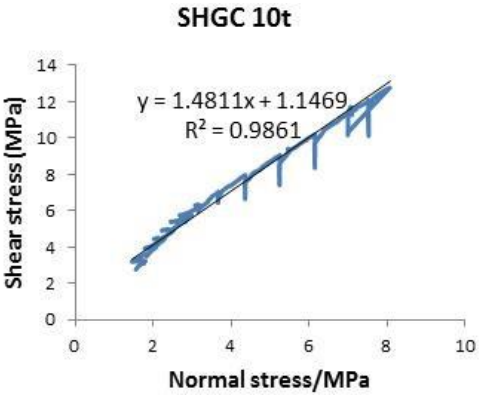

(j) T1-11

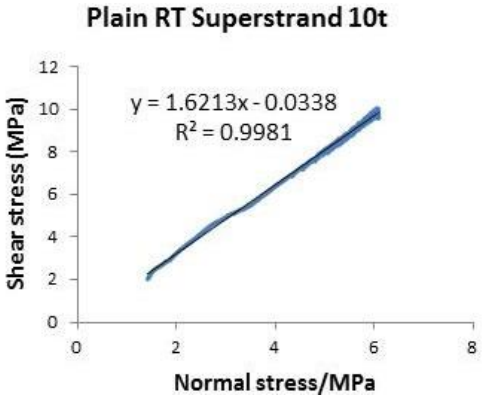

(k) T1-13

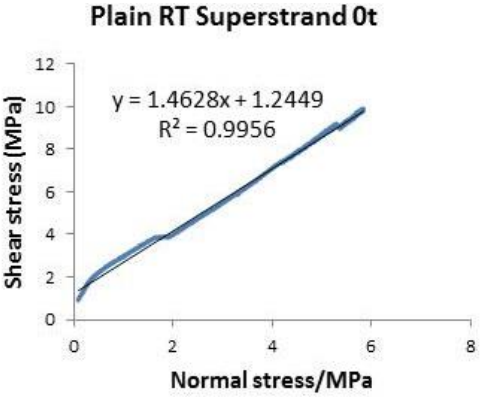

(l) T1-14

APPENDIX E

The following lists the failure modes of cable strands in double shear tests with joint friction: green, yellow and red represent un-broken, broken in tension and broken in shear, respectively. Note: normally no absolutely pure tension failure or shear failure existed in the tests. The classification of cable wire failure was based on the major pattern of each wire failure surface.

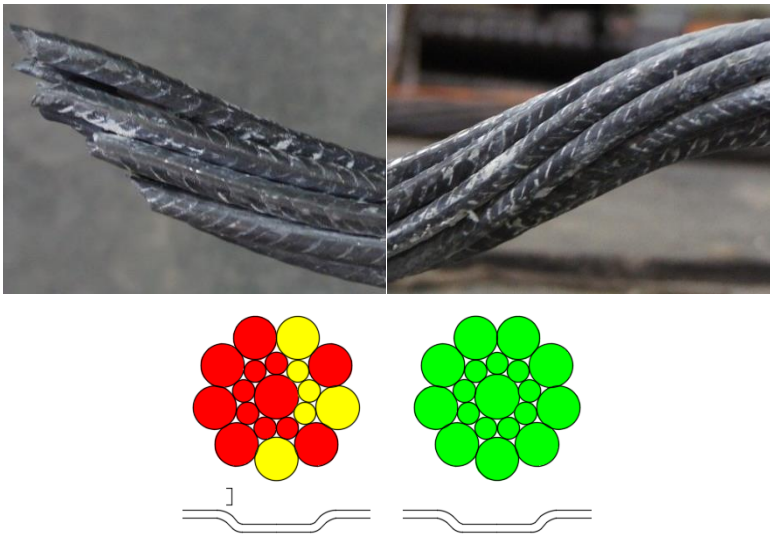

(a) T1-1

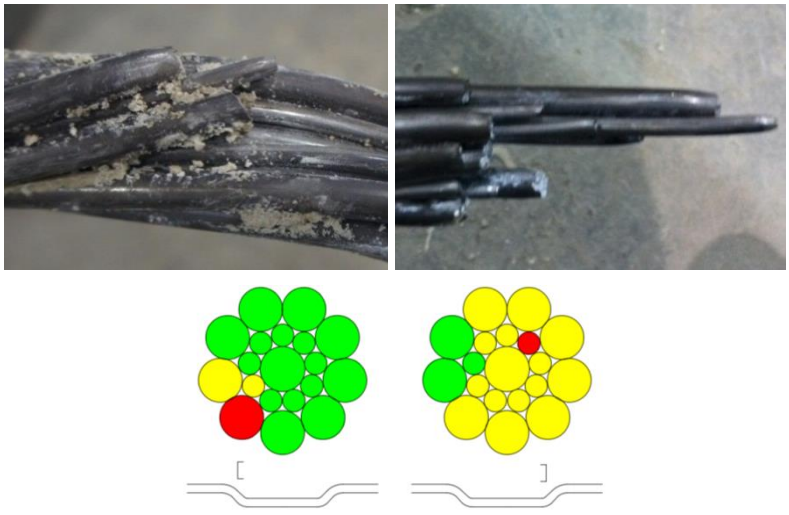

(b) T1-2

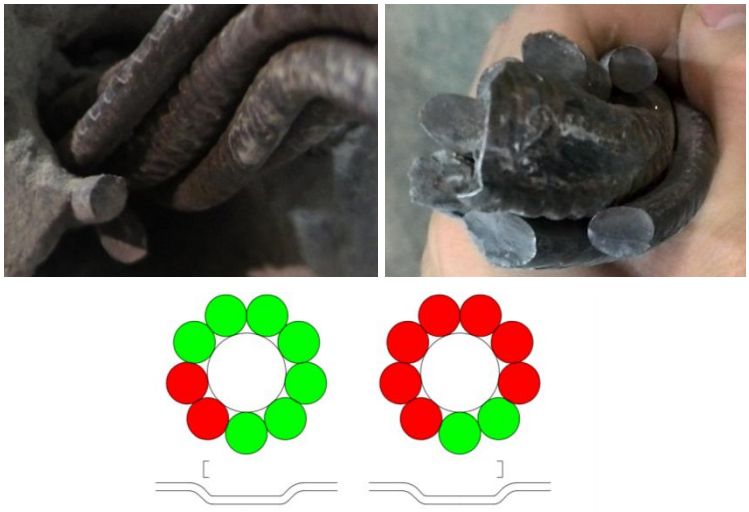

(c) T1-3

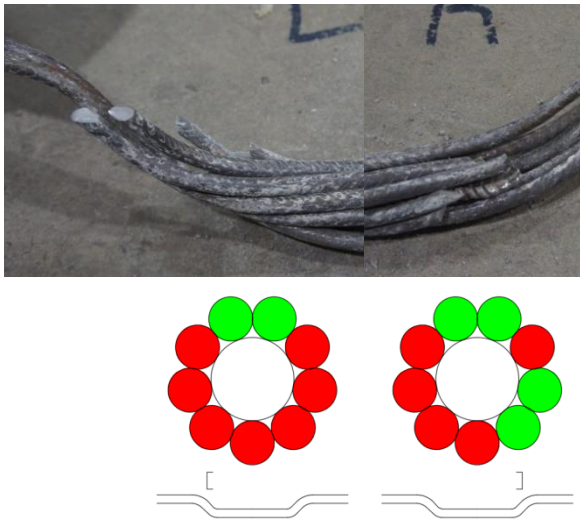

(d) T1-4

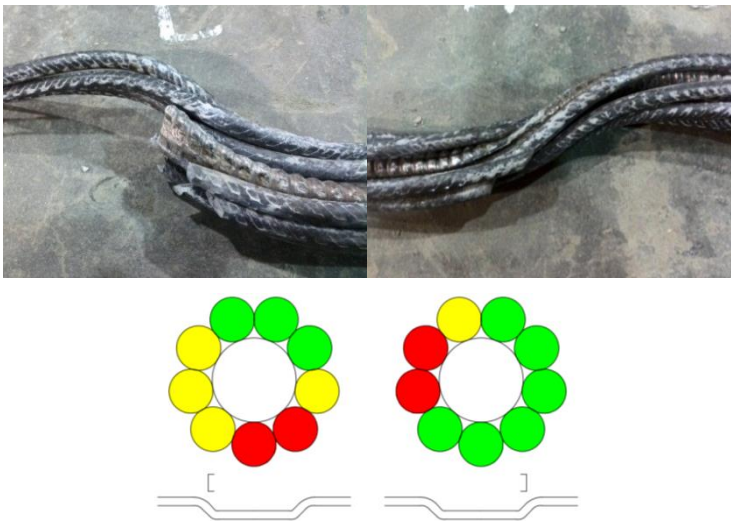

(e) T1-5

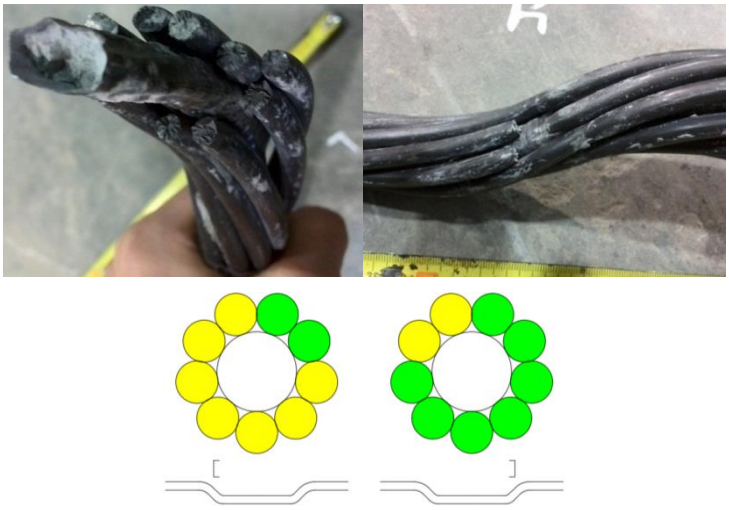

(f) T1-6

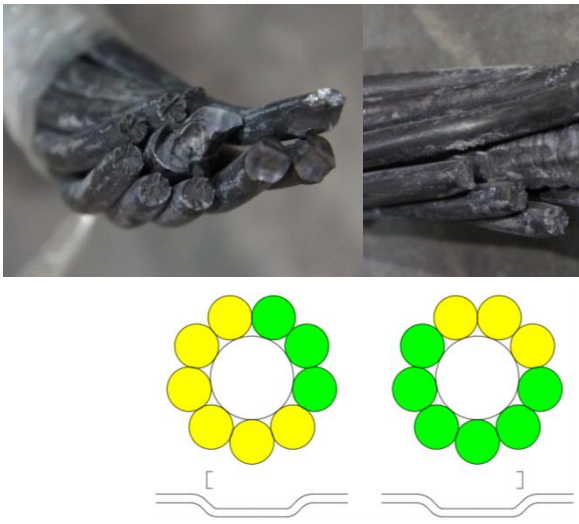

(g) T1-7

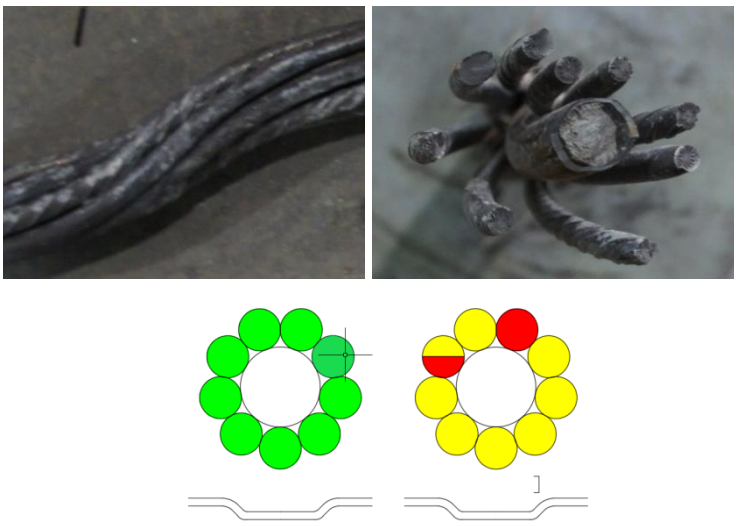

(h) T1-9

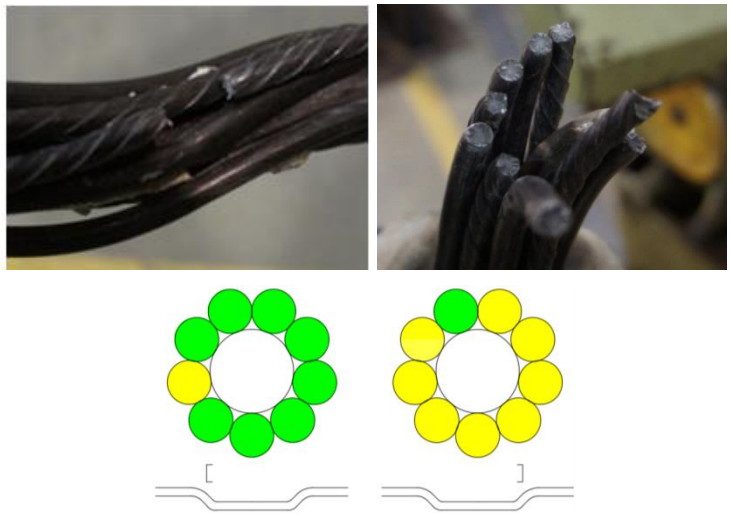

(i) T1-11

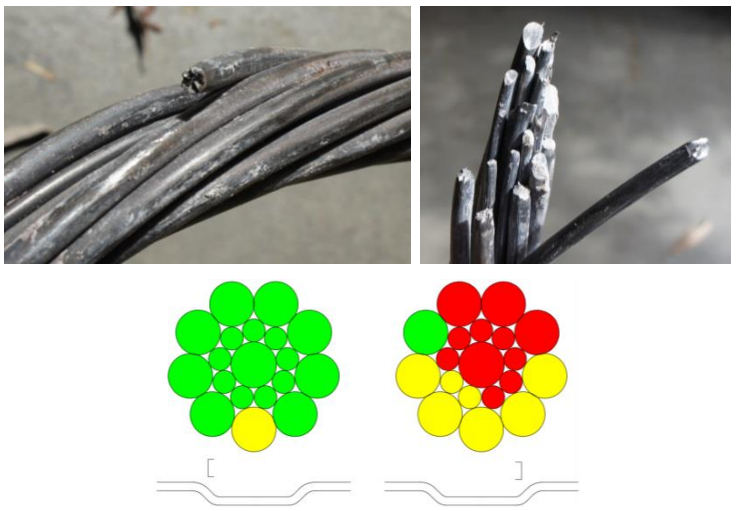

(j) T1-12

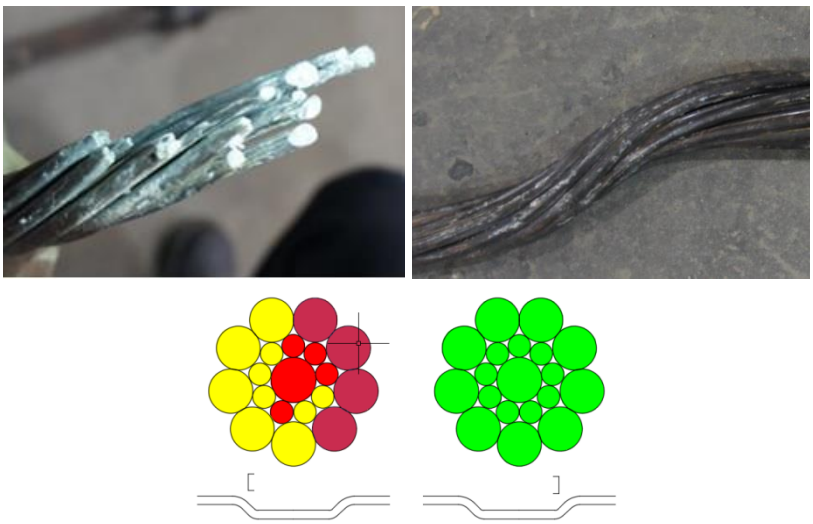

(k) T1-13

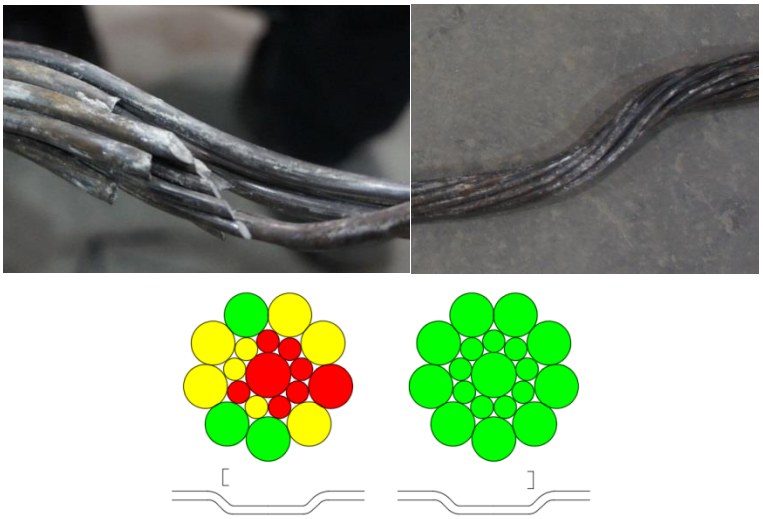

(l) T1-14

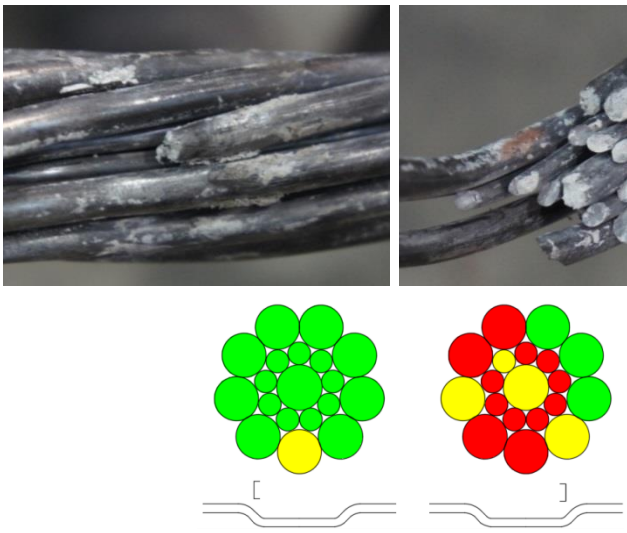

(m) T1-15

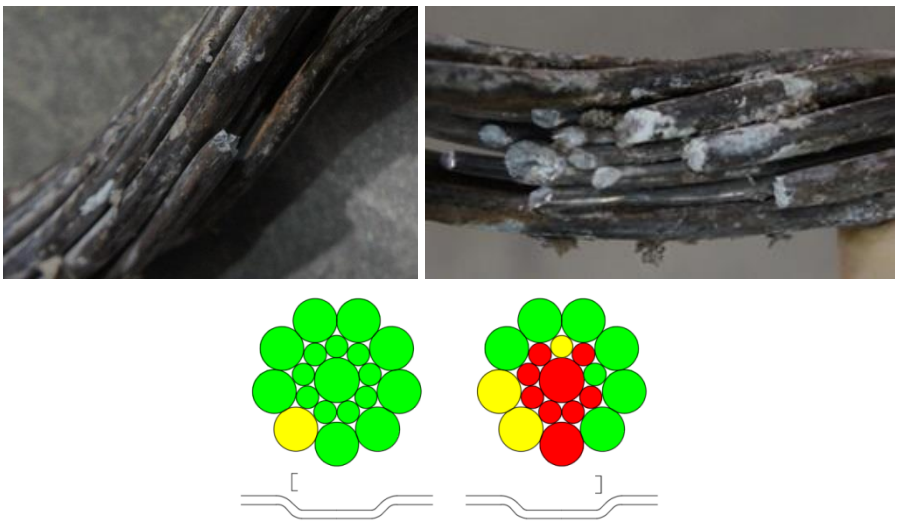

(n) T1-16

APPENDIX F

The following lists the failure modes of cable strands in double shear tests without joint friction: green, yellow and red represent un-broken, broken in tension and broken in shear, respectively. Note: normally no absolutely pure tension failure or shear failure existed in the tests. The classification of cable wire failure was based on the major pattern of each wire failure surface.

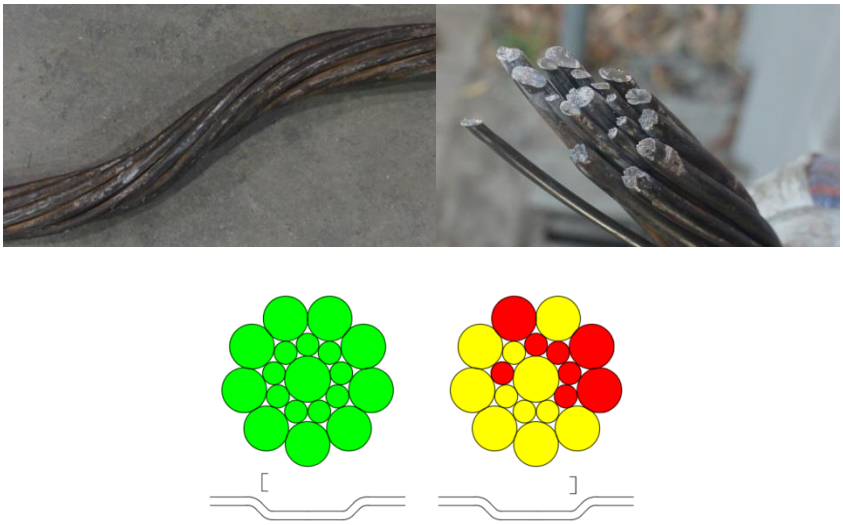

(a) T2-1

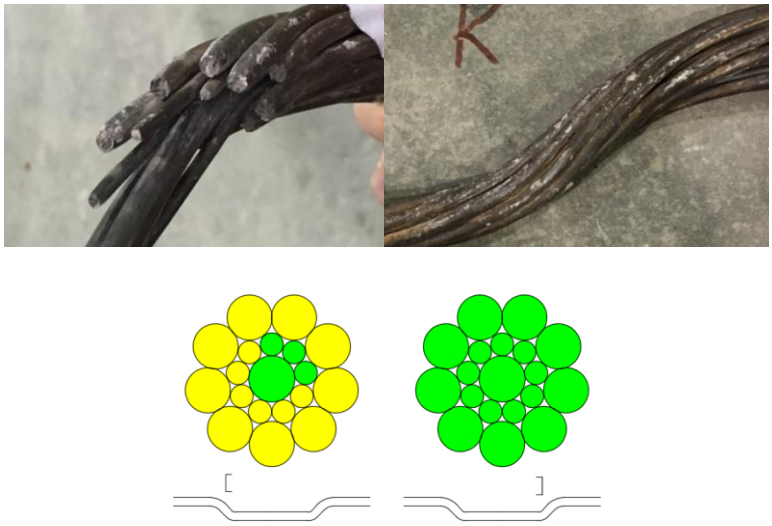

(b) T2-2

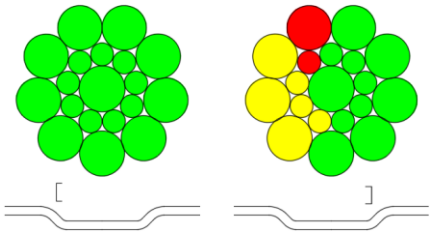

(c) T2-3

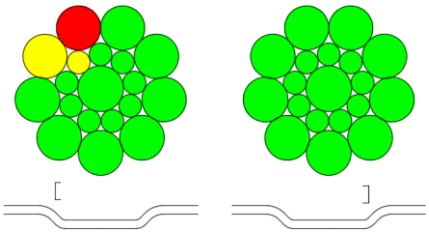

(d) T2-4

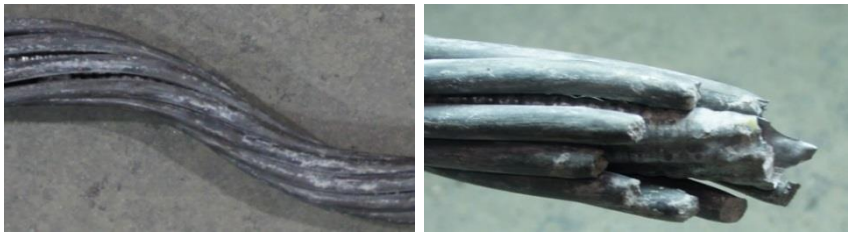

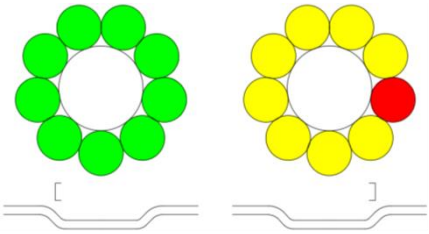

(e) T2-5

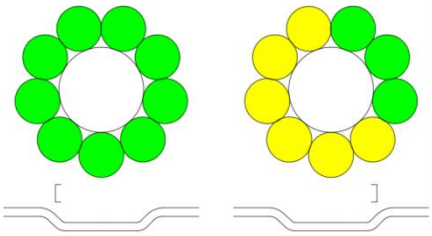

(f) T2-6

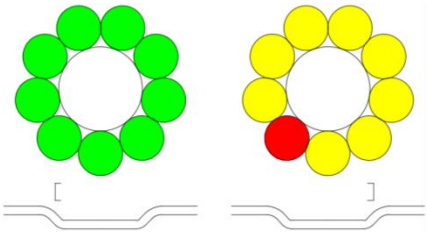

(g) T2-7

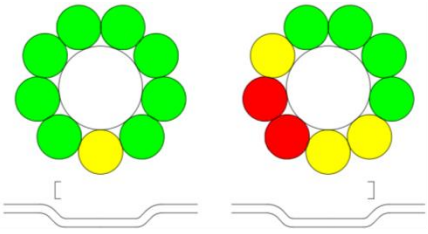

(h) T2-8